Three Dimensional Printing of Biopolymers

Henadira Appuhamilage Deshani Tharindika Gunasekera

(BEng Chemical Engineering, MSc Chemical Engineering)

Thesis Submitted for the Doctoral Philosophy of Engineering,
University of Nottingham

Department of Mechanical, Material and Manufacturing Engineering

October, 2019

Abstract

Annually, large proportions of waste are generated from plants, bird feathers, wool and animal hair. Currently, some of these are recycled while the rest are sent into landfilling which contributes to an increased pollution of the environment. The aim of this work was to provide an alternative use for these biopolymer materials by utilizing three dimensional printing (3PD) technology which will provide environmental and economically friendly solution to reduce waste. These bespoke 3DP parts can be used for biomedical (drug delivery), packaging and wastewater treatment applications.

Due to the presence of strong intra and inter molecular bonds, applications of biopolymers like cellulose and keratin are currently hindered. A wide variety of literature has been published on successful dissolution of these biopolymers in ionic liquids, casting on glass to form films and regeneration using an anti-solvent (mainly water) to remove the ionic liquid. This research attempts to fill the knowledge gap that exists between 3DP and biopolymers by utilizing a novel system. This will involve a biopolymer-ionic liquid-based ink and ink jet printing technology.

The first results chapter uses a DIMATIX ink-jet printer. Due to the viscosity restrictions with this printer, a co-solvent DMSO, was added as a rheological modifier to bring the viscosity of the inks within the printing range. The major limitation of this technique was the requirement of large quantities of co-solvent (32 to 47 wt%) while the amount of cellulose dissolved in the inks was

limited to less than 1.5 wt%. This was well below the cellulose loading that could be dissolved in ionic liquids.

In order to increase the cellulose loading, a PICO Pulse printer that does not have ink viscosity limitations was used. This allowed an increase in cellulose loading up to 13 wt%. More inks were formulated in ionic liquids using keratin and combination of keratin and cellulose (blends). When the printed films were left overnight at room temperature, they formed gel like films. The majority of films cracked after removed from the anti-solvent bath due to the loss of solvent. Characterisation experiments conducted on these films indicated the presence of large quantities of water and ionic liquid in the films.

This research has demonstrated that future work should focus on modifying the glass substrate surface and thereby minimizing the distortion of the pattern during printing. Modifications to the current printing set-up can be achieved by using a support material, printing into an anti-solvent bath and spraying the anti-solvent to maintain the shape of the pattern. A new printing method like binder jetting can also be used for future printing.

Acknowledgement

"He who begun a good work in me shall accomplish it"

Philippians 1:6

I will start by giving glory to God who has seen me through it all and been my ever present help in times of need.

I want to say a big thank you to my father, Mr. Gamini Gunasekera, mother, Mrs. Mano Gunasekera and sister, Miss Kasuni Gunasekera, who have been a strong pillar of support throughout my life. Living away from family over the past few years has not been easy, but they have always provided me with all the emotional and financial support, blessings and encouragement to complete my studies. My lovely grandparents Mr and Mrs Jayasekara have played a key role in my studies and their continuous support played a great part in where I am today and not to give up when faced with challenges.

My lovely husband, Mr Frank Ankrah and I have been part of this postgraduate research journey together for the last 4 years. He was always there to help me brainstorm ideas/questions throughout my PhD and kept me on track with my work. His emotional and spiritual support kept me moving forward steadily till the end.

Being part of the Centre for Additive Manufacturing (CfAM) over the past 4 years as a postgraduate research, I was exposed to world-class cutting-edge research in additive manufacturing. Coming from a chemical engineering field, this has opened a new career pathway for me. I would like to first thank my

supervisors, Prof. Ricky Wildman, Dr. Anna Croft and Prof. Chris Tuck for all their support, guidance and encouragement given to me.

Special thanks to my MSc supervisors, Dr. Anna Croft and Prof. George Chen and my lecturer for my yearlong module, Mr. Sean Moran, who helped me identify my strengths and supported me to actively plan my further studies and career. Also, a big thank you to all the post-docs, technicians, staff and other colleagues in CfAM. Special thanks to Dr. Yinfeng He for all the technical support he provided.

A big thank you to my family in Added Scientific LTD, for their understanding and support during the last phase of my thesis writing. To the warden and the tutors at Derby Hall who were always there to lift me up after a long day.

Finally, special thanks to Dr. Emmanuel Amissah and Pastor Israel. Y. Kemevor for the guidance and spiritual support all through these years.

I am grateful to God for bringing all these wonderful people into my life who have contributed in diverse ways to bring me this far.

God richly bless you all……..

List of Publications

Published

Three dimensional ink-jet printing of biomaterials using ionic liquids and co-solvents.

Deshani H. A. T. Gunasekera, SzeLee Kuek, Denis Hasanaj, Yinfeng He, Christopher Tuck, Anna K. Croft and Ricky D. Wildman.

Faraday Discussions 2016, 190, 509-523.

Tunable ionic control of polymeric films for inkjet based 3D printing.

Erno Karjalainen, Dominic J. Wales, Deshani H.A.T. Gunasekera, Jairton Dupont, Peter Licence, Ricky D. Wildman and Victor Sans.

ACS Sustainable Chemistry and Engineering 2018, 6(3), 3984-3991.

Proteins in ionic liquids: Reactions, applications and futures

A. Schindl, M. L. Hagen, S. Muzammal, H. A. D. Gunasekera, and A. K. Croft

Frontiers in Chemistry 2019, 7, 347

Manuscript in Preparation

Three dimensional printing of biomaterial-laden ionic liquids.

Deshani H. A. T. Gunasekera, Yinfeng He, Christopher Tuck, Anna K. Croft and Ricky D. Wildman.

Oral Presentations

Three dimensional printing of biomaterial-laden ionic liquids.

Deshani H. A. T. Gunasekera, Christopher Tuck, Anna K. Croft and Ricky D. Wildman.

Molten Salts Discussion Group, Summer Meeting 2017.

Table of Contents

Chapter 1 : Introduction 20
1.1 Background 20
1.2 Aims and Objectives 21
Chapter 2 : Literature Review 26
2.1 Background 26
2.2 Cellulose 27
2.2.1 Introduction to Cellulose 27
2.2.2 Cellulose Structure 29
2.2.3 Cellulose Solvents 32
2.3 Keratin 37
2.3.1 Introduction to Keratin 37
2.3.2 Keratin Structure 38
2.3.3 Keratin Solvents 43
2.4 Ionic Liquids 44
2.5 Dissolution Mechanism 47
2.5.1 Cellulose 48
2.5.2 Keratin 50
2.6 Current Literature on Cellulose and Keratin Dissolution using Ionic Liquids 51
2.7 Regeneration 64
2.8 Additive Manufacturing 68
2.8.1 Introduction to Additive Manufacturing 68
2.8.2 Current Literature on Biopolymer 3DP 70
2.8.3 Ink-Jet Printing Technologies 71
2.8.4 Comparison between different Ink-Jet Printing Technologies 74
2.8.5 Principles behind Ink-Jet Printing 76
2.9 Knowledge Gap 82
Chapter 3 : Materials and Methods 84
3.1 Introduction 84
3.2 Chemicals 85
3.3 Ink Preparation 86
3.3.1 Low Viscosity Inks 86
3.3.2 High Viscosity Inks 88
3.4 Printing 89
3.4.1 DIMATIX Ink-jet Printing 89
3.4.2 PICO Pulse Printing 100
3.4.3 Substrates Used for Printing 107
3.4.4 Printing Summary 107

3.5 Regeneration 109
3.6 Evaluation of Ink Physical Properties 111
3.6.1 Coulometric Karl Fischer Titration 111
3.6.2 Rheology 113
3.6.3 Surface Tension 117
3.6.4 Density 119
3.7 Optical Characterisation 119
3.8 Other Characterisation Methods Used 120
3.8.1 Thermogravimetric Analysis (TGA) 120
3.8.2 Fourier Transform Infrared (FTIR) Spectrometer 122
3.8.3 Elemental Analysis 123
Chapter 4 : Three-Dimensional DIMATIX ink-jet Printing of Cellulose using Ionic Liquids and Co-Solvents 124
4.1 Background 124
4.2 Justification 124
4.2.1 Cellulose Selection 124
4.2.2 Ionic Liquid Selection 125
4.2.3 Co-Solvent Selection 129
4.2.4 Anti-Solvent Selection 131
4.3 Results and Discussion 132
4.3.1 Physical Properties and Printability Parameter for Pure Chemicals 132
4.3.2 Preparation of Low Viscosity Inks: Cellulose and Ionic Liquid 134
4.3.3 Physical Properties and Printability Parameter for Low Viscosity Inks: Cellulose and Ionic Liquid 140
4.3.4 Preparation of Low Viscosity Inks: Cellulose, Ionic Liquid and Co-Solvent 142
4.3.5 Physical Properties and Printability Parameter for Low Viscosity Inks: Cellulose, Ionic Liquid and Co-Solvent 143
4.3.6 Ink-jet Printing 147
4.3.7 Regeneration and Characterisation 151
4.4 Chapter Summary 159
Chapter 5 : Three-Dimensional Printing of Cellulose using a PICO Pulse Printer 163
5.1 Background 163
5.2 Results and Discussion 164
5.2.1 Preparation of High Viscosity Inks: Cellulose and Ionic Liquid 164
5.2.2 Rheological Properties of High Viscosity Inks: Cellulose and Ionic Liquid 166
5.2.3 Printing Parameters Optimisation 169
5.2.4 Multi-Layer Printing and Regeneration 181

5.2.5 Optical Characterisations 188

5.2.6 Characterisation of Regenerated Cellulose 193

5.3 Chapter Summary 204

Chapter 6 : Three-Dimensional Printing of Wool and Blends using a PICO Pulse Printer 209

6.1 Background 209

6.2 Justification 209

6.3 Result and Discussion 210

6.3.1 Preparation of High Viscosity Inks: Wool and Ionic Liquid 210

6.3.2 Rheological Properties of High Viscosity Inks: Wool and Ionic Liquid 214

6.3.3 Printing Parameters Optimisation: Wool and Ionic Liquid 216

6.3.4 Multi-Layer Printing and Regeneration: Wool and Ionic Liquid 221

6.3.5 Characterisation of Regenerated Wool: Wool and Ionic Liquid 226

6.3.6 Preparation of High Viscosity Inks: Blend (cellulose and woo) and Ionic Liquid 230

6.3.7 Rheological Properties of High Viscosity Inks: Blend (cellulose and wool) and Ionic Liquid 233

6.3.8 Printing Parameters Optimisation: Blend (cellulose and wool) and Ionic Liquid 235

6.3.9 Multi-Layer Printing and Regeneration: Blend (cellulose and wool) and Ionic Liquid 237

6.3.10 Characterisation of Regenerated Wool: Blend (cellulose and wool) and Ionic Liquid 242

6.4 Chapter Summary 243

Chapter 7 : General Discussion 247

Chapter 8 : Conclusions and Future Work 253

8.1 General Discussion 253

8.2 Recommendations for Future Work 258

Chapter 9 : Appendix 263

Chapter 10 : References 296

List of Figures

Figure 1.1: Flowchart summarising the thesis structure 25
Figure 2.1: Schematic diagram of lignocellulose (Adapted from Lee H. et al., 2014) 27
Figure 2.2: Cellulose molecular structure (Adapted from Klemm D. et al., 1998; Wertz J. et al., 2010) 30
Figure 2.3: Intra- and intermolecular hydrogen bonds in cellulose (Adapted from Klemm D. et al., 1998; Pinkert A. et al., 2009) 31
Figure 2.4: Fringed fibril model (Adapted from Hearle J., 1958) 32
Figure 2.5: α -Amino acid structure (Adapted from Voet D. et al., 2016). 38
Figure 2.6: Peptide bond formation (Adapted from Voet D. et al., 2016) . 39
Figure 2.7: Secondary protein structure: α-helix (Adapted from Gunton J. et al., 2007; Voet D. et al., 2016) 40
Figure 2.8: Secondary protein structure: β-sheet (Adapted from Gunton J. et al., 2007; Voet D. et al., 2016) 41
Figure 2.9: Intra-chain crosslinks in wool (Adapted from Lewis D. and Rippon J., 2013) 41
Figure 2.10: Inter-chain crosslinks in wool (Adapted from Lewis D. and Rippon J., 2013) 42
Figure 2.11: Common anions and cations used in ionic liquids 45
Figure 2.12: Cellulose dissolution mechanism in ionic liquids (Adapted from Sashina E. and Novoselov N., 2009) 49
Figure 2.13: Cation structure for imidazolium based ionic liquids 55
Figure 2.14: General AM process (Adapted from Gibson I. et al., 2014) .. 70
Figure 2.15: Commonly used ink-jet printing technologies (Adapted from Le H., 1998) 72
Figure 2.16: Continuous ink-jet printing mechanisms (Adapted from Le H., 1998) 73
Figure 2.17: Drop-on-demand ink-jet printing mechanisms (Adapted from Derby B., 2010) 74
Figure 2.18: Drop formation sequence in a drop-on-demand ink-jet printer (Adapted from Martin G. *et al*., 2008) 78
Figure 2.19: Impact of a liquid drop on a solid surface (Adapted from Rein M., 1993) 79
Figure 2.20: Contact angle on different substrates (Adapted from Riobbo et al., 2001) 80
Figure 2.21: Effect of droplet spacing on line morphology (Adapted from Soltman D. and Subramanian V., 2008) 81
Figure 2.22: Knowledge gap addressed in this research 82
Figure 3.1: Summary of the experimental procedure used 84
Figure 3.2: Structures of the chemicals used 85
Figure 3.3: FUJIFILM DIMATIX DMP-2831 ink-jet printing procedure 90
Figure 3.4: DIMATIX ink-jet cartridge (Adapted from Fujifilm Dimatix Manual, 2010) 91
Figure 3.5: Consumables used to fill the DIMATIX ink-jet cartridge 92
Figure 3.6: Major components of the DIMATIX ink-jet printer (Adapted from Fujifilm Dimatix Manual, 2010) 93
Figure 3.7: Major components of the DIMATIX ink-jet printer carriage (Adapted from Fujifilm Dimatix Manual, 2010) 93
Figure 3.8: Cross section of the DIMATIX jetting mechanism (Adapted from Fujifilm Dimatix Manual, 2006) 95
Figure 3.9: Voltage Vs time behaviour for different segments in the waveform (Adapted from Fujifilm Dimatix Manual, 2006 and 2010) 97
Figure 3.10: Relationship between print direction, sabre angle and droplet spacing (Adapted from Eggenhuisen T. et al., 2015) 100

Figure 3.11: Cartridge alignment scale (Adapted from Fujifilm Dimatix Manual, 2010) 100
Figure 3.12 PICO Pulse printing procedure 101
Figure 3.13: Major component of the PICO Pulse printing set-up..... 103
Figure 3.14: PICO Pulse valve system (Adapted from Nordson, 2015a). 104
Figure 3.15: Schematic diagram of the PICO Pulse valve operating mechanism (Adapted from Nordson, 2015a) 104
Figure 3.16: (A) Fluid body seat cleaning locations and (B) Alignment of the fluid body seat and the cartridge (Adapted from Nordson, 2015a) .. 107
Figure 3.17: Coulometric Karl Fischer titration procedure..... 113
Figure 3.18: Rotational rheometes used (Adapted from Bohlin Instruments Limited, 1994)..... 114
Figure 3.19: Malvern Kinexus rotational rheometer operating procedure 115
Figure 3.20: Malvern Kinexus rotational rheometer front view 116
Figure 3.21: Forces acting on a liquid drop (Adapted from Yuan Y. and Lee R., 2013) 117
Figure 3.22 Major components of the KRUSS DSA100 drop shape analyser (Adapted from Berry J. et al., 2015)..... 118
Figure 3.23: KRUSS DSA100 drop shape analyser operating procedure 119
Figure 3.24: ATR technique (Adapted from Barbes L. et al., 2014) 122
Figure 4.1: TGA and TG curves for cellulose 135
Figure 4.2: TGA and DTG curves for [C_2C_1Im][OAc] 135
Figure 4.3: TGA and DTG curves for [C_4C_1Im][OAc] 136
Figure 4.4: Dissolution observations for samples containing DMSO and 1-butanol..... 142
Figure 4.5: Viscosity Vs time at fixed shear rate and temperature for sample 6 146
Figure 4.6: Viscosity Vs time at fixed shear rate and temperature for sample 7 147
Figure 4.7: Microscopic images showing missing drops and ligaments .. 149
Figure 4.8: Microscopic images for samples ink-jet printed on PET 149
Figure 4.9: SEM images for samples ink-jet printed on PET and dried for approximately 18 hrs at room temperature 150
Figure 4.10: SEM images for sample 6 ink-jet printed on PET and regenerated by leaving deionised water for different time intervals before heating for approximately 18 hours at 50 °C 153
Figure 4.11: SEM images for sample 7 ink-jet printed on PET and regenerated by leaving deionised water for different time intervals before heating for approximately 18 hours at 50 °C 154
Figure 4.12: WLI results for sample 6 ink-jet printed on PET and regenerated by leaving deionised water for different time intervals before heating for approximately 18 hours at 50 °C 155
Figure 4.13: WLI results for sample 7 ink-jet printed on PET and regenerated by leaving deionised water for different time intervals before heating for approximately 18 hours at 50 °C 156
Figure 4.14: WLI results for sample 6 ink-jet printed on glass and regenerated by leaving deionised water for different time intervals before heating for approximately 18 hours at 50 °C 157
Figure 4.15: WLI results obtained for sample 7 ink-jet printed on glass and regenerated by leaving deionised water for different time intervals before heating for approximately 18 hours at 50 °C 158
Figure 5.1: TGA curve for cellulose dried at isothermal conditions 165
Figure 5.2: Rheological properties of sample 11 ([C_2C_1Im][OAc] and cellulose) 167
Figure 5.3: Rheological properties of sample 12 ([C_4C_1Im][OAc] and cellulose) 168

Figure 5.4: Microscopic images obtained from the droplet formation study 173
Figure 5.5: Images obtained from the film formation study 181
Figure 5.6: Multi-layered film printed using cellulose and ionic liquid 182
Figure 5.7: Films obtained after straight regeneration 184
Figure 5.8: Gel film formed when sample 11 was left overnight 185
Figure 5.9: Films obtained after cellulose recovery 186
Figure 5.10: WLI results obtained for Sample 11 190
Figure 5.11: SEM image of untreated cellulose 191
Figure 5.12: SEM images obtained after the cellulose recovery process 193
Figure 5.13: FTIR spectra obtained after the cellulose recovery process 197
Figure 5.14: TGA and DTG curves for pure chemicals and films obtained from sample 11 200
Figure 5.15: TGA and DTG curves for pure chemicals and films obtained from sample 12 201
Figure 6.1: TGA and DTG curves for wool..... 211
Figure 6.2: Rheological properties of sample 13 ([C_2C_1Im][OAc] and wool) 215
Figure 6.3: Rheological properties of sample 14 ([C_4C_1Im][OAc] and wool) 215
Figure 6.4: Images obtained from the film formation study 221
Figure 6.5: Multi-layered films printed using wool and ionic liquid 222
Figure 6.6: Films obtained from sample 14 after the straight regeneration 223
Figure 6.7: Films obtained from sample 14 after wool recovery 224
Figure 6.8: TGA and DTG curves for pure chemicals and films obtained from sample 14 228
Figure 6.9: Rheological properties of sample 15 ([C_2C_1Im][OAc], cellulose and wool) 234
Figure 6.10: Rheological properties of sample 16 ([C_4C_1Im][OAc], cellulose and wool) 234
Figure 6.11:Multi-layered films printed using blends (cellulose and wool) 238
Figure 6.12: Films obtained after straight regeneration..... 239
Figure 6.13: Films obtained after the blend (cellulose and wool) recovery 240
Figure 7.1: Schematic diagram for cellulose and ionic liquid interaction mechanism 251
Figure 7.2: Schematic diagram for wool and ionic liquid interaction mechanism 251
Figure 9.1: Drop watcher screen (Adapted from Fujifilm Dimatix Manual, 2010)..... 263
Figure 9.2: Cartridge settings window (Adapted from Fujifilm Dimatix Manual, 2010)..... 264
Figure 9.3:Waveform editor window (Adapted from Fujifilm Dimatix Manual, 2010)..... 265
Figure 9.4: WLI results for sample 6 ink-jet printed on PET and dried for approximately 18 hours at room temperature..... 266
Figure 9.5: WLI results for sample 7 ink-jet printed on PET and dried for approximately 18 hours at room temperature..... 267
Figure 9.6: WLI results for sample 6 ink-jet printed on PET and regenerated by leaving deionised water for 30 minutes before heating for approximately 18 hours at 50 °C 268
Figure 9.7: WLI results obtained for sample 6 ink-jet printed on PET and regenerated by leaving deionised water for 1 hour 30 minutes before heating for approximately 18 hours at 50 °C 269

Figure 9.8: WLI results for sample 6 ink-jet printed on PET and regenerated by leaving deionised water for 2 hours before heating for approximately 18 hours at 50 °C 270
Figure 9.9: WLI results for sample 7 ink-jet printed on PET and regenerated by leaving deionised water for 30 minutes before heating for approximately 18 hours at 50 °C 271
Figure 9.10: WLI results for sample 7 ink-jet printed on PET and regenerated by leaving deionised water for 1 hour before heating for approximately 18 hours at 50 °C 272
Figure 9.11: WLI results for sample 7 ink-jet printed on PET and regenerated by leaving deionised water for 1 hour 30 minutes before heating for approximately 18 hours at 50 °C 273
Figure 9.12: WLI results for sample 7 ink-jet printed on PET and regenerated by leaving deionised water for 2 hours before heating for approximately 18 hours at 50 °C 274
Figure 9.13: WLI results obtained for sample 6 ink-jet printed on glass and regenerated by leaving deionised water for 30 minutes before heating for approximately 18 hours at 50 °C 275
Figure 9.14: WLI results obtained for sample 6 ink-jet printed on glass and regenerated by leaving deionised water for 1 hour before heating for approximately 18 hours at 50 °C 276
Figure 9.15: WLI results obtained for sample 6 ink-jet printed on glass and regenerated by leaving deionised water for 1 hour 30 minutes before heating for approximately 18 hours at 50 °C 277
Figure 9.16: WLI results for sample 6 ink-jet printed on glass and regenerated by leaving deionised water for 2 hours before heating for approximately 18 hours at 50 °C 278
Figure 9.17: WLI results for sample 7 ink-jet printed on glass and regenerated by leaving deionised water for 30 minutes before heating for approximately 18 hours at 50 °C 279
Figure 9.18: WLI results for sample 7 ink-jet printed on glass and regenerated by leaving deionised water for 1 hour before heating for approximately 18 hours at 50 °C 280
Figure 9.19: WLI results for sample 7 ink-jet printed on glass and regenerated by leaving deionised water for 1 hour 30 minutes before heating for approximately 18 hours at 50 °C 281
Figure 9.20: WLI results for sample 7 ink-jet printed on glass and regenerated by leaving deionised water for 2 hours before heating for approximately 18 hours at 50 °C 282
Figure 9.21: Graph b shows the FTIR spectra for [C_2C_1Im][OAc] (Adapted from Zhang B. et al., 2015) 283
Figure 9.22: Microscopic images obtained from the droplet formation study for sample 13 284
Figure 9.23: Microscopic images obtained from the droplet formation study for sample 14 285
Figure 9.24: Microscopic images obtained from the droplet formation study for sample 15 290
Figure 9.25: Microscopic images obtained from the droplet formation study for sample 16 291
Figure 9.26: TGA and DTG curves for ionic liquid and blend films obtained from sample 15 295
Figure 9.27: TGA and DTG curves for ionic liquid and blend films obtained from sample 16 295

List of Tables

Table 2.1: Lignocellulose composition in different plant species 28
Table 2.2: Summary of non-derivatising solvents used to dissolve cellulose 35
Table 2.3: Summary of cellulose solubility in selected ionic liquids 59
Table 2.4: Summary of keratin solubility in selected ionic liquids 62
Table 2.5: Summary of cellulose and keratin-based regenerated materials 66
Table 3.1: Low viscosity inks containing cellulose and ionic liquid..... 87
Table 3.2: Low viscosity inks containing cellulose, ionic liquid and co-solvent 87
Table 3.3: High viscosity inks containing cellulose and/or wool and ionic liquid..... 88
Table 3.4: Ink requirements for DIMATIX ink-jet printing (Fujifilm Dimatix, 2006; Fujifilm Dimatix, 2010) 96
Table 3.5: Explanation of the different segments in the waveform (Fujifilm Dimatix, 2006; Fujifilm Dimatix, 2010)..... 97
Table 3.6: Description of different parameters in the waveform (Fujifilm Dimatix, 2010) 99
Table 3.7: Description of PICO touch controller printing parameters (Nordson, 2015b) 105
Table 3.8: Summary of the printing conditions used in the droplet formation study 108
Table 3.9: Summary of shear rate and temperature ranges used 116
Table 4.1: Physical properties of commonly used ionic liquids..... 126
Table 4.2: Physical properties and printability parameters of the pure chemicals used 132
Table 4.3: Degradation temperatures of the pure chemicals used 138
Table 4.4: Physical properties of the low viscosity inks (cellulose and ionic liquid) used..... 141
Table 4.5: Experimental and theoretical densities of the low viscosity inks (cellulose, $[C_4C_1Im][OAc]$ and DMSO) 144
Table 4.6: Physical properties and printability parameters of the low viscosity inks (cellulose, $[C_4C_1Im][OAc]$ and DMSO)..... 145
Table 4.7: Jetting parameters for samples 6 and 7..... 148
Table 4.8: Average droplet diameter for ink-jet printed samples on PET 149
Table 4.9: Average height of a droplet for ink-jet printed samples on PET 151
Table 4.10: Average height of a droplet for ink-jet printed samples on glass 152
Table 5.1: Rheological properties of the high viscosity inks containing cellulose and ionic liquid 167
Table 5.2: Summary of constant printing parameters used 169
Table 5.3: Droplet formation study results 171
Table 5.4: Average droplet diameter results..... 172
Table 5.5: Microscopic images obtained from the line formation study for sample 11..... 176
Table 5.6: Microscopic images obtained from the line formation study for sample 12..... 178
Table 5.7: Summary of cellulose recovery observations 187
Table 5.8: Summary of elemental analysis results..... 194
Table 5.9: Summary of cellulose regeneration TGA results reported in literature 202
Table 5.10: Degradation temperatures for pure chemicals and films obtained from the cellulose recovery process 204

Table 6.1: Degradation temperatures for keratin 211
Table 6.2: Rheological properties of the high viscosity inks containing wool and ionic liquid 214
Table 6.3: Droplet formation study results 217
Table 6.4: Average droplet diameter results 218
Table 6.5: Summary of keratin recovery observations 225
Table 6.6: Degradation temperatures for pure chemicals and films obtained from the keratin recovery process 228
Table 6.7: Summary of keratin regeneration TGA results reported in literature 229
Table 6.8: Summary of cellulose and keratin based blends reported in literature 231
Table 6.9: Rheological properties of the high viscosity inks containing cellulose, wool and ionic liquid 233
Table 6.10: Droplet formation study results 236
Table 6.11: Average droplet diameter results 237
Table 6.12: Summary of blend (cellulose and wool) recovery observations 241
Table 6.13: Degradation temperatures for pure chemicals and films obtained from the blend recovery process 242
Table 8.1: Summary of PICO Pulse printing results 256
Table 9.1: Microscopic images obtained from the line formation study for sample 13 ([C_2C_1Im][OAc]) and wool 286
Table 9.2: Microscopic images obtained from the line formation study for sample 14 ([C_4C_1Im][OAc] and wool) 288
Table 9.3: Microscopic images obtained from the line formation study for sample 15 ([C_2C_1Im][OAc], cellulose and wool) 292
Table 9.4: Microscopic images obtained from the line formation study for sample 16 ([C_4C_1Im][OAc], cellulose and wool) 294

Abbreviations

List of Chemicals

[AMIM][Cl]	1-allyl-3-methylimidazolium chloride
[AMIM]OFo]	1-allyl-3-methylimidazolium formate
[BDMIM][Cl]	1-*N*-Butyl-2,3-dimethylimidazolium chloride
$[BF_4]$	Tetrafluoroborate
[Br]	Bromide
$[C_2C_1Im][Cl]$	1-ethyl-3-methylimidazolium chloride
$[C_2C_1Im][DEP]$	1-ethyl-3-methylimidazolium diethylphosphate
$[C_2C_1Im][DMP]$	1-ethyl-3-methylimidazolium dimethylphosphate
$[C_2C_1Im][Et_2PO_4]$	1-ethyl-3-methylimidazolium diethylphosphate
$[C_2C_1Im][(MeO)(H)PO_2]$	1-ethyl-3-methylimidazolium methyl phosphonate
$[C_2C_1Im][(MeO)(Me)PO_2]$	1-ethyl-3-methylimidazolium methyl methylphosphonate
$[C_2C_1Im][(MeO)_2PO_2]$	1-ethyl-3-methylimidazolium dimethyl phosphate
$[C_2C_1Im][OAC]$	1-ethyl-3-methylimidazolium acetate
$[C_4C_1Im][(C_6H_5)COO]$	1-butyl-3-methylimidazolium benzoate
$[C_4C_1Im][Cl]$	1-butyl-3-methylimidazolium chloride
$[C_4C_1Im][DBP]$	1-butyl-3-methylimidazolium dibutyl phosphate
$[C_4C_1Im][DMP]$	1-butyl-3-methylimidazolium dimethylphosphate
$[C_4C_1Im][H_2NCH_2COO]$	1-butyl-3-methylimidazolium aminoethanic acid salt
$[C_4C_1Im][HOCH_2COO]$	1-butyl-3-methylimidazolium glycollate
$[C_4C_1Im][H_2PO_4]$	1-butyl-3-methylimidazolium dihydrogenphosphate
$[C_4C_1Im][HSO_4]$	1-butyl-3-methylimidazolium hydrogensulfate
$[C_4C_1Im][HSCH_2COO]$	1-butyl-3-methylimidazolium thioglycollate
$[C_4C_1Im][OAc]$	1-butyl-3-methylimidazolium acetate
$[C_4C_1Im][OFo]$	1-butyl-3-methylimidazolium formate
$[Cu(NH_3)_4][OH]_2$	Cuprammonium hydroxide (Cuam)
[DBNE][DEP]	1-Ethyl-1,5-diazabicyclo[4.3.0]-non-5-enium diethylphosphate
[DBNH][OAc]	1,5-diazabicyclo[4.3.0]non-5-enium acetate
[DBNM][DMP]	1-methyl-1,5-diazabicyclo[4.3.0]non-5-enium dimethyl phosphate
[DCA]	Dicyanamide
$[DiMIM][Me_2PO_4]$	1,3-dimethylimidazolium dimethylphosphate
DMAc	N,N-dimethylacetamide
[DMEA][OFo]	*N,N*-dimethylethanolammonium formate
DMF	*N,N*-dimethylformamide
DMSO	Dimethyl sulfoxide
$[EtSO_4]$	Ethylsulfate
H_2	Hydrogen gas
H_2O	Water
I_2	Iodine

LiCl	Lithium chloride
$[Me(OEt)_2\text{-}Et\text{-}Im][OAc]$	1-ethyl-3-(2-methoxyethoxy)ethyl)imidazolium acetate
$[Me(OEt)_3\text{-}Et\text{-}Im][OAc]$	1-ethyl-3-(2-(2-methoxyethoxy)ethoxy)ethyl)imidazolium acetate
$[Me(OEt)_4\text{-}Et\text{-}Im][OAc]$	1-ethyl-3-(2-(2-(2-methoxyethoxy)ethoxy)ethoxy)ethyl)imidazolium acetate
$[Me(OEt)_2\text{-}Et_3N][OAc]$	Triethyl (2-methoxyethoxy)ethylammonium acetate
$[Me(OEt)_3\text{-}Et_3N][OAc]$	Triethyl (2-(2-methoxyethoxy)ethoxy)ethylammonium acetate
$[Me(OEt)_3\text{-}Et_3N][OFo]$	Triethyl (2-(2-methoxyethoxy)ethoxy)ethylammonium formate
N_2	Nitrogen gas
$[N_{2221}][DMP]$	Triethylmethylammonium dimethylphosphate
NaOH	Sodium hydroxide
$[Ni(NH_2CH_2CH_2)_3N][OH]_2$	Nitren
NMMO	N-methylmorpholine-N-oxide
[OTf]	Trifluoromethanesulfonate
$[PF_6]$	Hexafluorophosphate
$[Pb(NH_2(CH_2)_2NH_2)][OH]_2$	Pden
[SCN]	Thiocyanate
SiO_2	Silicon dioxide
SO_2	Sulphur dioxide
TBAF	Tetra butyl ammonium fluoride

List of Acronyms

3D	Three dimensional
3DP	Three dimensional printing
AFM	Atomic force microscope
AGU	Anhydroglucopyranose unit
ATR	Attenuated total reflectance
CAD	Computer aided design
CfAM	Centre for Additive Manufacturing
DP	Degree of polymerization
DTG	Derivative of the thermogravimetric curve
Eu	Eucalyptus
FTIR	Fourier transform infrared spectroscopy
GPC	Gel permeation chromatography
IR	Infrared radiation
LED	Light emitting diode
MCC	Microcrystalline cellulose
MSDS	Material safety data sheet
NMR	Nuclear magnetic resonance

O.D, regen and rtm	Overnight drying, regeneration and leave at room temperature
O.D, regen and vac. oven	Overnight drying, regeneration and leave in the vacuum oven
PET	Polyethylene terephthalate
PTFE	Polytetrafluoroethylene
PZT	Piezo element
SD	Standard duty
SEM	Scanning electron microscope
SLS	Selective laser sintering
STL	Stereolithography
Straight regen	Straight regeneration
TGA	Thermogravimetric analysis
UK	United Kingdom
UV-vis	Ultraviolet–visible spectroscopy
WLI	White light interferometry

List of Units

±	Plus-minus
≈	Approximately
<	Less than
≥	Greater than or equal to
°	Degree
%	Percentage
%/°C	Derivative weight
µm	Micrometre
µs	Microsecond
bar	Bar
°C	Degree Celsius
C	Coulomb
cm^{-1}	Per centimetre
°C/minute	Degree Celsius per minute
°C/min	Degrees Celsius per minute
C/mol	Coulombs per mole
g	Grams
g cm^{-3}	Grams per cubic centimetre
g/mol	Grams per mole
Hz	Hertz
Mass%	Percentage by mass
mg	Milligram
mL	Millilitre
mm	Millimetre
mN m^{-1}	Millinewton per meter
MPa	Mega pascal
mPa s	Millipascal-second
ms	Millisecond

mol%	Percentage by moles
m/s	Metre per second
nL	Nanolitre
nm	Nanometre
pL	Picolitre
ppm	Parts per million
rpm	Revolutions per minute
s	Second
s^{-1}	Per second
V	Volts
%ww	Percentage weight
wt%	Percentage by weight

List of Symbols

π*	Kamlet-Taft parameters; dipolarity/polarizability effects
ρ	Density
η	Viscosity
γ	Shear rate
σ	Surface tension/Shear stress
α	Alpha
α	Kamlet-Taft parameters; hydrogen bond acidity
β	Beta
β	Kamlet-Taft parameters; hydrogen bond basicity
C	Carbon
Cr	Chromium
d	Characteristic length
e	Electron
H	Hydrogen
H^+	Hydrogen ion
I^-	Iodide
n	Non-Newtonian index/Power law index
n	Degree of polymerization
N	Nitrogen
O	Oxygen
Oh	Ohnesorge number
Re	Reynolds number
v	velocity
W	Weight of ionic liquid + syringe
w	Weight of the syringe
We	Weber number
X_{IL}	Mole fraction of ionic liquid relative to co-solvent
Z	Printability parameter

Chapter 1 : Introduction

1.1 Background

The desire for high quality and precision-designed manufactured goods has been steadily increasing, putting strain on both resources and manufacture processes. As such, renewable chemicals from biomass are being looked towards to supply the material needs of tomorrow. In particular, biopolymeric materials such as cellulose, which can be derived from plants, and keratin, which is available in waste streams from animal processing, presents an opportunity to incorporate properties that nature has selected for over billions of years of evolution.

The environmental pollution (land, water and air) caused by these biopolymers contribute to greenhouse effect and global warming. According to the UK statistics on waste, wood waste output for the year 2014 was 2.3 million tonnes, which was 1.1 % of the total waste produced (Department of Environment Food and Rural Affair, 2016). Even though, some of the wood waste is currently recycled to manufacture panel boards, generate biomass, for animal bedding and other applications like equine, mulches and pathways (Tolvik Consulting Ltd, 2011), still a major proportion of non-hazardous wood waste is landfilled (24,503 tonnes in 2014) and incinerated (176,717 tonnes in 2014) (Department of Environment Food and Rural Affair, 2016) adding to pollution and processing cost. In terms of world keratin-based waste, it has

been projected to be around 4,500,000 tonnes per annum (Zoccola M. *et al*., 2009).

For many new industrial applications, three-dimensional printing (3DP) has shown promise as a mechanism for bespoke and waste-minimising manufacture. Limitations in cellulose and keratin solubility have restricted their use in 3DP, and to move towards better utilisation of renewable resources. Therefore, as a readily available resource both wood and animal waste can be used in conjunction with 3DP to bring value to waste. With the growing volumes of waste with population increase and industrialisation if this method is successful it opens a new manufacturing pathway where these biopolymers can be used for a wide variety of applications.

1.2 Aims and Objectives

Aims

The aim of this PhD was to identify routes by which 3DP of biopolymers will become possible.

Objectives

- Identify suitable ionic liquids which can act as a solvent for biopolymer dissolution.
- Prepare biopolymer inks using ionic liquids as the solvent and evaluate their rheological properties.

- Optimise the printing parameters and demonstrate printability of ionic liquid-laden biopolymers.
- Regenerate the printed samples to remove the ionic liquid.
- Characterise the properties of regenerated samples and evaluate the efficiency of the regeneration process.

1.3. Novelty of Research

The novelty of this research comes from;

- Preparation of different inks (low and high viscosity) for ink-jet printing using biopolymers and ionic liquids.
- Evaluating the rheological properties of these inks.
- Optimising the printing parameters and identifying different factors that govern the stable printability of droplets, lines and films.
- Regeneration of 3D printed films using different mechanisms.
- Assessing the efficiency of the regeneration process by characterising the regenerated films in terms of morphology, functional groups, chemical composition and thermal stability.

1.4 Thesis Structure & Chapter Outline

Chapter 2: Literature Review

This chapter aims to provide a brief overview of the structure of two natural biopolymers namely; cellulose and keratin and the limitations associated with the current solvents that are been used to dissolve them. Next the use of ionic

liquids as a solvent for biopolymer dissolution will be discussed, followed by regeneration (removal of ionic liquid after dissolution). Finally, the additive manufacturing process will be introduced and a detailed review on material jetting technology and the underlining theory will be discussed.

Chapter 3: Materials and Methods

This chapter provides information on the chemicals used and the ink preparation procedure. Next a detailed explanation of the two different material jetting technologies used (DIMATIX ink-jet printing and PICO Pulse printing), along with the regeneration process is provided. Other instruments used to evaluate ink physical properties, optical characterisation and properties of regenerated samples will also be discussed here along with the experimental procedure used for data collection and processing.

Chapter 4: Three-Dimensional DIMATIX Ink-Jet Printing of Cellulose using Ionic Liquids and Co-Solvents

Different low viscosity inks will be prepared using cellulose, ionic liquid and a co-solvent and their printability parameter will be used to select the inks suitable for DIMATIX ink-jet printing. The printed samples and the regenerated samples will be characterised to assess their morphology.

Chapter 5: Three-Dimensional Printing of Cellulose using PICO Pulse Printing

Cellulose and ionic liquid-based high viscosity inks will be printed using a PICO Pulse printer. The printing parameters will be optimised to identify the suitable

printing conditions to print films. Finally, the 3D printed films will be immersed in an anti-solvent and characterised using different techniques.

Chapter 6: Three-Dimensional Printing of Wool and Blends using PICO Pulse Printing

Wool and ionic liquid, and blend (cellulose, wool and ionic liquid)-based high viscosity inks will be printed using a PICO Pulse printer. The printing parameters will be optimised to identify the suitable printing conditions to print films. Finally, the 3D printed films will be immersed in an anti-solvent and characterised using different techniques.

Chapter 7: General Discussion

This chapter aims to bring together the main results obtained from the low viscosity (DIMATIX ink-jet printing) and high viscosity (PICO Pulse printing) ink preparation, printing and the outcomes from the biopolymer recovery process.

Chapter 8: Conclusions and Future Work

This chapter summarise the results obtained from DIMATIX ink-jet printing and PICO Pulse printing using different biopolymers. Limitations and future work will be also be suggested.

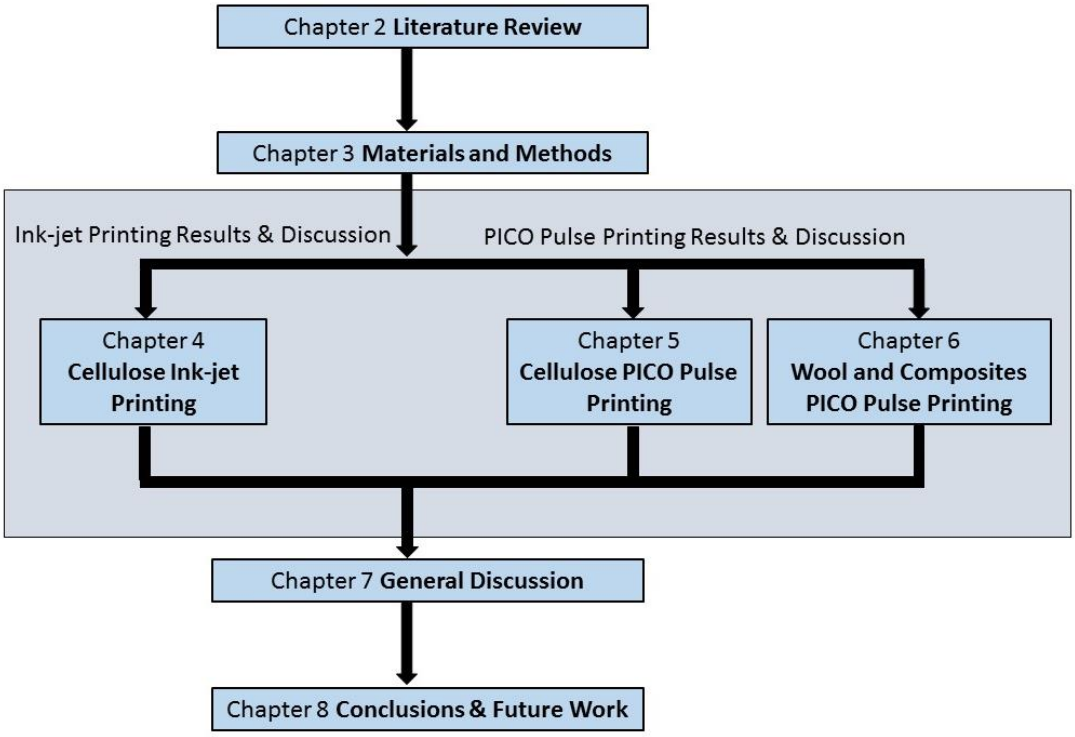


Figure 1.1: Flowchart summarising the thesis structure

Chapter 2 : Literature Review

2.1 Background

This chapter is comprised of three sections. Firstly, it will give an overview of two different biopolymers namely; cellulose and keratin. This is followed by their structures and limitations associated with the solvents currently used to dissolve them.

Secondly, it will provide a brief introduction to ionic liquids, their properties and advantages of using them as a solvent for biopolymer dissolution. Next a detailed review will be conducted on current research available on the dissolution mechanism of biopolymers (cellulose and keratin) in ionic liquids and factors that govern this dissolution process. This section will conclude looking into biopolymer regeneration and applications of these regenerated materials.

The final section will provide an overview of the additive manufacturing (AM) process and the current literature on the use of biopolymers in AM. Next, two different material jetting technologies (ink-jet printing and PICO Pulse printing) will be discussed along with different theories that govern these technologies.

2.2 Cellulose

2.2.1 Introduction to Cellulose

Lignocellulose is a composite material predominately comprising of cellulose, hemicellulose and lignin. There are also smaller quantities of pectin, protein, extractives and ash present (Chen H., 2014; Bajpai P., 2016). Figure 2.1 shows a schematic diagram of lignocellulose.

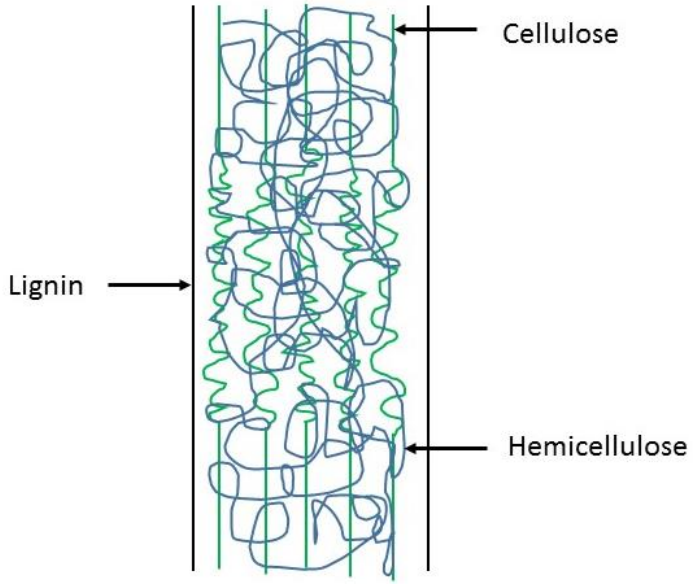


Figure 2.1: Schematic diagram of lignocellulose (Adapted from Lee H. *et al*., 2014)

Cellulose is the most abundant component for most plant species, except for, grass and wheat straw where the hemicellulose percentage is proportionately higher (Bajpai P., 2016) and cotton consists of only cellulose (Chen H., 2014). The dry weigh compositions vary among different lignocellulosic materials (Table 2.1) and are influenced by a variety of factors like plant species, age and growth conditions (Berrocal A. *et al*., 2004; Jørgensen H. *et al*., 2007; Bajpai

P., 2016). Generally, lignocellulose consists of 35 to 50 % cellulose, 20 to 35 % hemicellulose and 5 to 30 % lignin (Chen H., 2014).

Table 2.1: Lignocellulose composition in different plant species

Lignocellulose Material	Cellulose %	Hemicellulose %	Lignin %	Reference
Softwood - spruce	43.4	18	28.1	Tengborg C. *et al*., 1998
Cotton	100			Chen H., 2014
Hardwood	40-55	24-40	18-25	Bajpai P., 2016
Softwood	45-50	25-35	25-35	Bajpai P., 2016
Wheat straw	30	50	15	Bajpai P., 2016
Corn cobs	45	35	15	Bajpai P., 2016
Grasses	25-40	35-50	10-30	Bajpai P., 2016
Switchgrass	45	31.4	12	Bajpai P., 2016

Cellulose was selected for this research, both due to the natural abundance and the ease in obtaining purified material. Cellulose is the most abundant renewable organic compound present on the Earth because of its fundamental role in the plant cell wall (Chen H., 2014), although its availability is not limited to plant sources. A review conducted by Moon R. *et al*., (2011) highlighted wood, plant, animal tunicate (family of sea animals), algae (green, gray, red, yellow-green etc.) and bacteria (*Gluconacetobacter xylinus*) as cellulose sources. In addition, nine different cellulose-based particles can be obtained from cellulose sources. They include micro- and macro-scaled particles (*e.g.* wood fibre, plant fibre and microcrystalline cellulose) and nano-scaled particles (*e.g.* microfibrillated cellulose, nanofibrilated cellulose, cellulose nanocrystals, tunicate cellulose nanocrystals, algae cellulose particles and bacterial cellulose particles). All these particles have unique dimensions, morphology, crystallinity, crystal structure and properties (Moon R. *et al*., 2011).

Cellulose and its derivatives have been used for a wide variety of applications ranging from pharmaceutical (Shokri J. and Adibkia K., 2013), electronic (Baptista A. *et al*., 2013; Mahadeva S. *et al*., 2015), textile (Wertz J. *et al*., 2010), cosmetic (Wiechers S. *et al*., 2015) and many more. Hence, this renewable resource has many uses in different industries.

2.2.2 Cellulose Structure

At the molecular lever, cellulose is a linear syndiotactic homopolymer consisting of D-anhydroglucopyranose units (AGU) attached via β-1,4-glycosidic bonds (Klemm D. *et al*., 1998; Wertz J. *et al*., 2010; Olsson C. and Westman G., 2013). The glycosidic bond is formed at C-1 and C-4 positions (Wertz J. *et al*., 2010) and the oxygen is covalently bonded to C-1 and C-4 (Klemm D. *et al*., 2005; Moon R. *et al*., 2011). In this structure, the alternating monomer units are rotated 180 ° with respect to their neighbours (Klemm D. *et al*., 2005; Wertz J. *et al*., 2010; Olsson C. and Westman G., 2013). The AGU is formed when glucose loses a water molecule during polymerization. An acetal bond is formed when the hemiacetal in one glucose unit reacts with the alcohol in another (Olsson C. and Westman G., 2013). Cellulose molecular structure can also be described as an isotactic polymer where the dimer cellobiose is the repeating unit (Klemm D. *et al*., 1998; Olsson C. and Westman G., 2013). Figure 2.2 presents a diagram showing the molecular structure of cellulose and indicating the numbering of both the carbon and oxygen atoms.

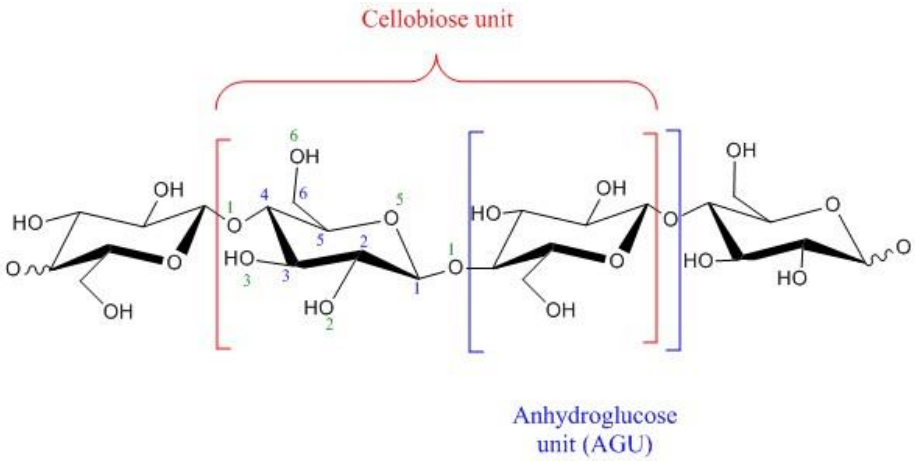


Figure 2.2: Cellulose molecular structure (Adapted from Klemm D. *et al*., 1998; Wertz J. *et al*., 2010)

In the AGU, a primary hydroxyl group is present at C-6 position and secondary hydroxyl groups at C-2 and C-3 positions (Klemm D. *et al*., 1998; Olsson C. and Westman G., 2013). These hydroxyl groups play an important role in cellulose dissolution (discussed in a later section). The oxygen atom of the glycosidic bond is known as O1, oxygen atoms of the primary and secondary hydroxyl are known as O6, O2 and O3 respectively. The last oxygen in the ring is given O5 (Wertz J. *et al*., 2010).

The composition of carbon, hydrogen and oxygen in cellulose is 44.44 %, 6.17 % and 49.39 % respectively. This gives cellulose the chemical formula $(C_6H_{10}O_5)_n$, where n represents the degree of polymerization (DP), i.e. the number of repeating units (Chen H., 2014). The average molecular mass can be calculated by multiplying the DP by the molecular mass of the AGU (Klemm D. *et al*., 1998). The DP can vary based on the origin and the pre-treatment method used for processing (Klemm D. *et al*., 1998; Klemm D. *et al*., 2005; Wertz J. *et al*., 2010; Olsson C. and Westman G., 2013). Therefore, all these factors can affect the

amount of cellulose that can be dissolved and the dissolution conditions that are needed.

Intramolecular hydrogen bonds in native crystalline cellulose are present between the hydroxyl group at C-2 position and the O6 (in the adjacent AGU), also between the hydroxyl group in C-3 position and the O5 (in the adjacent AGU) (Klemm D. *et al*., 1998). These intramolecular forces are responsible for chain stiffness (Olsson C. and Westman G., 2013) and they are illustrated in Figure 2.3. Due to the presence of hydrogen bonds, the solubility of cellulose in water reduces as the DP approaches 6 and above (Klemm D. *et al*., 1998). This implies that a simple solvent like, water is not suitable for cellulose dissolution and requires special solvent/s to break the intramolecular hydrogen bonding network.

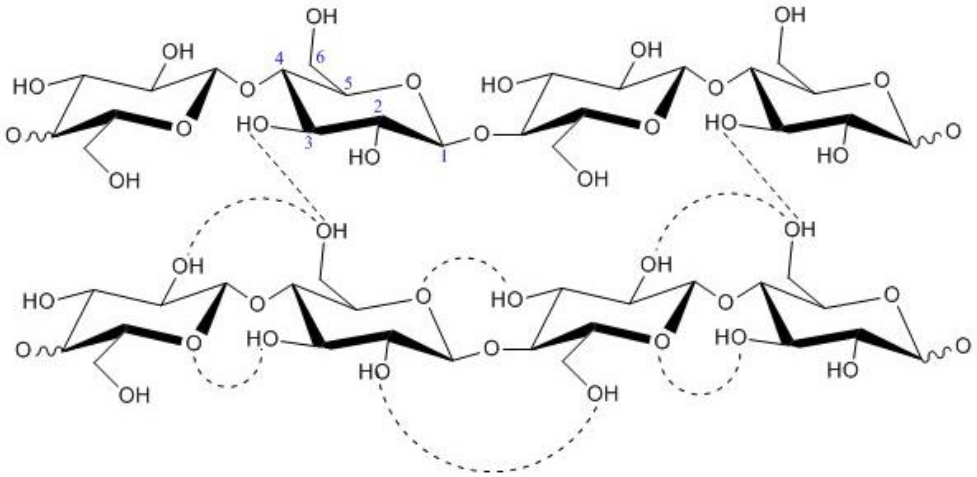


Figure 2.3: Intra- and intermolecular hydrogen bonds in cellulose (Adapted from Klemm D. *et al*., 1998; Pinkert A. *et al*., 2009)

Intermolecular hydrogen bonds are present between the hydroxyl group at C-6 position and O3 in another cellulose chain (Figure 2.3) (Klemm D. *et al*., 1998).

Cellulose is a long polymer with a high DP and a complex hydrogen bonding network, and this presents difficulties to its dissolution (Olsson C. and Westman G., 2013).

The presence of strong intermolecular forces gives rise to the cohesion between cellulose chains (Klemm D. *et al*., 1998; Olsson C. and Westman G., 2013). These cellulose chains then aggregate to form a two-phase model known as the fringed fibril model which was proposed by Hearle in 1958. This consist of crystalline (highly ordered) and amorphous (low order) regions (Hearle J., 1958). A schematic diagram of the fringed fibril model is shown in Figure 2.4. The morphology of different cellulose-based products can be compared against the fringed fibril model to identify the changes in its crystallinity.

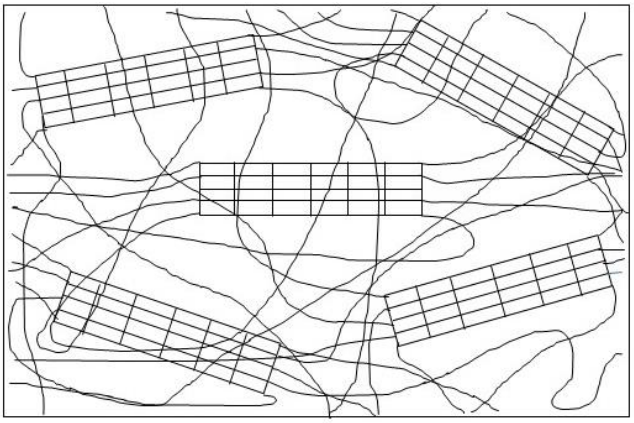


Figure 2.4: Fringed fibril model (Adapted from Hearle J., 1958)

2.2.3 Cellulose Solvents

The polymeric structure present possesses challenges in the dissolution of cellulose. As such, many solvents for cellulose dissolution have been examined

and can be classified into two groups; as derivatising and non-derivatising. Derivatising solvents, dissolve cellulose by reacting to form an unstable ester, ether or acetal derivative (Wertz J. *et al*., 2010) and non-derivatising solvents, dissolve cellulose via intermolecular interactions (Wertz J. *et al*., 2010; Medronho B. and Lindman B., 2014). The dissolution of cellulose in the presence of these solvents generally occur via breaking the intra- and intermolecular hydrogen bonding network in cellulose and a detailed study can be found in Medronho B. and Lindman B., (2014).

The most significant derivatising solvent based industrial system for cellulose dissolution is the viscose process. It uses carbon disulphide and sodium hydroxide to produce rayon fibres, films, castings and sponges (Wertz J. *et al*., 2010). Even though the viscose process is commercialized there are major environmental and safety problems due to the use of carbon disulphide as it is toxic, flammable and explosive (Wertz J. *et al*., 2010; Wang S. *et al*., 2016a). Also, the process requires large quantities of raw materials and despite the raw material recovery in the process, waste (water, alkali acid and exhaust air) is still generated which is an environmental concern. Another disadvantage is the degradation of the cellulose backbone (Wang H. *et al*., 2012).

NMMO (N-methylmorpholine-N-oxide) is the most industrially successful method for the non-derivatising solvent based cellulose dissolution (Olsson C. and Westman G., 2013). The process patented in 1970 by Johnson (Johnson D., 1970) is now industrially used to make textile fibres (*e.g. of brands:* Lyocell,

Tencel, Alceru and Newcell) (Liebert T., 2010; Wertz J. *et al*., 2010). Despite, its ability to dissolve higher cellulose concentrations (up to 23 %) and excellent solvent recovery (between 99.6-99.7 %) (Klemm D. *et al*., 2005; Olsson C. and Westman G., 2013), the major drawbacks of this solvent are poor thermal stability (Olsson C. and Westman G., 2013), fibrillation (fibres undergo local separation in wet conditions and under mechanical stress) which reduces its application (Fang K. *et al*., 2003; Klemm D. *et al*., 2005; Liebert T., 2010; Periyasamy A. and Khanum R., 2012) and side reactions that leads to the formation of by-products (e.g. morpholine and *N*-methylmorpholine). Some problems associated with these side reactions and by-products include; cellulose degradation, fibre staining and reduced fibre performance (Rosenau T. *et al*., 2001).

Several detailed studies have been conducted by Heinze T. and Koschella A., (2005), Liebert T., (2010), Wertz J. *et al*., (2010), Olsson C. and Westman G., (2013), Medronho B. and Lindman B., (2014) and Wang S. *et al*., (2016a) on other derivatising and non-derivatising cellulose solvents. Some of the most common non-derivatising solvents used for cellulose dissolution along with their drawbacks that limits their application are summarised in Table 2.2.

Table 2.2: Summary of non-derivatising solvents used to dissolve cellulose

Solvent Type	Examples	Disadvantages
Aqueous inorganic metal complexes	Cuam - $[Cu(NH_3)_4][OH]_2$ Nitren - $[Ni(NH_2CH_2CH_2)_3N][OH]_2$ Pden – $[Pb(NH_2(CH_2)_2NH_2)][OH]_2$	• Some metal complexes are coloured and not suitable for analytical applications (*e.g.* light scattering) (Saalwächter K. *et al*., 2000). • Cupro process which uses the metal complex cuam is commercialized at a high expense (Wang S. *et al*., 2016a).
Aqueous bases	$NaOH/H_2O$ NaOH/Urea NaOH/Poly(ethylene glycol)	• $NaOH/H_2O$ - solubility is limited to cellulose with low crystallinity and DP and this solvent does not fully destroy the semicrystalline regions in cellulose (Liebert T., 2010; Medronho B. and Lindman B., 2014). • NaOH/Urea - solubility dependent on dissolution temperature, cellulose molecular weight and crystallinity (Qi H. *et al*., 2008a). • Solvent systems involving NaOH and other additives means that additives need to be recovered and reused (Olsson C. and Westman G., 2013).
N,N-dimethylacetamide/Lithium chloride (DMAc/LiCl)		• Difficult to recycle the expensive solvent as it has a low volatility (Liebert T., 2010; Wang S. *et al*., 2016a). • DMAc/LiCl/cellulose system needs to be distilled to remove water as it can reduce cellulose solubility and this requires time and solvent (Olsson C. and Westman G., 2013; Wang S. *et al*., 2016a).

Solvent Type	Examples	Disadvantages
Tetra butyl ammonium fluoride/Dimethyl sulfoxide (TBAF/DMSO)		• TBAF is hygroscopic, the control of water in the solvent mixture is critical (Sharma R. and Fry J., 1983; Olsson C. and Westman G., 2013). • Removal of water from the DMSO/TBAF.$3H_2O$ leads to the formation of FHF^- ions which make cellulose insoluble in the presence of DMSO (Sharma R. and Fry J., 1983; Liebert T., 2010).

Due to the disadvantages associated with the traditional solvents and the increasing drive to shift to environmentally friendly and sustainable systems means that alternative solvents for cellulose dissolution must be considered.

2.3 Keratin

2.3.1 Introduction to Keratin

Protein can be found in animals, plants and bacteria (Silva N. *et al*., 2014). Keratin is a type of a protein that can be sourced from the skin, hair, horns, nails, beaks and teeth of different mammals, reptiles, birds and fish (McKittrick J. *et al*., 2012). A detailed list of keratin sources can be found in McKittrick J. *et al*., (2012).

Depending on the sulphur content, keratin can be categorised as either hard or soft keratin. Hard keratins, like wool have high sulphur content and therefore more covalent (disulphide) crosslinks (Simpson W. and Crawshaw G., 2002; Zoccola M. *et al*., 2009; McKittrick J. *et al*., 2012). The term 'wool' is often used to define animal hair that can be obtained from different breeds of domestic sheep, cashmere and angora goats, camels, yak hair etc. (Simpson W. and Crawshaw G., 2002). Soft keratins can be found in the outer layer of the skin and have low sulphur content and therefore less covalent (disulphide) crosslinks (Zoccola M. *et al*., 2009; McKittrick J. *et al*., 2012).

Different studies have summarised applications of keratin-based materials; these include biomedical (Rouse J. and Van Dyke M., 2010; Silva N. *et al*., 2014; Sharma S. and Gupta A., 2016) and cosmetic applications, as a fertilizer, a flame retardant (Sharma S. and Gupta A., 2016), in leather and textile industries (Lewis D. and Rippon J., 2013; Sharma S. and Gupta A., 2016) and many more. As a natural fibre wool is biodegradable and widely used commercially (*e.g.* textile industry) (Lewis D. and Rippon J., 2013). Therefore, wool was selected for this research.

2.3.2 Keratin Structure

Protein are polymers of α-amino acids, which are made up of a central α-carbon attached to a carboxylic acid group (COOH), an amino group (NH_2), a hydrogen atom (H) and a side chain (R) (Figure 2.5). The side chains (R) differ in terms of size and chemical nature with 20 common types of amino acids (Gunton J. *et al*., 2007; Lewis D. and Rippon J., 2013; Voet D. *et al*., 2016). A summary of different amino acid compositions in wool can be found in Lewis D. and Rippon J. (2013) and Zoccola M. *et al*., (2009).

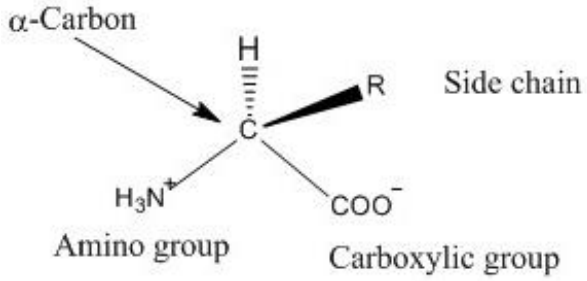


Figure 2.5: α -Amino acid structure (Adapted from Voet D. *et al*., 2016)

Protein formation occurs via condensation of two amino acids to form a dipeptide bond. This reaction is shown in Figure 2.6, where the carbon atom in the carboxyl group of one amino acid and the nitrogen atom in the amino group of another amino acid are bonded by eliminating a water molecule. When a large number of amino acids combine together like this, they form a protein, which is also known as a polypeptide (Gunton J. *et al*., 2007; Lewis D. and Rippon J., 2013 Voet D. *et al*., 2016). Such structures can be considered as polyamides (Lewis D. and J. Rippon, 2013; Silva N. *et al*., 2014). Due to the incorporation of different amino acids, polypeptides can have different compositions and form a wide variety of proteins (Gunton J. *et al*., 2007).

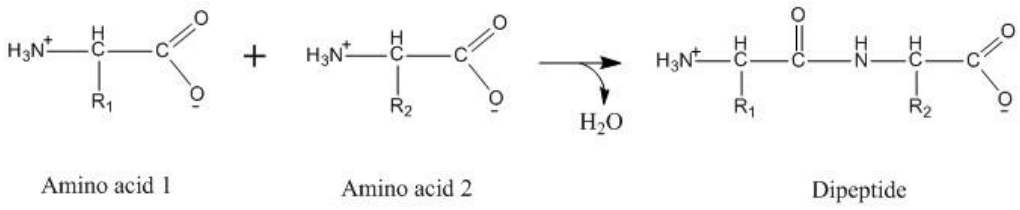


Figure 2.6: Peptide bond formation (Adapted from Voet D. *et al*., 2016)

Protein structure can be explained at four different levels; primary, secondary, tertiary and quaternary. The sequence of the monomer units (amino acids) in the protein is referred to the primary structure (Gunton J. *et al*., 2007; Voet D. *et al*., 2016). This sequence has directionality and is conventionally referred to form the *N*-terminus (terminal ammonium group) to the *C*-terminus (terminal carboxylate group), following the polymerisation direction carried out in natural living systems (Voet D. *et al*., 2016).

The conformation of the primary structure (peptide backbone) gives rise to two different secondary structures namely; α-helices and β-sheets which are held together by hydrogen bonds. As shown in Figure 2.7, α-helix is a helical structure with hydrogen bonds formed between the H atom in N-H group and the O atom in the C=O group. This gives rise to two hydrogen bonds per peptide link maxing it very stable (Gunton J. *et al*., 2007; Voet D. *et al*., 2016).

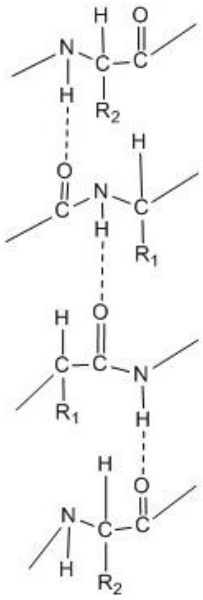


Figure 2.7: Secondary protein structure: α-helix (Adapted from Gunton J. *et al*., 2007; Voet D. *et al*., 2016)

The second most common secondary structure the β-sheet (Figure 2.8) is formed between two polypeptide chains which are linked side by side in a parallel manner. Here the N-H and C=O bonds are at right angles to the peptide backbone and keep alternating (upwards and downwards) (Gunton J. *et al*., 2007; Voet D. *et al*., 2016). Wool polypeptide consists of α-helices (Zoccola M. *et al*., 2009; McKittrick J. *et al*., 2012; Lewis D. and Rippon J., 2013) but can convert to a β-sheet form when stretched (Cao J., 2000; Cao J., 2002).

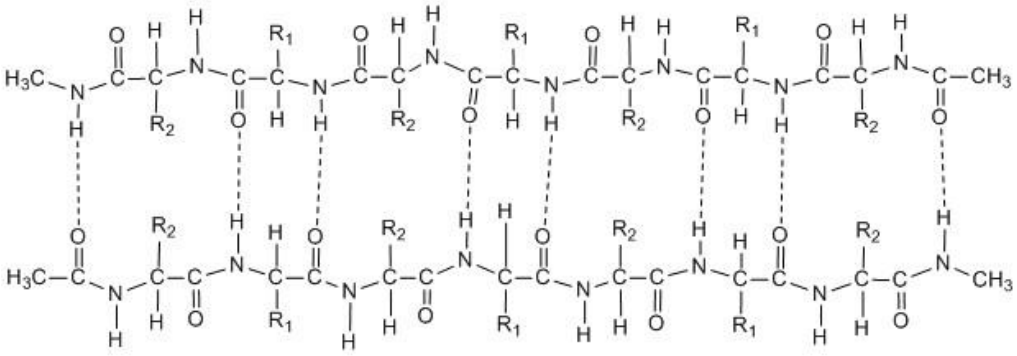


Figure 2.8: Secondary protein structure: β-sheet (Adapted from Gunton J. *et al*., 2007; Voet D. *et al*., 2016)

The tertiary structure is the 3D arrangement of peptide backbone depending on the side chain (Gunton J. *et al*., 2007). Based on the type of the side chain attached to the amino acid, the peptide backbone can have covalent crosslinks and non-covalent bonds/interactions (Darby N. and Creighton T., 1993; Lewis D. and Rippon J., 2013) that are responsible for protein folding (Gunton J. *et al*., 2007). Non-covalent bonds/interactions can be further sub-divided into hydrogen bonds, ionic bonds/electrostatic interactions, hydrophobic interactions and van der Waals interactions (Darby N. and Creighton T., 1993; Lewis D. and Rippon J., 2013). These covalent crosslinks and non-covalent bonds/interactions can exist within the same chain (intra-chain) and between two polypeptide chains (inter-chain) (Lewis D. and Rippon J., 2013), providing structuring for the protein (Figures 2.9 and 2.10).

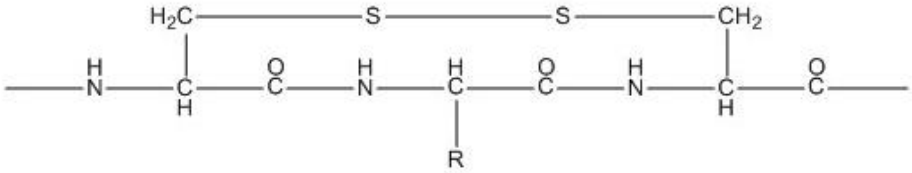


Figure 2.9: Intra-chain crosslinks in wool (Adapted from Lewis D. and Rippon J., 2013)

In the final level (quaternary), several polypeptides combine to make a large macromolecule (Gunton J. *et al*., 2007). The complicated protein structure that is present in keratin provides challenges for its dissolution.

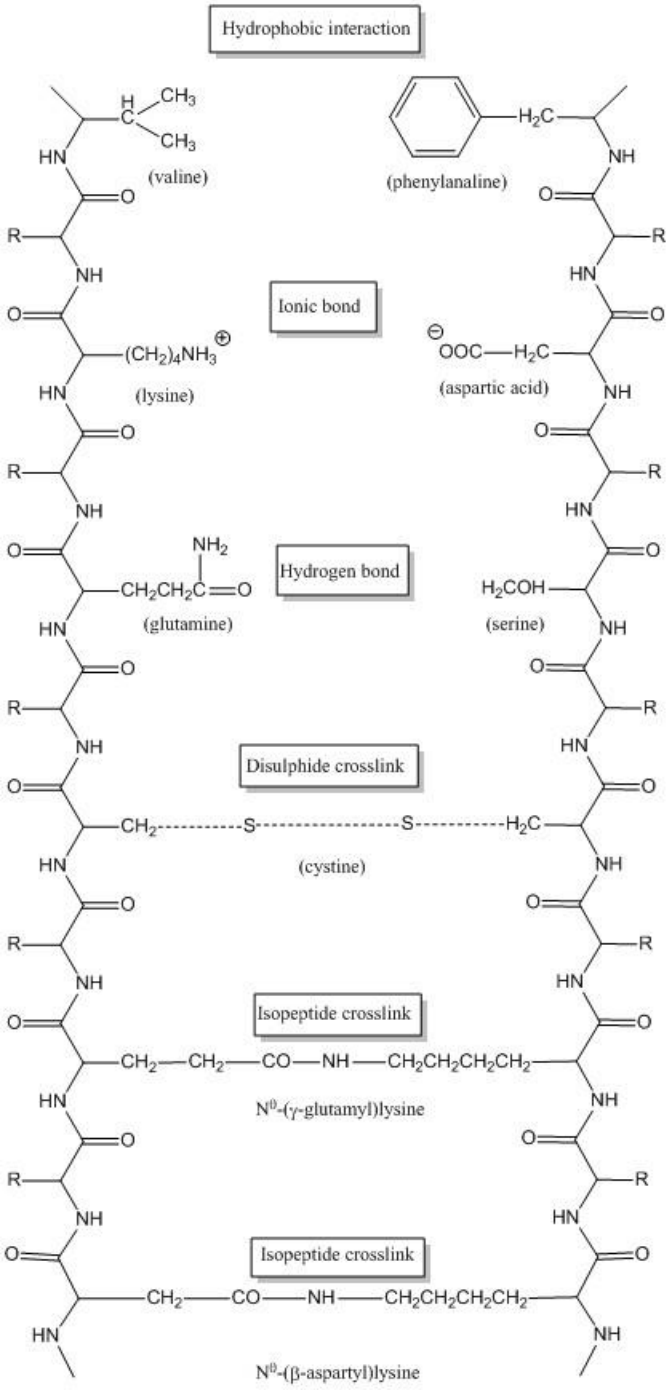


Figure 2.10: Inter-chain crosslinks in wool (Adapted from Lewis D. and Rippon J., 2013)

2.3.3 Keratin Solvents

Mixtures of different solvents, where each solvent plays a key role in breaking covalent and/or non-covalent bonds, have been generally required for keratin dissolution (Xie H. *et al*., 2005). In addition, cleavage of either the disulphide crosslinks or peptide backbone is often carried out to make dissolution more tractable, for example by oxidation of disulphide crosslinks using peroxide (Poole A. *et al*., 2009), reduction of disulphide crosslinks using a mixture of thiol (2-mercaptoethanol) and urea (Maclaren J. , 1962; Yamauchi K. *et al*., 1996; Schrooyen P. *et al*., 2000; Schrooyen P. *et al*., 2001) or sodium sulphide (Poole A. *et al*., 2011), sulfitolysis, where the disulphide crosslinks are broken by sulfite (Poole A. *et al*., 2009), the Shindai method using tris-hydrochloric acid, urea, thiourea and 2-mercaptoethanol (Fujii T. and Li D., 2008; Wong S. *et al*., 2016), alkali hydrolysis using sodium hydroxide (Nagai Y. and Nishikawa T., 1970; Tsuda Y. and Nomura Y., 2014) and a combination of enzyme and alkaline technology (Dalev P., 1994). Some of the physiochemical methods include; high density steam flash-explosion (Zhao W. *et al*., 2012), using superheated water (Yin J. *et al*., 2007) and hydrothermal treatment (Lamoolphak W. *et al*., 2008).

Even though, 2-mercaptoethanol and urea are widely used to break the crosslinks without damaging the protein backbone and gives a high yield, these solvents are expensive, limiting their application in industry and reduction using sodium sulphide is a complicated process (Poole A. *et al*., 2009; Poole A. *et al*., 2011). The chemicals used for most of the chemical methods listed above (*e.g.* sulfite, thiol and peroxide) are often toxic and difficult to use and

physicochemical methods require rigorous reaction conditions (*e.g*. pressure and temperature) (Zhao W. *et al*., 2012). Some other disadvantages highlighted for these keratin solvents include; volatility, corrosive nature, not environmentally friendly, difficulty to recycle, pollute the environment, not renewable, multi-step process and keratin degradation leading to regenerated keratin with a lower value (Hameed N. and Guo Q., 2009; Idris A. *et al*., 2013; Ji Y. *et al*., 2014; Zheng S. *et al*., 2015; Liu X. *et al*., 2017; Zhang Z. *et al*., 2017a). Similar to cellulose solvents, there is a growing demand to develop new solvents for keratin dissolution which are able to overcome the disadvantages associated with the traditional/existing solvents.

2.4 Ionic Liquids

The discovery of ionic liquids dates back to the 19th century where, a 'red oil' was formed as a by-product during Friedel-Crafts reaction, between benzene and chloromethane in the presence of a catalyst (aluminium chloride) to form toluene. It was after the discovery of nuclear magnetic resonance spectroscopy (in mid-19th century), the structure of this red oil was discovered as a salt (Wilkes J., 2002). In 1888 Gabriel, synthesized an ammonium based ionic liquid ethanolammonium nitrate, with a melting point of 52 to 55 °C (Zhao S. *et al*., 2013). The first room temperature ionic liquid, ethylammonium nitrate was synthesized by Walden in 1914 (Wilkes J., 2002; Zhao S. *et al*., 2013; Welton T., 2018).

Ionic liquids are defined as liquids that consist of ions and have a melting point/glass transition temperature less than 100 °C (Wilkes J., 2002; Pinkert A. *et al*., 2009; Freemantle M., 2010). The term 'room-temperature ionic liquids' is used to define ionic liquids that exist as a liquid either at or around room temperature and often consisting of either a large nitrogen or phosphorus based organic cation attached to linear alkyl chains and either an organic or inorganic anion (Wilkes J., 2002; Marsh K. *et al*., 2004; Freemantle M., 2010). Several different synonyms and abbreviations have been used in literature to define these salts (Freemantle M., 2010; Hallett J. and Welton T., 2011). Ionic liquids with different properties (chemical, physical and biological) can be designed by changing the cation/anion, incorporating specific features to the cation/anion and by mixing simple ionic liquids (Freemantle M., 2010). Some of the common cations and anions used in literature are shown in Figure 2.11.

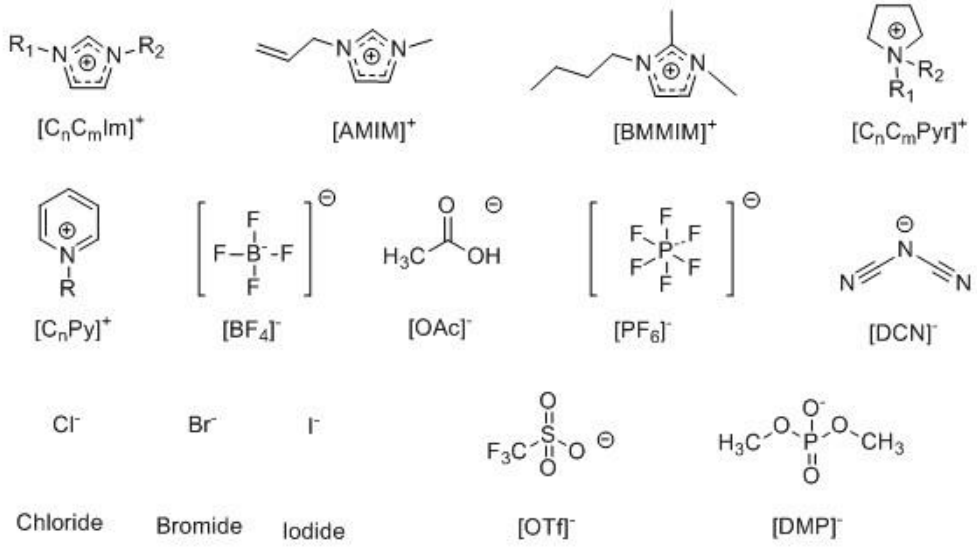


Figure 2.11: Common anions and cations used in ionic liquids

Ionic liquids have been used and proposed for a diverse range of applications. Some of these include; separation and extraction (gas separation, metal extraction, membranes), for biological applications (antimicrobial agent, drug delivery) (Freemantle M., 2010; Patel D. and Lee J., 2012), electrochemical applications (batteries, fuel cells, solar cells) (Freemantle M., 2010; Patel D. and Lee J., 2012, Watanabe M. *et al*., 2017), as a catalyst (Freemantle M., 2010; Oliver-Bourbigou H. *et al*., 2010), as a solvent and electrolyte in analytical applications (chromatography, gas sensors, spectroscopy), as a lubricant (Freemantle M., 2010) and to dissolve different carbohydrates (Freemantle M., 2010; Oliver-Bourbigou H. *et al*., 2010; Patel D. and Lee J., 2012). Ionic liquids are also able to dissolve a variety of organic and inorganic gases, liquids and solids (Freemantle M., 2010). Examples of other commercial and pilot scale applications of ionic liquids are summarised by Freemantle M., (2010) and Oliver-Bourbigou H. *et al*., (2010).

According to Ranke and his co-workers' ionic liquids are classified as 'green solvents' because they have;

- *Negligible vapour pressure* - therefore they don't evaporate at ambient temperatures and pressures, and results in no air pollution and health issues (Ranke J. *et al*., 2007; Pinkert A. *et al*., 2009; Freemantle M., 2010).
- *Non-flammable* - therefore fast, exothermic oxidations can be reduced significantly in an accident (Ranke J. *et al*., 2007).
- *Non-toxic* - ionic liquids are generally considered non-toxic (Ranke J. *et al*., 2007).

Detailed studies on the 'greenness' of ionic liquids can be found in Ranke J. *et al*., (2007) and Wang H. *et al*., (2012). Even though the term 'green solvent' has been used to define ionic liquids, this has lately been challenged (Ranke J. *et al*., 2007; Freemantle M., 2010). Nevertheless, utilizing ionic liquids reduce the impact to the environment as they have a higher product yield leading to lower wastage, reactions can be conducted easily, recyclability of the ionic liquid which lowers process cost and increased reaction rates which improves the energy efficiency of the process (Earle M. and Seddon K., 2010; Freemantle M., 2010).

Another important property of ionic liquids that makes them a suitable solvent to replace traditional solvents for biopolymer dissolution is their high thermal stability (300 to 400 °C), which means higher temperatures can be used to conduct experiments and the ionic liquid does not degrade (Pinkert A. *et al*., 2009; Freemantle M., 2010). Therefore, these properties have attracted the use of ionic liquids to dissolve different biopolymers.

2.5 Dissolution Mechanism

Ionic liquids have gained increased attention as a solvent for biopolymer dissolution due to its unique properties discussed above. A brief review on some of the existing theories and studies that have been conducted on the cellulose and keratin dissolution mechanism in the presence of ionic liquids is provided below.

2.5.1 Cellulose

NMR studies (Remsing R. *et al*., 2006; Remsing R. *et al*., 2008; Youngs T. *et al*., 2011) and simulation studies (Novoselov N. *et al*., 2007; Liu H. *et al*., 2010; Youngs T. *et al*., 2011) have confirmed that the solvation is governed by the interaction and formation of hydrogen bonds between the ionic liquid anion and the cellulose hydroxyl group hydrogen atom. This solvation mechanism does not change with the anion structure (Remsing R. *et al*., 2008).

Other studies conducted by Youngs T. *et al*., (2007), Zhang J. *et al*., (2010), El Seoud O. *et al*., (2011), Liu Z. *et al*., (2011) and Lu B. *et al*., (2014a) have proposed a different dissolution mechanism where the ionic liquid anion and cation both participates. According to Lu B. *et al*., (2014a), hydrogen bonds are formed between the ionic liquid anion (oxygen atom) and the cellulose hydroxyl group hydrogen atoms at C-3 and C-6 positions breaking the intra- and intermolecular hydrogen bonds. The intramolecular hydrogen bonds in cellulose are further broken by the interaction of the acidic protons of the imidazolium cation (H2) with the cellulose oxygen at C-2 position and the ether oxygen atom at O5.

Rabideau B. *et al*., (2013), used a molecular dynamics simulation study to investigate the dissolution mechanism of small bundles of cellulose in different ionic liquids. They reported that the anion forms bonds with the exterior hydroxyl groups in cellulose resulting in negatively charged ions and loosening

the intramolecular interactions present in cellulose. Cations then associate with these ions by pushing them apart and facilitating cellulose dissolution.

The dissolution mechanism proposed by Sashina E. and Novoselov N. (2009), for imidazolium based ionic liquids was somewhat different (Figure 2.12). Here the ionic liquid anion forms hydrogen bonds with the cellulose hydroxyl group. However, the anion still maintains its bond with the cation and the cation does not interact directly with the cellulose hydroxyl group due to steric hindrance.

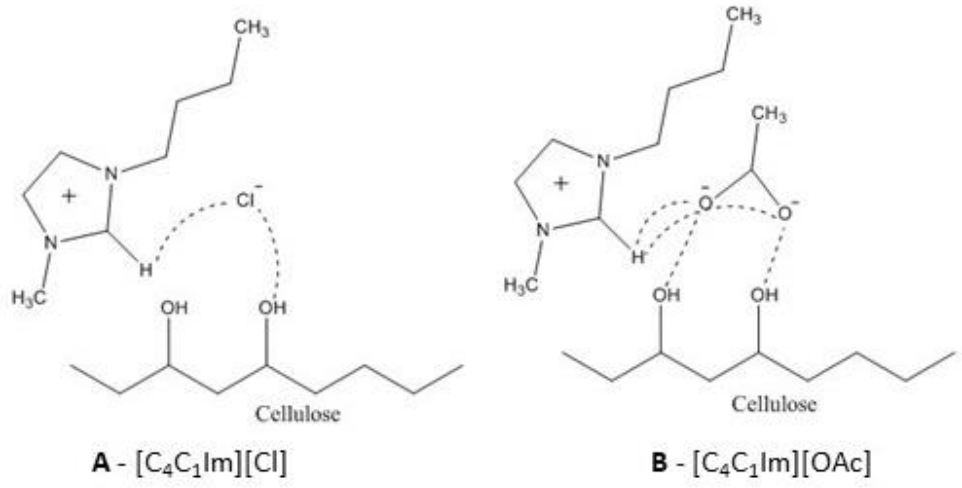


Figure 2.12: Cellulose dissolution mechanism in ionic liquids (Adapted from Sashina E. and Novoselov N., 2009)

Factors like the cation chain length can affect the cellulose dissolution (Sashina E. and Novoselov N., 2009). Zhang H. *et al*., (2005), stated that the interaction between the cellulose hydroxyl oxygen atom and the cation [AMIM] was due to its smaller size and the presence of a small electronic chemical structure due to the alkyl group. Another study involving [C_2C_1Im], concluded that steric hindrance can be overcome through the association at the most acidic H2 proton (Zhang J. *et al*., 2010). According to Novoselov N. *et al*., (2007), cations

like [C_4C_1Im] does not form bonds with the hydroxyl group oxygen atom due to steric hindrance.

Different conclusions have been made regarding the interaction and bonds formed between the ionic liquid cation and cellulose. These include weak van der Waals interactions (Youngs T. *et al*., 2007), hydrophobic interactions (Liu H. *et al*., 2010), covalent bonds (Heinze T. *et al*., 2008). According to Remsing R. *et al*., (2008) and Youngs T. *et al*., (2011), the role of the cation was not significant in cellulose solvation. It is evident that the cation plays an important role in cellulose dissolution. However, the presence of contradicting and different theories does not help to reach a conclusion. Therefore, more research has to be conducted on this matter (Wang H. *et al*., 2012; Zhang J. *et al*., 2017b).

2.5.2 Keratin

Keratin fibre is composed of an outer layer (cuticle) and an inner layer (cortex). The dissolution process starts with the swelling of the cuticle followed by the cortex. Then the cortex becomes transparent indicating the loss of its crystallinity. Cuticle takes longer to dissolve due to the high amount of disulphide bonds present (Chen J. *et al*., 2014). According to Wang M. *et al*., (2014) for imidazolium cation and chloride anion based ionic liquids the combined effect of the anion and cation was responsible for breaking the covalent and non-covalent interactions in keratin.

2.6 Current Literature on Cellulose and Keratin Dissolution using Ionic Liquids

The first use of ionic liquids in cellulose dissolution was reported in 1934, where N-alkylpyridinium salt was used (Graenacher C., 1934). Then in 2002, Swatloski and co-workers used 1-butyl-3-methylimidazolium acetate ([C_4C_1Im]) cation based ionic liquids as a non-derivatising solvent for cellulose dissolution (Swatloski R. *et al*., 2002). Since then, a large number of studies and reviews have been conducted on cellulose dissolution using ionic liquids (Pinkert A. *et al*., 2009; Mäki-Arvela P. *et al*., 2010; Oliver-Bourbigou H. *et al*., 2010; Meng Z. *et al.,* 2012; Wang H. *et al*., 2012; Brandt A. *et al*., 2013; Badgujar K. and Bhanage B., 2015).

Keratin dissolution using ionic liquids is still at a very early stage and only few studies have been published. An imidazolium cation coupled with a chloride-based anion has been commonly used in literature to dissolve different types of keratin (Xie H. *et al*., 2005; Hameed N. and Guo Q., 2009; Sun *et al*., 2009; Hameed N. and Guo Q., 2010; Idris A. *et al*., 2013; Li R. and Wang D., 2013; Ji Y. *et al*., 2014; Wang M. *et al*., 2014; Zheng S. *et al*., 2015).

The amount of biopolymer that can be dissolved in an ionic liquid cannot be described based on a single parameter but the combined effect of a wide range of properties need be considered. These include; type of anion and cation, properties of the ionic liquid (*e.g.* hydrogen bond basicity, hygroscopicity and viscosity), dissolution conditions (*e.g.* mixing and heating) and the type and

source of the biopolymer. This section will briefly review some of the existing literature based on these factors.

In terms of the anion; [Cl] (Swatloski R. *et al*., 2002), [OFo] (Fukaya Y. *et al*., 2006), [(MeO)(R)PO_2] (where R = H, Me and MeO) (Fukaya Y. *et al*., 2008) and [OAc] (Xu A. *et al*., 2010), have high hydrogen bond accepting ability (good basicity) and exhibit excellent cellulose solubility. Low basicity anions like; [$EtSO_4$], [OTf] and [DCA] (Zhao H. *et al*., 2009; Xu A. *et al*., 2010) or large, non-coordination anions like; [PF_6], [BF_4], [SCN] and [Br] (Swatloski R. *et al*., 2002) reduce cellulose solubility. Nevertheless, this does not mean all ionic liquids with a good basicity anion are able to dissolve cellulose. The type of cation also influences cellulose solubility (Mäki-Arvela P. *et al*., 2010). Similar results were reported for keratin where solubility reduced when a large, non-coordinating anion (Xie H. *et al*., 2005; Wang M. *et al*., 2014; Zheng S. *et al*., 2015; Wang L. *et al*., 2016b) or an anion with a low hydrogen ion accepting ability (Ji Y. *et al*., 2014) was used.

Even though, chloride-based ionic liquids exhibited good cellulose and keratin solubility (Tables 2.3 and 2.4), they are difficult to use as they exist as solids at room temperature, having high melting points (Fukaya Y. *et al*., 2006; Zhao H. *et al*., 2008; Vitz J. *et al*., 2009) and needs to be heated above their melting point, which requires input of energy. In addition, these ionic liquids are hygroscopic (Zhao H. *et al*., 2008; Vitz J. *et al*., 2009) and forms highly viscous solutions (Vitz J. *et al*., 2009; Zavrel M. *et al*., 2009). Some chloride based ionic

liquids ([C_4C_1Im][Cl]) have shown a higher tendency to cellulose degradation (Vitz J. *et al*., 2009) and became thicker or formed a crystalline solid when cooled down to room temperature (Swatloski R. *et al*., 2002; Vitz J. *et al*., 2009).

Dissolution studies conducted by Vitz J. *et al*., (2009), observed cellulose degradation in acetate based ionic liquids ([C_2C_1Im][OAc] and [C_4C_1Im][OAc]) by a colour change. Overall, ionic liquids based on formate [OFo] and acetate [OAc] coupled with a good cation have been identified as suitable solvents for cellulose (Mäki-Arvela P. *et al*., 2010) and keratin (Chen J. *et al*., 2014; Zheng S. *et al*., 2015) dissolution.

An odd-even effect on cellulose solubility was observed for imidazolium cation based ionic liquids with chloride as the anion (up to 6 carbon units), where even numbered, short chain cations having higher cellulose dissolution (Erdmenger T. *et al*., 2007; Vitz J. *et al*., 2009). It is not clear the reason behind this behaviour (Erdmenger T. *et al*., 2007) but, lower cellulose solubility as the number of carbon units increase (6 and 8 carbon units) has been explained due to the overall reduction in chloride concentration (Swatloski R. *et al*., 2002). However, for imidazolium cation based ionic liquid with even numbered carbon units, the cation chain length had minimum effect on keratin dissolution (Zheng S. *et al*., 2015).

Ionic liquids based on cations like imidazolium, pyridinium and allyl have shown excellent biopolymer solubility. Higher cellulose solubility in aromatic based

ionic liquids (*e.g.* imidazolium and pyridinium) was due to the lower electrostatic strength between the cation and anion due to charge delocalization in the aromatic ring (Fernandes A. *et al*., 2011) enabling the anion to freely form hydrogen bonds with cellulose (Wang H. *et al*., 2012).

As outlined in the dissolution mechanism the cation chain length can also influence the biopolymer solubility in ionic liquid. A large cation introduces steric hindrance making it difficult for the cation to interact with the cellulose hydroxyl oxygen atoms (Kosan B. *et al*., 2008; Lu B. *et al*., 2014a) and thereby reduce the number of hydrogen bonds formed between cellulose and the cation and reduce cellulose solubility (Zhao H. *et al*., 2008). For keratin, ionic liquids with a long cation chain length makes it difficult to penetrate into the keratin structure (Idris A. *et al*., 2013).

As shown in Figure 2.13, [AMIM] cation has a smaller size compared to [C_4C_1Im] cation. This is because [AMIM] has three carbon atoms and a double bond attached to the nitrogen compared to four carbon atoms in [C_4C_1Im]. Therefore, [AMIM] cation based ionic liquid showed higher cellulose (Zhang H. *et al.,* 2005) and keratin (Li R. and Wang D., 2013; Wang M. *et al*., 2014) solubility. A similar behaviour was observed between [C_2C_1Im] and [C_4C_1Im] cation based ionic liquids, where solubility decreased with increasing cation size (Kosan B. *et al*., 2008; Zavrel M. *et al*., 2009; Liu Z. *et al*., 2011). However, these results contradict some studies conducted on cellulose (Barthel S. and Heinze T., 2006; Erdmenger T. *et al*., 2007; Vitz J. *et al*., 2009) and keratin

solubility (Idris A. *et al*., 2013; Ji Y. *et al*., 2014). This is because the biopolymer solubility did not decrease when the cation chain length was increased.

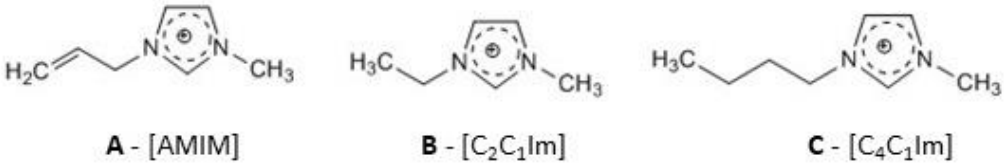


Figure 2.13: Cation structure for imidazolium based ionic liquids

Side chains attached to the cation (like a hydroxyl group), can reduce cellulose (Zhao H. *et al*., 2008; Lu B. *et al*., 2014a) and keratin (Zheng S. *et al*., 2015) solubility by forming hydrogen bonds with the anion. Therefore, Lu B. *et al*., (2014a) proposed for efficient cellulose dissolution a cation having acidic protons, the absence of a highly electronegative atom (*e.g.* oxygen or nitrogen) or a bulk group is recommended. In conclusion, when selecting a suitable ionic liquid for biopolymer dissolution the type of cation and anion must be carefully selected to achieve higher dissolutions.

Kamlet-Taft model has been commonly used to determine the solvation properties of ionic liquids (Badgujar K. and Bhanage B., 2015). A UV-vis spectrometer is used in the presence of different dyes to determine the Kamlet-Taft parameters: hydrogen bond donating ability-acidity (α), hydrogen bond accepting ability-basicity (β) and dipolarity/polarizability effects (π^*) (Kamlet M. and Taft R., 1976; Taft R. and Kamlet M., 1976; Crowhurst L. *et al*., 2003).

Dried cellulose has a hydrogen bond basicity of 0.60 (Spange S. *et al*., 1998). According to Badgujar K. and Bhanage B., (2015), ionic liquids having a hydrogen bond basicity of 0.82 or more are considered as good cellulose solvents. Imidazolium cation based ionic liquids with anions like [BF_4] (β = 0.376), [PF_6] (β = 0.207), [OTf] (β = 0.464) and [DCA] (β = 0.621) have a very low hydrogen bond basicity (Crowhurst L. *et al*., 2003; Xu A. *et al*., 2010), and this explains their poor cellulose solubility (Swatloski R. *et al*., 2002; Zhao H. *et al*., 2009; Xu A. *et al*., 2010). According to Xu A. *et al*., (2010), higher cellulose solubility in [C_4C_1Im] [OAc] was due to its high hydrogen bond basicity (1.161). They also found a linear relationship between hydrogen bond basicity and cellulose solubility, where solubility increased with hydrogen bond basicity. Similar results on higher cellulose and keratin solubility in ionic liquids with high hydrogen bond basicity was reported by Fukaya Y. *et al*., (2006), Fukaya Y. *et al*., (2008), Zhang J. *et al*., (2010) and Liu X. *et al*., (2017). However, only hydrogen bond basicity cannot be used to select a suitable ionic liquid-based solvent for biopolymer dissolution. Other Kamlet-Taft parameters (Liu X. *et al*., 2017) and ionic liquid viscosity (Fukaya Y. *et al*., 2008) can sometimes supersede the hydrogen bond basicity.

In terms of the ionic liquid properties, hygroscopic ionic liquids reduce cellulose and keratin solubility as it introduces competition for hydrogen bonds (Swatloski R. *et al*., 2002; Vitz J. *et al*., 2009; Zhang Z. *et al*., 2017a). When the ionic liquid viscosity is low, it is able to dissolve higher quantities of cellulose and keratin at a lower temperature (Fukaya Y. *et al*., 2006; Fukaya Y. *et al*.,

2008; Idris A. *et al*., 2013) as it enhances cellulose dispersion (Fukaya Y. *et al*., 2008) and ion mobility (Pinkert A. *et al*., 2009; Ghosh A. *et al*., 2014). Another advantage of low viscosity ionic liquid is that, they are easy to use (Wang H. *et al*., 2012). Ionic liquid viscosity can be reduced by using smaller ionic size (Fukaya Y. *et al*., 2006; Fukaya Y. *et al*., 2008), presence of water and heating (Vitz J. *et al*., 2009; Zhang Z. *et al*., 2017a). However, the amount of water has to be maintained at an optimum level in order to reduce recycling cost and dissolution time (Zhang Z. *et al*., 2017a).

Other than the type of ionic liquid used and its properties, dissolution conditions can also play a major role in cellulose and keratin solubility. Mixing increases cellulose solubility (Zhang H. *et al*., 2005; Zavrel M. *et al*., 2009) as it enhances mass transfer (Zavrel M. *et al*., 2009). High-power ultrasound was also able to dissolve cellulose much faster compared to conventional heating as the system temperature can reach up to 150 °C (Mikkola J. *et al*., 2007). Microwave heating has also proven to increase cellulose solubility. However, cellulose tend to degrade (Swatloski R. *et al*., 2002; Vitz J. *et al*., 2009; Wang H. *et al*., 2012), because microwave, heating happens much quicker and ionic liquids are highly effective at absorbing microwave radiation, potentially leading to explosions if the container is sealed (Wang H. *et al*., 2012) due to pressure build up.

The temperature dependence off cellulose and keratin solubility has been investigated by Swatloski R. *et al*., (2002), Xie H. *et al*., (2005), Zhang H. *et al*., (2005), Fukaya Y. *et al*., (2006), Fukaya Y. *et al*., (2008), Zavrel M. *et al*., (2009);

Xu A. *et al*., (2010), Liu Z. *et al*., (2011); Idris A. *et al*., (2013); Chen J. *et al*., (2014); Lu B. *et al*., (2014a), Wang M. *et al*., (2014) and Wang L. *et al*., (2016b). Generally, cellulose and keratin solubility increase with temperature. This is because at higher temperatures the viscosity of the ionic liquid is reduced and the ion mobility is increased, which enhances mixing and the complex intra- and intermolecular network is disrupted (Zavrel M. *et al*., 2009; Xu A. *et al*., 2010; Ghosh A. *et al*., 2014; Zheng S. *et al*., 2015). However, further increasing the temperature the solution can become dark indicating keratin degradation (Wang L. *et al*., 2016b) and protein modification (Ghosh A. *et al*., 2014). Also, for cellulose it has been reported that degradation (DP was lowered) occurred at higher temperatures (Liu Z. *et al*., 2011).

From the cellulose and keratin dissolution summary shown in Tables 2.3 and 2.4, it can be seen that based on the type and source there can be a significant difference in biopolymer solubility. Other than this particle type and size can also affect the solubility (Badgujar K. and Bhanage B., 2015).

Table 2.3: Summary of cellulose solubility in selected ionic liquids

Ionic Liquid	Cellulose Type	Solubility	Dissolution Conditions	Ionic Liquid Water Content	Reference
$[C_2C_1Im][OAc]$	Cellulose (Linters, DP 795)	16 wt%			Hermanutz F. *et al*., 2008
	Eucalyptus (Eu-569)	19.6 %			Kosan B. *et al*., 2008
	Cellulose (Avicel PH-101)	15 wt%	110 °C		Zhao H. *et al*., 2008
	MCC	15 %	80 °C, 48 hours		Gericke M. *et al*., 2009a
	Cellulose (Avicel PH-101)	8 %	100°C, maximum 1 hour	6762 ppm[a]	Vitz J. *et al*., 2009
	Cellulose	15 wt%	110 °C		Zhao H. *et al*., 2009
	Cotton pulp	16 wt%	90 °C, 7 hours		Liu Z. *et al*., 2011
$[C_4C_1Im][OAc]$	Eucalyptus (Eu-569)	18.9 %			Kosan B. *et al*., 2008
	Cellulose	10 wt%	90 °C		Sashina E. and Novoselov N., 2009
	Cellulose (Avicel PH-101)	12 %	100°C, maximum 1 hour		Vitz J. *et al*., 2009
	MCC	15.5 wt%	70 °C	[b]	Xu A. *et al*., 2010
	Cotton pulp	15 wt%	90 °C, 7 hours		Liu Z. *et al*., 2011
$[Me(OEt)_2\text{-}Et\text{-}Im][OAc]$	Cellulose (Avicel PH-101)	12 wt%	110 °C		Zhao H. *et al*., 2008
$[Me(OEt)_3\text{-}Et\text{-}Im][OAc]$	Cellulose (Avicel PH-101)	12 wt%	110 °C		Zhao H. *et al*., 2008
	Cellulose	12 wt%	110 °C		Zhao H. *et al*., 2009
$[Me(OEt)_4\text{-}Et\text{-}Im][OAc]$	Cellulose (Avicel PH-101)	10 wt%	110 °C		Zhao H. *et al*., 2008
$[Me(OEt)_2\text{-}Et_3N][OAc]$	Cellulose (Avicel PH-101)	10 wt%	110 °C		Zhao H. *et al*., 2008
$[Me(OEt)_3\text{-}Et_3N][OAc]$	Cellulose (Avicel PH-101)	10 wt%	110 °C		Zhao H. *et al*., 2008
	Cellulose	10 wt%	110 °C		Zhao H. *et al*., 2009

Ionic Liquid	Cellulose Type	Solubility	Dissolution Conditions	Ionic Liquid Water Content	Reference
[AMIM][Cl]	MCC (dissolved pulp)	14.5 wt%	80 °C		Zhang H. *et al*., 2005
	MCC (DP=250)	≈ 11 wt%	100 °C	[b]	Fukaya Y. *et al*., 2006
	MCC (Avicel)	27 wt%	Sonicate for 22 minutes		Mikkola J. *et al*., 2007
$[C_2C_1Im][Cl]$	Cellulose (Avicel)	12 %	80 °C, 12 hours		Barthel S. and Heinze T., 2006
	Cellulose (Avicel)	10 wt%	100 °C, 15 minutes		Erdmenger T. *et al*., 2007
	Eucalyptus (Eu-569)	15.8 %			Kosan B. *et al*., 2008
	Cellulose (Avicel PH-101)	10-14 %	100 °C, maximum 1 hour		Vitz J. *et al*., 2009
	Cotton pulp	14 wt%	90 °C, 7 hours		Liu Z. *et al*., 2011
$[C_4C_1Im][Cl]$	Cellulose pulp (DP≈1000)	10 wt%	100 °C		Swatloski R. *et al*., 2002
	Cellulose (Avicel)	18 %	83 °C, 12 hours		Heinze T. *et al*., 2005
	Cellulose (Avicel)	18 %	80 °C, 12 hours		Barthel S. and Heinze T., 2006
	Cellulose (Avicel)	20 wt%	100 °C, 15 minutes		Erdmenger T. *et al*., 2007
	MCC (Avicel)	8 wt%	Sonicate for 10 minutes		Mikkola J. *et al*., 2007
	MCC	13 wt%	100 °C, 24 hours		Kadokawa J. *et al*., 2008
	Eucalyptus (Eu-569)	13.6 %			Kosan B. *et al*., 2008
	Cellulose (Avicel PH-101)	10 wt%	110 °C		Zhao H. *et al*., 2008
	Cellulose pulp	14 %	90 °C	<0.5%[c]	Chen X. *et al*., 2009
	MCC (Avicel PH-101)	10 wt%	80 °C, 24 hours		Gericke M. *et al*., 2009bC
	Cellulose	5 wt%	90 °C		Sashina E. and Novoselov N., 2009
	MCC (Avicel)	10 %	80 °C, 24 hours		Sescousse R. *et al*., 2010

Ionic Liquid	Cellulose Type	Solubility	Dissolution Conditions	Ionic Liquid Water Content	Reference
$[C_4C_1Im][Cl]$	Cotton pulp	13 wt%	90 °C, 7 hours		Liu Z. *et al*., 2011
[BDMIM][Cl]	Eucalyptus (Eu-569)	12.8 %			Kosan B. *et al*., 2008
[AMIM][OFo]	MCC (DP=250)	≈ 22 wt%	85 °C	[b]	Fukaya Y. *et al*., 2006
	α-Cellulose	10 wt%	60 °C, 2 hours	0.2%[c]	Lu F. *et al*., 2014b
$[C_4C_1Im][OFo]$	MCC	12.5 wt%	70 °C	[b]	Xu A. *et al*., 2010
$[Me(OEt)_3\text{-}Et_3N][OFo]$	Cellulose	10 wt%	110 °C		Zhao H. *et al*., 2009
$[C_4C_1Im][HSCH_2COO]$	MCC	13.5 wt%	70 °C	[b]	Xu A. *et al*., 2010
$[C_2C_1Im][(MeO)(H)PO_2]$	MCC (DP=200-250)	10 wt%	45 °C, 30 minutes	[b]	Fukaya Y. *et al*., 2008
$[C_2C_1Im][(MeO)(Me)PO_2]$	MCC (DP=200-250)	10 wt%	55 °C, 30 minutes	[b]	Fukaya Y. *et al*., 2008
$[C_2C_1Im][(MeO)_2PO_2]$	MCC (DP=200-250)	10 wt%	65 °C, 30 minutes	[b]	Fukaya Y. *et al*., 2008
$[C_4C_1Im][(C_6H_5)COO]$	MCC	12 wt%	70 °C	[b]	Xu A. *et al*., 2010
$[C_4C_1Im][H_2NCH_2COO]$	MCC	12 wt%	70 °C	[b]	Xu A. *et al*., 2010
$[C_4C_1Im][HOCH_2COO]$	MCC	10.5 wt%	70 °C	[b]	Xu A. *et al*., 2010
$[C_2C_1Im][Et_2PO_4]$	Cellulose (Avicel PH-101)	12-14 %	100°C, maximum 1 hour	5865 ppm[c]	Vitz J. *et al*., 2009
$[DiMIM][Me_2PO_4]$	Cellulose (Avicel PH-101)	10 %	100°C, maximum 1 hour		Vitz J. *et al*., 2009

[a] - As received from supplier
[b]- Dried ionic liquid
[c]- Synthesized

Table 2.4: Summary of keratin solubility in selected ionic liquids

Ionic Liquid	Keratin Type	Solubility	Dissolution Conditions	Reference
$[C_2C_1Im][DMP]$	Wool keratin	8 wt%	130 °C, 1.5 hours	Zheng S. *et al.*, 2015
	Goat wool	8 wt%	120 °C, 2.5 hours	Liu X. *et al*., 2017
$[C_4C_1Im][DMP]$	Wool keratin	8 wt%	130 °C, 1.5 hours	Zheng S. *et al*., 2015
	Wool	5.0 % [a]	120 °C, N_2, 10.5 hours	Wang L. *et al*., 2016b
[DBNM][DMP]	Goat wool	8 wt%	120 °C, 3.5 hours	Liu X. *et al*., 2017
$[C_4C_1Im][H_2PO_4]$	Wool	5.0 %[a]	120 °C, N_2, 17 hours	Wang L. *et al*., 2016b
$[C_4C_1Im][HSO_4]$	Wool	5.0 % [a]	120 °C, N_2, 13.5 hours	Wang L. *et al*., 2016b
$[C_4C_1Im][DBP]$	Wool	5.0 % [a]	120 °C, N_2, 12 hours	Wang L. *et al*., 2016b
[AMIM][Cl]	Wool keratin	8 wt%	130 °C, N_2, 10 hours	Xie H. *et al*., 2005
	Turkey feathers	50 wt%	130 °C, N_2, 10 hours	Idris A. *et al*., 2013
	Wool keratin	21 wt%	130 °C, 11 hours	Li R. and Wang D., 2013
	Duck feather	≈ 5 wt%	120 °C, 60 minutes	Ji Y. *et al*., 2014
	Human hair	19 wt%	130 °C, 8 hours	Wang M. *et al*., 2014
$[C_4C_1Im][Cl]$	Wool keratin	11 wt%	130 °C, N_2, 10 hours	Xie H. *et al*., 2005
	Wool	5 wt%	100 °C	Hameed N. and Guo Q., 2009
	Chicken feather	23 wt%	100 °C, N_2, 48 hours	Sun *et al*., 2009
	Wool	5 wt%	100 °C, 10 hours	Hameed N. and Guo Q., 2010
	Turkey feathers	50 wt%	130 °C, N_2, 10 hours	Idris A. *et al*., 2013
	Wool keratin	15 wt%	130 °C, 9 hours	Li R. and Wang D., 2013
	Duck feather	≈ 5 wt%	120 °C, 60 minutes	Ji Y. *et al*., 2014
	Human hair	13 wt%	130 °C, 8 hours	Wang M. *et al*., 2014
	Wool keratin	8 wt%	130 °C, 5 hours	Zheng S. *et al*., 2015

Ionic Liquid	Keratin Type	Solubility	Dissolution Conditions	Reference
$[C_4C_1Im][OAc]$	Wool keratin	8 wt%	130 °C, 10 minutes	Zheng S. *et al*., 2015
[DBNH][OAc]	Goat wool	8 wt%	120 °C, 0.33 hours	Liu X. *et al*., 2017
[choline][thioglycolate]	Turkey feathers	45 wt%	130 °C, N_2, 10 hours	Idris A. *et al*., 2013
[DBNE][DEP]	Goat wool	8 wt%	120 °C, 3 hours	Liu X. *et al*., 2017
$[C_2C_1Im][DEP]$	Goat wool	8 wt%	120 °C, 1.5 hours	Liu X. *et al*., 2017

[a] wool fibre to ionic liquid mass ratio

2.7 Regeneration

The regeneration process involves an anti-solvent, where the solvent used for the biopolymer dissolution (ionic liquid in this case) is removed allowing the biopolymer to precipitate. Regeneration has opened the pathway for the utilization of biopolymers to manufacture different materials for a diverse range of applications (Sun N. *et al*., 2011; Wang S. *et al*., 2016a; Zhang J. *et al*., 2017b). A summary of cellulose and keratin-based regenerated materials that can be formed from different cellulose/keratin-ionic liquid mixtures along with commonly used anti-solvents are presented in Table 2.5.

Some researchers have also explored the recovery of the ionic liquid from the anti-solvent-ionic liquid mixture (Heinze T. *et al*., 2005; Zhang H. *et al*., 2005; Erdmenger T. *et al*., 2007; Mikkola J. *et al*., 2007; Hameed N. and Guo Q., 2009; Hameed N. and Guo Q., 2010; Liu Z. *et al*., 2011; Li R. and Wang D., 2013; Ji Y. *et al*., 2014; Idris A. *et al*., 2014; Tran C. and Mututuvari T., 2015; Zheng S. *et al*., 2015; Tran C. and Mututuvari T., 2016; Tran C. *et al*., 2016b; Liu X. *et al*., 2017; Tran C. *et al*., 2017). This is an important step towards waste reduction and the sustainability of the regeneration process. However, the major limitations in recovering the ionic liquid are it is expensive and requires lot of energy (Zhang Z. *et al*., 2017a).

Zavrel M. *et al*., (2009), explained the regeneration phenomena between cellulose and water as a solute-displacement, where water shields the ionic

liquid ions by forming a hydrodynamic shell, preventing its interaction with cellulose. This leads to a reformation of the hydrogen bonds in cellulose causing it to precipitate and leading to a disordered structure. According to Zhang H. *et al*., (2005), during dissolution the intra-and intermolecular hydrogen bonds are broken destroying the crystalline structure of cellulose. However, the regeneration process does not allow cellulose to crystallize back to its original state. Therefore, reduce its crystallinity.

From Table 2.5, it is evident that regenerated materials from cellulose and keratin can be used for different applications and the regeneration procedure determines the final shape of the regenerated material. Some literature has reported the formation of a gel type material when an ionic liquid and biopolymer mixture was left at room temperature (Kadokawa J. *et al*., 2007; Tran C. and Mututuvari T., 2015; Tran C. and Mututuvari T., 2016; Tran C. *et al*., 2016b; Tran C. *et al*., 2017) and/or introduced into an anti-solvent (Zhang H. *et al*., 2005; Mikkola J. *et al*., 2007; Aaltonen O. and Jauhiainen O., 2009; Deng M. *et al*., 2009). A review conducted by Marr P. and Marr A.(2016), defines a 'gel' as a two-phase heterogeneous mixture between a liquid (dispersed phase) and a solid (continuous phase). A polymer gel is formed, when the continuous phase is composed of a polymer (like cellulose) and an ionogel is formed when an ionic liquid is used as the dispersed phase. These ionogels exhibit properties of both the ionic liquid and the biopolymer (Le Bideau J. *et al*., 2011; P. C. Maar and A. C. Maar, 2016).

Table 2.5: Summary of cellulose and keratin-based regenerated materials

Regenerated Material Type	Regeneration Method	Ionic Liquid	Anti-Solvent	Application	Reference
Cellulose powder	Rapid mixing	$[C_4C_1Im][Cl]$	Water/ethanol/ acetone		Swatloski R. *et al*., 2002
Cellulose fibres and rods	Extrusion	$[C_4C_1Im][Cl]$	Water		Swatloski R. *et al*., 2002
	Spinning	[AMIM][Cl]	Water	• Carbon nanotubes	Zhang H. *et al*., 2007
	Electrospinning	$[C_4C_1Im][Cl]$	Water		Quan S. *et al*., 2010
	Electrospinning	$[C_2C_1Im][OAc]$	Water		Brown E. *et al*., 2012
Cellulose films	Cast onto a glass plate/slide	[AMIM][Cl]	Water		Zhang H. *et al*., 2005
		$[C_4C_1Im][Cl]$	Water		Kadokawa J. *et al*., 2008
		$[C_4C_1Im][Cl]$	Water		Liu Z. *et al*., 2011
		[AMIM][Cl]	Water	• Packaging	Reddy K. *et al*., 2014
		$[C_2C_1Im][OAc]$	Water	• Food packaging • Medical applications	Pang J. *et al*., 2015
		[AMIM][Cl]	Water	• Packaging	Reddy K. *et al*., 2017

Regenerated Material Type	Regeneration Method	Ionic Liquid	Anti-Solvent	Application	Reference
Cellulose foams	Cast onto a glass template	$[C_4C_1Im][Cl]$	Water	• Thermal and sound insulation • Packaging • Filter material • Catalysis • Medical applications	Deng M. *et al.*, 2009
Cellulose aerogels	Poured onto a petri dish	$[C_4C_1Im][Cl]$	Ethanol	• Nanofibrillar aerogels	Aaltonen O. and Jauhiainen O., 2009
	Cast onto a glass dish	$[C_4C_1Im][Cl]$	Methanol followed by tert-butanol	• Polymer support for protein adsorption	Oshima T. *et al*., 2014
Keratin particles	Rapid mixing	$[C_4C_1Im][Cl]$	Ethanol/water	• Removal of Cr(VI) ions in waste water	Sun P. *et al*., 2009
Keratin films and molded samples	Cast onto a Teflon plate	[DMEA][OFo]	Water		Idris A. *et al*., 2014
	Spread on glass	$[C_4C_1Im][Cl]$ [AMIM][Cl]	Water/methanol/methanol		Li R. and Wang D., 2013
Keratin membranes	Cast onto a glass slide	$[C_4C_1Im][Cl]$ $[C_4C_1Im][Cl]$	Methanol Water		Xie H. *et al*., 2005 Hameed N. and Guo Q., 2009

The next section will discuss a well-established manufacturing method that can be used to produce cellulose/keratin-based materials with specific shapes and dimensions.

2.8 Additive Manufacturing

2.8.1 Introduction to Additive Manufacturing

The term 'Additive Manufacturing' (AM) is defined as "a process of joining materials to make objects from 3D model data, usually layer upon layer, as opposed to subtractive manufacturing methodologies" (ASTM,2013). It is also known as additive techniques, additive layer manufacturing, additive fabrication, additive processes, freeform fabrication, direct digital manufacturing, rapid prototyping, rapid manufacturing, solid freeform fabrication, layer manufacturing and 3D printing (3DP) (ASTM, 2013; Petrovic V. *et al*., 2011; Guo N. and Leu M., 2013; Ambrosi A. and Pumera M., 2016). Some of the advantages of using AM, compared to conventional manufacturing techniques like injection moulding and cutting based machinery, include; generating less waste with recycling of the waste possible, the requirement for less energy during manufacture, avoidance of the need for expensive tools, moulds or punches, and the ability to easily create and revise a design (Petrovic V. *et al*., 2011; Berman B., 2012; Ambrosi A. and Pumera M., 2016).

The stages involved in creating a 3D object are illustrated in Figure 2.14. First, a software model that defines the external geometry of either the prototype

or the actual part is made. Next the CAD file is converted to STL format which describes the external surface of the CAD file and calculates each layer before transferring to the AM machine. Then the machine is setup where the user specifies setup parameters (*e.g.* temperature, layer thickness, time etc.) and physically prepares the machine (loading build materials, inserting and bringing the build platform to the home position). Once the machine is setup layer by layer, the manufacturing process will start. When the part is fully built, the part is removed from the build platform. Based on the final application during post-processing, the part may need additional cleaning and removal of support material (Gibson I. *et al*., 2014).

Over the past few decades a growing body of literature has reported different AM processes (Kruth J. *et al*., 1998; Pham D. and Gault R., 1998; Levy G. *et al*., 2003; Petrovic V. *et al*., 2011; Wong K. and Hernandez A., 2012; Guo N. and Leu M., 2013; Ambrosi A. and Pumera M., 2016; Ngo T. *et al*., 2018). These technologies uses a variety of materials like polymers, metals, ceramics and composites to produce parts layer by layer (Kruth J. *et al*., 1998; Levy G. *et al*., 2003; Petrovic V. *et al*., 2011; Guo N. and Leu M., 2013; Ambrosi A. and Pumera M., 2016; Ngo T. *et al*., 2018) that have been successfully used in many applications in the fields of aerospace, automobile, medical and energy (Levy G. *et al*., 2003; Petrovic V. *et al*., 2011; Wong K. and Hernandez A., 2012; Guo N. and Leu M., 2013; Ambrosi A. and Pumera M., 2016; Liaw C. and Guvendiren M., 2017, Ngo T. *et al*., 2018).

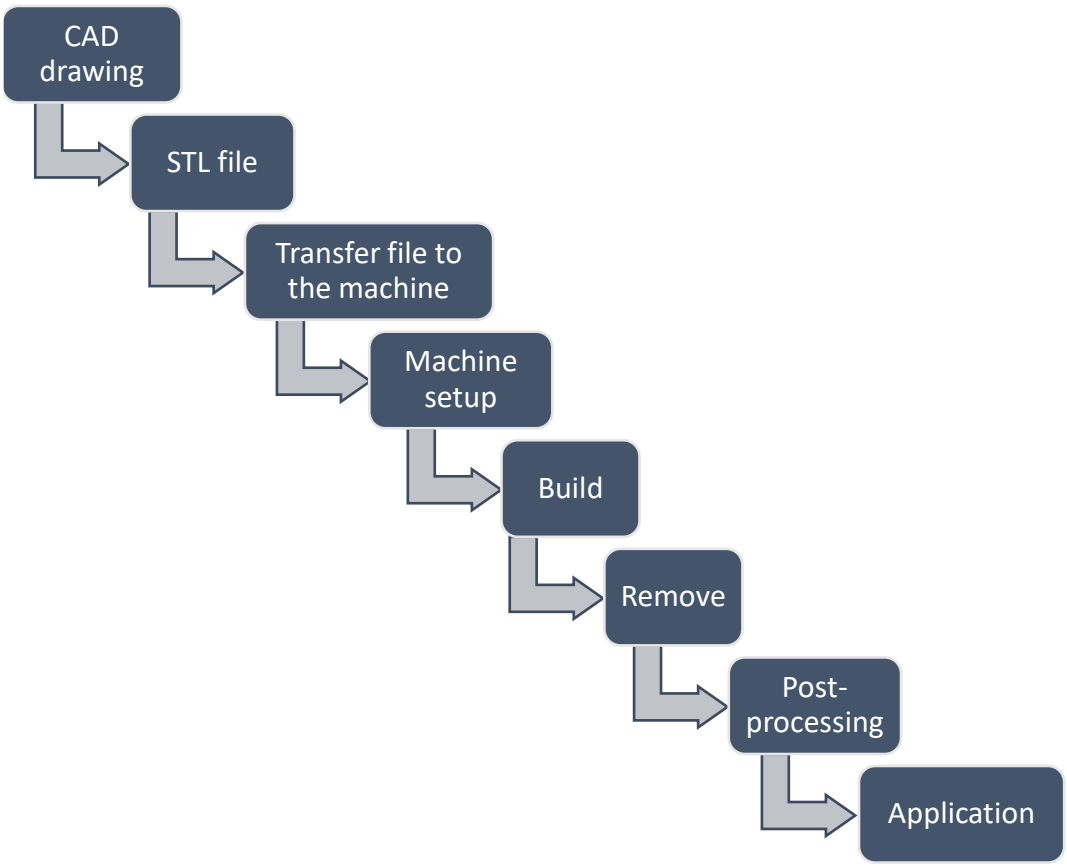


Figure 2.14: General AM process (Adapted from Gibson I. *et al*., 2014)

2.8.2 Current Literature on Biopolymer 3DP

Extrusion and ink-jet printing have been successfully used to demonstrate the viability of 3DP cellulose (Haverhals L. *et al*., 2012; Markstedt K. *et al*., 2014; Sweely K. *et al*., 2014). Haverhals L. *et al*., (2012), ink-jet printed a mixture of $[C_2C_1Im][OAc]$ and acetonitrile onto a cellulosic paper and regeneration was achieved using a water bath. In another study Sweely K. and co-workers exhibited ink-jet printing $[C_2C_1Im][OAc]$, carbon black and microcrystalline cellulose onto a cotton paper. Again, water was used to remove ionic liquid (Sweely K. *et al*., 2014). Markstedt K. *et al*., (2014), used extrusion to print cellulose and $[C_2C_1Im][OAc]$ cylinders of approximately 25 mm high on a

vertical agar support (made from agar and water). In addition to this Li L. *et al*., (2018), 3D-printed cellulose and NMMO using extrusion printing and Holland S. *et al*., (2018), ink-jet printed a food-based ink containing xanthan gum onto cellulose powder. Recently, Nulwala H. *et al*., (2018) conducted a review highlighting applications and opportunities on 3D printed ionic liquids-based inks.

Research on 3DP biopolymer-ionic liquids mixtures is at a very early stage and to the best of our knowledge no attempt has been made to ink-jet print a biopolymer-ionic liquid mixture. If this method is successful it will open a new pathway of applications and a manufacturing method to utilize biopolymer-based wastes.

2.8.3 Ink-Jet Printing Technologies

Ink-jet printing is one of the most promising technologies which is widely used. Ink-jet printers can be divided into two categories: as continuous and drop-on-demand (Le H., 1998; de Gans B. *et al*., 2004; Martin G. *et al*., 2008; Derby B., 2010). Figure 2.15 shows a summary of different types of continuous and drop-on-demand ink-jet printers that are commonly used.

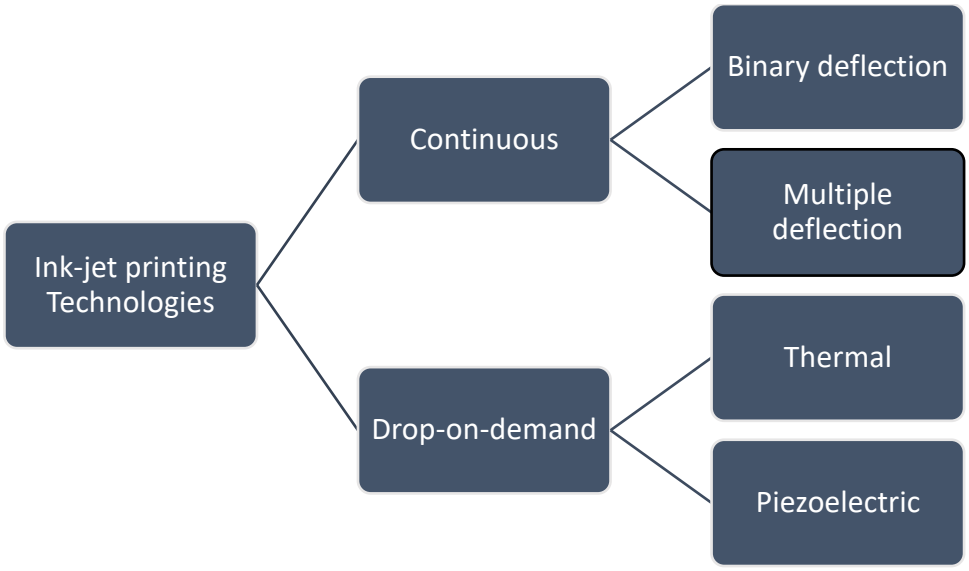


Figure 2.15: Commonly used ink-jet printing technologies (Adapted from Le H., 1998)

In continuous ink-jet printing, the ink is ejected under pressure via a nozzle (Martin G. *et al*., 2008; Derby B., 2010). The Rayleigh instability causes the stream to break and form droplets (Derby B., 2010). Some of the droplets from this stream are chosen for printing by applying a charge to them (Martin G. *et al*., 2008), while the uncharged droplets are deflected into a gutter for recycling (Le H., 1998; Martin G. *et al*., 2008; Derby B., 2010). Based on the mechanism for droplet deflection, continuous ink-jet printing is further divided into two categories (Le H., 1998). In binary deflection the substrate is located where the printing is required and the charged droplets are deflected there (Le H., 1998; Derby B., 2010) (Figure 2.16A). In multiple deflection the charged droplets are deflected onto the substrate at different levels based on their charge (Le H., 1998; Martin G. *et al*., 2008) (Figure 2.16B).

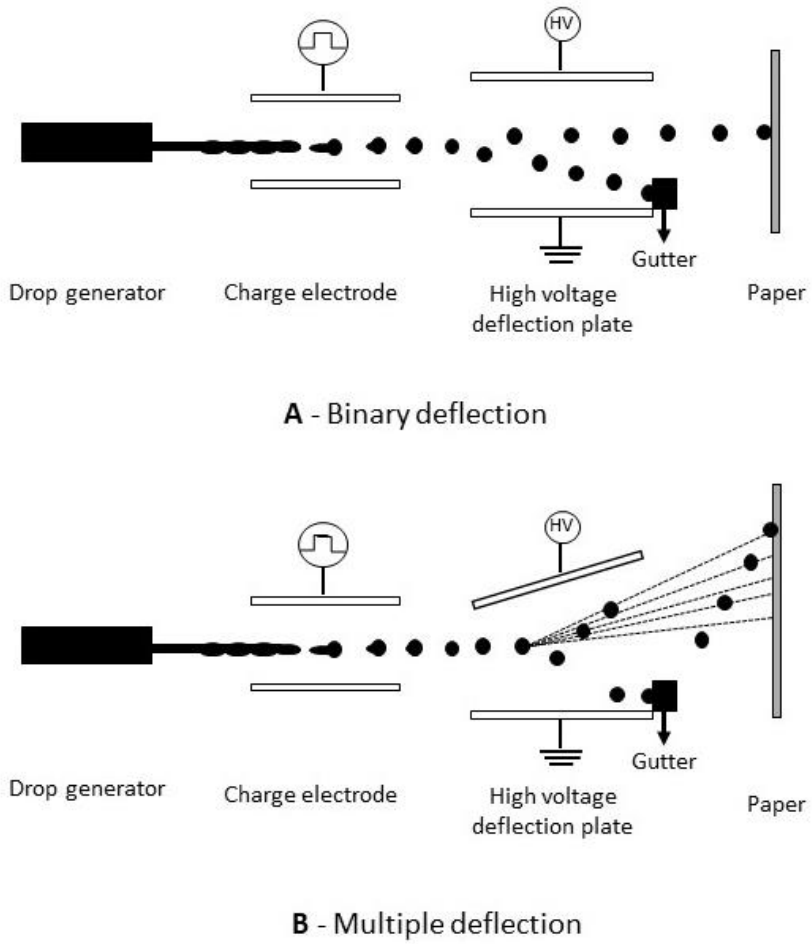


Figure 2.16: Continuous ink-jet printing mechanisms (Adapted from Le H., 1998)

Unlike continuous ink-jet printing, drop-on-demand ink-jet printing produces droplets only when needed. The nozzle is placed on the desired printing location on the substrate and a pressure pulse is exerted on the fluid either thermally or piezo electrically (Le H., 1998; de Gans B. *et al*., 2004; Martin G. *et al*., 2008; Derby B., 2010). Drops are ejected from the nozzle if this pressure pulse exceeds a threshold value (Derby B., 2010). Thermal drop-on-demand ink-jet printers (Figure 2.17A) have a thin film heater inside the ink chamber. A current is passed via this heater, which heats the ink near it above its boiling point causing the formation of a small water vapour pocket/bubble. This forces the ink out of the nozzle. When the current is switched off, the bubble collapses

rapidly due to heat transfer, causing the ink to break (Le H., 1998; de Gans B. *et al*., 2004; Derby B., 2010). In a piezoelectric drop-on-demand ink-jet printer (Figure 2.17B), a piezoelectric material deforms causing a sudden change in ink volume and passes an acoustic pressure signal to the nozzle. This results in the formation of a liquid droplet at the nozzle. When adequate pressure is present, this drop is ejected (Le H., 1998; de Gans B. *et al*., 2004).

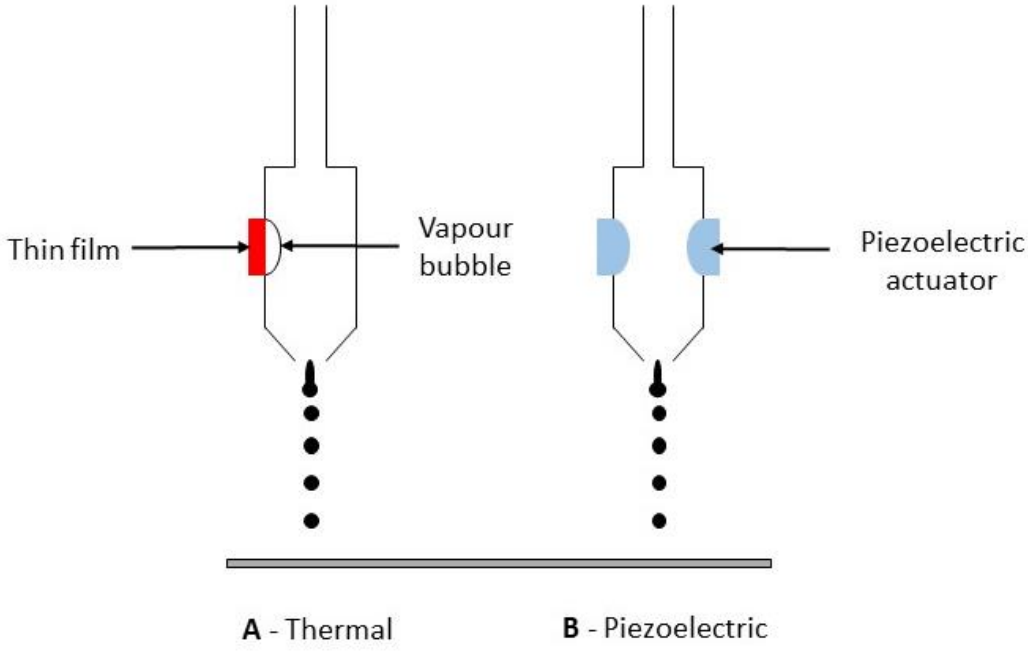


Figure 2.17: Drop-on-demand ink-jet printing mechanisms (Adapted from Derby B., 2010)

2.8.4 Comparison between different Ink-Jet Printing Technologies

Some of the major disadvantages of continuous ink-jet printers, relative to drop-on-demand printers, that limit their application include; generation of droplets with a diameter slightly bigger than the nozzle diameter, formation of ink droplets even in the absence of printing, recycling of ink after exposure to the printing environment can cause contamination, only a few fluids are

suitable for this application and the drops having poor spatial resolution once printed (Derby B., 2010).

Given the limitations with continuous ink-jet printing, majority of ink-jet printing is based on the drop-on-demand technology (Le H., 1998). Some of the advantages of drop-on-demand ink-jet printing include; production of smaller droplets (de Gans B. *et al*., 2004; Derby B., 2010), cost-effectiveness in terms of ink delivery, compared to continuous ink-jet printing, as drops are produced only when needed (Derby B., 2010) and excellent placement accuracy (de Gans B. *et al*., 2004). The droplet size is generally roughly equal to the nozzle diameter, but this printing technique has the added benefit of being able to control the drop size and ejection velocity by varying the pressure pulse (Derby B., 2010). An important characteristic that is required in drop-on-demand ink-jet printers is that the ink should dry/solidify on the printed substrate and not in the nozzle. Various techniques have been developed at the nozzle (cleaning) and substrate (use of heaters, dryers etc.) to overcome this issue (Martin G. *et al*., 2008).

Thermal drop-on-demand ink-jet printers are not commonly used as they require an ink with a high vapour pressure at ambient conditions (Derby B., 2010). This restriction limits the number of fluids that can be used (de Gans B. *et al*., 2004; Derby B., 2010). Secondly, piezoelectric drop-on-demand ink-jet printers allow drop size and velocity to be easily controlled by changing the pulse. Therefore, piezoelectric drop-on-demand ink-jet printers are widely

used in industrial applications and a substantial body of literature has been published relating to this approach (Derby B., 2010). Since continuous ink-jet printing involves charge to direct the ink onto the substrate, it is not suitable to print inks involving ionic liquids. These benefits mean that this study will be focused on drop-on-demand ink-jet printers.

2.8.5 Principles behind Ink-Jet Printing

This section will provide an overview of different principles that govern the ink-jet printing process. These include; the printability parameter which determines the printability of an ink, formation of individual drops from a jet of ink, impact of an individual drop on a substrate and droplet spacing which effects the quality and precision of the final printed pattern.

Printability Parameter

In order to determine the printability of an ink, the physical properties of the ink must be examined. In addition to this, ink-jet print heads are designed for different types of inks and have specifications in terms of ink viscosity, surface tension and temperature. This can be used as a guideline when selecting an ink or when formulating an ink mixture.

The printability parameter (Z) determines if an ink can be printed. It is calculated using different dimensionless quantities like the Reynolds number (Re) (ratio between inertial and viscous forces), Weber number (We) (ratio

between kinetic and surface energy) and Ohnesorge number (Oh) (ratio between viscous, inertial and surface tension forces).

$$\mathrm{Re} = \frac{\rho \mathrm{v} \mathrm{d}}{\eta} \quad \text{(Equation 1)}$$

$$\mathrm{We} = \frac{v^2 \rho d}{\sigma} \quad \text{(Equation 2)}$$

$$\mathrm{Oh} = \frac{\sqrt{We}}{Re} = \frac{\eta}{\sqrt{\sigma \rho d}} \quad \text{(Equation 3)}$$

$$Z = \frac{1}{\mathrm{Oh}} = \frac{\sqrt{\sigma \rho \mathrm{d}}}{\eta} \quad \text{(Equation 4)}$$

Where ρ, η and σ are the density, viscosity and surface tension of the fluid, respectively d is the characteristic length and v is the velocity (Martin G. *et al*., 2008; Derby B., 2010).

For ink-jet printing, it is generally recommended to have the printability parameter between 1 and 10 (Gibson I. *et al*., 2014). This is because, when it is low (< 1), the ink is too viscous, it does not have enough energy to break and this prevents ejection of drops. When the printability parameter is high (> 10), the ink has a very high surface tension and results in satellite drops (Derby B., 2010). Therefore, viscosity and surface tension of the ink are the crucial physical parameters that needs to be tuned to achieve successfully ink-jet printing.

Droplet Formation

In a drop-on-demand ink-jet printer, the drop leaves the nozzle as a jet with a long-extended tail/ligament connected to the ink in the nozzle (Figure 2.18A). After some time, the tail/ligament breaks and some ink will return to the nozzle and some either connects to the drop, or breaks, forming small satellite drops (Figure 2.18B) (Martin G. *et al*., 2008; Derby B. 2010). Satellite drops that do not merge with the leading drop can give rise to drops with poor precision, resolution and accuracy. The distance between the nozzle and the substrate must be maintained at a minimum to enable drop merge during flight and to prevent the drop diverging from its original path due to drag from air currents (Derby B., 2010). Therefore, during printing other than the distance between the substrate and the nozzle, different printing parameters like voltage, temperature, pressure, waveform, frequency, etc. and the physical properties of the ink need to be optimised to obtain a drop, where the satellite has enough velocity to merge with the main drop.

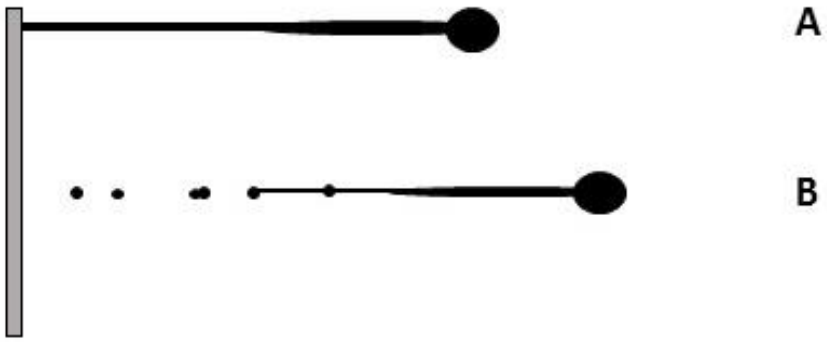


Figure 2.18: Drop formation sequence in a drop-on-demand ink-jet printer (Adapted from Martin G. *et al*., 2008)

Droplet Impact on the Substrate

Detailed studies on a liquid drop impact on a solid substrate have been conducted by Rein M. (1993), Rioboo R. *et al*., (2001), Rioboo R. *et al*., (2002), Yarin A. (2006) and Derby B., (2010). According to Rein M. (1993), a liquid drop can either bounce, spread or splash on a solid surface (Figure 2.19). For stable printing in this study the liquid drops need to spread, and the extent of this spreading is governed by wettability.

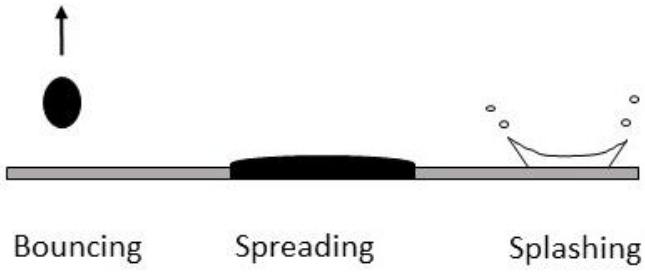


Figure 2.19: Impact of a liquid drop on a solid surface (Adapted from Rein M., 1993)

Wettability is defined as the ability of a liquid drop to spread on a solid surface and quantified using the contact angle (Riobbo *et al*., 2001). Contact angle is the angle formed by the tangent to the liquid drop at its contact point with the substrate and can be used to define the hydrophobicity of the substrate (Dey T. and Naughton D., 2016; Yuan Y. and Lee R., 2013).

As shown in Figure 2.20 on a non-wetting surface (hydrophobic) a compact liquid drop is formed with less contact with the substrate and the liquid drop has a higher contact angle (> 90 °) and on a wetting surface (hydrophilic) the liquid drop spread on the surface and has a lower contact angle (< 90 °) (Yuan

Y. and Lee R., 2013; Dey T. and Naughton D., 2016). A review conducted by Dey T. and Naughton D. (2016), summarises different methods that can be used to modify substrates and thereby either increase or decrease the wettability.

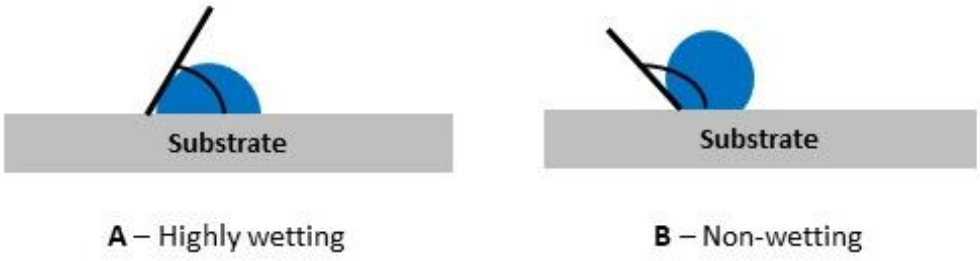


Figure 2.20: Contact angle on different substrates (Adapted from Riobbo *et al*., 2001)

Droplet Spacing

Once the drop is ejected from the nozzle and it is deposited on the substrate, depending on the droplet spacing (specified during printing) it can either print an individual drop or merge to form a shape. Droplet spacing is defined as the distance between adjacent drops and calculated using the droplet diameter (Zhang F. *et al*., 2016).

Soltman D. and Subramanian V. (2008), studied the effect of droplet spacing on the morphology of printed lines. When the droplet spacing was very high (> 2 times the droplet radius) individual drops with no overlap were formed (Figure 2.21A). As the droplet spacing was reduced, a scalloped line was observed where the individual drops overlapped but still had their curved contact lines. Lower droplet spacing restricted the movement of the ink, resulting in a narrow-scalloped line (Figure 2.21B). Reducing the droplet spacing further

produced a uniform line that was smooth and straight on all sides. Compared to all the different line morphologies printed, this uniform line was the narrowest (Figure 2.21C). Further decreasing the droplet spacing resulted in a bulged line, where bulging occurred between uniform regions (Figure 2.21D). This study demonstrated that, frequency, substrate temperature and droplet spacing must be optimised in order to form uniform patterns. He Y. *et al*., (2016), Zhang F. *et al*., (2016) and Hu G. *et al*., (2017) also observed similar results on line morphology as the droplet spacing was varied.

Stringer J. and Derby B. (2010), suggested that stable line formation is bounded by two limits. The lower bound (minimum line width) at higher droplet spacing and the upper bound (maximum line width) at lower droplet spacing. In conclusion, droplet spacing determine the resolution and quality of the printed pattern and it is affected by a variety of printing parameters.

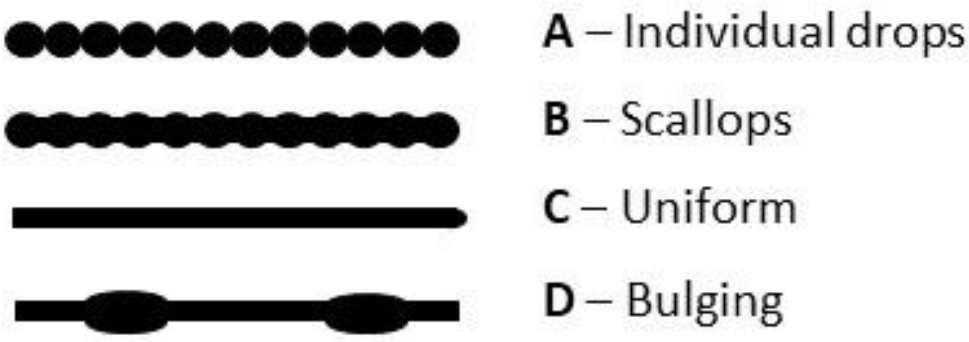


Figure 2.21: Effect of droplet spacing on line morphology (Adapted from Soltman D. and Subramanian V., 2008)

2.9 Knowledge Gap

In conclusion applications of biopolymers have been hindered due to strong intra- and intermolecular forces present in them. Ionic liquids have been identified as a feasible and efficient solvent compared to traditional solvents used to break the strong bonds present in biopolymers. A large number of literature studies have reported the use of different ionic liquids to dissolve biopolymers and methods to obtain regenerated materials for different applications. Similarly, AM is an industrialized process that manufactures 3D printed parts from a wide variety of materials. As outlined in Figure 2.22, this research will attempt to fill the knowledge gap that exist between 3DP and biopolymers by utilizing a novel system. This will involve a biopolymer-ionic liquid-based inks, 3D printed and regenerated to obtain parts with specific dimensions.

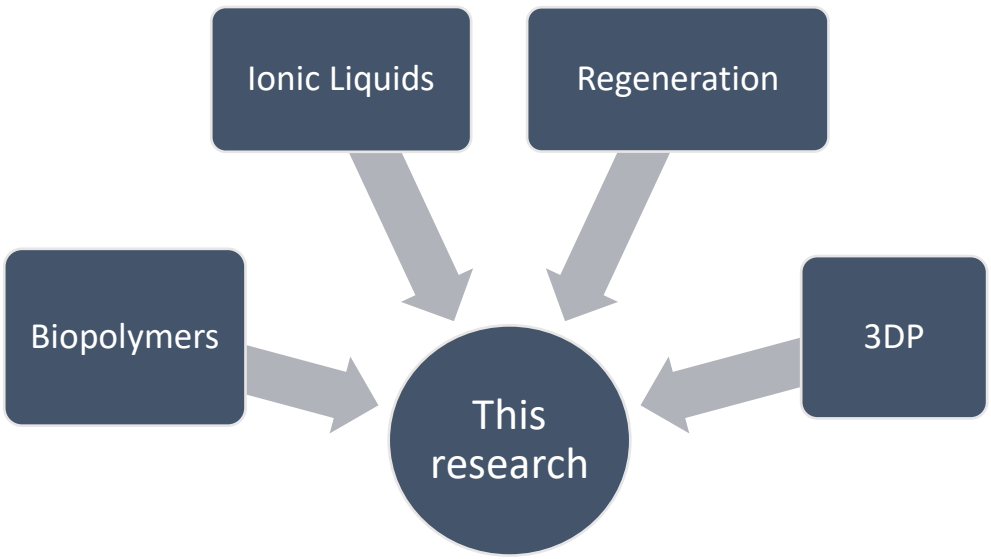


Figure 2.22: Knowledge gap addressed in this research

These 3D printed parts can be used in biomedical, packaging and wastewater treatment applications (Deng M. *et al.*, 2009; Sun P. *et al*., 2009; Reddy K. *et al*., 2014; Rosewald M. *et al*., 2014; Pang J. *et al*., 2015; Tran C. and Mututuvari T., 2015; Tran C. and Mututuvari T., 2016; Tran C. *et al*., 2016a; Tran C. *et al*., 2016b; Reddy K. *et al*., 2017; Tran C. *et al*., 2017; Tran C. *et al*., 2018). Currently, a large number of literature has reported the production of films using cellulose and keratin blends for drug delivery systems (Rosewald M. *et al*., 2014; Tran C. and Mututuvari T., 2015; Tran C. and Mututuvari T., 2016; Tran C. *et al*., 2016a; Tran C. *et al*., 2016b; Tran C. *et al*., 2017; Tran C. *et al*., 2018). Using 3DP printing to manufacture with these materials means complicated, bespoke parts can be manufactured in smaller quantities (Ngo T. *et al*., 2018).

Implementing this system in an industrial scale would involve dissolution of biopolymer in the ionic liquid, 3DP and regeneration to remove the ionic liquid. Major cost contributor comes from the printing technology used. Ink-jet printing was selected since it has a medium cost compared to other printing technologies like selective laser sintering (SLS) (Valot L. *et al*., 2019). This system can be made environmentally friendly by incorporating biodegradable solvents and recycling used solvent. This will also reduce the costs associated with purchase and wastage of raw materials.

Chapter 3 : Materials and Methods

3.1 Introduction

This chapter describes the chemicals, ink preparation procedure, printing technologies (DIMATIX ink-jet printing and PICO Pulse printing), regeneration procedure and characterisation methods used in this study. Figure 3.1 presents a flowchart summarising the experimental procedure used.

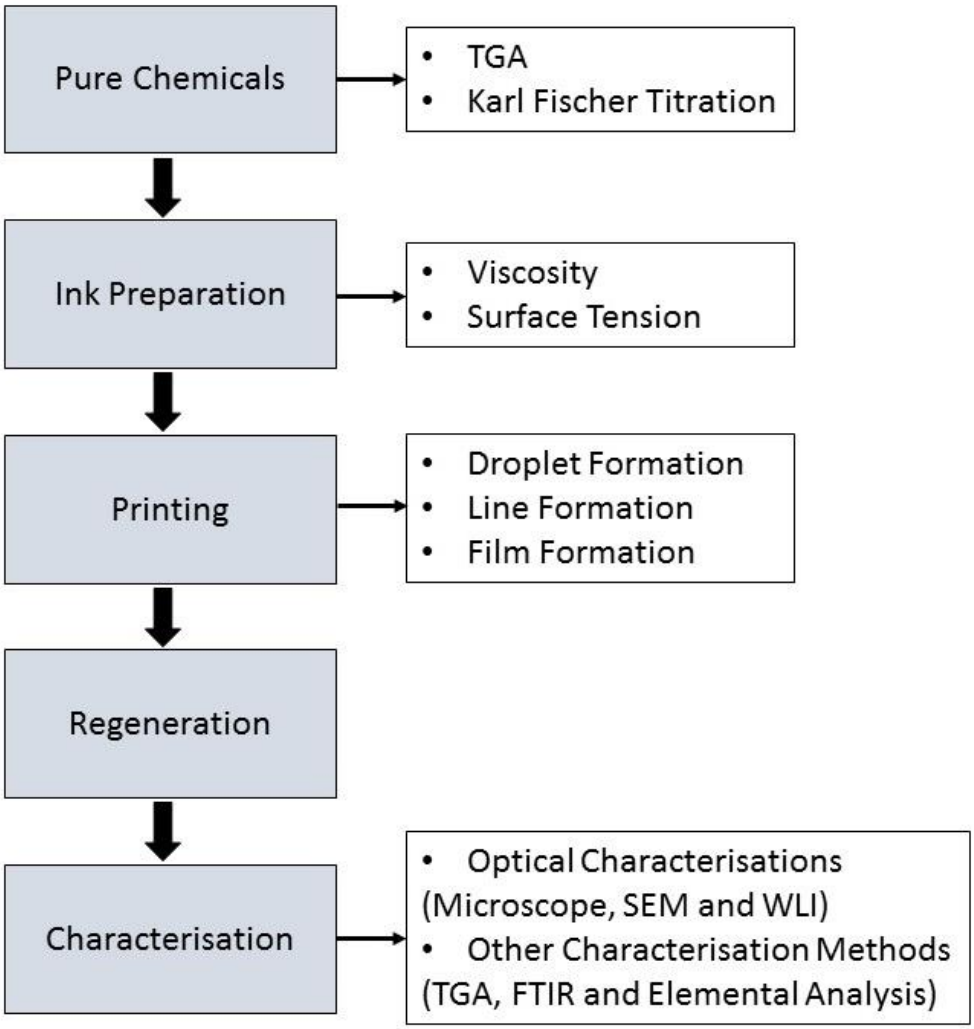


Figure 3.1: Summary of the experimental procedure used

3.2 Chemicals

Ionic liquids: 1-ethyl-3-methylimidazolium acetate [C_2C_1Im][OAc] (purity ≥ 95 %) and 1-butyl-3-methylimidazolium acetate [C_4C_1Im][OAc] (purity ≥ 95 %) were purchased from Sigma Aldrich (UK). Co-solvents: 1-butanol and dimethyl sulfoxide (DMSO) were purchased from Thermo Fisher Scientific (UK). Microgranuallar cellulose was purchased from Sigma Aldrich (UK) and wool was sourced from British spun wool. Deionized water was obtained from the laboratory. All the chemicals were used as received, except for cellulose which was dried in an oven (Lenton) for 3 hours at 60 °C (for low viscosity inks) and for 5 minutes at 100 °C (for high viscosity inks) before use.

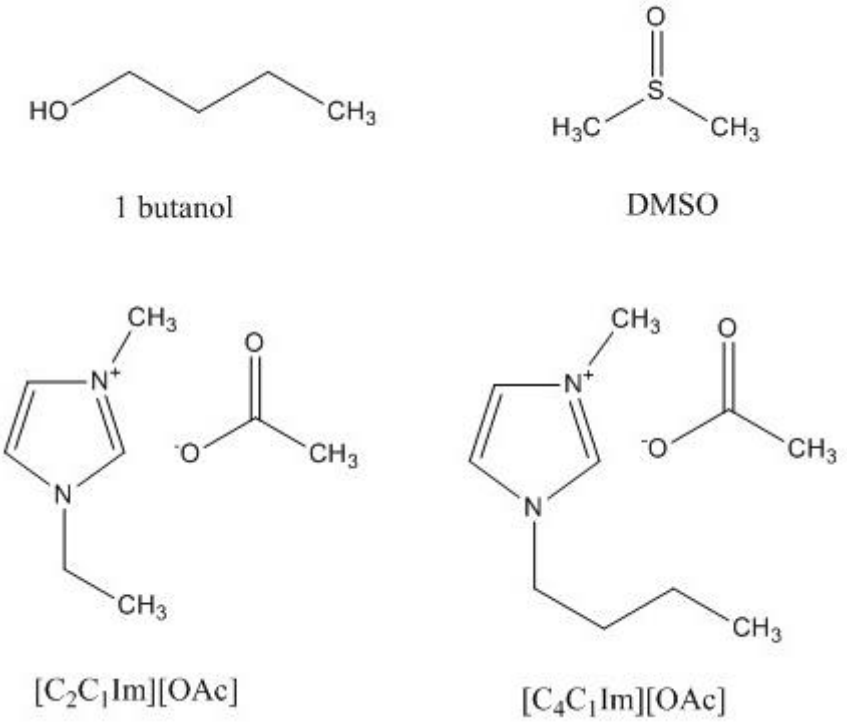


Figure 3.2: Structures of the chemicals used

3.3 Ink Preparation

Two different inks; low viscosity (for DIMATIX ink-jet printing) and high viscosity (for PICO Pulse printing) were prepared in this study. The ink preparation procedure is described below.

3.3.1 Low Viscosity Inks

The mass of cellulose used was calculated by taking 2 and 5 % of the ionic liquid mass (Table 3.1). The required quantity of cellulose was weighed using a four figure digital balance (Denver Instruments) and placed into a glass vial. The ionic liquid was measured out using a 1 mL ink-jet syringe and was added to the cellulose. To investigate the effect of adding a co-solvent on cellulose dissolution and the physical properties of the resultant solution, two different percentages of cellulose (calculated as above) and three different percentages of co-solvents (50, 70 and 90 % of the ionic liquid mass) were then added to samples containing cellulose and $[C_4C_1Im][OAc]$ (Table 3.2). The amount of cellulose, ionic liquid and co-solvent in all the samples was also calculated as wt % (Tables 3.1 and 3.2). To create the final formulation, the mixtures were stirred using a magnetic stirrer at 800 rpm whilst heating in an oil bath at 100 °C (for samples 1 to 4) and 80 °C (for samples 5 to 10), and visually observed until no particulate matter remained.

Table 3.1: Low viscosity inks containing cellulose and ionic liquid

Sample	Cellulose (g)	$[C_2C_1Im][OAc]$ (g)	$[C_4C_1Im][OAc]$ (g)	Cellulose (%)	Cellulose (wt %)	Ionic Liquid (wt %)
1	0.1643	8.2		2.0	2.0	98
2	0.4108	8.2		5.0	4.8	95
3	0.1688		8.4	2.0	2.0	98
4	0.4220		8.4	5.0	4.8	95

Table 3.2: Low viscosity inks containing cellulose, ionic liquid and co-solvent

Sample	Cellulose (g)	$[C_4C_1Im][OAc]$ (g)	DMSO (g)	1-Butanol (g)	Cellulose (%)	Co-Solvent (%)	Cellulose (wt %)	$[C_4C_1Im][OAc]$ (wt %)	Co-Solvent (wt %)
5	0.1266	6.3	3.2		2.0	50	1.3	66	33
6	0.1266	6.3	4.4		2.0	70	1.2	58	41
7	0.1055	5.3	4.7		2.0	90	1.0	52	47
8	0.1266	6.3		3.2	2.0	50	1.3	66	33
9	0.1846	3.7	1.8		5.0	50	3.2	65	32
10	0.3165	6.3		3.2	5.0	50	3.2	65	32

3.3.2 High Viscosity Inks

The high viscosity inks (Table 3.3) were prepared by weighing the required mass of cellulose and/or wool using a four-figure digital balance (Denver Instruments) and placed into a glass vial. The ionic liquid was measured out using a 1 mL ink-jet syringe and was added to cellulose and/or wool. For sample 13 and 14 wool was gradually added in increments of 0.5 to 1 g. For sample 15 and 16, first cellulose was fully dissolved in the ionic liquid to give a clear solution before wool was added. The glass vial was then immersed in an oil bath (at 100 °C) and the mixtures were stirred using a magnetic stirrer (at 800 rpm) until no particulate matter remained. The amount of cellulose, wool and ionic liquid in all the samples were also calculated as a wt % in Table 3.3.

Table 3.3: High viscosity inks containing cellulose and/or wool and ionic liquid

Sample	Cellulose (g)	Wool (g)	$[C_2C_1Im][OAc]$ (g)	$[C_4C_1Im][OAc]$ (g)	Cellulose (wt %)	Wool (wt %)	$[C_2C_1Im][OAc]$ (wt %)	$[C_4C_1Im][OAc]$ (wt %)
11	1.8415		12.3		13		87	
12	1.4067			12.7	10			90
13		3.0810	12.3			20	80	
14		4.3320		12.7		25		75
15	0.7034	0.7034	12.3		5	5	90	
16	0.7034	0.7034		12.7	5	5		90

3.4 Printing

Two different printing methods; DIMATIX ink-jet printing and PICO Pulse printing were used in this study. A step-by-step description of the printing procedure, major components of each printer, nozzle cleaning procedure and the substrates used for printing are presented in this section.

3.4.1 DIMATIX Ink-jet Printing

The ink-jet printer used in this study was a FUJIFILM DIMATIX DMP-2831, which is a piezoelectric drop-on-demand printer. Low viscosity inks (Table 3.2) were printed using this printer. Figure 3.3 shows the steps involved in loading the cartridge to obtaining the final printed pattern.

First, the cartridge containing the ink and the cleaning pad were inserted into the DIMATIX ink-jet printer. This step was followed by selecting the cartridge settings. Next, a drop watcher was used to examine the nozzles. The cartridge settings selected earlier can be optimised here to obtain the required ink performance. These include parameters like; waveform, voltage, temperature, cleaning cycles (before, during and after printing) and selecting the nozzle/s that will be used for printing. Next, the pattern to be printed was selected and the sabre angle was adjusted. The substrate was then loaded and its specifications (substrate thickness and temperature) were specified. A fiducial camera was used to set the print origin (based on the location of the substrate). Finally, the printing parameters were confirmed, and printing begins.

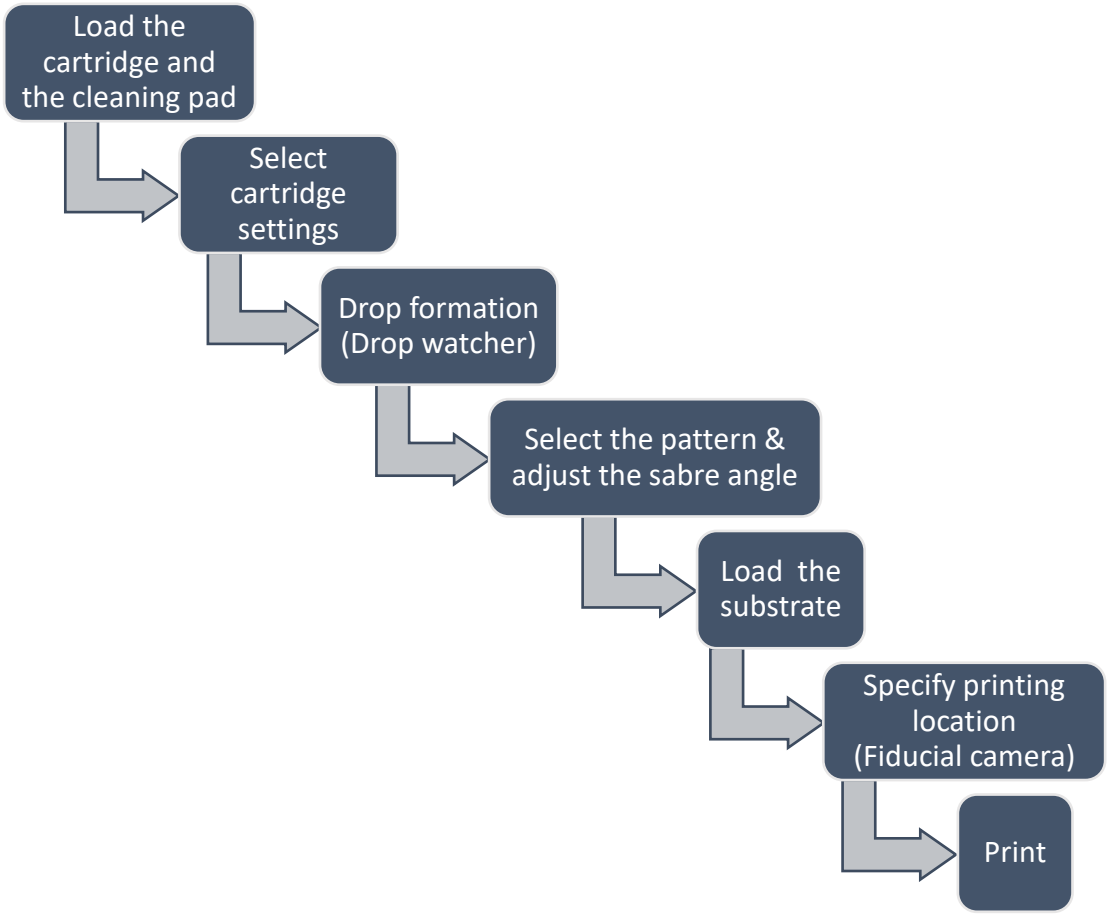


Figure 3.3: FUJIFILM DIMATIX DMP-2831 ink-jet printing procedure

DIMATIX Ink-jet Cartridge

The cartridge purchased from FUJIFILM DIMATIX consists of a fluid module and a jetting module (Figure 3.4). The ink was filled into the polypropylene fluid bag inside the fluid case via the fill port. The piezo-driven jetting module, consisting of 16 nozzles each having a diameter of 21 µm and a 254 µm spacing between them. They are able to produce a 10 pL drop volume and a built-in heater to adjust the ink viscosity by heating the cartridge up to 70 °C (Fujifilm Dimatix, 2008; Fujifilm Dimatix, 2010).

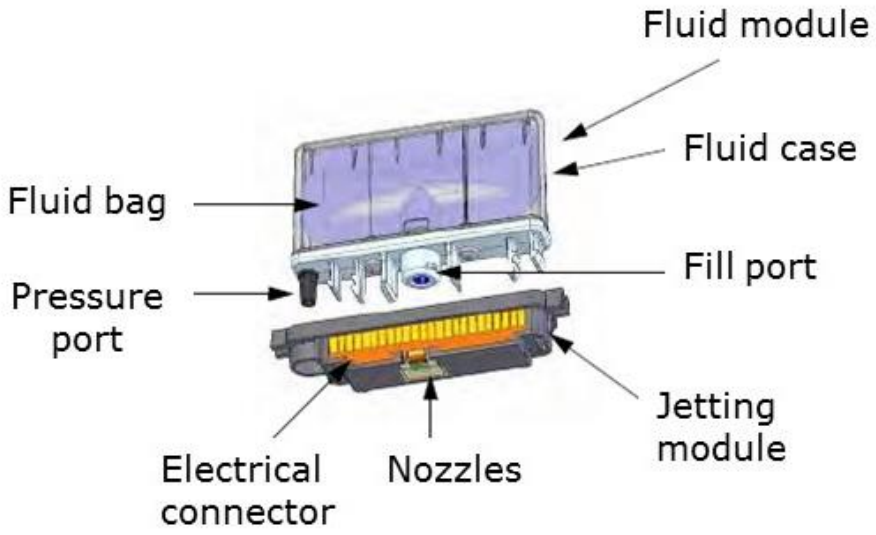


Figure 3.4: DIMATIX ink-jet cartridge (Adapted from Fujifilm Dimatix Manual, 2010)

The consumables used to fill the DIMATIX ink-jet cartridge are shown in Figure 3.5. First, the required volume of ink was measured using a 1 mL ink-jet syringe and transferred to the DIMATIX fluid module using a 5 µm nylon syringe filter (Cole-Parmer) and the fill needle (supplied with the cartridge). The syringe filter was used to prevent any particles from blocking the nozzle. When filling the DIMATIX fluid module, care must be taken to reduce the formation of air bubbles by tapping into the fluid module. The fluid module was filled with approximately 2 mL of ink and the jetting module was attached before installing into the print carriage in the DIMATIX ink-jet printer (Figures 3.6 and 3.7) (Fujifilm Dimatix, 2010).

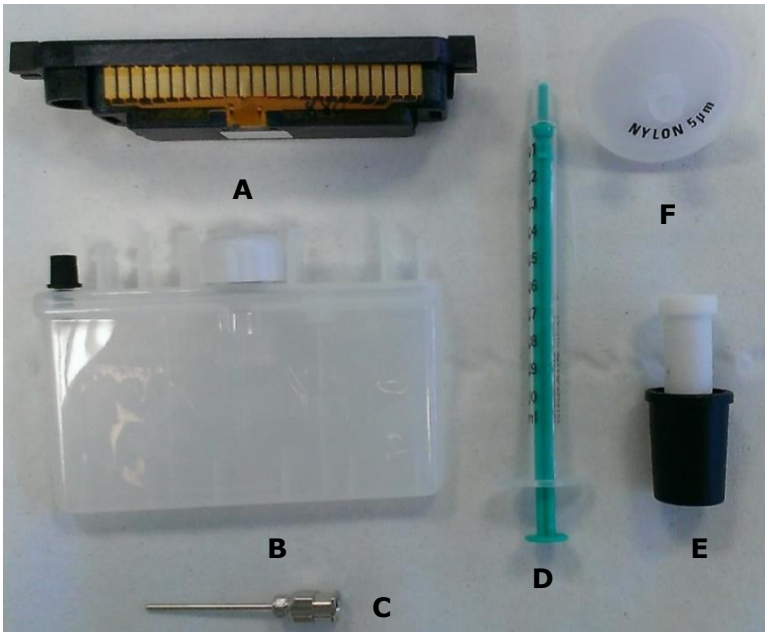


Figure 3.5: Consumables used to fill the DIMATIX ink-jet cartridge

(A) DIMATIC jetting module (B) DIMATIX fluid module (C) Fill needle (D) 1 mL ink-jet syringe (E) Cleaning pad and (F) 5 µm Nylon syringe filter

Major Components of the DIMATIX Ink-jet Printer

Figure 3.6, presents the major components of the DIMATIX ink-jet printer (platen, print carriage, maintenance station blotting pad and drop watcher). The platen is connected to a vacuum system, which passes vacuum through the platen holes. This helps to secure the substrate on the platen and prevents it from moving during printing. Also, the platen can be heated up to 60 °C. The print carriage moves horizontally over the substrate during printing. Figure 3.7 illustrates the major components of the print carriage. The cartridge is inserted to the cartridge holder and the fiducial camera is used to locate the substrate, specify the print origin, view and capture images of the printed pattern (Fujifilm Dimatix, 2008; Fujifilm Dimatix, 2010).

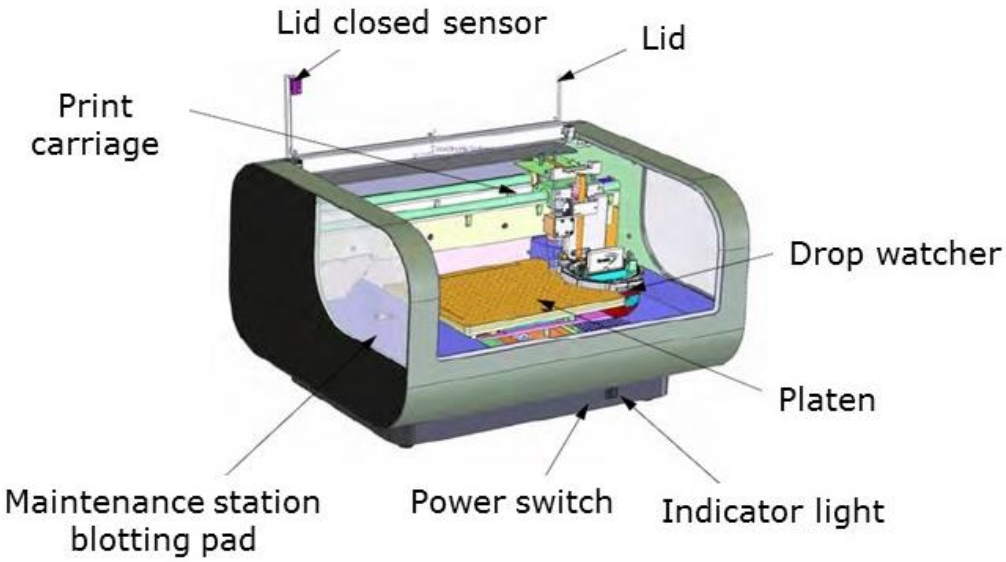


Figure 3.6: Major components of the DIMATIX ink-jet printer (Adapted from Fujifilm Dimatix Manual, 2010)

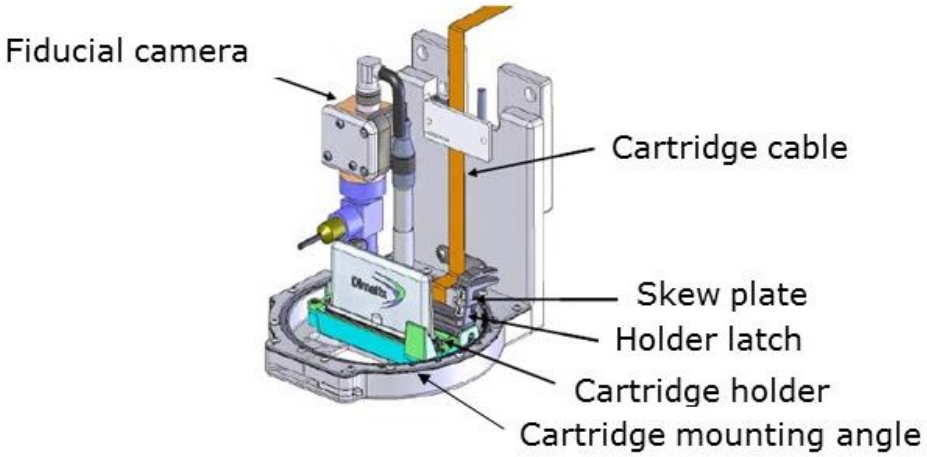


Figure 3.7: Major components of the DIMATIX ink-jet printer carriage (Adapted from Fujifilm Dimatix Manual, 2010)

The maintenance station blotting pad (cleaning pad) (Figure 3.5) is an absorbent pad that touches the face plate of the cartridge around the nozzle plate. During cartridge cleaning the print carriage moves to the left side of the platen (maintenance station) (Figure 3.6). The cartridge is cleaned by applying

air pressure to the fluid bag inside the fluid module via the pressure port (Figure 3.4), which forces the ink to leave the nozzle (Fujifilm Dimatix, 2010). During printing, when the cleaning cycles were unable to unblock the nozzles, the cartridge was manually cleaned using a polyester wipe.

The drop watcher (Figure 3.6), consists of a camera that allows to view the jetting nozzles, the faceplate around the nozzles and the actual jetting of the ink. Any fluid that is jetted during this process is captured by the drop watcher pad. When drop watcher is activated the print carriage moves to the right-hand side of the platen (Figure 3.6) (Fujifilm Dimatix, 2010). The drop watcher screen is shown in Appendix Figure 9.1.

The jetting performance through the nozzles can be viewed from the drop watcher screen by selecting the required nozzle/s (3 to 7 in the case of Appendix Figure 9.1). Cleaning cycles to improve jetting and the jetting frequency is also specified here. The velocity of the drops can be calculated using the strobe delay. If the strobe delay is set at 100 µs, the strobe LED captures an image of the drops after 100 µs. The distance travelled during this time along with the strobe delay time can be used to calculate the drop velocity. The manufacturer has recommended a drop velocity range between 7 to 9 m/s (Fujifilm Dimatix, 2010).

Ink-jet Printing Mechanism

Figure 3.8 shows a cross section of the DIMATIX jetting mechanism. The process of printing starts with removing any air in the pumping chamber (priming) and it is filled with ink. Then a voltage is applied to the piezo element (PZT) causing it to bend, pushing the membrane and the fluid chamber. As a result, the ink inside the chamber is pushed resulting in droplet ejection. Next the voltage is removed, and the piezo element moves back to its original position and the ink is pulled back into the chamber. Finally, the chamber is filled with ink which is supplied from the cartridge reservoir and kept at a small negative pressure to avoid flooding at the nozzle (Fujifilm Dimatix, 2006).

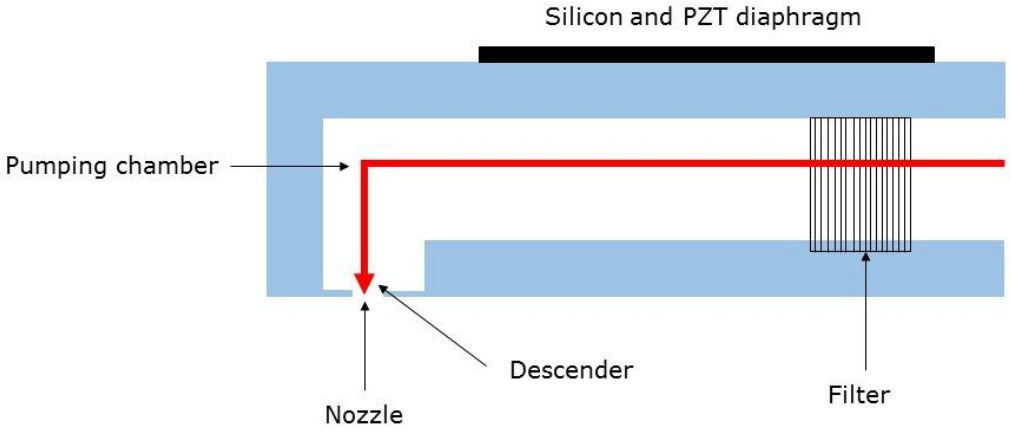


Figure 3.8: Cross section of the DIMATIX jetting mechanism (Adapted from Fujifilm Dimatix Manual, 2006)

In order to achieve optimum drops, the manufacturer has recommended ink physical properties which can be used as a guideline when formulating a new ink. Some of the important ink physical properties are summarised in Table 3.4.

Table 3.4: Ink requirements for DIMATIX ink-jet printing (Fujifilm Dimatix, 2006; Fujifilm Dimatix, 2010)

Ink Property	Manufacturer's Acceptable Range	Remarks
Viscosity	12 to 18 mPa s	**High viscosity** – Increase the cartridge temperature to reduce viscosity. **Low viscosity** – Adjust the waveform or reformulate the ink.
Surface tension	28 to 32 mN m^{-1}	**High surface tension** – The air inside the pumping chamber cannot be fully removed during the priming step and this prevents jetting. **Low surface tension** – Flooding at the nozzle.
Low volatility	Boiling point > 100 °C	**High volatility** - Ink can evaporate and form a layer around the nozzle which obstructs jetting.
Degassed	N/A	**Air/dissolved gas** - Can hinder jetting.
Particle size	Particles should not agglomerate	**High particle size** - Particles can block the nozzle.

A waveform is used to control the drop formation in a DIMATIX ink-jet printer. It consists of four segments and the zero segment is linked to the last segment (Phase 4) (Figure 3.9). The three main parameters associated with each segment in the waveform are; voltage, slew rate and duration. Voltage refers to how far the fluid chamber membrane is bent, slew rate refers to how fast it is been bent and duration refers to how long it's been bent. Table 3.5 provides an explanation of these segments in the waveform (Fujifilm Dimatix, 2006; Fujifilm Dimatix, 2010).

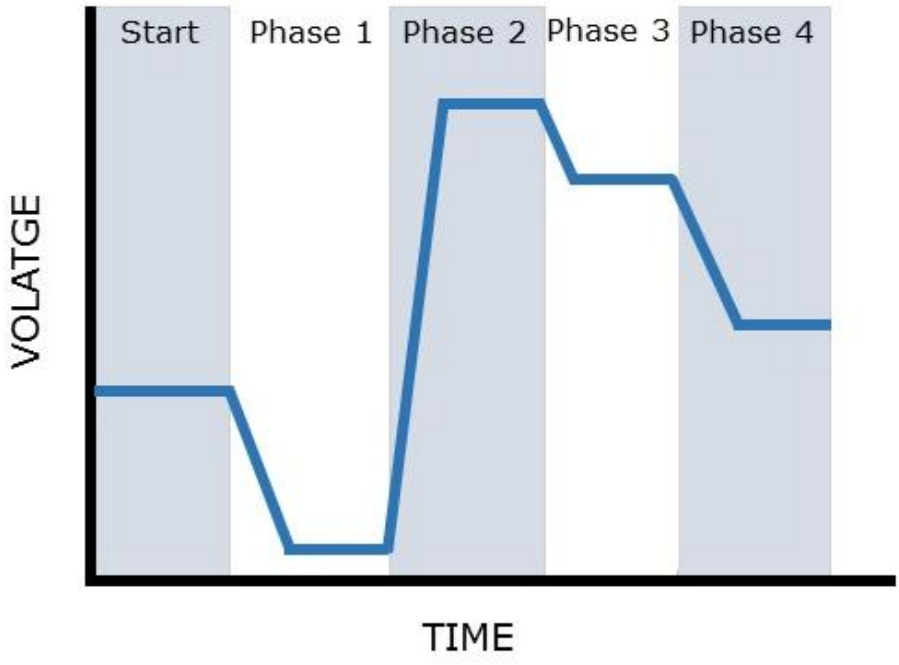
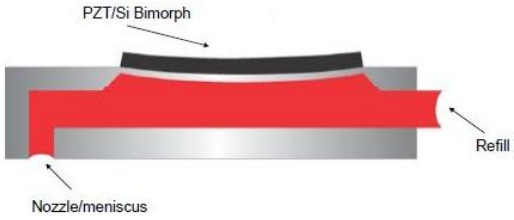
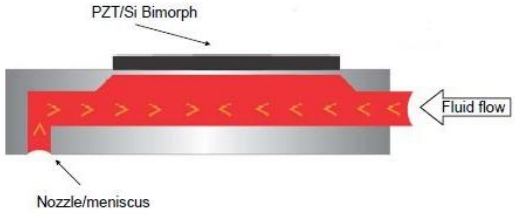
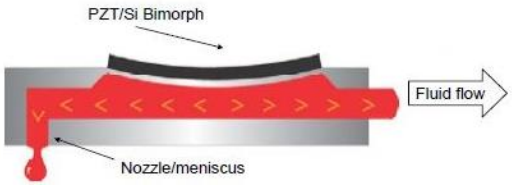
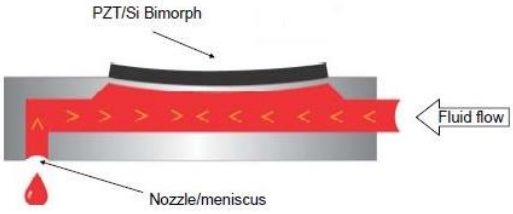


Figure 3.9: Voltage Vs time behaviour for different segments in the waveform (Adapted from Fujifilm Dimatix Manual, 2006 and 2010)

Table 3.5: Explanation of the different segments in the waveform (Fujifilm Dimatix, 2006; Fujifilm Dimatix, 2010)

Segment	Main Observations
Phase 0 (Start/Standby) 	• Initially the piezo element is slightly depressed.
Phase 1 	• Voltage decrease to zero (the piezo element returns to neutral straight/relaxed position). • Fluid chamber is filled with ink (supplied by the cartridge reservoir). • Meniscus at the nozzle pulled up.

Segment	Main Observations
Phase 2 	• Voltage increase (piezo element deflects, and the fluid chamber compressed). • Drop ejection.
Phase 3 and 4 (Return to Standby) 	• Voltage decreases (fluid chamber decompressed partially and refilled with ink). • Meniscus at the nozzle pulled back.

As explained before, cartridge settings can be changed using the cartridge settings window (Appendix Figure 9.2) and the waveform editor window (Appendix Figure 9.3). The individual amplitudes of the nozzles (jetting voltage) can be varied between 0 and 40 V and can be used to optimise the velocity of the drops. The cartridge temperature was initially set based on the ink viscosity results and later optimised depending on the ink performance. The meniscus vacuum represents the height of the meniscus at the nozzle. Next the nozzles that will be used for printing were selected (jets to use) and the cartridge print height is the distance between the print head and the substrate (varied based on the thickness of the substrate) (Fujifilm Dimatix, 2010).

The waveform (Appendix Figure 9.3), is responsible for activating the electrical signal required for drop ejection. A description of each parameter in the

waveform is provided in Table 3.6. There are two different waveforms in the waveform editor. During printing, the jetting waveform is transferred to the printing nozzles and the non-jetting waveform to the non-printing (idle) nozzles (Fujifilm Dimatix, 2010).

Table 3.6: Description of different parameters in the waveform (Fujifilm Dimatix, 2010)

Parameter	Description
Level	Percent of the amplitude relative to the value given in cartridge settings window.
Slew rate	Gradient of the line in the waveform during voltage ramps.
Duration	Length of the segment.
Duration scalar	Scale factor for the waveform pulse width.
Width	Overall pulse time width for the waveform.
Maximum jetting frequency	Should be less than the value specified in Appendix Figure 9.1.

Sabre Angle

The cartridge mounting angle also known as the sabre angle (Figure 3.7) is the angle formed between the cartridge and the printing direction. It is used to change the droplet spacing and the resolution of the final printed pattern. This is illustrated in Figure 3.10. The droplet spacing is the distance between two nozzles when the cartridge is aligned at a specific sabre angle. Therefore, it is the distance between the centre of adjacent drops in the X and Y direction. For the FUJIFILM DIMATIX-DMP 2831 ink-jet printer the relationship between the sabre angle, resolution and droplet spacing is provided in a table by the

manufacturer (Fujifilm Dimatix, 2010). A close-up view of the cartridge alignment scale, which uses a Vernier scale to change the sabre angle for the cartridge is presented in Figure 3.11.

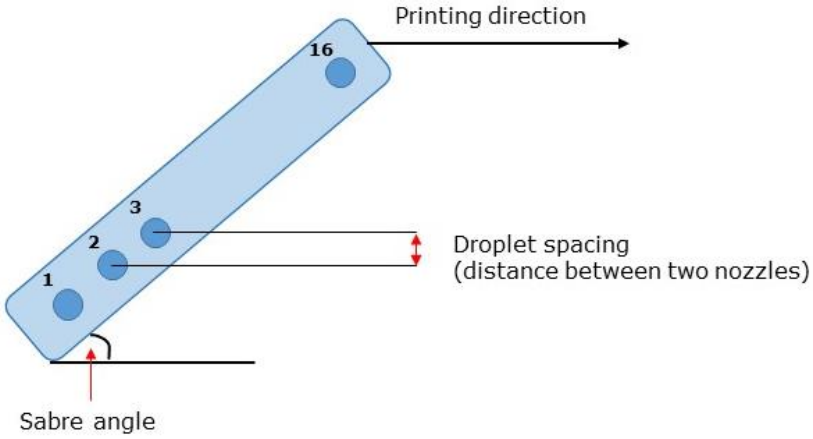


Figure 3.10: Relationship between print direction, sabre angle and droplet spacing (Adapted from Eggenhuisen T. et al., 2015)

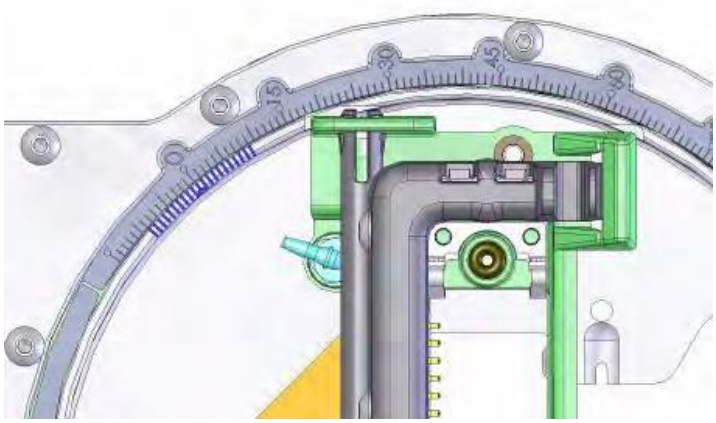


Figure 3.11: Cartridge alignment scale (Adapted from Fujifilm Dimatix Manual, 2010)

3.4.2 PICO Pulse Printing

The PICO Pulse printer used in this study was developed in the Centre for Additive Manufacturing (CfAM) laboratory using a Nordson EFD PICO Pulse valve, Nordson EFD PICO touch controller and a stage from Aerotech. High

viscosity inks (Table 3.3) were printed using this printer. Figure 3.12 shows the steps involved in loading the syringe barrel to obtaining the final printed pattern.

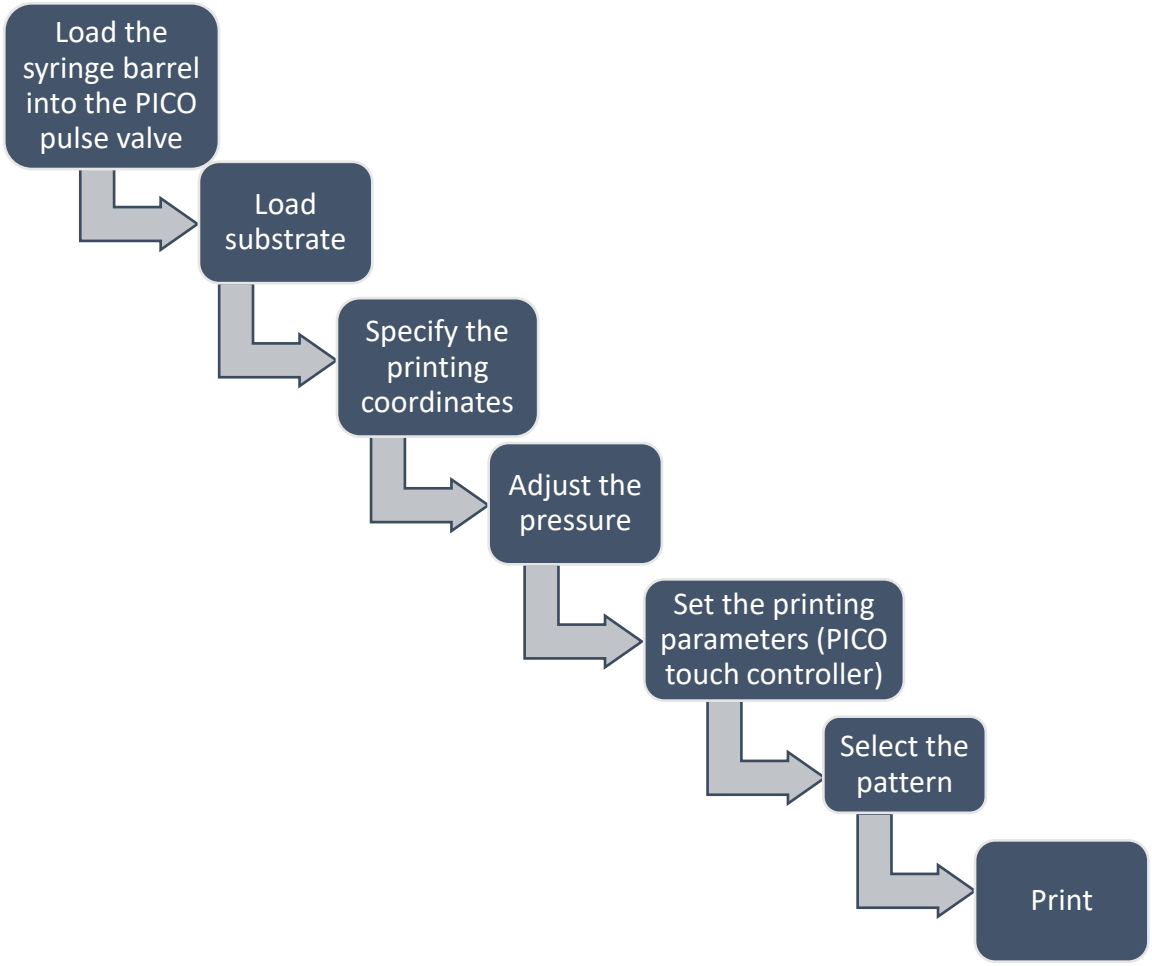


Figure 3.12 PICO Pulse printing procedure

First, the syringe barrel containing the ink was inserted into the PICO Pulse valve. This step was followed by attaching the substrate on to the substrate holder. Next, the Z coordinate of the PICO Pulse valve was adjusted and the printing coordinates (X, Y and Z) were specified into a program developed using LabVIEW. Next, the pressure required to push the ink inside the syringe barrel was adjusted using a pressure regulator. The printing parameters (valve

parameters, temperature and waveform) were then specified in the PICO touch controller and the pattern was loaded into a LabVIEW computer program along with the droplet spacing, number of layers and the frequency for the movement of the stage. Finally, the printing parameters were confirmed, and printing begins.

Major Components of the PICO Pulse Printing Set-Up

Figure 3.13 presents the major components of the PICO Pulse printing set-up (PICO Pulse valve, PICO touch controller, pressure regulator, syringe barrel, computer, substrate holder and the stage). The ink was manually filled into the syringe barrel and the surface was cleaned using a dry tissue. A piston was then inserted into the syringe barrel before inserting into the PICO Pulse valve. The piston prevents contamination (air and ink coming to contact). A pressure regulator which pushes the ink using compressed air (up to 6 bar) was then connected to the syringe barrel.

The substrate was placed on the substrate holder which was connected to a compressed air source and a computer. The compressed air pass through the holes in the substrate holder and helps to secure the substrate on the substrate holder and prevents its movement during printing. The substrate holder was attached to a stage, where the movement of the substrate in the X and Y direction can be controlled using a LabVIEW computer program. The PICO Pulse valve was mounted onto a Z stage, where its movement was again controlled using a LabVIEW program.

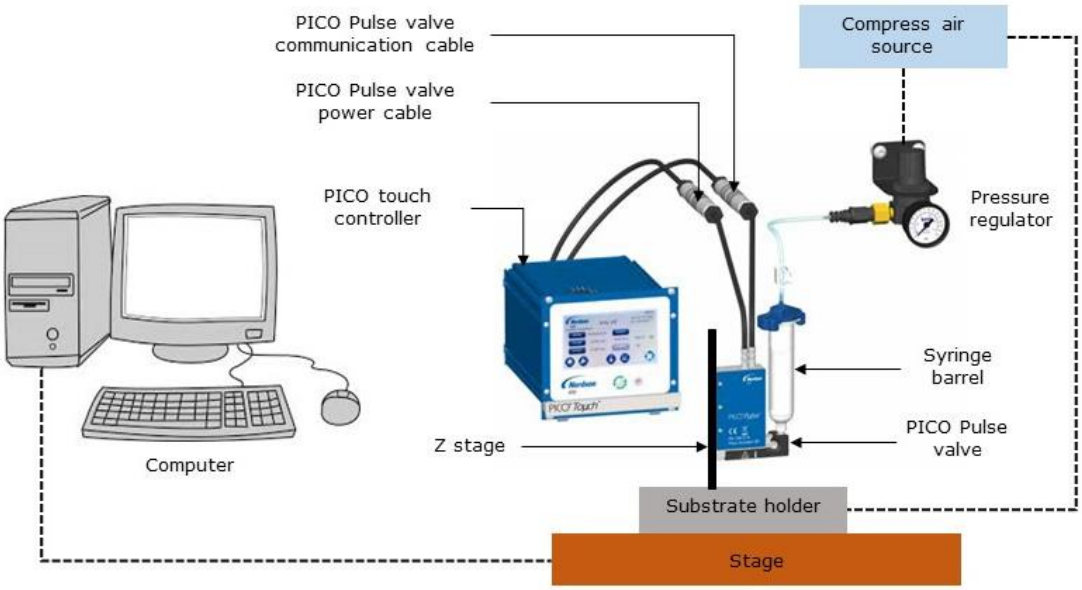


Figure 3.13: Major component of the PICO Pulse printing set-up

The PICO Pulse valve is an electrically operated, piezo-actuated dispensing valve that is used to deposit fluid, which is pneumatically supplied via a syringe barrel. The major advantages of the PICO Pulse valve include; the ability to dispense micro-deposits (0.5 nL), the fluid body assembly (Figure 3.14) can be easily dismantled to clean, jets inks with varying viscosities, can be easily added into an automated system as it has a number of mounting holes and the installation angle does not affect its performance (Nordson, 2015a).

The PICO Pulse valve system as shown in Figure 3.14, consists of a piezo actuator and a fluid body assembly. A Standard Duty (SD) piezo actuator, E seat geometry fluid body assembly (50 and 150 µm orifice) and a M5 × female Luer lock, straight, stainless steel fluid inlet fitting was used. A SD piezo actuator was used as they are designed for general purposes. The PICO Pulse valve

was connected to the the PICO touch controller where the printing parameters were specified.



Figure 3.14: PICO Pulse valve system (Adapted from Nordson, 2015a)

PICO Pulse Printing Mechanism

The piezo actuator (Figure 3.14) is responsible for driving the PICO Pulse valve. A lever positioned in the piezo actuator imparts the piezo movement to a rod. This movement is then passed on to a shutoff ball stem (made of ceramic) in the valve seat (at the lower end of the rod). When the valve is closed, the shutoff ball is lowered (nozzle closed) and when lifted, the fluid flows through the nozzle (nozzle open) (Nordson, 2015a). A schematic diagram of the PICO Pulse valve operating mechanism is illustrated in Figure 3.15.

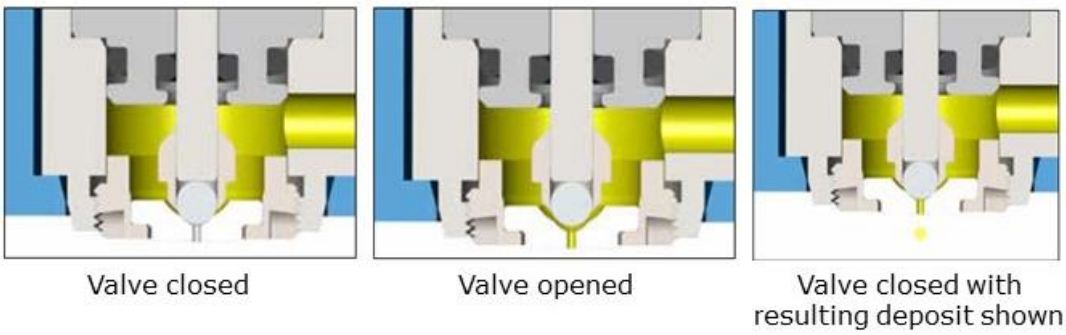


Figure 3.15: Schematic diagram of the PICO Pulse valve operating mechanism (Adapted from Nordson, 2015a)

The PICO Touch controller (Figure 3.13) is a touch screen interface that controls the PICO Pulse valve (Nordson, 2015b). A description of the printing parameters in each screen in the PICO touch controller is provided in Table 3.7.

Table 3.7: Description of PICO touch controller printing parameters (Nordson, 2015b)

Secondary Screen	Parameter	Description
Valve	Mode	System operating mode (timed, continuous)
	Pulse	Length of valve opening (minimum 100 µs)
	Cycle	Time between deposits (2 ms to 9.9999 s)
	Count	Number of deposits per cycle (1 to 9999)
	Frequency	How fast the valve is operating (in Hz) at the selected settings (green - safe operating frequency)
	Power	On – Valve closed; Off – Valve open
	Purge	Used to purge
Heaters	Mode	Turn valve heater on/off
	Setting	Heater temperature (maximum 100 °C)
	Actual	Actual temperature of the heater
Wave profile	Close volts	Voltage at which the valve closes (Higher voltage ensures good sealing force)
	Stroke	Voltage to initiate each cycle
	Open	How fast the valve opens (200 to 500 µs)
	Close	How fast the valve closes (200 to 2000 µs)

Cleaning Procedure

To ensure the nozzle and its surrounding was clean, after every print the nozzle was purged and wiped with a foam tipped bud (RS Components Ltd, UK). The following procedure was used to clean the fluid body assembly (Figure 3.14).

First the valve was purged with the ink followed by the ionic liquid (pure ionic liquid similar to that in the ink) and finally with deionised water. As the ink can

precipitate in the presence of deionised water the nozzle was first purged with ionic liquid before purging with deionised water. During this cleaning step, the valve heater was switched off and the cleaning liquids (ionic liquid and deionised water) were separately filled into two syringe barrels and the system was depressurized during installation. When necessary, pressure was used to push the cleaning fluids. Once purged with the cleaning fluids, the system was depressurized and the syringe barrel and the fluid body assembly were removed from the PICO Pulse valve (Nordson, 2015a).

The fluid body assembly was dismantled and the fluid body seat (Figure 3.16A), sealing screw, fluid inlet fitting and the cartridge were cleaned using deionised water and a brush (supplied by Nordson). Once cleaned compressed air was blown through the fluid body seat to fully dry. Finally, the fluid body assembly was assembled back (the cartridge must align with the fluid body seat as shown in Figure 3.16B (Nordson, 2015a). The fluid body assembly was then inserted into to the PICO Pulse valve and purged with ionic liquid (pure ionic liquid similar to that in the ink) followed by the ink. After cleaning the fluid body assembly, it was first purged with ionic liquid followed by the ink to ensure fluid path was fully opened as any remaining water residues can precipitate the biopolymer inside the nozzle.

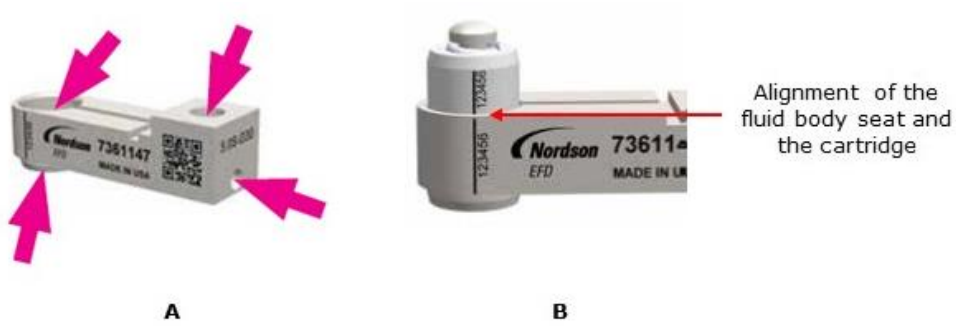


Figure 3.16: (A) Fluid body seat cleaning locations and (B) Alignment of the fluid body seat and the cartridge (Adapted from Nordson, 2015a)

3.4.3 Substrates Used for Printing

Polyethylene terephthalate (PET) and glass slides were used as the substrates. Before use the PET sheet was wiped using a polyester wipe. If glass slides were recycled, they were first washed thoroughly with deionised water followed by isopropanol and allowed to dry at room temperature. For all the printing experiments substrates were at room temperature. In the DIMATIX printer a substrate height between 100 to 200 µm was used for PET and 1200 µm for glass slides. In PICO Pulse printing a substrate height of 1.0 mm was used for glass slides.

3.4.4 Printing Summary

For DIMATIX ink-jet printing, the physical properties of the formulated inks (rheology and surface tension) were first determined to identify the inks that were within the printing range. Then, a 3 × 3 mm square having an array of single drops were printed using these inks at a droplet spacing of 150 µm. The diameter of these printed drops was measured using an optical microscope

(Nikon ECLIPSE LV100ND) and ImageJ Software. The samples were then regenerated using deionised water.

For PICO Pulse printing, the rheological properties were determined to study the ink behaviour. However, the ink viscosity does not affect its printing ability, as the PICO Pulse valve is capable of jetting inks with varied viscosities (Nordson, 2015a). The droplet formation study was carried out, where a dot pattern (16 individual drops) was printed at different temperatures (40, 65 and 90 °C), pressures (3 and 5 bar) and pulse times (0.3 and 0.7 ms). PICO Pulse printing involves a wide variety of printing parameters (Table 3.7). Therefore, optimisation of printing parameters was conducted using only three main variables. The upper, middle and lower ranges were used as a guideline for this study (Table 3.8). The diameter of the printed drops was measured using an optical microscope (Nikon ECLIPSE LV100ND) and ImageJ Software.

Table 3.8: Summary of the printing conditions used in the droplet formation study

Printing Condition	Temperature (°C)	Pressure (bar)	Pulse Time (ms)
A	40	3	0.3
B	40	5	0.3
C	40	3	0.7
D	40	5	0.7
E	65	3	0.3
F	65	5	0.3
G	65	3	0.7
H	65	5	0.7
I	90	3	0.3
J	90	5	0.3
K	90	3	0.7
L	90	5	0.7

The best printing conditions from the droplet formation study were selected for the line formation study. The droplet diameter was used to determine the droplet spacing required to achieve different droplet overlaps (20, 40, 60 and 80 %) (calculated using Equation 5) and lines were printed at these droplet spacing's. The intention here was to optimise the droplet spacing that is required to print a uniform line. Again, the average line width was measured using an optical microscope (Nikon ECLIPSE LV100ND) and the best printing conditions were selected for the film formation study. The final printing parameters were selected based on the quality of the printed films, and it was used to print films with 1 and 5 layers (9.2×9.2 mm) which were then regenerated using deionised water.

$$\text{Droplet spacing} = \text{Droplet diamter}\left(1 - \frac{\text{overlap}}{100}\right) \qquad \text{(Equation 5)}$$

3.5 Regeneration

The printed samples were regenerated by immersing in deionised water. As the dimensions of the ink-jet printed and PICO Pulse printed samples were not similar, two different approaches were used.

For the ink-jet printed samples the main aim was to vary the time for which the printed pattern was soaked in water. The ink-jet printed samples were regenerated by adding 0.1 mL of deionised water at room temperature. Deionised water was left on the ink-jet printed samples for different time

intervals (30 minutes, 1 hour, 1 hour 30 minutes or 2 hours) before heating in an oven at 50 °C (Lenton) for approximately 18 hours.

PICO Pulse printed samples were treated in three different ways to investigate the best method to regenerate the biopolymer.

- **Straight regeneration (straight regen)** – Immediately after printing the samples were soaked in deionised water for 15 minutes and then left at room temperature.
- **Overnight drying, regeneration and leave at room temperature (O.D, regen and rtm)** – Printed samples were dried overnight at room temperature, soaked in deionised water for 15 minutes and then left room temperature.
- **Overnight drying, regeneration and leave in the vacuum oven (O.D, regen and vac. oven)** – Printed samples were dried overnight at room temperature, soaked in deionised water for 15 minutes and then transferred into a vacuum oven (Thermo Scientific) for 30 minutes.

The term 'overnight drying' was used to describe samples that were PICO Pulse printed and left drying overnight at room. The properties of the samples obtained after immersing in deionised water were examined using different characterisation methods which will be discussed next.

3.6 Evaluation of Ink Physical Properties

This section will provide a brief summary of the techniques used to determine the physical properties of the inks. These include; Coulometric Karl Fischer titration, rheology, surface tension and density.

3.6.1 Coulometric Karl Fischer Titration

Method

Coulometric Karl Fischer titration is used to determine the water (moisture) content in different substances. The apparatus consists of an anode and a cathode chamber. The anolyte in the anode chamber consist of a solvent (methanol or ethanol), a base (imidazole), sulphur dioxide (SO_2) and iodide salts. As shown in Equation 6, electrochemical oxidation results in the generation of iodine in the anode chamber. The catholyte in the cathode chamber facilitates the completion of the electrochemical reaction where, hydrogen ions (H^+) are reduced to hydrogen gas (H_2) (Equation 7) (Dominguez V. *et al*., 2010; Mettler Toledo, 2011).

Anode reaction: $2\mathrm{I}^- \rightarrow \mathrm{I}_2 + 2\mathrm{e}^-$ (Equation 6)

Cathode reaction: $2\mathrm{H}^+ + 2\mathrm{e}^- \rightarrow \mathrm{H}_2$ (Equation 7)

The solvent (ROH), sulphur dioxide and the base (B) reacts to form alkylsulfite (Equation 8). When the sample is injected into the system, water in the sample reacts with alkylsulfite and iodine to form alkylsulfate (Equation 9) (Dominquez V. *et al*., 2010).

$$ROH + SO_2 + B \rightarrow BH^+ + RSO_2^- \quad \text{(Equation 8)}$$

$$H_2O + RSO_2 + I_2 + 2B \rightarrow 2BH^+I^- + RSO_3^- \quad \text{(Equation 9)}$$

The water content in the sample is calculated by the current required to produce iodine. According to the Faraday constant, each mole carries a charge of 96,485 C. From Equation 6 and 9, 2 moles of iodide ions are needed to produce 1 mole of iodine, which reacts with, 1 mole of water. Therefore, 192,970 C/mol needed to react with 1 mole of water. Considering the molar mass of water (18.015 g/mol), this equates to the consumption 10.712 C of electrical current for every 1 mg of water (Mettler Toledo, 2011).

Experimental Procedure

Water content of the ionic liquids was determined by a Mitsubishi CA100 Coulometric Karl Fischer titration, and the procedure is summarised in Figure 3.17. A 1 mL ink-jet syringe (with a needle attached at the end) was used to draw out approximately 1 mL of ionic liquid. Excess ionic liquid around the needle and syringe was cleaned using a dry tissue. The system calculates the water content in the sample using the following equation;

$$\text{Water content (ppm)} = \frac{\text{Microgram count}}{W - w} \quad \text{(Equation 10)}$$

Where, W is the weight of the ionic liquid and syringe and *w* is the weight of the empty syringe (O,Mahony A. *et al*., 2008). The water content in ppm is converted to a percentage using the following conversion; 1 % = 10,000 ppm.

All the measurements were carried out in triplicate and the average was recorded.

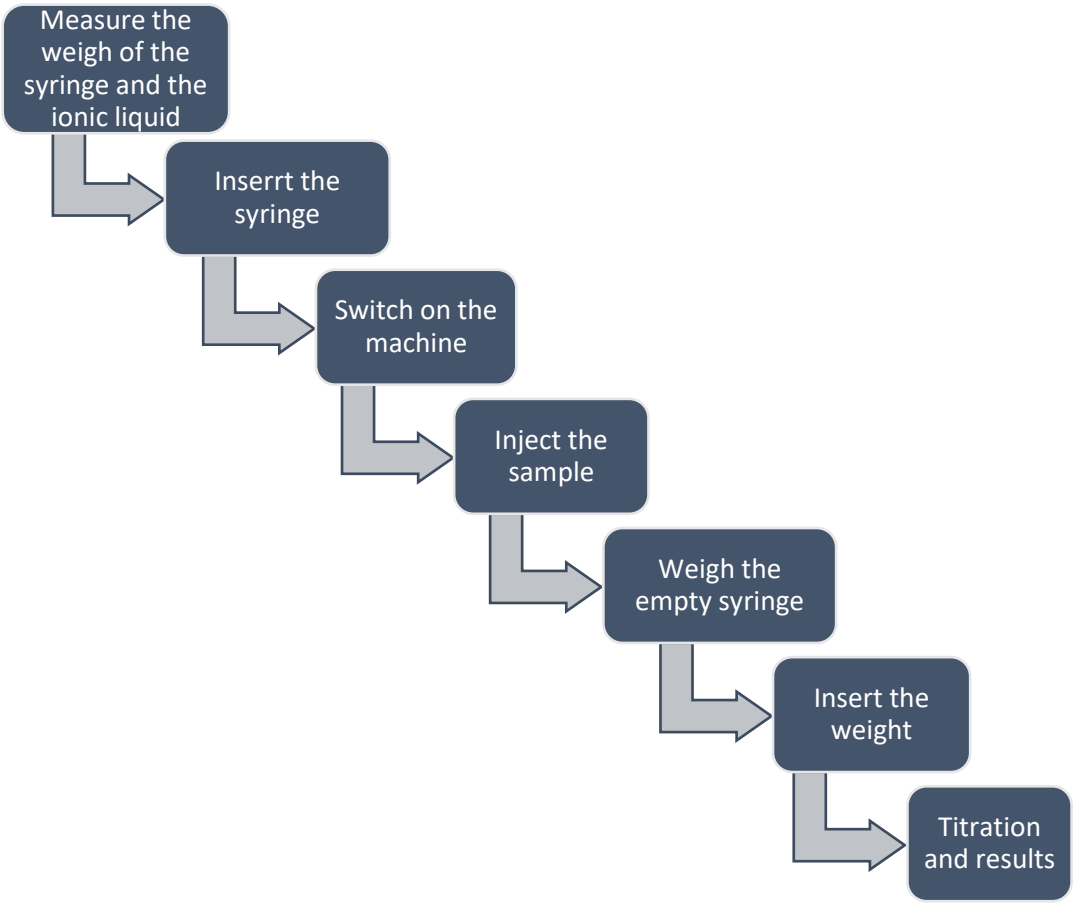


Figure 3.17: Coulometric Karl Fischer titration procedure

3.6.2 Rheology

Method

Rheology is the study of flow and deformation of materials, and viscosity is resistance to this flow (Barnes H., 2000). Viscosity measurements were carried out using a rotational rheometer from Malvern Kinexus, using a cone-plate geometry (cone angle 4 ° and cone diameter 40 mm) and a cup and bob geometry (cup size of C14 (DIN) and bob diameter of 14 mm) (Figure 3.18). In

the cone-plate geometry, the cone is truncated so that the tip does not touch the plate, and this prevents it from wearing. Therefore, a gap size of 0.15 mm was used. In a rotational rheometer a torque is applied, and the viscosity of the sample can be calculated at a given shear rate or shear stress (Barnes H., 2000).

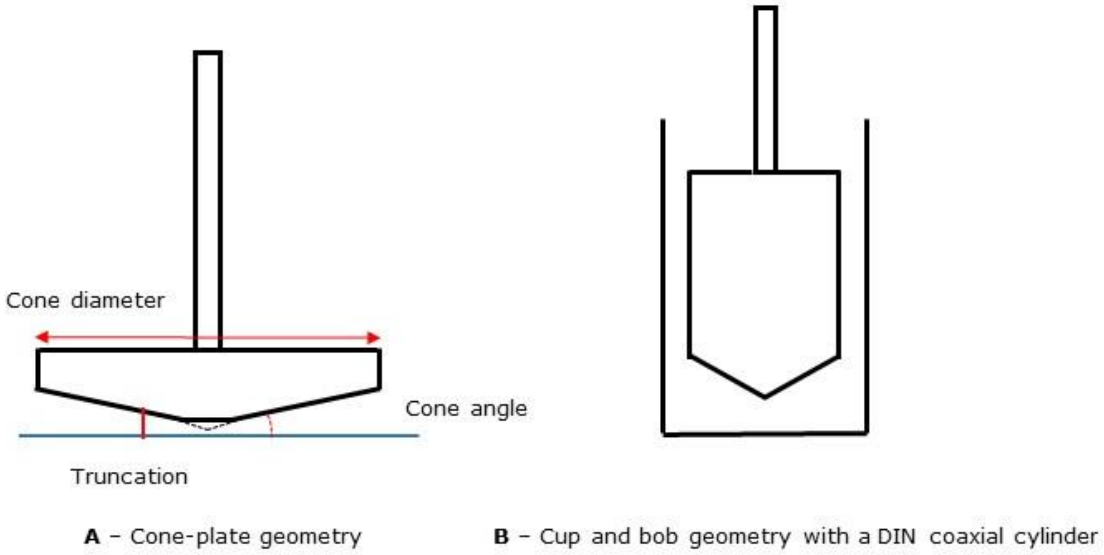


Figure 3.18: Rotational rheometes used (Adapted from Bohlin Instruments Limited, 1994)

For Newtonian fluids, shear stress (σ) is proportional to shear rate (γ) (Equation 11) and for Non-Newtonian fluids, a power law fluid model (like Ostwald de Waele) can be used to calculate the viscosity (Equation 12).

Newtonian fluids: $\sigma = \eta\gamma$ (Equation 11)

Non-Newtonian fluids: $\eta = m\gamma^{n-1}$ (Equation 12)

Where η is the viscosity and n is the power law index. Equation 12 can be rearranged on a log scale to give Equation 13. The gradient from this graph can be used to determine the material properties. When $n < 1$ the material is shear

thinning and when $n > 1$ the material is shear thickening (Bohlin Instruments Limited, 1994; Barnes H., 2000).

$$\log \eta = \log m + (n-1)\log \gamma \qquad \text{(Equation 13)}$$

Experimental Procedure

The cone-plate geometry was used to measure the viscosities of the chemicals (ionic liquids, deionised water), low viscosity (Tables 3.1 and 3.2) and high viscosity inks (Table 3.3) and cup and bob geometry was used to measure the viscosities of the co-solvents (DMSO and 1-butanol). A summary of the operating procedure for the rheometer is given in Figure 3.19. The location of the environment controller and the geometry (cone-plate or cup and bob) is shown in Figure 3.20.

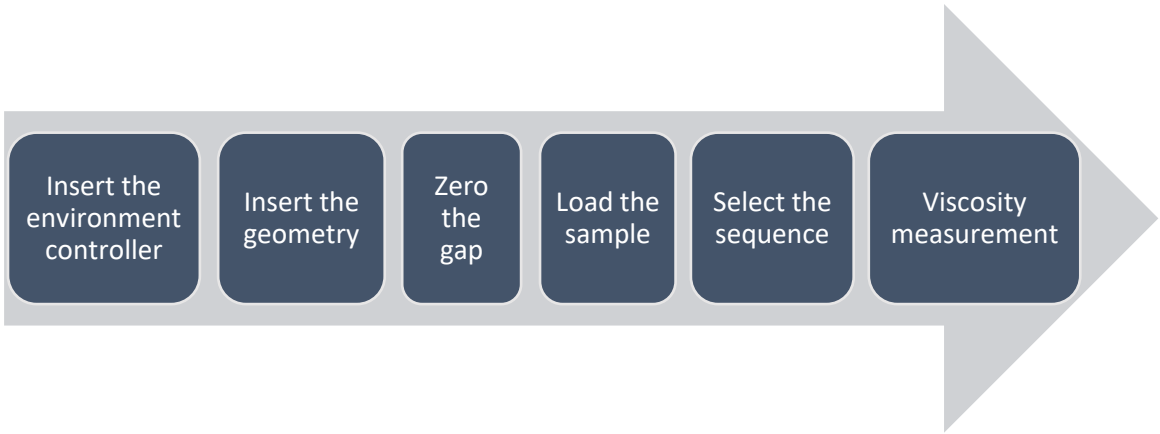


Figure 3.19: Malvern Kinexus rotational rheometer operating procedure



Figure 3.20: Malvern Kinexus rotational rheometer front view

The cone-plate geometry and the cup and bob geometry required approximately 1.19 and 3.5 mL of sample respectively. In the cone-plate geometry excess sample (during sample loading) was cleaned using a dry tissue. The operation of the rheometer was monitored real time using the rSpace software. The sequence in the rSpace software contained the information relevant for the measurements (Table 3.9). All the rheological properties were measured in triplicate using a new sample each time and the average viscosity at the highest shear rate was used, except for sample 2 (Table 3.1) where the average viscosity was calculated at a shear rate of 631 s^{-1}.

Table 3.9: Summary of shear rate and temperature ranges used

Sample Type	Shear Rate Range	Temperature Range
Pure chemicals	10 to 1000 s^{-1}	25°C
Low viscosity inks	1 to 1000 s^{-1}	60°C
High viscosity inks	1 to 100 s^{-1}	40 to 90°C

3.6.3 Surface Tension

Method

Surface tension governs the shape of a liquid drop. A pure liquid has a zero net force since all the molecules are been equally pulled in different directions by the neighbouring molecules. At the same time the molecules near the surface experience an unbalanced net force due to the absence of neighbouring molecules in all the directions (Figure 3.21). Therefore, the neighbouring molecules pulls them inwards causing an internal pressure. This results in the droplet shrinking its surface to attain the lowest surface free energy, also known as the surface tension (Yuan Y. and Lee R., 2013).

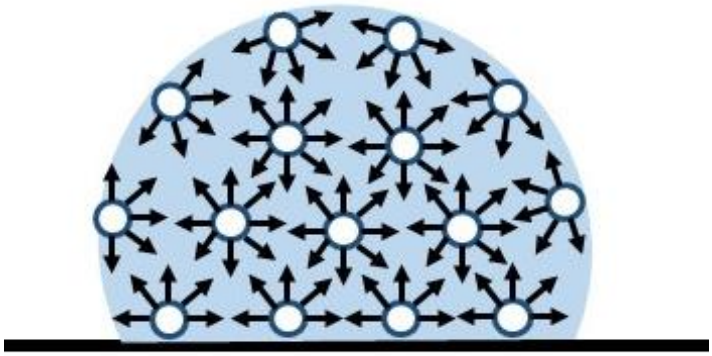


Figure 3.21: Forces acting on a liquid drop (Adapted from Yuan Y. and Lee R., 2013)

A drop suspended from another drop is defined as a pendant drop and its shape at equilibrium is governed by surface tension or interfacial tension and gravity (Song B. and Springer J., 1996; Arashiro E. and Demarquette N., 1999; Berry J. *et al*., 2015). The pendant drop method uses the Young-Laplace equation to calculate the surface tension or interfacial tension. A drop shape analyser captures an image and a drop profile is extracted from it. Then, the Young-

Laplace equation is iteratively solved using an automated computerized method (Berry J. *et al*., 2015).

Experimental Procedure

Surface tension of the pure chemicals (ionic liquids, co-solvents and deionised water) and the low viscosity inks (Table 3.2), was measured at room temperature (assumed to be 25 °C) using a KRUSS DSA100 drop shape analyser. The Young-Place equation was iteratively solved real time by the KRUSS DSA software. The major components of the KRUSS DSA100 drop shape analyser are shown in Figure 3.22.

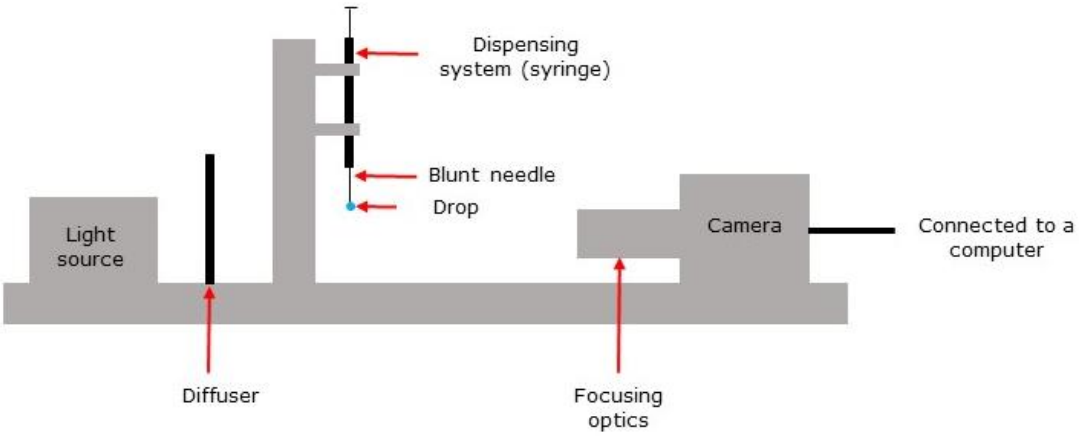


Figure 3.22 Major components of the KRUSS DSA100 drop shape analyser (Adapted from Berry J. *et al*., 2015)

A brief summary of the experimental procedure is illustrated in Figure 3.23. Approximately, 1 mL of the sample was loaded into an ink-jet syringe and inserted into the dispensing system. Drop ejection was achieved by specifying a dosing volume and using an automatic dosing system (controlled by the KRUSS DSA100 software) to push the syringe, until a drop was suspended from

the needle with the maximum volume. Measurements were taken six times and the average was recorded.

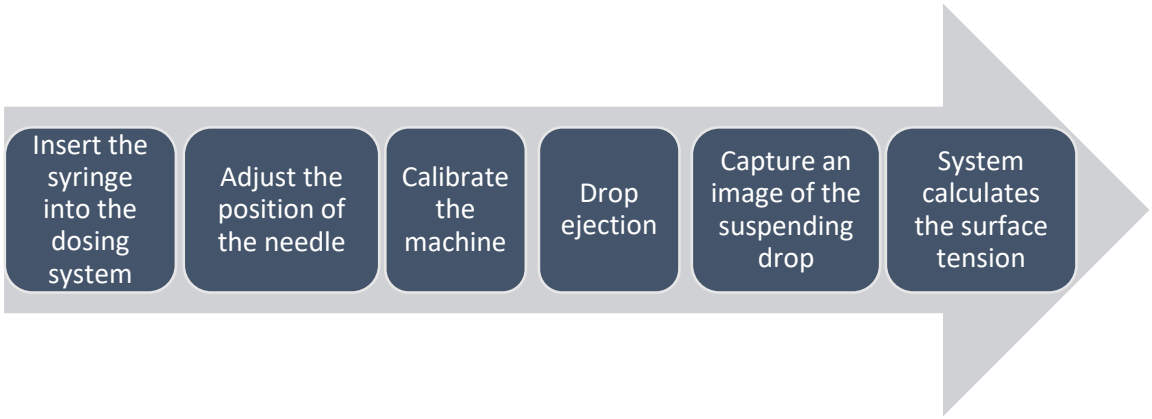


Figure 3.23: KRUSS DSA100 drop shape analyser operating procedure

3.6.4 Density

Density of the pure chemicals were used along with the mass or volume of each chemical used in the formulation to calculate the theoretical densities (Equation 14). Experimental densities were calculated by measuring the mass of either 0.2 or 0.5 mL of ink. All the experimental density measurements were carried out in triplicate and the average was recorded.

$$\text{Density} = \frac{\text{Total mass}}{\text{Total volume}} \qquad \text{(Equation 14)}$$

3.7 Optical Characterisation

Optical images of the printed samples were obtained using a microscope (Nikon ECLIPSE LV100ND). Scanning electron microscope (SEM) images of untreated cellulose were obtained from a Hitachi TM3030 TableTop SEM and for regenerated samples using a Philips XL30 SEM.

Surface profile analysis of the regenerated samples was performed using a white light interferometry (WLI) from Bruker Contour GT. This is a non-contact method that can be used to measure the height of a sample quickly. A beam splitter is used to divide the white light between the sample and a reference mirror. The reflected light from these two surfaces combine to form an interference pattern known as a 'fringe'. This Interference data is captured at regular time intervals and analysed by a computer algorithm (Devillez A. *et al*., 2004).

All regenerated samples analysed using the SEM and WLI were coated with platinum to ensure reduced charging during SEM and provide reflectivity for WLI.

3.8 Other Characterisation Methods Used

This section will provide a brief summary of the characterisation techniques used on pure chemicals, inks and the regenerated materials. These include; Thermogravimetric analysis (TGA), Fourier transform infrared (FTIR) spectrometer and Elemental analysis.

3.8.1 Thermogravimetric Analysis (TGA)

Method

TGA measures the mass of a sample as its temperature is changed using a temperature controlled program. The sample is placed in a thermo-balance (analytical balance coupled with an electronically programmed furnace). The

outputs from the TGA experiment can be displayed as an integral or a differential thermogravimetric curve. The integral form also known as the TGA curve, plots the mass or the percentage mass (mass divided by the mass at time zero) against time or temperature. The differential curve also known as the DTG curve, is the derivative of the TG curve (Vyazovkin S., 2012). In this work degradation temperature is defined as the temperature where the maximum degradation occurred (highest downward peak in the DTG curve) (Cao Y. and Mu T., 2014).

Experimental Procedure

TGA for the pure chemicals (cellulose, wool and ionic liquids) and the regenerated samples (obtained by immersing the PICO Pulse printed samples in deionised water) was performed using a Perkin Elmer Thermogravimetric Analyser TGA 4000. The weight loss was measured real time using the TGA software. All the samples were heated from 50 to 900 °C at a heating rate of 10 °C/minute. In order to maintain consistency of the analysis the sample weight was kept at 12 mg throughout all the experiments. Cellulose drying time was determined by performing a TGA at isothermal conditions (constant temperature of 100 °C) and a holding time of 45 minutes. All the TGA experiments were conducted under air except for pure wool, where a nitrogen flow rate of 20 mL/min was used.

3.8.2 Fourier Transform Infrared (FTIR) Spectrometer

Method

FTIR uses ATR (attenuated total reflectance) technique to produce a spectrum of the sample. As show in Figure 3.24, infrared radiation (IR) is directed at the ATR crystal and this reflect from the crystal creating an evanescent wave on the sample. The reflected energy from the evanescent wave passes through a detector (Barbes L. *et al*., 2014). The detector covert this energy to a spectrum showing the absorbance against the wavenumber. Since, each molecule has a specific IR range this can be used to identify the molecules present in the sample (ThermoFischer Scientific, 2013).

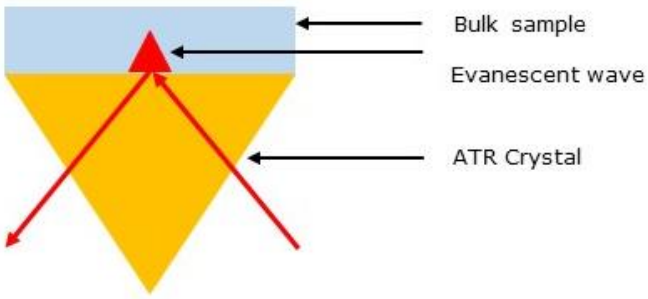


Figure 3.24: ATR technique (Adapted from Barbes L. *et al*., 2014)

Experimental Procedure

FTIR spectrum for the pure chemicals (cellulose and ionic liquids) and the regenerated samples (obtained by immersing the PICO Pulse printed samples in deionised water) was obtained using a Frontier FTIR spectrometer from Perkin Elmer and the measurements were recorded by the FTIR software. Wavenumber range from 550 to 4000 cm^{-1} was used for all the samples. A total of 5 scans were performed and baseline corrected to obtain the final spectrum.

3.8.3 Elemental Analysis

Method

Elemental microanalysis was used to determine the carbon, hydrogen and nitrogen composition in a sample. Here the sample is combusted in the presence of pure oxygen gas in a high temperature furnace (975 °C). The products obtained from combustion is detected by thermal conductivity detectors which record the carbon, hydrogen and nitrogen content in the sample.

Experimental Procedure

Elemental analysis was performed on the pure chemicals (cellulose and ionic liquid), high viscosity formulations (Table 3.3) and regenerated samples using a CE440 elemental analyser from Exeter Analytical. All the measurements were carried out in duplicate and the average was recorded.

Chapter 4 : Three-Dimensional DIMATIX ink-jet Printing of Cellulose using Ionic Liquids and Co-Solvents

4.1 Background

Cellulose dissolution using ionic liquids have been well-documented in the literature over the past few decades (Chapter 2 Section 2.6). In this chapter cellulose was dissolved in the ionic liquids $[C_2C_1Im][OAc]$ and $[C_4C_1Im][OAc]$; with the co-solvents, 1-butanol and DMSO used as rheological modifiers to ensure consistent printing. An attempt was made to print these inks (cellulose + ionic liquid + co-solvent) using a FUJIFILM DIMATIX ink-jet printer. Successfully printed samples were immersed in deionised water to remove the ionic liquid and the resulting structural changes were assessed using SEM and WLI.

4.2 Justification

4.2.1 Cellulose Selection

As discussed in Chapter 2 Section 2.2.1, depending on the particle size (nano, micro and macro), cellulose forms nine different particle types (Moon R. *et al*., 2011). The most commonly used cellulose type for cellulose dissolution using ionic liquids has been microcrystalline cellulose (MCC) (Table 2.3). Therefore, MCC was selected for this study.

MCC is manufactured under different brand names (Avicel, Emcocel, Microcel, Vivapur) and is widely used in the pharmaceutical and food industries (Levis S. and Deasy P., 2001; Moon R. *et al*., 2011; Vehovec T. *et al*., 2012; Thoorens G. *et al*., 2014). It is made up of aggregated bundles of cellulose crystallites giving rise to a porous nature (Levis S. and Deasy P., 2001).

4.2.2 Ionic Liquid Selection

Based on the literature review conducted in Chapter 2 Section 2.6, short chain imidazolium cations coupled with an acetate or chloride anion exhibited excellent cellulose dissolution. Table 4.1 presents a summary of the physical properties of some these ionic liquids.

Even though other ionic liquids may have shown good cellulose solubility, they have been poorly characterised in terms of their physical properties. According to Fendt S. *et al*., (2011), the major disadvantages of using chloride anion-based ionic liquids compared to acetate anion-based ionic liquids include that they exist as solids at room temperature with higher viscosities, and that they are hygroscopic. Other studies have also made similar conclusions about chloride anion-based ionic liquids (Fukaya Y. *et al*., 2006; Zhao H. *et al*., 2008; Vitz J. *et al*., 2009).

Table 4.1: Physical properties of commonly used ionic liquids

Ionic Liquid	Water Content	Temperature (°C)	Viscosity (mPa s)	Surface Tension (mN m^{-1})	Reference
[AMIM][Cl]		30	685		Zhang H. *et al*., (2005)
		25	2090		Fukaya Y. *et al*., (2006)
	0.59 %ww	33.85	790[a]		Lopes J. *et al*., (2016)
$[C_2C_1Im][Cl]$		79.85	96[b]		Chen T. *et al*., (2010)
		79.85	62[c]		Chen T. *et al*., (2010)
		80	65		Fendt S. *et al*., (2011)
	0.0076 mass%	60.05		62.60	Součková M. *et al*., (2017)
	0.0076 mass%	60.05		62.56	Součková M. *et al*., (2017)
$[C_4C_1Im][Cl]$		24.85		48.2	Ghatee M. and Zolghadr A., (2008)
		80	142		Fendt S. *et al*., (2011)
		40	625		El Seoud O. *et al*., (2011)
		75	217		Hiraga Y. et al., (2017)
	0.03 mass%	35.08		49.64	Součková M. *et al*., (2017)
	0.03 mass%	29.96		50.32	Součková M. *et al*., (2017)
$[C_2C_1Im][OAc]$		20	162		Bonhôte P. *et al*., (1996)
	1.2 mass%	25	162		Fendt S. *et al*., (2011)
	0.124 wt%	25	143.61		Freire M. *et al*., (2011)
		25		38.1	Guan W. *et al*., (2011)
	0.046 wt%	24.95		47.1	Almeida H. *et al*., (2012a)

Ionic Liquid	Water Content	Temperature (°C)	Viscosity (mPa s)	Surface Tension (mN m^{-1})	Reference
$[C_2C_1Im][OAc]$	0.13 mass%	25	132.91	42.9	Quijada-Maldonado E. *et al*., (2012)
		25		38.2	Ma X. *et al*., (2013)
	0.12 mass%	25	139	47.1	Castro M. *et al*., (2014)
	0.09 mass%	25	138.4		Pinto A. *et al*., (2014)
	0.125 mass%	25	141.1		Nazet A. *et al*., (2015)
$[C_4C_1Im][OAc]$	1.1%	24.85	440		Crosthwaite J. *et al*., (2005)
		40	81		El Seoud O. *et al*., (2011)
	0.85 mass%	25	485		Fendt S. *et al*., (2011)
		25		35.2	Guan W. *et al*., (2011)
	0.085 wt%	25	297	36.4	Almeida H. *et al*., (2012b)
		25		39.2	Xu A. *et al*., (2012a)
		30	288.8		Xu A. *et al*., (2012b)
		25		35.4	Ma X. *et al*., (2013)
		20	549.9		Haghtalab A. and Shojaeian A., (2014)
	0.03 mass%	25	447.5	37.61	Safarov J. *et al*., (2014)
	0.027 %	20	592.3		Hiraga Y. *et al*., (2015)

[a] – Measured under vacuum
[b] – Simulation value
[c] – Experimental value

From the ionic liquid physical properties summary presented in Table 4.1, it is evident that acetate anion-based ionic liquids have low viscosities at lower temperatures compared to the chloride anion-based ionic liquids. As the ink needs to be within the operating viscosity range of the DIMATIX ink-jet printer, it is not recommended to use an ionic liquid that has a higher viscosity at room temperature. This is because the solution viscosity increases during the dissolution process (Zhang H. *et al*., 2005) and as the cellulose loading is increased (Hermanutz F. *et al*., 2008; Kosan B. *et al*., 2008; Chen X. *et al*., 2009; Gericke M. *et al*., 2009a; Gericke M. *et al*., 2009b; Quan S. *et al*., 2010; Sescousse R. *et al*., 2010; Liu Z. *et al*., 2011; Lu F. *et al*., 2014b).

Acetate anion-based ionic liquids like $[C_2C_1Im][OAc]$ exist as a liquid at room temperature. They are biodegradable, non-toxic and non-corrosive (Hermanutz F. *et al*., 2008; Zavrel M. *et al*., 2009; Liebert T., 2010). In terms of the cation chain length it was found that, longer imidazolium cation length resulted in an increased toxicity (Docherty K. *et al*., 2005). Therefore, it is recommended to use a short alkyl chain based ionic liquid. A study conducted on aquatic toxicity of ionic liquids found that aquatic toxicity increased in the following order; ammonium, pyridinium, imidazolium, triazolium and tetrazolium. Imidazolium ionic liquids also, exhibited higher aquatic toxicity compared to commonly used solvents like acetonitrile, acetone and methanol (Couling D. *et al*., 2006).

Therefore, considering all the factors discussed above both $[C_2C_1Im][OAc]$ and $[C_4C_1Im][OAc]$ were selected for cellulose dissolution. Both these ionic liquids exist as a liquid at room temperature. Therefore, they don't need to be heated to convert to liquid state before dissolving in the biopolymer. Also, successful regeneration of cellulose dissolved in an imidazolium cation-based ionic liquid (Chapter 2 Section 2.7) means that the biopolymer becomes a solid when added to an anti-solvent bath after printing. However, modifications to the choice of ionic liquid can be made in the future when an efficient 3DP and regeneration system is developed.

4.2.3 Co-Solvent Selection

When a co-solvent is added to a cellulose ionic liquid system it should not have any effect on cellulose dissolution (Fort D. *et al*., 2007; Brown E. *et al*., 2012). However, the purpose of the co-solvent is to facilitate cellulose swelling (Quan S. *et al*., 2010) and reduce the solution viscosity (Heinze T. *et al*., 2005; Fort D. *et al*., 2007; Gericke M. *et al*., 2009b; Quan S. *et al*., 2010; Fendt S. *et al*., 2011; Brown E. *et al*., 2012; Olsson C. and Westman G., 2013; Andanson J. *et al*., 2014; Sweely K. *et al*., 2014) without causing the cellulose to precipitate (Heinze T. *et al*., 2005; Gericke M. *et al*., 2009b). According to Brown E. *et al*., (2012), the decrease in the solution viscosity was due to the reduction in the quantity of ionic liquid used for cellulose dissolution. However, Pinkert A. *et al*., (2009) suggest that a co-solvent is able to reduce the aggregation of ions and thereby reduce the ionic liquid viscosity.

Co-solvents like, dimethyl sulfoxide (DMSO) (Heinze T. *et al*., 2005; Fort D. *et al*., 2007; Gericke M. *et al*., 2009b; Quan S. *et al*., 2010; Brown E. *et al*., 2012; Andanson J. *et al*., 2014; Sweely K. *et al*., 2014), lithium salts (*e.g.* lithium acetate, lithium chloride, lithium bromide, lithium perchlorate and lithium nitrate) (Xu A. *et al*., 2010), *N,N*-dimethylformamide (DMF) (Gericke M. *et al*., 2009b), γ-butyrolactone (Brown E. *et al*., 2012), ethanol (Sweely K. *et al*., 2014) and acetonitrile (Brown E. *et al*., 2012; Sweely K. *et al*., 2014) have been used in literature for cellulose ionic liquid systems. However, DMSO has been commonly used to successfully dissolve cellulose and reduce the viscosity of the resulting solutions. Hence, DMSO was selected as a starting co-solvent. A common solvent available in the laboratory (1-butanol) was also used to investigate its suitability in reducing the cellulose ionic liquid solution viscosity.

The purpose was the co-solvent was to reduce the viscosity of the ionic liquid and cellulose solution without causing cellulose to precipitate. As reported previously the co-solvent can reduce the aggregation of ions. Therefore, it is crucial to monitor the quantity of co-solvent added as too much can destroy the ionic properties of the ionic liquid and turns the solution to an organic solvent. The co-solvent was added in increments in order to investigate the optimum quantity that is needed to reduce the viscosity within the printing range and still retain the ionic liquid properties.

4.2.4 Anti-Solvent Selection

Several different anti-solvents have been used in literature for cellulose regeneration from ionic liquids (Table 2.5). According to a molecular simulation study conducted by Gupta and co-workers on cellulose regeneration (from a cellulose and $[C_4C_1Im][OAc]$ mixture) using different anti-solvents (water, ethanol and acetone), they concluded that complete cellulose regeneration occurred in the presence of water. This is because the interaction between cellulose-ionic liquid was weakest in the presence of water and the interaction between cellulose-cellulose was strongest in the presence of water. Therefore, water had the highest ability in breaking the cellulose-ionic liquid hydrogen bonds and forming cellulose-cellulose hydrogen bonds (Gupta K. *et al*., 2013a).

Another molecular simulation study conducted by the same group concluded that, the dissolution mechanism was governed by the interaction between the acetate anion and cellulose. The regeneration mechanism was due to destruction of hydrogen bonds between cellulose and acetate anion, and reformation of hydrogen bonds between cellulose (cellulose-cellulose) and acetate anion and water. Also, increasing the water concentration (cellulose acetate hydrogen bonds decrease and cellulose-cellulose hydrogen bonds increase) and temperature (cellulose contacts increases) both resulted in an increase in regeneration (Gupta K. *et al*., 2013b).

4.3 Results and Discussion

4.3.1 Physical Properties and Printability Parameter for Pure Chemicals

Physical properties and the printability parameter for the pure chemicals used are shown in Table 4.2. The printability parameter, *Z*, which is a combination of physical properties of the fluid was calculated using Equation 4 (sample calculation provided in Appendix). The characteristic length d was taken as the length of the nozzle, which was 21 µm.

Table 4.2: Physical properties and printability parameters of the pure chemicals used

Chemical	Density (g cm^{-3})	Viscosity at 25 °C (mPa s)	Surface Tension (mN m^{-1})	Printability Parameter, *Z*
$[C_2C_1Im][OAc]$	1.0	85.47 ± 5.03	39.94 ± 0.54	0.34
$[C_4C_1Im][OAc]$	1.1	278.00 ± 15.74	30.30 ± 0.78	0.093
Deionised Water	1.0	2.99 ± 0.31	71.64 ± 0.51	13
DMSO	1.1	4.11 ± 1.03	29.99 ± 1.01	6.4
1-Butanol	0.81	4.31 ± 0.01	30.12 ± 0.91	5.2

Densities of the pure chemicals were obtained from the Material Safety Data Sheets (MSDS). Ionic liquids are hygroscopic, and it is generally recommended to use a closed rheometer (Vitz J. *et al*., 2009). Therefore, all the viscosity measurements were conducted using a closed system. Cup and bob geometry was used to measure the viscosities of the co-solvents to avoid evaporation. This evaporation may be due to the volatile nature of the co-solvents and may be due to the smaller sample volume (1.19 mL) used in the cone plate method compared to cup and bob method (3.5 mL). It was assumed that room temperature was 25 °C and this was used to measure the viscosities and surface

tension of the pure chemicals. The shear rate experienced by the ink during printing (10^5 s^{-1}) is much higher (de Gans B. *et al*., 2004) than the range that can be measured from the rheometer. In addition, increasing the shear rate to a higher value can result in material splashing and this reduces the accuracy of the measurements. Therefore, a shear rate range of 10 to 1000 s^{-1} was used and the average viscosities in Table 4.2 was recorded at the highest shear rate.

Both $[C_2C_1Im][OAc]$ and $[C_4C_1Im][OAc]$ had very high viscosities that exceed the printing range for the DIMATIX ink-jet printer. The surface tension of $[C_4C_1Im][OAc]$ was within the DIMATIX ink-jet printing range. However, $[C_2C_1Im][OAc]$ had a higher value than the recommended range. Overall, the printability parameter of both the ionic liquids was less than 1 as they both had the highest viscosity, and this prevents drop ejection during printing (Derby B., 2010). Therefore, the ionic liquids were not with in the acceptable range for ink-jet printing. The printability parameter of deionised water was more than 10 as it had the highest surface tension and this, could lead to satellite drops during printing (Derby B., 2010).

Experimental and simulation studies have shown reductions in ionic liquid viscosity and surface tension with increasing temperature (Crosthwaite J. *et al*., 2005; Ghatee M. and Zolghadr A., 2008; Chen T. *et al*., 2010; El Seoud O. *et al*., 2011; Fendt S. *et al*., 2011; Freire M. *et al*., 2011; Almeida H. *et al*., 2012a; Almeida H. *et al*., 2012b; Quijada-Maldonado E. *et al*., 2012; Xu A. *et al*., 2012a; Xu A. *et al*., 2012b; Ma X. *et al*., 2013; Castro M. *et al*., 2014; Haghtalab A. and

Shojaeian A., 2014; Pinto A. *et al*., 2014; Safarov J. *et al*., 2014; Hiraga Y. *et al*., 2015; Nazet A. *et al*., 2015; Lopes J. *et al*., 2016; Hiraga Y. *et al*., 2017; Součková M. *et al*., 2017). Even though, the pure ionic liquids exhibited viscosities higher than the DIMATIX ink-jet printing range at 25 °C, the ink can be heated up to 70 °C during printing, which should be sufficient to reduce the viscosity within the printing range.

Comparing the experimental results for viscosity and surface tension for $[C_2C_1Im][OAc]$ and $[C_4C_1Im][OAc]$ in Table 4.2 against the literature values in Table 4.1, these physical properties are clearly governed by a combination of parameters. These include; water content, temperature, ionic liquid preparation procedure (laboratory or off-the-shelf). This preliminary study has provided basic understating on the physical properties of different chemicals that will be used to formulate inks.

4.3.2 Preparation of Low Viscosity Inks: Cellulose and Ionic Liquid

In order to identify a suitable temperature for cellulose dissolution in ionic liquids, a TGA analysis was performed for cellulose and the ionic liquids. A heating range between 1 to 20 °C/minutes has been generally used in TGA analysis (Vyazovkin S., 2012). Therefore, all TGA measurements in this study were conducted at a heating rate of 10 °C/minute. The results obtained are presented in Figures 4.1, 4.2 and 4.3 along with the DTG curves.

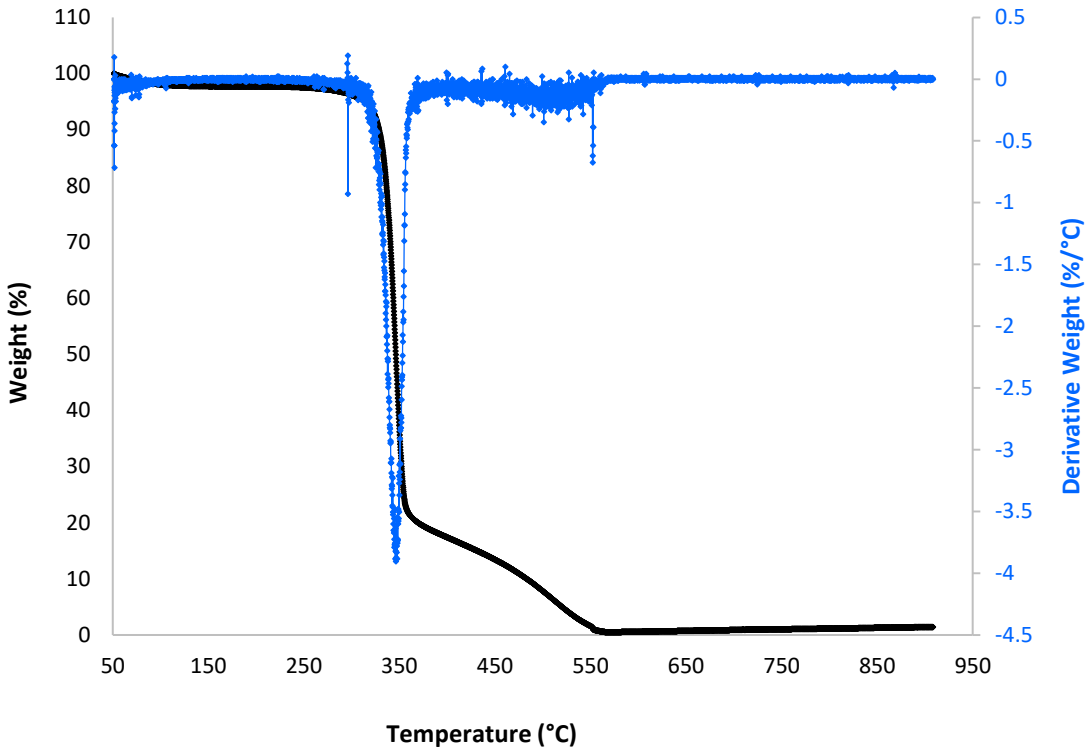


Figure 4.1: TGA and TG curves for cellulose

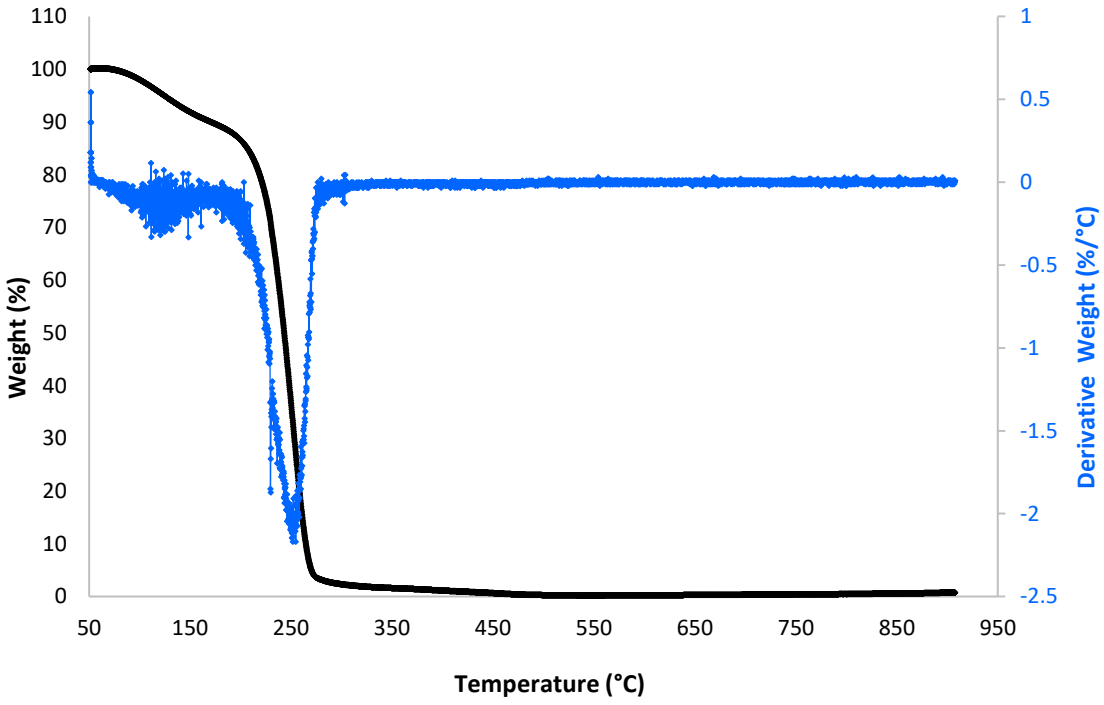


Figure 4.2: TGA and DTG curves for $[C_2C_1Im][OAc]$

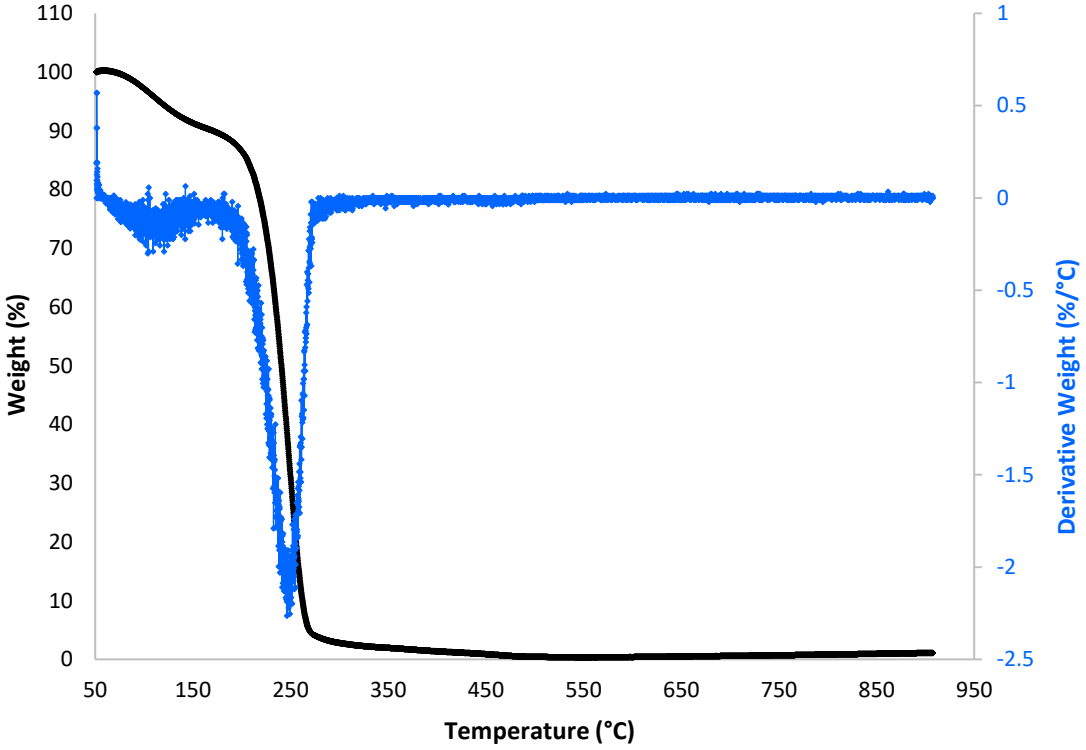


Figure 4.3: TGA and DTG curves for $[C_4C_1Im][OAc]$

In Figure 4.1, the initial weight loss was due the volatilization and vaporization of absorbed or bound water (Liu Z. *et al*., 2011; Lan W. *et al*., 2013; Shen W. *et al*., 2014; Leal G. *et al*., 2015; Yeng L. *et al*., 2015; Reddy K. *et al*., 2017). For cellulose, this was between 50 to 150 °C where the weight loss was approximately 3 %. Then there was a rapid weight loss, relating to dehydration, thermal decomposition and degradation (Kadokawa J. *et al*., 2008; Shen W. *et al*., 2014; Leal G. *et al*., 2015; Yeng L. *et al*., 2015; Reddy K. *et al*., 2017). This step resulted in cellulose been fully burnt as a result of oxidative thermal degradation and loss of its crystallite structure (Yeng L. *et al*., 2015). For cellulose, this occurred via a two-step thermal degradation between 250 to 370 °C and 370 to 550 °C where the weight loss was 77 % and 18 % respectively. The final slow weight loss was due to cellulose pyrolysis, decomposition and

formation of carbon dioxide and carbon monoxide (Shen W. *et al*., 2014). Compared with literature (Table 4.3), MCC studied in this work had a lower thermal stability, indicating the presence of fewer hydrogen bonds resulting in a less ordered packing of cellulose chains and therefore a lower crystallite size (Kim U. *et al*., 2010; Poletto M. *et al*., 2013).

For the ionic liquids, the initial weight loss between 50 to 150 °C was about 9 % (Figures 4.2 and 4.3). The water content in ionic liquids was investigated using a Karl Fischer Coulomteric titration and it was 1.67 (± 0.138) % and 1.54 (± 0.00153) % for $[C_2C_1Im][OAc]$ and $[C_4C_1Im][OAc]$ respectively. Karl Fischer Coulomteric titration measured the water content based on the reaction between iodine and water. However, TGA measured the volatile components, which included water and other impurities (Nogueira R. *et al*., 2012). The ionic liquids used had a purity of ≥ 95 %. Hence the difference between the water contents observed between the two techniques used.

TGA results also indicated that the absorbed or bound water of the ionic liquids was higher compared cellulose. This could be due to the presence of impurities and the hygroscopic nature of the ionic liquids. Unlike cellulose the ionic liquids exhibited a one-step thermal degradation (Figures 4.2 and 4.3).

Table 4.3: Degradation temperatures of the pure chemicals used

Raw Material	Degradation Temperature (°C)	Reference
Cellulose	345	In this work
	375	Quan S. *et al*., (2010)
	350	Lan W. *et al*., (2013)
	353	Poletto M. *et al*., (2013)
	360	Poletto M. *et al*., (2013)
	350	Shen W. *et al*., (2014)
	350	Leal G. *et al.,* (2015)
	338	Yeng L. *et al*., (2015)
	394	Reddy K. *et al*., (2017)
$[C_2C_1Im][OAc]$	250	In this work
	244	Cao Y. and Mu T., (2014)
$[C_4C_1Im][OAc]$	245	In this work
	242	Cao Y. and Mu T., (2014)

Cellulose was dried in an oven for 3 hours at 60 °C before use. Mikkola J. *et al*., (2007), did not observe any significant variation in cellulose dissolution time when dried or non-dried cellulose was used. The main purpose of this drying step was to remove any absorbed or bound water in cellulose, as it can reduce its solubility in ionic liquid. However, this drying step was undertaken as a preliminary study since the amount of cellulose in the inks prepared was very low. Cellulose was dried at 100 °C when the desired cellulose loading was much higher (for samples 11, 12, 15 and 16 in Table 3.3).

Initial samples (samples 1 to 4) consisting of cellulose and ionic liquid were prepared at very low cellulose loadings (2 and 4.8 wt%). This was because literature has suggested higher viscosities when the cellulose loading was higher (Hermanutz F. *et al*., 2008; Kosan B. *et al*., 2008; Chen X. *et al*., 2009; Gericke M. *et al*., 2009a; Gericke M. *et al*., 2009b; Quan S. *et al*., 2010; Sescousse R. *et al*., 2010; Liu Z. *et al*., 2011; Lu F. *et al*., 2014b) and this may not

be within the printing range of the DIMATIX ink-jet printer. The mass of cellulose was within 10 % error margin of the theoretical mass. The dissolution experiments were carried out at 800 rpm as there was no formation of air bubbles and separation of the mixtures at this speed, and it was assumed that additional heat was not produced by the magnetic stirrer (Fukaya Y. *et al*., 2008). An oil bath was used to ensure constant heating.

A common dissolution temperature range used in the literature has between 100 to 110 °C (Table 2.3). A study conducted by Baranyai K. *et al*., (2004), concluded that if imidazolium cation based ionic liquids are kept at a higher temperature for a longer time period (approximately 10 hours) degradation can occur at a lower temperature. Therefore, it can be assumed that the ionic liquids may have a probability to degrade at a temperature less than 250 °C over a longer dissolution period. Barthel S. and Heinze T., (2006) and Heinze T. *et al*., (2005) used a dissolution temperature 10 °C above the ionic liquid melting point. Both the ionic liquids used in this research had a very low melting temperatures as they exist as liquids at room temperature. From the TGA results (Table 4.3) no degradation was observed for the pure chemicals around 100 °C. Therefore, 100 °C was selected as a suitable dissolution temperature for samples containing cellulose and ionic liquid (samples 1 to 4).

Cellulose dissolution in ionic liquids has been studied under a microscope by Zhang H. *et al*., (2005), Zavrel M. *et al*., (2009), Liu Z. *et al*., (2011) and Andanson J. *et al*., (2014). During dissolution, the cellulose fibres initially swelled forming

a thick gel which later became thinner (Liu Z. *et al*., 2011). The size and number of cellulose particles reduced with time (Zavrel M. *et al*., 2009; Andanson J. *et al*., 2014) and the dissolution rate decreased with time, possibly due to the increase in viscosity (Zhang H. *et al*., (2005).

Since water acts as an anti-solvent facilitating cellulose regeneration, low water levels in the ionic liquid should be ensured. Successful dissolution of the samples prepared suggests that the amount of water in the ionic liquids had a minimum or negligible effect in this system.

4.3.3 Physical Properties and Printability Parameter for Low Viscosity Inks: Cellulose and Ionic Liquid

The physical properties of the low viscosity inks containing cellulose and ionic liquid, are presented in Table 4.4. It was assumed that there was negligible deviation in measured cellulose mass and ionic liquid volumes and the density was similar to the theoretical density. Considering the maximum printing temperature of 70 °C for the DIMATIX cartridge, viscosity measurements were taken at 60 °C. A shear rate range of 10 to 1000 s^{-1} was used and the average viscosities for all the samples were recorded at the highest shear rate, except for sample 4 ($[C_4C_1Im][OAc]$ and 4.8 wt% cellulose) where the viscosity was recorded at a shear rate of 631 s^{-1}. This was due to a limitation in the rheometer, which can be overcome by either reducing the gap to avoid splashing (cone-plate geometry) or by measurement of the viscosity using an enclosed system (*e.g.* cup and bob geometry).

Table 4.4: Physical properties of the low viscosity inks (cellulose and ionic liquid) used

Sample	Ionic Liquid	Cellulose (wt %)	Density (g cm^{-3})	Viscosity at 60 °C (mPa s)
1	$[C_2C_1Im][OAc]$	2.0	1.0	87.30 ± 2.56
2	$[C_2C_1Im][OAc]$	4.8	0.99	290.70 ± 22.21
3	$[C_4C_1Im][OAc]$	2.0	1.0	163.90 ± 7.58
4	$[C_4C_1Im][OAc]$	4.8	1.0	723.13 ± 49.53

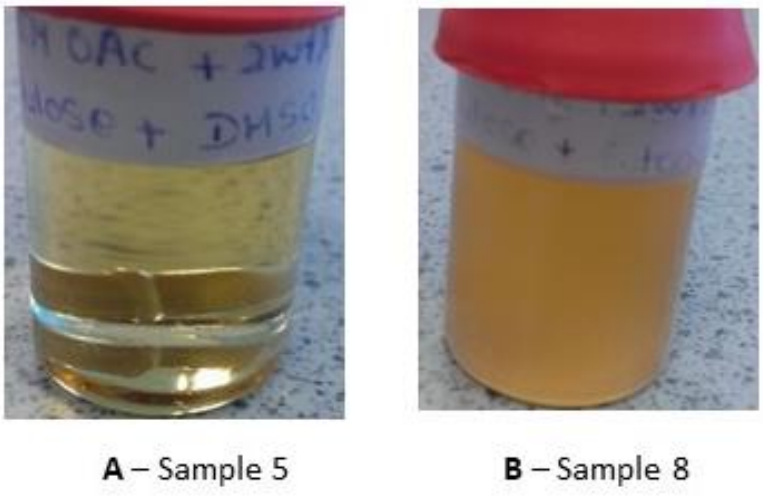
As the cellulose loading increased, from 2.0 to 4.8 wt% and when the cation size increased, the viscosity increased (Table 4.4). Similar trends in viscosity with increased cellulose loading and ion size were reported by Fukaya Y. *et al*., (2006), Fukaya Y. *et al*., (2008), Hermanutz F. *et al*., (2008), Kosan B. *et al*., (2008), Chen X. *et al*., (2009), Gericke M. *et al*., (2009a), Gericke M. *et al*., (2009b), Quan S. *et al*., (2010), Sescousse R. *et al*., (2010), Liu Z. *et al*., (2011) and Lu F. *et al*., (2014b). The pure ionic liquid $[C_2C_1Im][OAc]$, had a lower viscosity at room temperature (85.47 mPa s) compared to $[C_4C_1Im][OAc]$ (278 mPa s). Therefore, this explains the lower viscosity of samples 1 and 2 compared to samples 3 and 4.

The viscosity of the ionic liquid and cellulose solutions were higher than the printing range, even at 60 °C. Whilst increasing the temperature is known to decrease the viscosity, temperature modulation in this printing system was limited by the maximum working temperature for the DIMATIX cartridge (70 °C). Therefore, different concentrations of co-solvents (DMSO and 1-butanol) were added to reduce the viscosity. As an initial study $[C_4C_1Im][OAc]$

was selected to further study the dissolution of cellulose in the presence of different co-solvents.

4.3.4 Preparation of Low Viscosity Inks: Cellulose, Ionic Liquid and Co-Solvent

Dissolution conditions used for the samples containing co-solvents were similar to the low viscosity inks consisting of cellulose and ionic liquids (in Chapter 4 Section 4.3.2) except for the dissolution temperature. When the initial dissolution experiments were conducted at 100 °C, the lids popped out from the glass vials. As the mixture was heated the particles may have gained lot of kinetic energy converting them into gas. Even though the volume of this gas increased with time, since the lids were closed, pressure build up from the evaporating solvents exerted force on the glass vial pushing the lid away. Therefore, the dissolution temperature was reduced to 80 °C. Figure 4.4, shows the dissolution observations for samples 5 and 8.



A – Sample 5 **B** – Sample 8

Figure 4.4: Dissolution observations for samples containing DMSO and 1-butanol

Samples containing DMSO dissolved easily compared to samples containing 1-butanol, where a cloudy solution formed, which resulted in a precipitate at room temperature. Therefore, the printability parameter for samples containing 1-butanol (samples 8 and 10 in Chapter 3 Table 3.2) was not calculated. DMSO is a polar aprotic co-solvent (Gericke M. *et al*., 2009b; Brown E. *et al*., 2012) and does not form hydrogen bonds by hydrogen donation. On the other hand, 1-butanol is a polar protic solvent and can form hydrogen bonds. Therefore, it can be assumed that when 1-butanol was added, it competed with cellulose to form hydrogen bonds with the ionic liquid and thus reduced the cellulose solubility.

Compared to the samples containing solely cellulose and ionic liquid, the samples containing the co-solvent DMSO dissolved faster. This suggests that the presence of a co-solvent has reduced the ionic liquid viscosity, facilitating its interaction with cellulose. Successful dissolution of the samples containing DMSO suggests that the amount of water in the ionic liquids had a minimum or negligible effect in this system.

4.3.5 Physical Properties and Printability Parameter for Low Viscosity Inks: Cellulose, Ionic Liquid and Co-Solvent

Theoretical and experimental densities for the samples containing cellulose, ionic liquid and co-solvents are presented in Table 4.5. From the results the percentage difference was less than ± 1.5 %. Since the deviation was minimum

and to keep the printability parameter calculation consistent with Table 4.2, theoretical density was used in Table 4.6.

Table 4.5: Experimental and theoretical densities of the low viscosity inks (cellulose, $[C_4C_1Im][OAc]$ and DMSO)

Sample	Cellulose (wt %)	$[C_4C_1Im][OAc]$ (wt %)	DMSO (wt %)	Experimental Density (g cm^{-3})	Theoretical Density (g cm^{-3})	Percentage Difference
5	1.3	66	33	1.05	1.06	0.47
6	1.2	58	41	1.07	1.06	- 0.49
7	1.0	52	47	1.08	1.07	- 0.88
9	3.2	65	32	1.06	1.04	- 1.22

Viscosity (at 60 °C) and surface tension (at room temperature) measurements were conducted similar to before and the average viscosity at the highest shear rate (1000 s^{-1}) was recorded in Table 4.6. Initially 33 wt% of DMSO was added and the viscosity was measured, then DMSO concertation was increased from 41 to 47 wt% to bring the sample viscosity within the DIMATIX ink-jet printing range. It can be seen from the rheological properties (Table 4.6), increasing the concentration of DMSO reduced the viscosity. This confirms the previous findings in literature regarding the role of DMSO as a co-solvent (Heinze T. *et al*., 2005; Gericke M. *et al*., 2009b; Quan S. *et al*., 2010; Brown E. *et al*., 2012; Andanson J. *et al*., 2014; Sweely K. *et al*., 2014). For sample 9, viscosity was more than 90 mPa s at 60 °C, which was much higher than the printing range.

Table 4.6: Physical properties and printability parameters of the low viscosity inks (cellulose, $[C_4C_1Im][OAc]$ and DMSO)

Sample	Cellulose (wt %)	$[C_4C_1Im][OAc]$ (wt %)	DMSO (wt %)	Viscosity at 60 °C (mPa s)	Surface Tension (mN m^{-1})	Printability Parameter, *Z*
5	1.3	66	33	28.49 ± 2.12	36.71 ± 0.18	1.0
6	1.2	58	41	19.64 ± 1.13	35.58 ± 0.64	1.4
7	1.0	52	47	15.66 ± 1.32	36.06 ± 0.41	1.8
9	3.2	65	32	91.27 ± 2.21	37.15 ± 0.43	0.31

Even though the viscosity was recorded at a shear rate of 1000 s^{-1}, the actual shear rate during printing will be much higher (10^5 s^{-1}) and the rheometer is unable to measure the viscosity at this shear rate (de Gans B. *et al*., 2004). Again, the surface tension was measured at room temperature. However, at 60 °C the actual surface tension will be lower than the value recorded (Ghatee M. and Zolghadr A., 2008; Almeida H. *et al*., 2012a; Almeida H. *et al*., 2012b; Xu A. *et al*., 2012a; Ma X. *et al*., 2013; Castro M. *et al*., 2014; Safarov J. *et al*., 2014; Součková M. *et al*., 2017) and this changes the actual printability parameter during printing. Therefore, these results can be used as an initial estimate of the ink properties and optimisation of the printing parameters during printing is essential.

Comparing the surface tension and viscosity of $[C_4C_1Im][OAc]$ in Table 4.2 with the inks in Table 4.6, it can be seen that when mixed to create the formulations, surface tension increased and the viscosity decreased. The surface tension (Table 4.6) and density (Table 4.5) remain approximately the same (compared

to Table 4.2) and, the characteristic length of the nozzle being a constant, results in the printability parameters (*Z*) being mainly affected by the sample viscosity. Since the printability parameter (*Z*) was within the acceptable range (between 1 and 10) for samples 6 and 7 they were chosen for ink-jet printing.

To further study the rheological behaviour exhibited by these inks (samples 6 and 7), viscosity was measured against time at a fixed shear rate (1000 s^{-1}) and temperature (60 °C). From the results (Figures 4.5 and 4.6), it can be seen that both the samples showed thixotropic behaviour, exhibiting shear thinning. When the viscosity decreased under shearing it was easier for the ink to pass through the nozzle. When the shear was removed, viscosity increased and the printed pattern can retain its shape (Detsch R. *et al*., 2008; Faddoul R. *et al*., 2012). This is a useful property of the formulated ink that can be used in ink-jet printing to eject droplets at a viscosity lower than that recorded in Table 4.6.

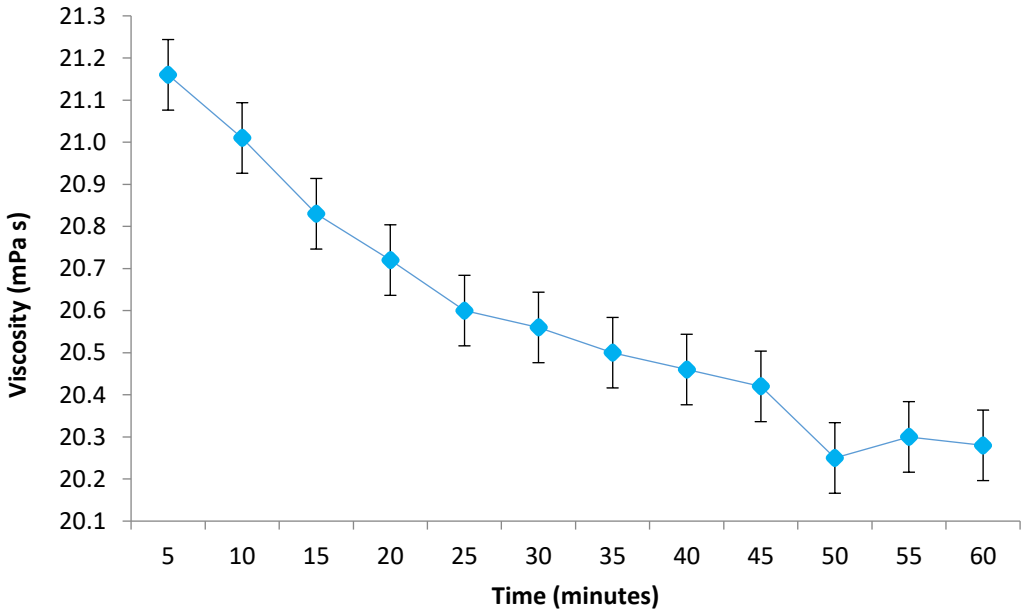


Figure 4.5: Viscosity Vs time at fixed shear rate and temperature for sample 6

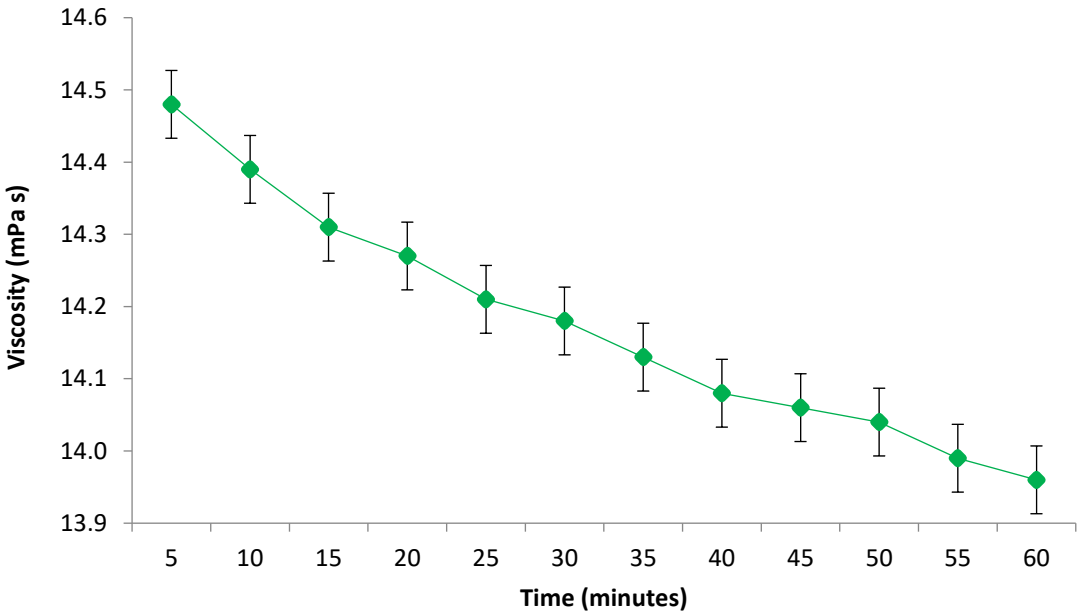


Figure 4.6: Viscosity Vs time at fixed shear rate and temperature for sample 7

4.3.6 Ink-jet Printing

When printing sample 6, the nozzles were blocked more easily than for sample 7, possibly due to sample 6 processing a viscosity higher than the manufacturer's acceptable viscosity range (12-18 mPa s). When observing the drops using the drop watcher in the DIMATIX Drop Manager Software, frequency, waveform and voltage were adjusted until acceptable drops that merged with the leading drop were formed. Jetting parameters for samples 6 and 7 are presented in Table 4.7.

Table 4.7: Jetting parameters for samples 6 and 7

Segment	Sample 6			Sample 7		
	Level (%)	Slew Rate	Duration (µs)	Level (%)	Slew Rate	Duration (µs)
1	0	0.65	4.416	0	0.65	3.584
2	60	0.93	4.160	100	0.93	3.712
3	0	0.64	4.032	27	0.60	3.392
4	100	0.93	2.176	40	0.80	0.832
Duration Scalar			1		1	
Width			14.784 µs		11.520 µs	
Maximum Jetting Frequency			1.0 Hz		1.5 Hz	
Jetting Voltage			35 V		35 V	

A 3 × 3 mm square having an array of single drops was printed, with a droplet spacing of 150 µm (sabre angle 36.2°). Printing was achieved using a single nozzle at 55 °C. Figure 4.7, shows the array of drops printed using samples 6 and 7. From the microscopic images obtained, it can be seen that some drops were missing (Figure 4.7A), which may be due to a blockage in the nozzle (occasional nozzle failure and a drop was not deposited). Small drops were also deposited next to the large drop (Figure 4.7B) indicating the formation of small ligaments alongside the primary drop. To overcome these problems, the ink can be reformulated to reduce the viscosity and the waveform can be modified (He Y. *et al*., 2016). Although, there were some printing difficulties, overall both the samples were able to print stable drops (Figure 4.8).

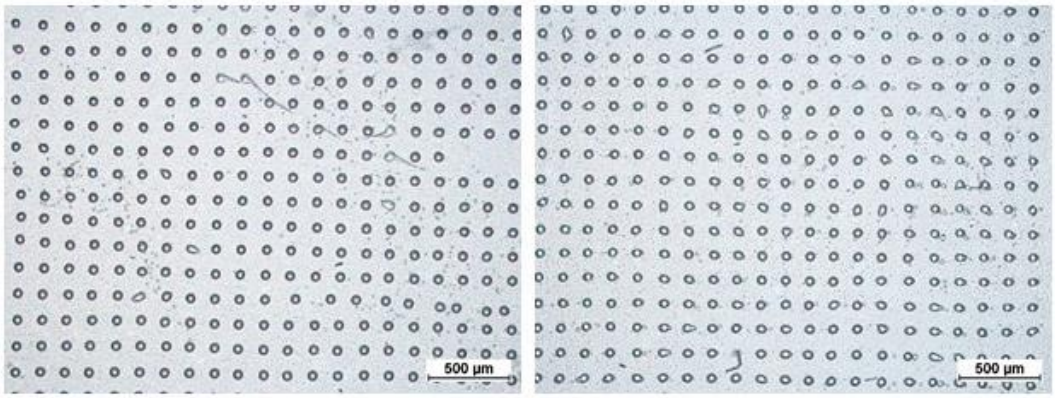


Figure 4.7: Microscopic images showing missing drops and ligaments

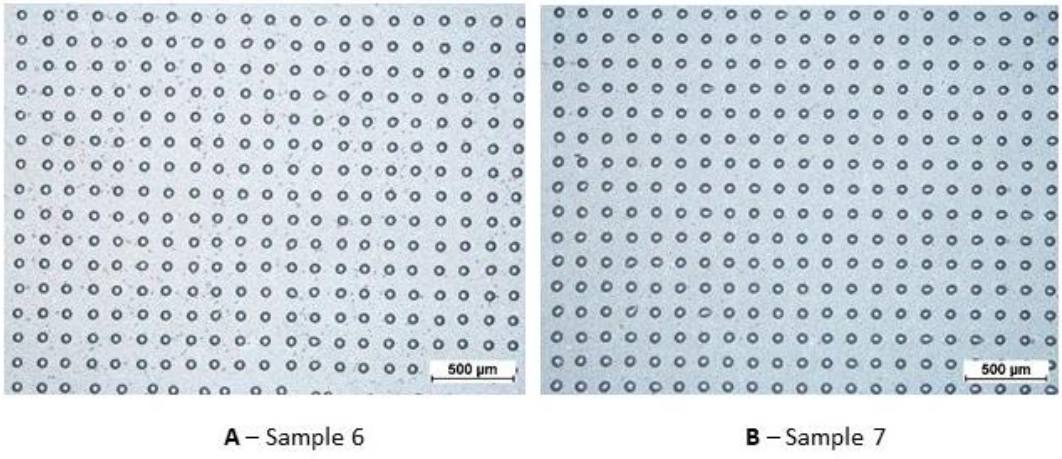


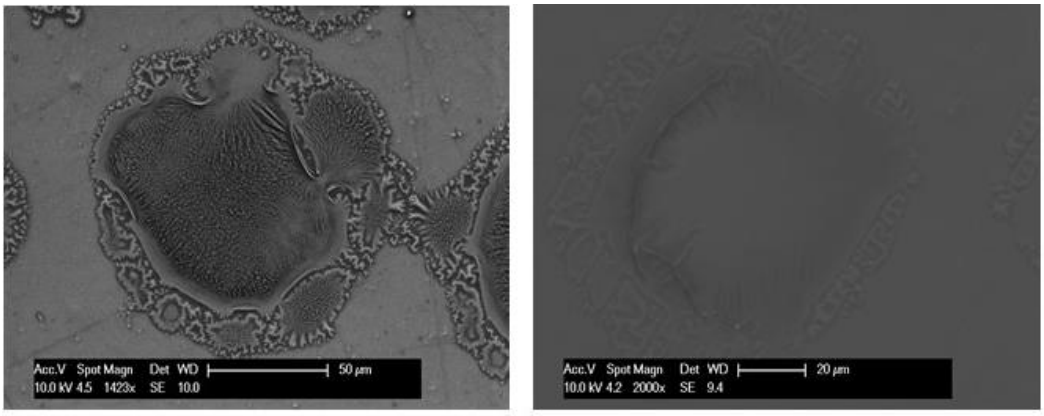
Figure 4.8: Microscopic images for samples ink-jet printed on PET

The average droplet diameters of the printed drops were measured using a microscope and using the ImageJ software. Table 4.8 clearly shows that the percentage difference between these two methods was less than 7 %.

Table 4.8: Average droplet diameter for ink-jet printed samples on PET

	ImageJ Analyzed Diameter (µm)	**Microscope Measured Diameter (µm)**	**Percentage Difference**
Sample 6	133 ± 4.12	125 ± 4.11	6.15
Sample 7	131 ± 4.79	127 ± 6.06	3.09

The ink-jet printed samples were left overnight at room temperature to observe the surface of the printed dots. The SEM images (Figure 4.9) shows there was more material deposited in sample 6 compared to sample 7. The principle difference between these two samples was the amount of cellulose and DMSO. Since sample 7 had a higher DMSO loading, it is possible that it started to evaporate at room temperature leaving less residual mass in sample 7 compared to sample 6.



A – Sample 6 **B** – Sample 7

Figure 4.9: SEM images for samples ink-jet printed on PET and dried for approximately 18 hrs at room temperature

To further study the distribution of materials in the droplet, surface profile analysis was performed using white light interferometry. The surface profile image indicated that the height of the surface, corresponding to the amount of material deposited, differs (Appendix Figures 9.4 and 9.5). This was further investigated by calculating the average height of the ink-jet printed droplet obtained from the surface profile data. From Table 4.9, sample 6 showed a higher height over both *X* and *Y* axes, compared those printed using sample 7. This is consistent with the results obtained from the SEM.

Table 4.9: Average height of a droplet for ink-jet printed samples on PET

	Average Height in *X* Direction (nm)	**Average Height in *Y* Direction (nm)**
Sample 6	510	530
Sample 7	180	85

4.3.7 Regeneration and Characterisation

The regeneration experiments were conducted by adding 0.1 mL of deionised water and leaving it on the ink-jet printed samples for different time intervals. Based on the size of the ink-jet printed pattern (3 × 3 mm), the volume of deionised water added was kept to a minimum to avoid the printed sample been washed off fully. It was assumed that leaving deionised water for a longer time interval (2 hours) would remove more ionic liquid than leaving it for a short time interval (30 minutes). These samples were then heated at a moderate temperature of 50 °C with the intention of drying off the deionised water.

Figures 4.10 and 4.11 compare the scanning electron microscopy images obtained from regenerated ink-jet printed samples from samples 6 (41 wt% DMSO) and 7 (47 wt% DMSO). As seen from the images, characterisation of the morphology of the regenerated cellulose was challenging, due to the presence of debris on and around the printed droplets. These debris could even be due to the deionised water drying on the printed pattern.

Surface profile images were obtained, and they indicated that the central region of the drop was sunken, creating a concave residue (Figures 4.12 and 4.13 and Appendix Figures 9.6 to 9.12). A study conducted by Wang H. *et al*.,

(2009), found that $[C_4C_1Im][OAc]$ was responsible for PET degradation. In their work, 3.4 wt% of PET dissolved in $[C_4C_1Im][OAc]$ at 150 °C. Even though the ink-jet printed samples were treated at a maximum temperature of 50 °C in this study, the surface profile images suggest some degree of PET degradation. This was not observed for non-regenerated samples. Hence, it is likely have been caused during the time in the oven.

Further ink-jet printing was carried out using glass as the substrate, and the surface profile images, which are shown in Figures 4.14 and 4.15 (Appendix Figures 9.13 to 9.20), reveal no evidence of a sunken central region in the drop. This shows the possibility of forming 3D structures on glass as an improved printing substrate, relative to PET. The average droplet height was also calculated (Table 4.10) and no trend in the droplet height was observed with the regeneration time.

Table 4.10: Average height of a droplet for ink-jet printed samples on glass

Sample	**Regeneration Time**	**Average Height**	
		in *X* Direction (nm)	**in *Y* Direction (nm)**
Sample 6	30 minutes	620	645
	1 hour	830	890
	1 hour and 30 minutes	1010	810
	2 hours	620	605
Sample 7	30 minutes	685	585
	1 hour	595	210
	1 hour and 30 minutes	475	645
	2 hours	445	555

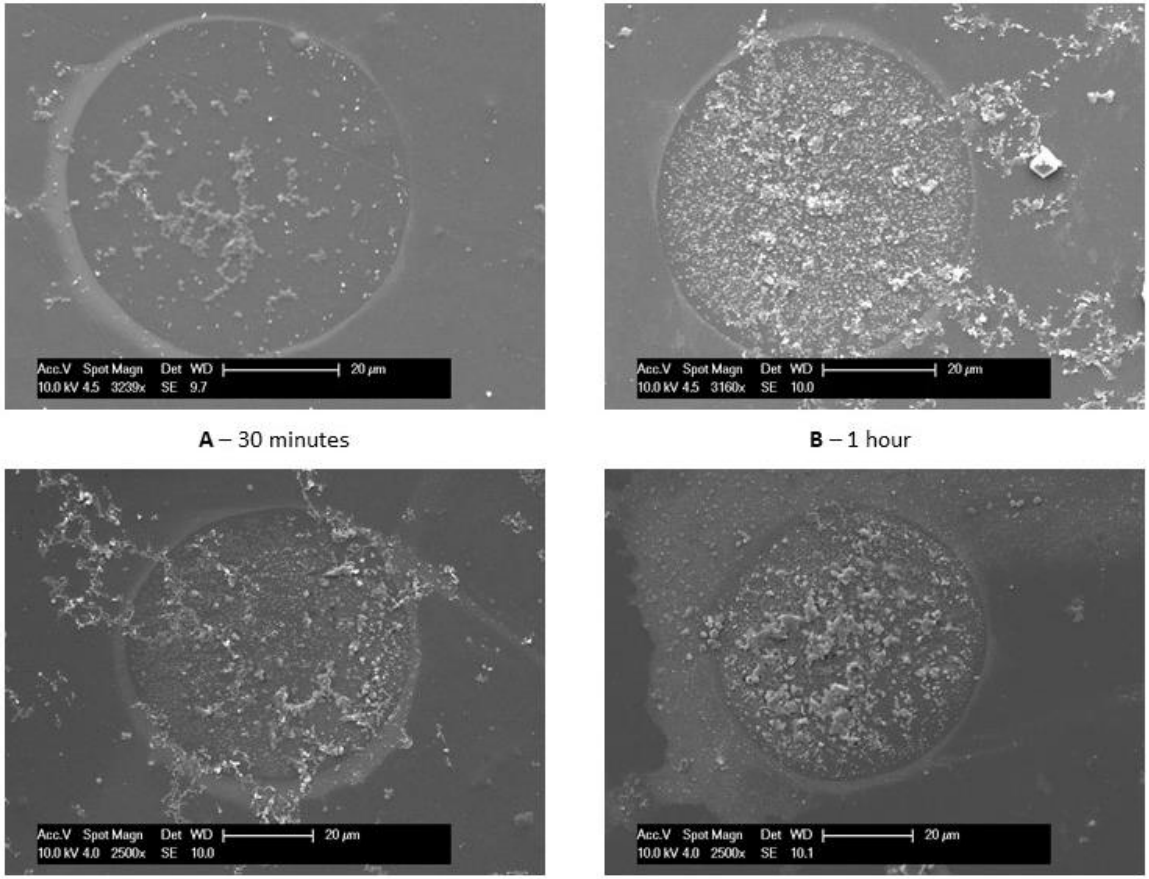


Figure 4.10: SEM images for sample 6 ink-jet printed on PET and regenerated by leaving deionised water for different time intervals before heating for approximately 18 hours at 50 °C

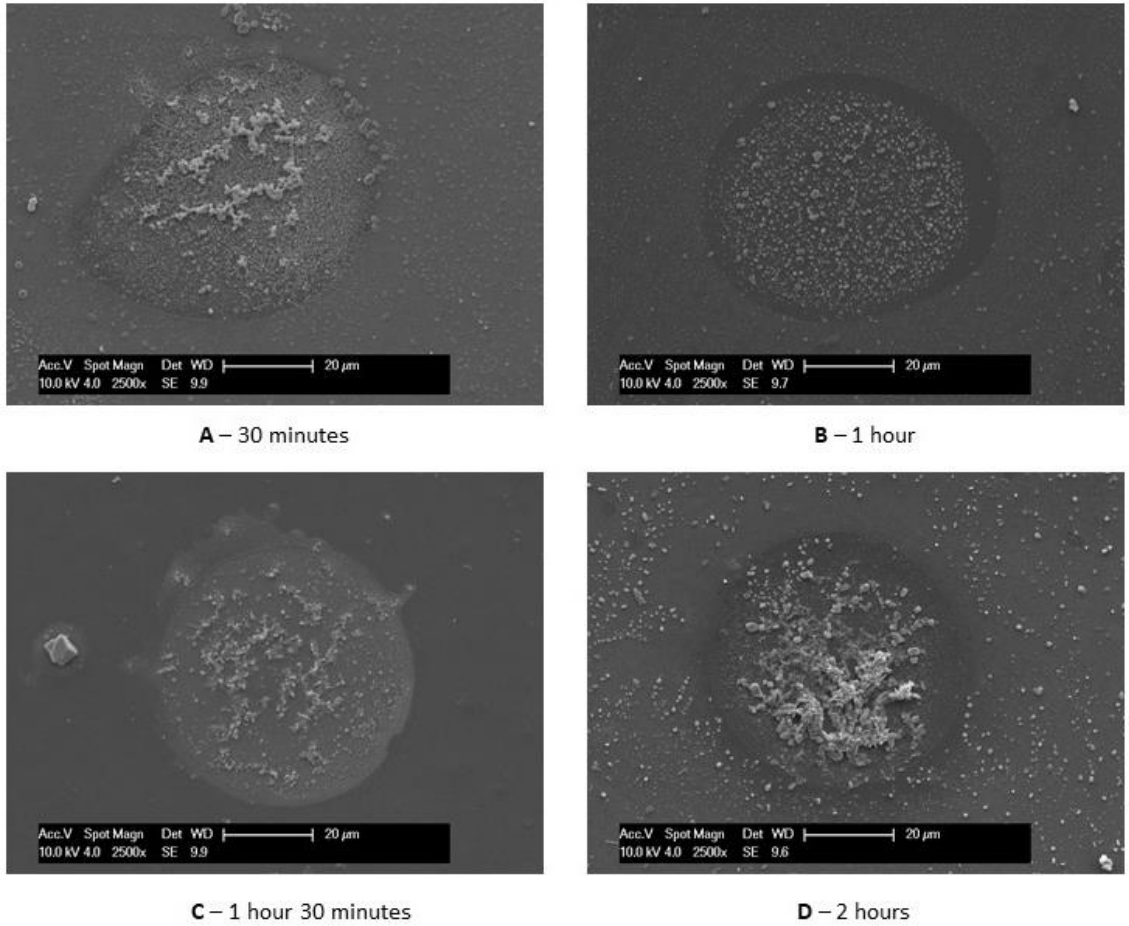


Figure 4.11: SEM images for sample 7 ink-jet printed on PET and regenerated by leaving deionised water for different time intervals before heating for approximately 18 hours at 50 °C

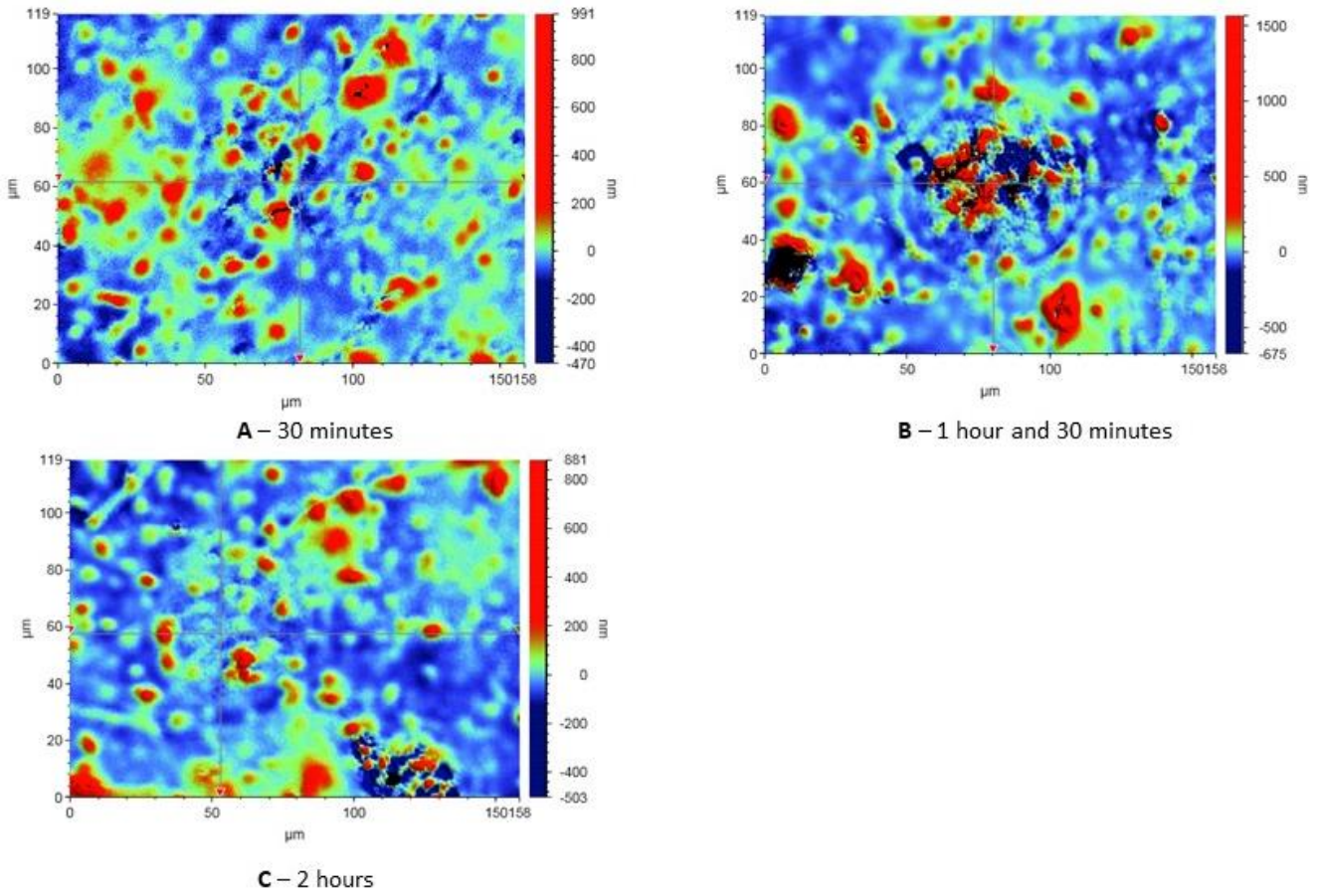


Figure 4.12: WLI results for sample 6 ink-jet printed on PET and regenerated by leaving deionised water for different time intervals before heating for approximately 18 hours at 50 °C

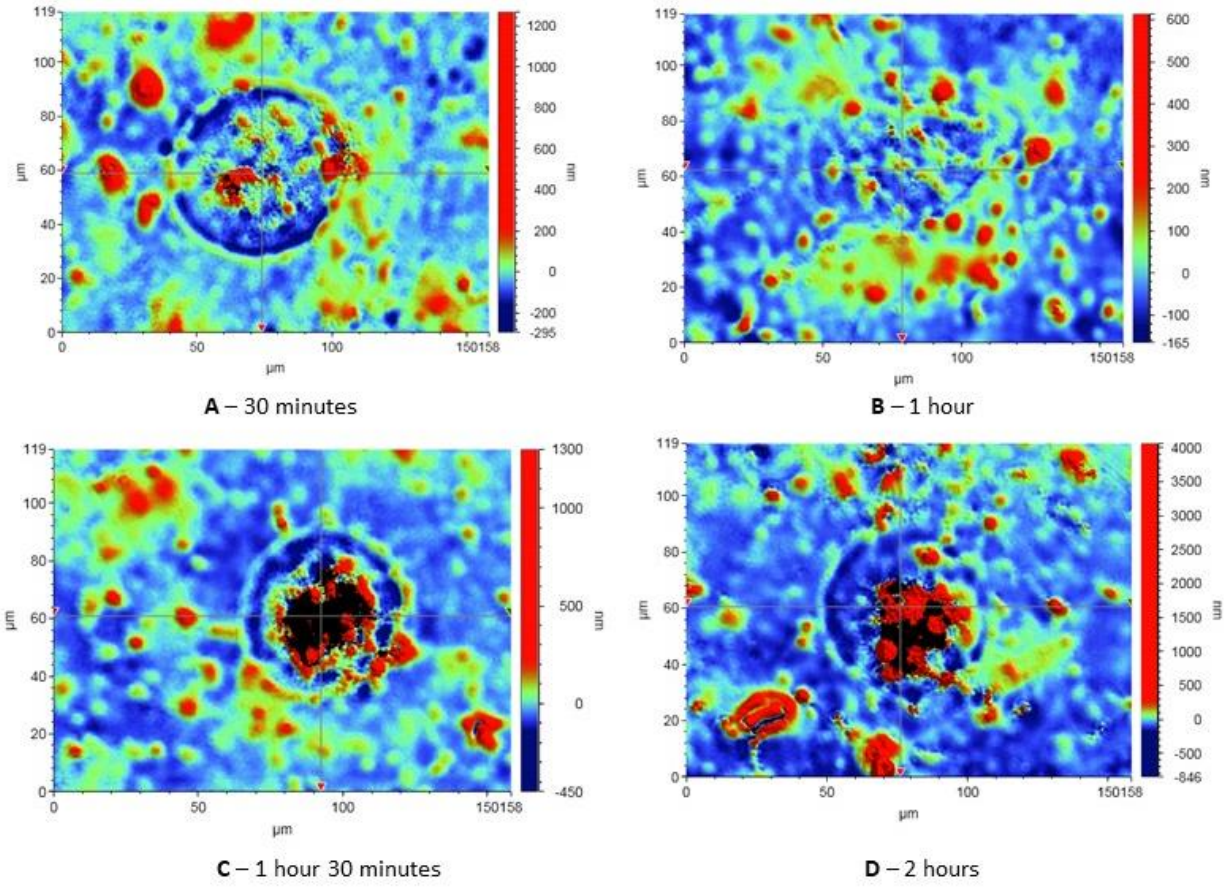


Figure 4.13: WLI results for sample 7 ink-jet printed on PET and regenerated by leaving deionised water for different time intervals before heating for approximately 18 hours at 50 °C

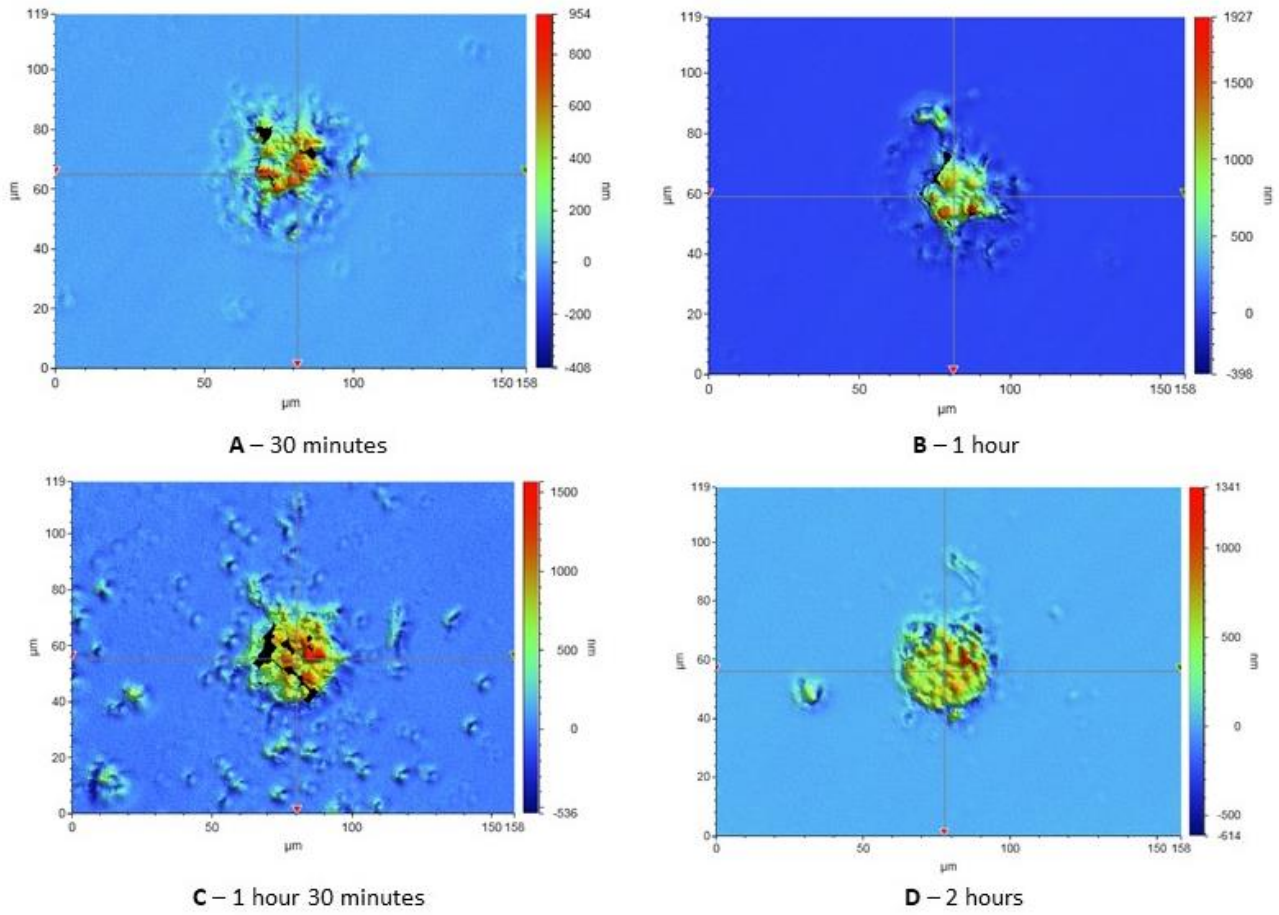


Figure 4.14: WLI results for sample 6 ink-jet printed on glass and regenerated by leaving deionised water for different time intervals before heating for approximately 18 hours at 50 °C

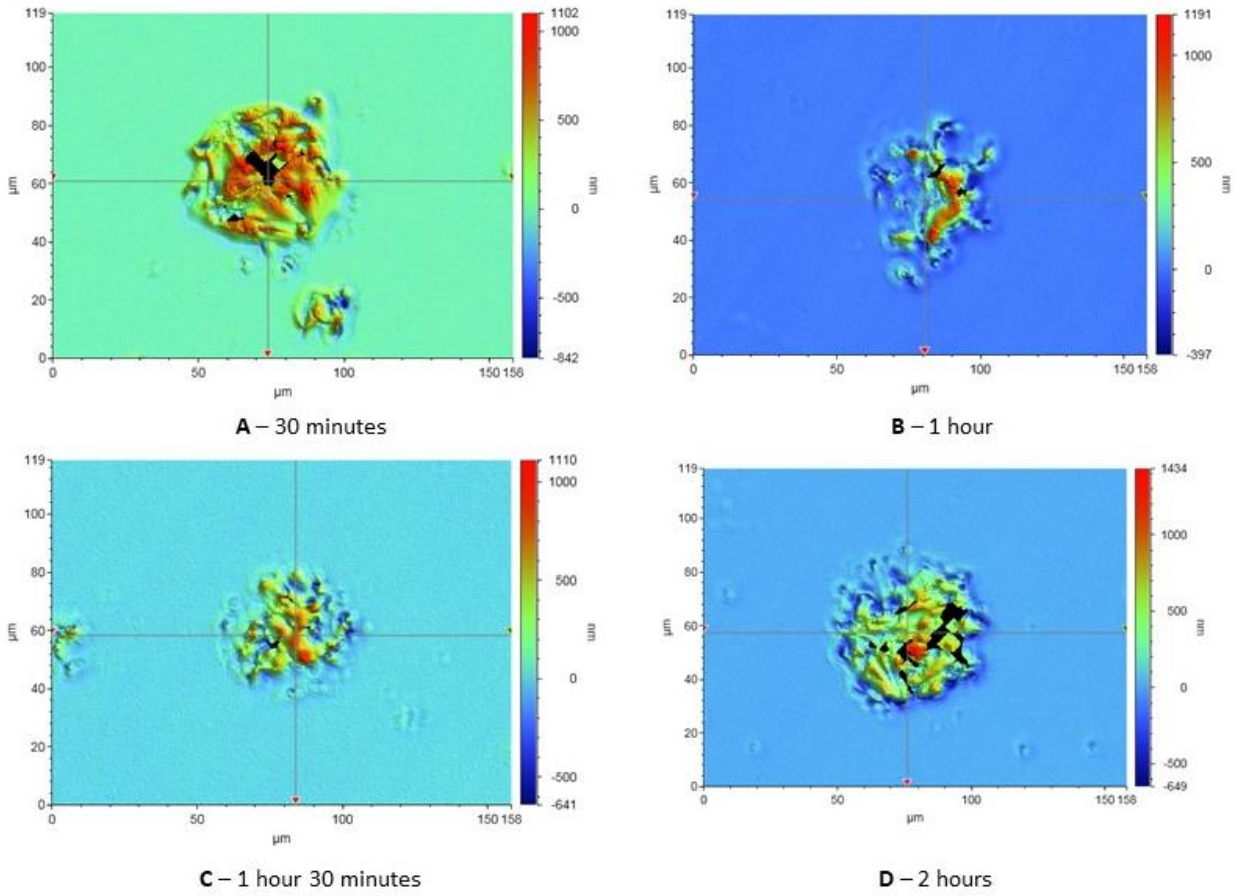


Figure 4.15: WLI results obtained for sample 7 ink-jet printed on glass and regenerated by leaving deionised water for different time intervals before heating for approximately 18 hours at 50 °C

4.4 Chapter Summary

- Physical properties of the pure chemicals (ionic liquids and co-solvents) were investigated at 25 °C. From the results it was evident that the viscosities of the pure chemicals were not within the DIMATIX ink-jet printing range (12-18 mPa s). Except for the ionic liquid $[C_2C_1Im][OAc]$, the other chemicals had a surface tension within the DIMATIX ink-jet printing range (28-32 mN m^{-1}). Overall, the printability parameter of the pure chemicals was not within the acceptable range (1-10).
- The TGA study revealed that the absorbed or bound water for the ionic liquid was about 9 % which was much higher than that of cellulose (3 %). Although ionic liquids are hygroscopic, successful dissolution of the samples in this study has proved that the absorbed or bound water of the ionic liquids was not a hindrance for cellulose dissolution.
- For cellulose the rapid weight loss occurred via a two-step thermal degradation and for the ionic liquids it was a one-step thermal degradation.
- Cellulose dissolved in the ionic liquids $[C_2C_1Im][OAc]$ and $[C_4C_1Im][OAc]$ resulted in high viscosity solutions that were not suitable for ink-jet printing. These results also showed that, increase in cation size and cellulose loading resulted in an increase in the solution viscosity.
- Samples containing the co-solvents were dissolved at 80 °C (10 °C lower than those containing cellulose and ionic liquid). The co-solvent may have been converted to gas at higher temperatures and exerted pressure on the glass vial pushing the lid away.

- Samples containing DMSO dissolved faster and showed a reduced viscosity, whilst maintaining cellulose solubility. Sample 3 (containing 2 wt% cellulose) and had a viscosity of 163.90 ± 7.58 mPa s at 60 °C and by the addition of DMSO (cellulose loading was 1 to 1.3 wt%) the viscosity was less than 30 mPa s at 60 °C. Similar results were observed for samples containing 4.8 wt% cellulose.
- The use of an alternative co-solvent 1-butanol resulted in precipitation of cellulose due to hydrogen bond competition.
- Both samples 6 and 7 showed thixotropic shear thinning behaviour, where the viscosity decreased during shearing and increased when the shearing was removed.
- Different concentrations of the co-solvent DMSO (41 wt% and 47 wt%) were able to bring the solutions within the DIMATIX ink-jet printing range. However, this gave a preliminary idea on the ink properties and the printing parameters were optimised during printing to obtain stable drops. This was why the samples were printed at 55 °C, even though the experimental results suggested they were printable at 60 °C.
- The ink-jet printed samples indicated that some drops were missing, and small ligaments were formed. This implies a blockage in the nozzle and formation of small ligaments that did not return to the nozzle or merge with the leading drop but demonstrates that printing using such equipment is possible. Modifying the ink formulation and waveform would help to overcome these problems in future.

- Both SEM and WLI resulted showed that more ink was deposited on drops printed using sample 6 compared to sample 7. This may be due to the increased loading of DMSO in sample 7 (47 wt%).
- The non-solvent deionised water was added to regenerate the ink-jet printed samples on both PET and glass. Data obtained from WLI studies exhibited structural distortion for regenerated samples printed on PET, potentially related to the degradation of the substrate during the heating step.
- Glass substrates exhibited no such issues, and as such are recommended to be used instead of PET for future characterisation and applications.
- During regeneration, leaving deionised water for different time intervals did not show any effect on the height of the regenerated pattern. However, further experiments must be conducted on the composition of the drop to observe if there was any effect on the time the sample was left on the anti-solvent and the amount of ionic liquid removed.
- The preliminary work presented herein provides the basis for 3DP of biopolymeric materials, by demonstrating that utilisation of a co-solvent with an ionic liquid was able to modulate liquid printability to a suitable range. However, with DIMATIX ink-jet printing the viscosity of the ink was restricted to be within 12 to 18 mPa s and this meant the inks contained approximately 52 to 58 wt% of DMSO. This high composition of DMSO has the tendency to hinder the ionic properties and turn the ink to an organic solvent. Therefore, further characterisation experiments were not conducted on these samples using TGA.

- The next results chapters (chapter 5 and 6) will focus on a different printing technology that does not limit the ink based on the viscosity. This means that the co-solvent addition will no longer be needed, and more biopolymer can be dissolved.

Chapter 5 : Three-Dimensional Printing of Cellulose using a PICO Pulse Printer

5.1 Background

In Chapter 4, the main limitation for not being able to print the inks consisting of cellulose and ionic liquid was due to their viscosity not falling within the DIMATIX ink-jet printing range (12-18 mPa s). Therefore, the co-solvent; DMSO was added to reduce the viscosity to ensure the inks were within the printing range. However, this meant that the amount of cellulose dissolved in the inks was limited to be less than 1.5 wt%, which was well below the cellulose loading that can be dissolved in the ionic liquids; $[C_2C_1Im][OAc]$ and $[C_4C_1Im][OAc]$. DMSO, is widely used in biological research. However, increased DMSO concentrations (0.5 to 6 %) can lead to cytotoxic properties. Therefore, in biomedical applications, it is recommended to keep the DMSO concentration at a minimum (Qi W. *et al*., 2008b). In this chapter, a new printing technology; PICO Pulse printing was adopted to overcome these problems and increase the cellulose loading.

Chapter 5, focused on preparing cellulose-based high viscosity inks with the ionic liquids; $[C_2C_1Im][OAc]$ and $[C_4C_1Im][OAc]$. Next, droplets, lines and films were printed at different printing parameters (pressure, temperature, pulse time and droplet spacing) to optimise the printing conditions. The optimum printing parameters were used to print single and multi-layered films which

were immersed in deionised water to remove the ionic liquid. Finally, these films were characterised to evaluate the morphology, chemical composition, functional groups and thermal stability.

5.2 Results and Discussion

5.2.1 Preparation of High Viscosity Inks: Cellulose and Ionic Liquid

From the TGA results conducted in Chapter 4 (Chapter 4 Section 4.3.2), the absorbed or bound water in cellulose was roughly 3 %. Compared to the low viscosity inks (Tables 3.1 and 3.2), the high viscosity inks (Table 3.3) had a higher cellulose loading. Therefore, another TGA was performed at isothermal conditions to determine the time required to completely remove any absorbed or bound water in cellulose.

A known mass of cellulose was heated to 100 °C and the weight loss was recorded over a period of 45 minutes. From the TGA curve shown in Figure 5.1, it was evident that majority of the weight loss occurred within the first 5 minutes and it was approximately 0.12 %. However, compared to the TGA obtained in Chapter 4 Section 4.3.2, the absorbed or bound water was very insignificant in Figure 5.1. It is likely that the water was strongly bound as part of the hydrogen bonding network. Based on these results, cellulose was dried at 100 °C for 5 minutes before dissolution when preparing the high viscosity inks.

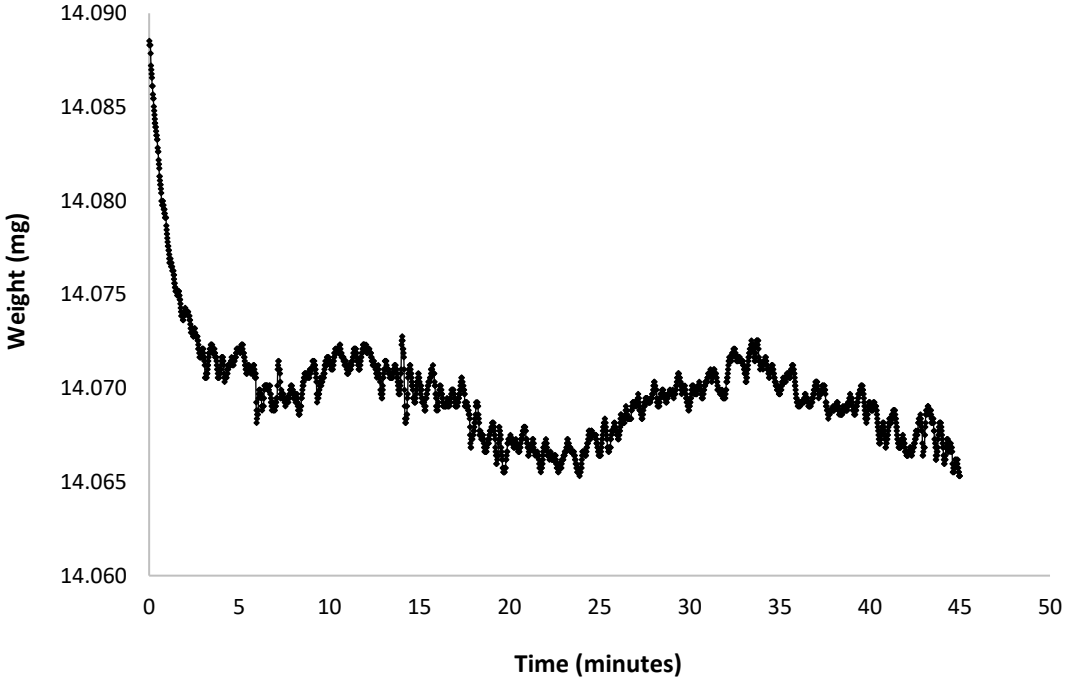


Figure 5.1: TGA curve for cellulose dried at isothermal conditions

The dissolution conditions used to prepare the high viscosity inks (temperature 100 °C, stirring speed 800 rpm and oil bath) were similar to those used before (Chapter 4 Section 4.3.2). The samples were occasionally stirred manually using a spatula to enhance the dissolution process. Cellulose loading in the samples was gradually increased to 5 wt%, 10 wt% and in 1wt% increment after that with the intention to identify the maximum cellulose loading at full dissolution. For $[C_2C_1Im][OAc]$ and for $[C_4C_1Im][OAc]$ these values were 13 wt% (sample 11) and 10 wt% (sample 12) respectively. These dissolution results further support the higher cellulose dissolution reported by Kosan B. *et al*., (2008), Zavrel M. *et al*., (2009) and Liu Z. *et al*., (2011) in short-chain cation-based ionic liquids. Also, $[C_2C_1Im][OAc]$ had a lower viscosity compared to $[C_4C_1Im][OAc]$ (Table 4.2). Hence, the viscosity trend is in good agreement with Fukaya Y. *et al*.,

(2006) and Fukaya Y. *et al*., (2008), where a low viscosity ionic liquid was able to dissolve higher quantities of cellulose.

The inks containing cellulose and either $[C_2C_1Im][OAc]$ or $[C_4C_1Im][OAc]$, when left at room temperature (assumed to be 25 °C), showed an increase in viscosity. Similar observations were made by Zhang H. *et al*., (2005), where the viscosity increased for a [AMIM][Cl] and cellulose mixture when cooled down to room temperature. Hence, for handling, these inks were heated for 5 minutes at 100 °C before filling into the syringe barrel.

5.2.2 Rheological Properties of High Viscosity Inks: Cellulose and Ionic Liquid

Rheological properties of the high viscosity inks containing cellulose and ionic liquid (samples 11 and 12) were investigated between 40 and 90 °C. The selection of the temperature range was based on the operating range of the PICO Pulse valve (maximum temperature 100 °C). A shear rate range of 1 to 100 s^{-1} was used and the average viscosities in Table 5.1 was recorded at the highest shear rate. Similar to DIMATIX ink-jet printing the actual shear rate experienced by the ink during PICO Pulse printing is much higher. Therefore, this rheological study will provide a basic understating on the ink rheological properties.

Figures 5.2 and 5.3 present the logarithmic curve of viscosity Vs shear rate. The non-Newtonian index (*n*) was calculated at different temperatures using the gradient (Equation 13) and shown along with the ink viscosities in Table 5.1.

Viscosity was not recorded at 40 °C due to a limitation in the experimental conditions used. Ink viscosity was very high (> 14,000 mPa s) and the shear rate range (1 to 100 s^{-1}) used was not able to record the viscosity of the ink at 40 °C. Future experiments can be conducted at a higher shear rate to overcome this.

Table 5.1: Rheological properties of the high viscosity inks containing cellulose and ionic liquid

Temperature (°C)	Sample 11		Sample 12	
	Viscosity (mPa s)	Non-Newtonian Index (*n*)	Viscosity (mPa s)	Non-Newtonian Index (*n*)
50	14430 ± 448	0.97	14810 ± 340	0.97
60	8504 ± 321	0.99	8050 ± 338	0.99
70	5220 ± 190	0.99	4555 ± 292	0.99
80	3349 ± 125	1.00	2720 ± 233	1.00
90	2230 ± 78	1.00	1791 ± 76	1.00

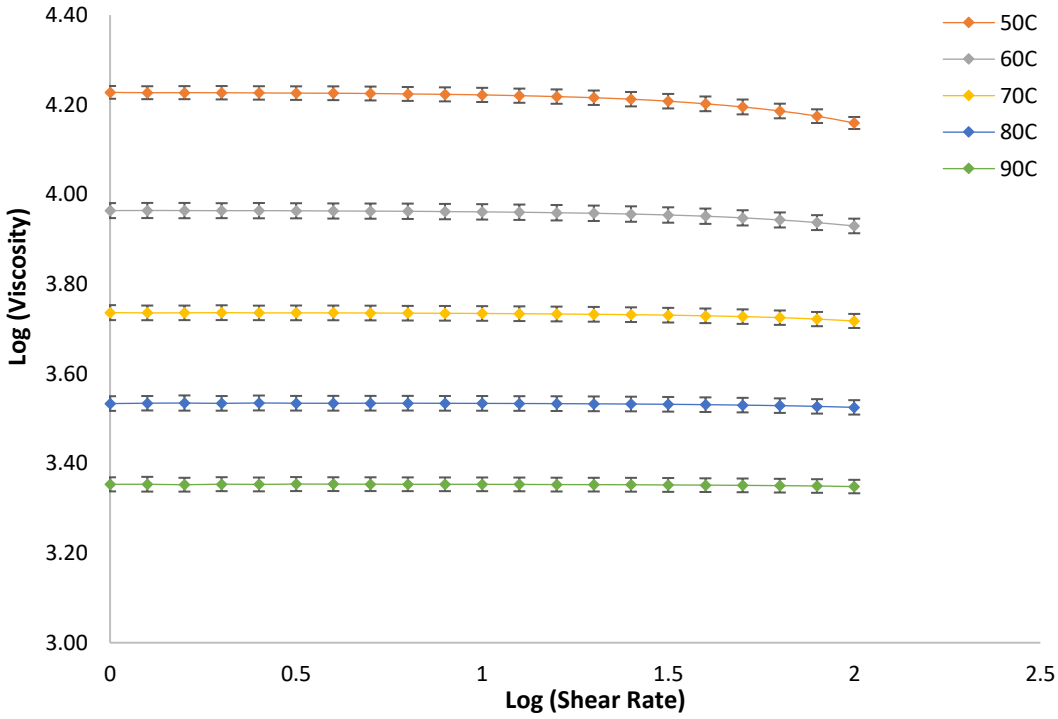


Figure 5.2: Rheological properties of sample 11 ($[C_2C_1Im][OAc]$ and cellulose)

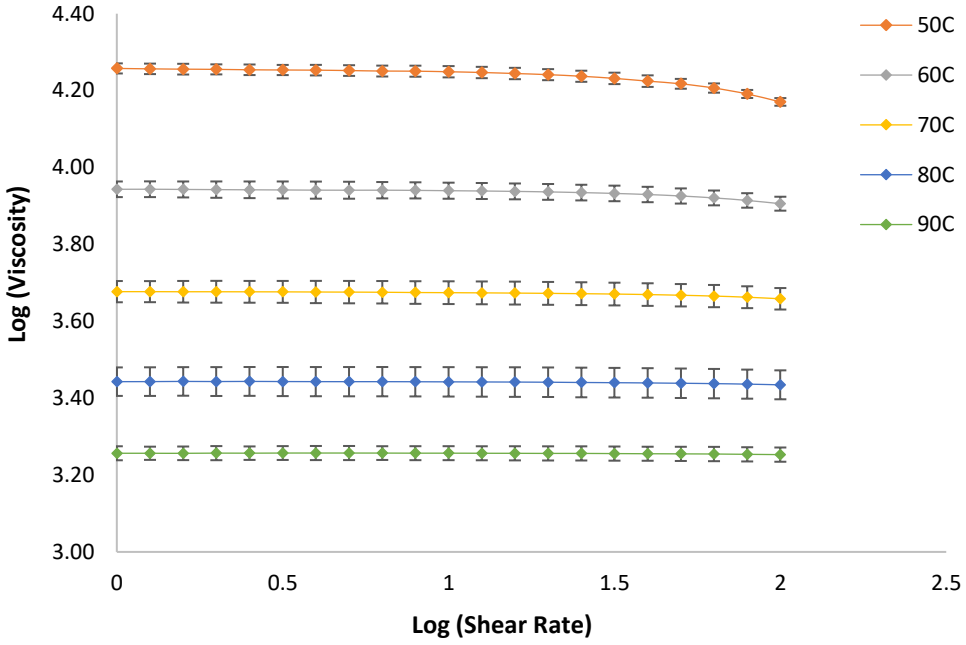


Figure 5.3: Rheological properties of sample 12 ($[C_4C_1Im][OAc]$ and cellulose)

At higher temperatures, as the kinetic energy of the molecules increases, this increases the distance between them, reducing the intermolecular forces and resulting in a lower overall viscosity (He C. and Wang Q., 1999). Newtonian behaviour was exhibited for both samples 11 ($[C_2C_1Im][OAc]$ and cellulose) and 12 ($[C_4C_1Im][OAc]$ and cellulose), similar to Sescousse R. *et al*., (2010) where the shear stress applied was proportional to the deformation of the liquid making it relatively easy to jet. Although these results contradict with those reported by Gericke M. *et al*., (2009a) and Lu F. *et al*., (2014b), where Newtonian behaviour was observed at low cellulose loading and shear thinning behaviour at higher cellulose loading and shear rates. According to Chen X. *et al*., (2009), the shear thinning behaviour was due to the decrease in entanglements with shearing and the dissolution of macromolecules at higher shear rates.

5.2.3 Printing Parameters Optimisation

Optimisation of the printing parameters was achieved by selecting three variables (temperature, pressure and pulse time) and printing droplets (droplet formation study), lines (line formation study) and films (film formation study) at different droplet spacings and observing the droplet shape and repeatability.

From the rheology results (Table 5.1), it was evident that the temperature played a significant role in the ink viscosity. Pressure determines the force applied to the ink in the syringe barrel and the pulse time is the length of valve opening. At high temperatures (low ink viscosity), increasing both pressure and pulse time ensures more ink can be filled into the fluid chamber and thus a higher jetting volume (Yang H. *et al*., 2013). Therefore, these three variables are interrelated and can have a great impact on the quality of the printed pattern and were therefore selected as the variables for the printing parameter optimisation study. Other printing parameters (Table 5.2) were kept constant throughout all the printing studies.

Table 5.2: Summary of constant printing parameters used

Parameter	Value
Open	0.25 ms
Close	0.2 ms
Cycle	10.00 ms
Stroke	75 %
Frequency	100 Hz
Volts	120 V

Droplet Formation Study

For the droplet formation study, individual drops were printed on a glass substrate at a droplet spacing of 1300 µm. These drops were printed with different printing conditions (Table 5.3). The selection of temperature (40, 65 and 90 °C), pressure (3 and 5 bar) and pulse time (0.3 and 0.7 ms) was based on the operating ranges specified by the manufacturer. The PICO Pulse valve operates from room temperature to 100 °C. Therefore, the lower, middle and upper working ranges for the PICO Pulse valve temperature were used. The pressure regulator operates between 0 and 6 bar. Lower pressures are not recommended due to air entrapment (air sucked inside because of limited ink supply) and at higher pressures satellite drops are formed (Wang L. *et al*., 2013). Hence, moderate pressure values of 3 and 5 bar were chosen. The pulse time was kept short to reduce the volume of ink filled into the fluid chamber (Yang H. *et al*., 2013) and to obtain small droplets.

The distance between the nozzle and the substrate also affects the quality of the printed pattern. As such, this distance must be larger than the droplet size to prevent the droplets coming into contact with the substrate and generating satellite drops, which can form at larger distances (Wang L. *et al*., 2013). The distance between the nozzle and the substrate was kept at 3 mm. A summary of the results and the microscopic images obtained from the droplet formation study are presented in Table 5.3 and Figure 5.4. Since, there were no satellite drops formed, it can be assumed that the distance between the nozzle and the substrate used was appropriate.

The droplet formation study revealed that no ink was ejected at 40 °C, possibly due to higher ink viscosity. At 90 °C the ink formed a bulge around the nozzle, which may be due to low ink viscosity, where the ink did not have enough energy to break from the nozzle. Stable droplets were printed at 65 °C. The connecting lines between the drops may be due the formation of a small ligament that did not merge with the leading drop. Some of the printed droplets also had air bubbles trapped, which disappeared within a few minutes.

Table 5.3: Droplet formation study results

Printing Condition	Temperature (°C)	Pressure (bar)	Pulse Time (ms)	Sample 11	Sample 12
A	40	3	0.3	No ink ejected from the nozzle	No ink ejected from the nozzle
B	40	5	0.3		
C	40	3	0.7		
D	40	5	0.7		
E	65	3	0.3	Printing	Printing
F	65	5	0.3		
G	65	3	0.7		
H	65	5	0.7		
I	90	3	0.3	No printing, bulging in the nozzle observed	No printing, bulging in the nozzle observed
J	90	5	0.3		
K	90	3	0.7		
L	90	5	0.7		

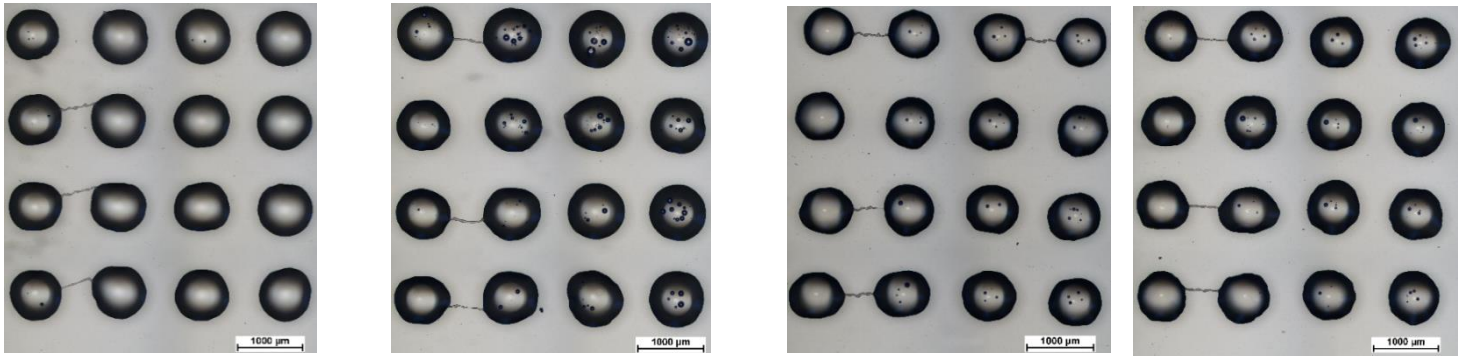
The average droplet diameter of the printed drops was measured using a microscope and ImageJ software (Ashrafmansouri S. and Esfahany M., 2015) (Table 5.4). For each printing condition, three sets of samples were printed and the average diameter using ImageJ was calculated based on the circular drops printed (non-circular droplets were removed). When calculating the average diameter using the microscopic method, data was expressed as the mean

± standard deviation, where n=6 (2 droplets from each print making a total of 6 droplets were used). Both the methods used to measure the droplet diameter produced similar results, but the sample size used in the ImageJ was higher, leading to a higher accuracy. Therefore, the average droplet diameter obtained from the ImageJ was used in all the calculations.

Table 5.4: Average droplet diameter results

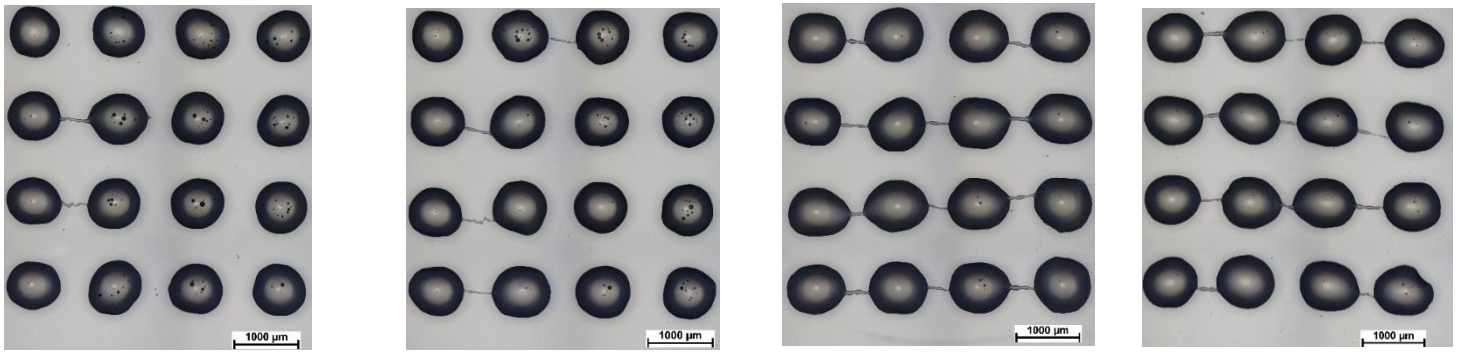
Sample	Printing Condition	ImageJ Analyzed Diameter (μm)	Microscope Measured Diameter (μm)
11	E	835 ± 22	837 ± 17
	F	841 ± 29	847 ± 11
	G	781 ± 43	768 ± 50
	H	805 ± 29	799 ± 36
12	E	840 ± 23	814 ± 13
	F	861 ± 20	847 ± 7
	G	895 ± 32	869 ± 20
	H	901 ± 26	886 ± 29

Sample 11: $[C_2C_1Im][OAc]$ and cellulose



Printing Condition E **Printing Condition F** **Printing Condition G** **Printing Condition H**

Sample 12: $[C_4C_1Im][OAc]$ and cellulose



Printing Condition E **Printing Condition F** **Printing Condition G** **Printing Condition H**

Figure 5.4: Microscopic images obtained from the droplet formation study

The microscopic images (Figure 5.4) and the average droplet diameter (Table 5.4) results revealed an increase in droplet diameter as the pressure was increased from 3 to 5 bar. At higher pressure, more ink was pushed through the syringe barrel into the PICO Pulse valve, leading to the formation of bigger droplets. It was assumed that when the valve was opened for a longer time (0.7 ms) more ink will be deposited (higher droplet diameter). However, this behaviour was not observed for sample 11. This printing study also did not show a higher droplet diameter at printing condition H (for sample 11), where the pressure and the pulse time was the highest. For the cellulose ionic liquid-based inks, it can be concluded that the droplet diameter was mainly dependent on the pressure and the ability to eject the ink from the nozzle was dependent on the ink temperature

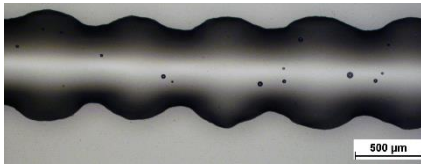
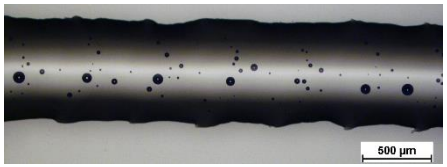
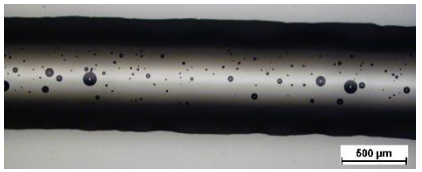
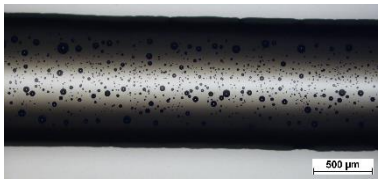
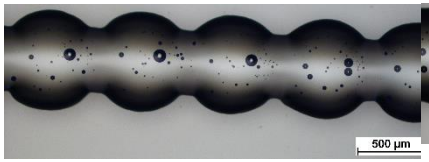
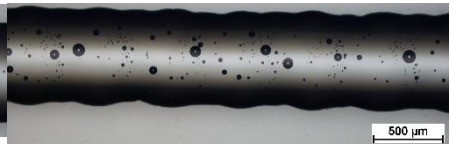
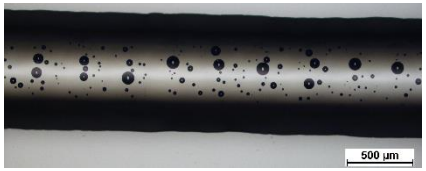
Line Formation Study

The average droplet diameter (Table 5.4) was used to calculate the droplet spacing required to print lines with different overlaps (20, 40, 60 and 80 %) using Equation 5. The calculated droplet spacing was rounded off to the nearest ten. The idea behind this study was to identify a suitable droplet spacing to form a uniform line. The microscopic images of the printed lines, along with the average line width (measured using the microscope, data expressed as the mean ± standard deviation, where n=6) are shown in Tables 5.5 and 5.6.

The microscopic images for the line formation study indicated an increase in line width as the droplet spacing decreased. The effect of droplet spacing on

droplet overlap to form lines has been investigated by Soltman D. and Subramanian V., (2008), He Y. *et al*., (2016); Zhang F. *et al*., (2016) and Hu G. *et al*., (2017). At 20 % overlap (highest droplet spacing) all the lines printed showed a scalloped shape, indicating there was not enough ink to merge and cover the printing area (Zhang F. *et al*., 2016; Hu G. *et al*., 2017). Further increasing the overlap to 40 %, majority of the printing conditions showed a scalloped line except for printing conditions G and H for sample 11. At an overlap of 60 % a uniform line was observed even though for some printing conditions the line still had some scallop behaviour. At 80 % overlap, the line width was maximum, due to the increased overlapping between the drops at lower droplet spacing leading to a higher volume of ink deposited over the printing area (He *at al*., 2016; Hu G. *et al*., 2017). Overall, lines printed at an overlap of 60 % showed a line with uniform edges compared to the others and therefore this condition was chosen to print films.

Table 5.5: Microscopic images obtained from the line formation study for sample 11

	20 % Overlap	40 % Overlap	60 % Overlap	80 % Overlap
Printing Condition E				
Droplet spacing (µm)	670	500	335	170
Average line width (µm)	N/A	N/A	858 ± 20	1150 ± 23
Printing Condition F				
Droplet spacing (µm)	675	505	340	170
Average line width (µm)	N/A	N/A	897 ± 12	1219± 47

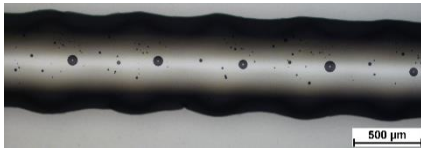
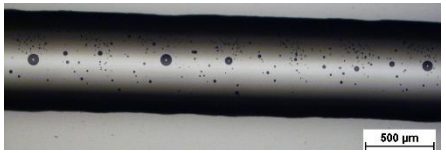
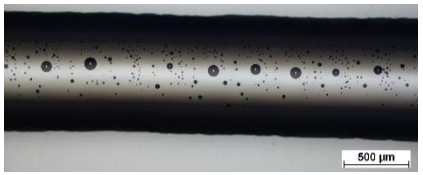
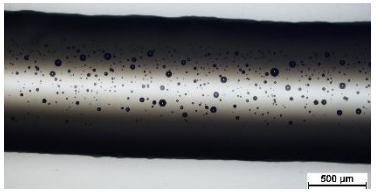
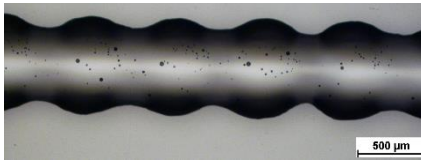
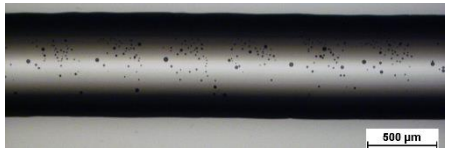
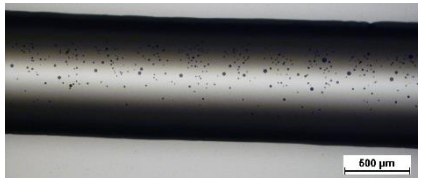
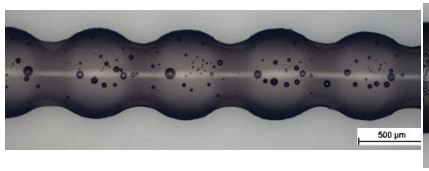
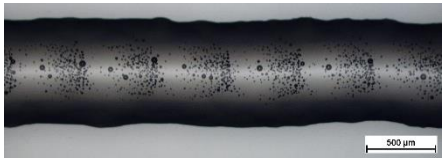
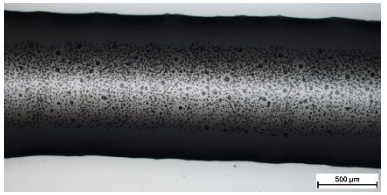
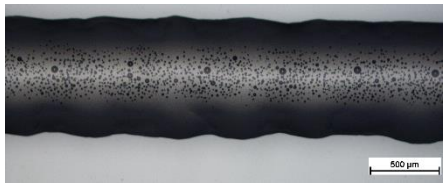
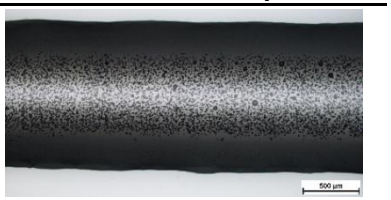
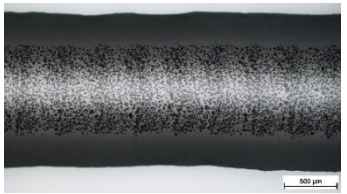
	20 % Overlap	40 % Overlap	60 % Overlap	80 % Overlap
Printing Condition G				
Droplet spacing (µm)	625	470	315	155
Average line width (µm)	N/A	758 ± 30	902 ± 14	1201 ± 32
Printing Condition H				
Droplet spacing (µm)	645	485	320	160
Average line width (µm)	N/A	740 ± 32	925 ± 27	1274 ± 41

Table 5.6: Microscopic images obtained from the line formation study for sample 12

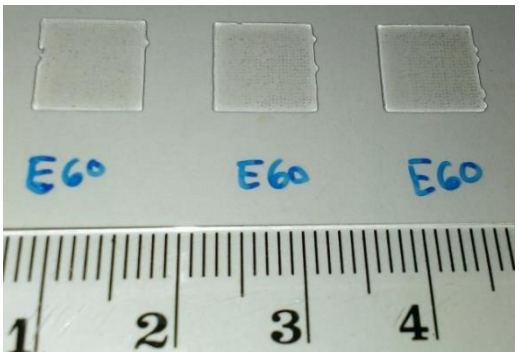
	20 % Overlap	**40 % Overlap**	**60 % Overlap**	**80 % Overlap**
Printing Condition E				
Droplet spacing (µm)	670	505	335	170
Average line width (µm)	N/A	N/A	969 ± 25	1292 ± 33
Printing Condition F				
Droplet spacing (µm)	690	520	345	170
Average line width (µm)	N/A	N/A	902 ± 53	1238 ± 16

	20 % Overlap	40 % Overlap	60 % Overlap	80 % Overlap
Printing Condition G				
Droplet spacing (µm)	715	540	360	180
Average line width (µm)	N/A	N/A	983 ± 23	1366 ± 58
Printing Condition H				
Droplet spacing (µm)	720	540	360	180
Average line width (µm)	N/A	N/A	1015 ± 62	1409 ± 45

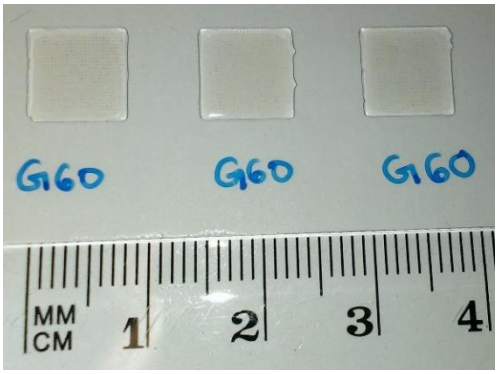
Film Formation Study

Films for sample 11 ($[C_2C_1Im][OAc]$ and cellulose), were printed at 2 different overlaps (40 and 60%) using the printing conditions E and G. These printing conditions were selected over F and H due to low pressure (3 bar). However, at 40 % overlap the individual drops didn't merge to form a uniform film. This was not the case at 60 % overlap (Figure 5.5A and B). Based on the results obtained for sample 11, films for sample 12 ($[C_4C_1Im][OAc]$ and cellulose) was printed at 60 % overlap at printing conditions E, F, G and H. Successful film printing was achieved only at printing conditions E and F (Figure 5.5C and D). With printing condition G and H, only a few lines of the film were printed, and the ink bulged at the nozzle. This may be due to the longer pulse time depositing a higher volume of ink.

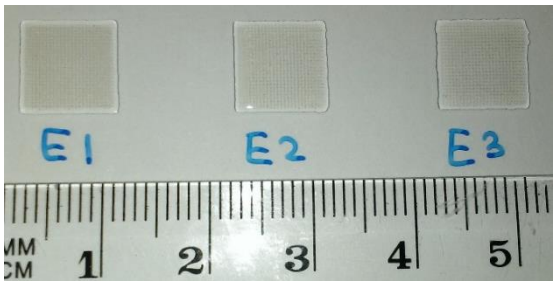
Similar to the droplet and line formation study, the trapped air bubbles disappeared within a few minutes. For both the inks, printing condition E was selected to print multi-layer films, as it had the lowest pulse time and pressure therefore were more likely to produce smaller drops without causing any bulging in the nozzle.



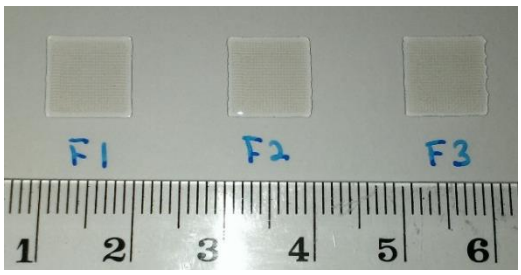
A Sample 11
Printing Condition E
Droplet Spacing: 335



B Sample 11
Printing Condition G
Droplet Spacing: 315



C Sample 12
Printing Condition E
Droplet Spacing: 335



D Sample 12
Printing Condition F
Droplet Spacing: 345

Figure 5.5: Images obtained from the film formation study

5.2.4 Multi-Layer Printing and Regeneration

The optimised printing parameters were used to print multi-layer (5 layers) films (Figure 5.6). This demonstrated the possibility of forming 3D structures using a cellulose and ionic liquid-based ink. Compared to the single layer films (Figure 5.5), as the number of layers increased, the ink was not uniformly distributed across the printing area. Instead, majority of the ink was concentrated in the centre. When an ink continues to spread on previously deposited ink which was not solidified, it is not able to hold its shape or of those

deposited on it giving rise to a time dependant deformation known as creeping (Emori K. *et al*., 2019). However, in AM this is referred as sagging behaviour. This results in a difference in morphology between the printed films and the original film pattern (He Y. *et al*., 2017a; He Y. *et al*., 2017b). This can be overcome by incorporating a support material (He Y. *et al*., 2017a; He Y. *et al*., 2017b), modifying the substrate surface (Dey T. and Naughton D., 2016) or spraying the anti-solvent during printing. Support material can be printed to help support the build material (cellulose and ionic liquid). It can be removed manually, dissolving in a solvent or by heating (Fahad M. *et al*., 2013).

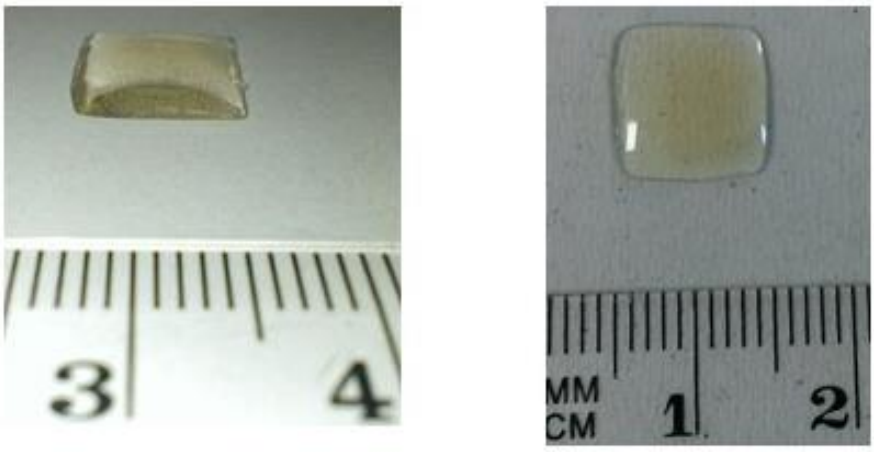


Figure 5.6: Multi-layered film printed using cellulose and ionic liquid

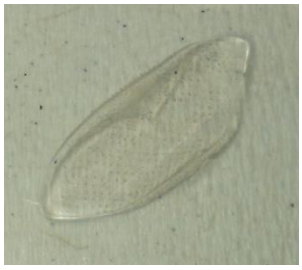
Single layer and multi-layered 3D printed films were regenerated using three different methods; straight regeneration (straight regen), overnight drying, regeneration and leave at room temperature (O.D, regen and rtm) and overnight drying, regeneration and leave in the vacuum oven (O.D, regen and vac. oven) (Chapter 3 Section 3.5).

Printed samples were fully immersed in a glass petri dish containing deionised water for 15 minutes. In Chapter 4, the WLI results showed that there was no pattern between the regeneration time and the height of the regenerated cellulose samples (Chapter 4 Section 4.3.7). Therefore, 15 minutes was chosen as a starting point. Since regeneration has generally been conducted at room temperatures, it was assumed that the room temperature was 25 °C. In order to avoid surface distortion of the printed films, the glass slide (where the film was printed) was placed in a frame before immersing in deionised water.

Rapid mixing, extrusion and casting are some of the common methods reported in literature for cellulose regeneration (Table 2.5). Ionic liquid-cellulose solutions have also been left in a humid environment to absorb moisture before regeneration (Aaltonen O. and Jauhiainen O., 2009) and regenerated cellulose has been dried in the atmosphere (Pang J. *et al*., 2015 and Reddy K. *et al*., 2017) or in a vacuum oven (Heinze T. *et al*., 2005; Zhang H. *et al*., 2005, Deng M. *et al*., 2009 and Liu Z. *et al*., 2011). Building on this literature, the purpose of the regeneration experiments, was to determine if leaving the printed films overnight at room temperature (overnight drying) and in a vacuum oven had any influence on the morphology, composition and thermal properties.

Single and multi-layered films printed using sample 11 ($[C_2C_1Im][OAc]$ and cellulose) and 12 ($[C_4C_1Im][OAc]$ and cellulose) did not maintain its shape when soaked in deionised water straight after printing (straight regen) (Figure 5.7).

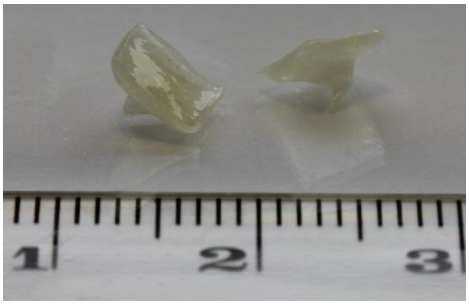
These films were printed at 65 °C in a molten state and were immersed in deionised water immediately. The loss in shape could possibly be due to deionised water at room temperature attracted to the ionic liquid, drawing the ions out from the cellulose ionic liquid matrix too quickly and breaking the film structure. Zhang H. *et al*., (2005), reported that the thickness of cellulose-ionic liquid films cast on to a glass plate was maintained at 0.5 mm to avoid the curling effect of dried regenerated cellulose. Therefore, the thickness of the printed film can also affect the final shape. Observations made during the cellulose recovery process are provided in Table 5.7. Since the films were not able to retain their shape, this straight regen procedure is not suitable for 3DP.



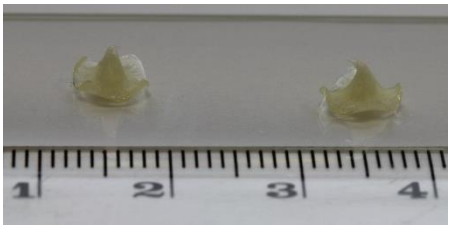
A Sample 11: 1 layer



B Sample 12: 1 layer



C Sample 11: 5 layers



D Sample 12: 5 layers

Figure 5.7: Films obtained after straight regeneration

When the printed films were left overnight at room temperature, some ink spread out leaving a film with a gel nature (Figure 5.8). This spreading maybe due to the combined effect of the sagging behaviour and the gravitational pressure. Overnight drying, allowed the rearrangement of hydrogen bonds into a more stable organised manner and heat was lost to the atmosphere and the molecules lost their kinetic energy that was holding them in the liquid state, causing a gel-like film to form. The formation of a gel film was similar to that reported by Kadokawa J. *et al*., (2007), where cellulose and $[C_4C_1Im][Cl]$ was kept between two glass plates at room temperature for a week and a gel was formed. A solution of MCC, nano-SiO_2 and $[C_2C_1Im][OAc]$ when cast on a glass slide formed a gel-like film (Song H. *et al*., 2013).

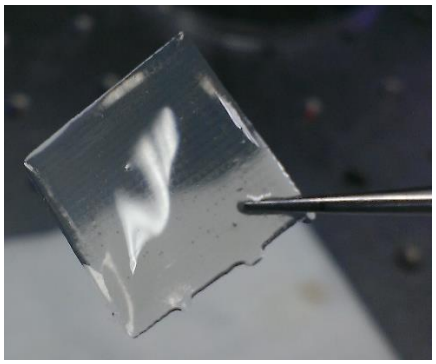
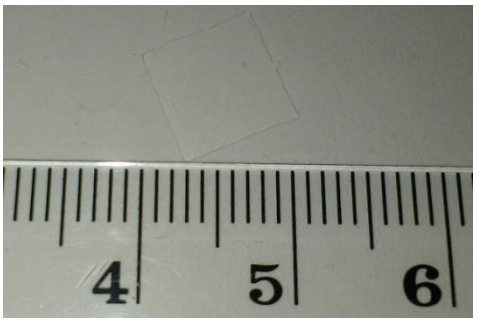


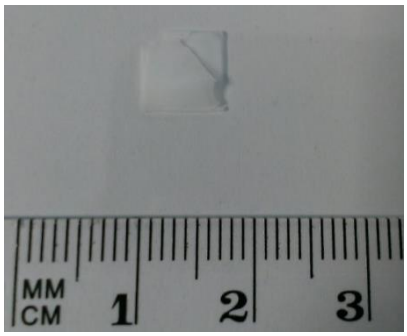
Figure 5.8: Gel film formed when sample 11 was left overnight

Both single and multi-layered, overnight dried films slowly turned white when immersed in deionised water and a very light yellow/white coloured films after leaving at room temperature or in the vacuum oven and were also able to maintain the shape (Figure 5.9). The colour change that occurred after the cellulose recovery process may be due to the manner in which ionic liquid and cellulose ordered on the microscale and removal of ionic liquid from the

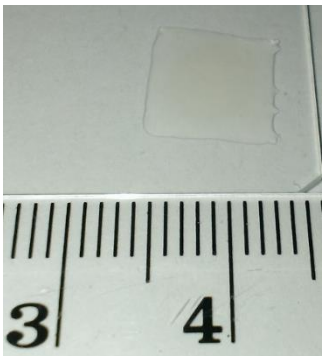
printed films. The only variation between sample 11 and 12 was the cation chain length. Sample 11 had a shorter cation ([C_2C_1Im]) compared to sample 12 ([C_4C_1Im]). This may have affected the differences in the observations made during the cellulose recovery process (Figure 5.9 and Table 5.7).



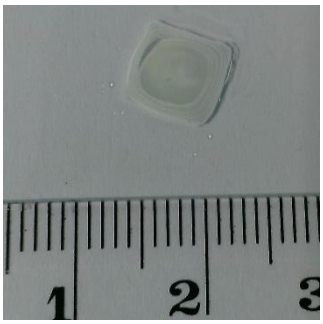
A Sample 11: 1 layer – O.D, regen and rtm



B Sample 12: 1 layer – O.D, regen and rtm



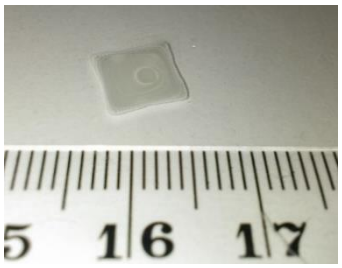
C Sample 11: 5 layers – O.D, regen and rtm



D Sample 12: 5 layers – O.D, regen and rtm



E Sample 11: 5 layers – O.D, regen and vac. oven



F Sample 12: 5 layers – O.D, regen and vac. oven

Figure 5.9: Films obtained after cellulose recovery

Table 5.7: Summary of cellulose recovery observations

Ionic Liquid	Anti-Solvent	Observations	Reference
$[C_2C_1Im][OAc]$	Deionised water	Transparent film when immersed in water and after left at room temperature. The final films did not maintain its shape.	Straight regen 1 layer In this work
		White/pale yellow film when immersed in water and turned pale yellow after left at room temperature. The final films did not maintain its shape.	Straight regen 5 layers In this work
		White film when immersed in water and turned pale yellow/white after left at room temperature/in the vacuum oven. The final films were easily foldable.	O.D, regen and rtm and O.D, regen and vac. dry In this work
$[C_4C_1Im][OAc]$	Deionised water	White film when immersed in water and after left at room temperature. The final films did not maintain its shape.	Straight regen 1 layer In this work
		White/pale yellow film when immersed in water and turned pale yellow after left at room temperature. The final film did not maintain its shape.	Straight regen 5 layers In this work
		White/pale yellow film when immersed in water and after left at room temperature. The final films formed cracks.	O.D, regen and rtm In this work
		White/pale yellow film when immersed in water and after left in the vacuum oven.	O.D, regen and vac. dry In this work
[AMIM][Cl]	Water	Transparent gel	Zhang H. *et al*., 2005
[AMIM][Cl]/ $[C_4C_1Im][Cl]$	Ethanol	Gel	Mikkola J. *et al*., 2007

Ionic Liquid	Anti-Solvent	Observations	Reference
$[C_4C_1Im][Cl]$	Water	Flexible gel	Kadokawa J. *et al*., 2007
$[C_4C_1Im][Cl]$	Ethanol	Opaque, shiny white gel, soft and compressible	Aaltonen O. and Jauhiainen O., 2009
$[C_4C_1Im][Cl]$	Water	Transparent gel	Deng M. *et al*., 2009

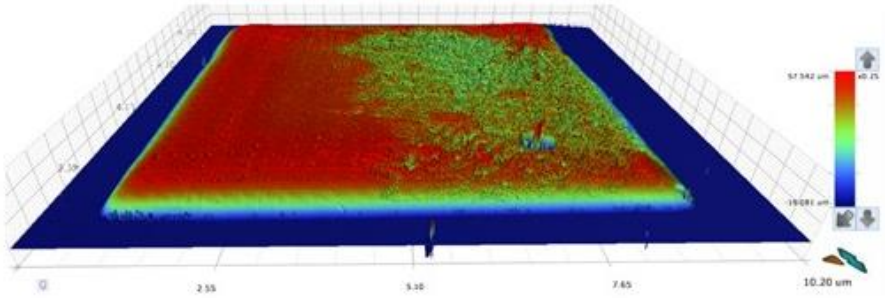
Visually, both films obtained by O.D, regen rtm and O.D, regen and vac. oven were similar, and further characterisation experiments were conducted in order to understand the differences between them.

5.2.5 Optical Characterisations

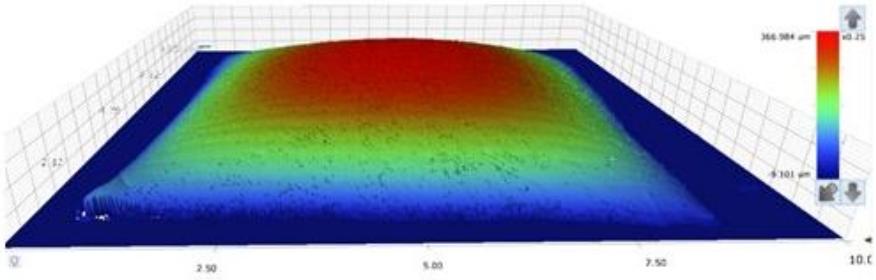
White Light Interferometry (WLI)

Films obtained after the cellulose recovery process for sample 11 ($[C_2C_1Im][OAc]$ and cellulose), were further analysed by WLI (Figure 5.10). Due to the soft nature of the films, this is a suitable non-contact technique to obtain surface height measurements compared to atomic force microscope (AFM). The average thickness for one layer film was between 15 to 18 µm. When the number of layers increased, similar to Figure 5.6, the majority of the ink was concentrated in the centre, giving rise to a maximum height between 340 to 360 µm. This roughly makes each layer 68 to 72 µm thick, which was much higher than average layer thickness based on one-layer films. One possible reason for this increase in height may come from retention of bound water in

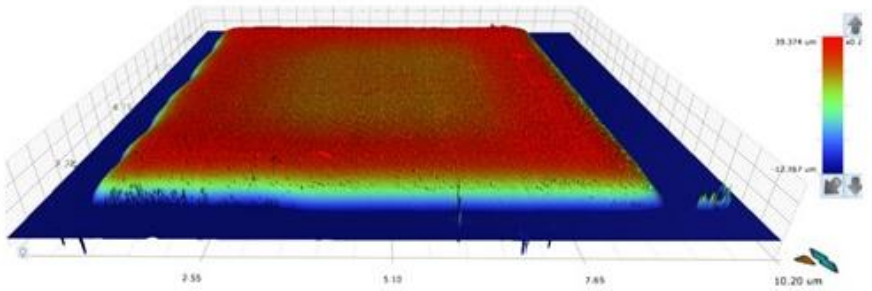
the film, even after leaving at room temperature/vacuum oven, which would have been lost in the thinner films with higher relative surface area.



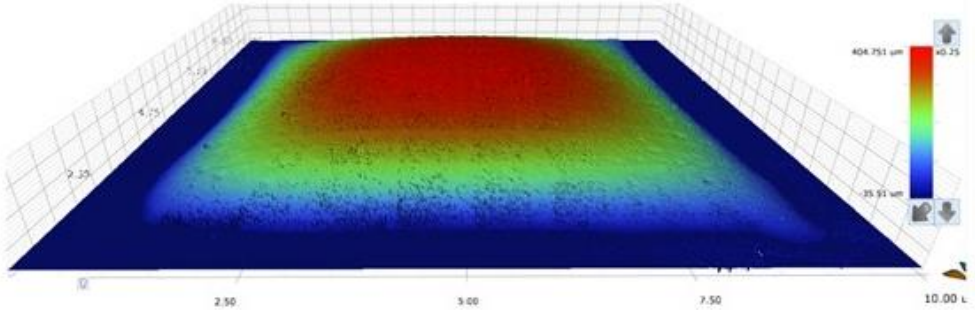
A 1 layer – O.D, regen and rtm



B 5 layers – O.D, regen and rtm



C 1 layer – O.D, regen and vac. dry



D 5 layers – O.D, regen and vac. dry

Figure 5.10: WLI results obtained for Sample 11

Scanning Electron Microscopy (SEM)

Untreated cellulose (Figure 5.11) was used as a benchmark for a qualitative comparison of morphology of the films obtained after the cellulose recovery process (Figure 5.12). From the SEM images it can be seen that undissolved cellulose was not present in the films, rather the cellulose fibres were connected into a homogeneous macrostructure giving rise to a conglomerate nature (Swatloski R. *et al*., 2002; Mikkola J. *et al*., 2007). At higher cellulose concentrations, a heterogeneous morphology has been observed due to an increase in chain entanglements and decrease in free chain mobility (Bang Y. *et al*., 1999; Liu Z. *et al*., 2011).

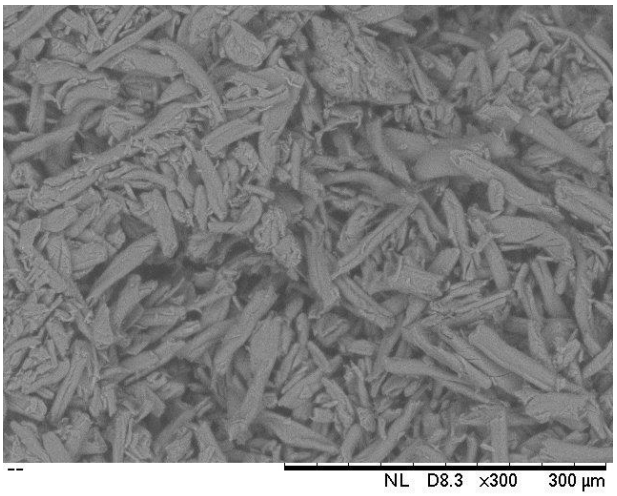
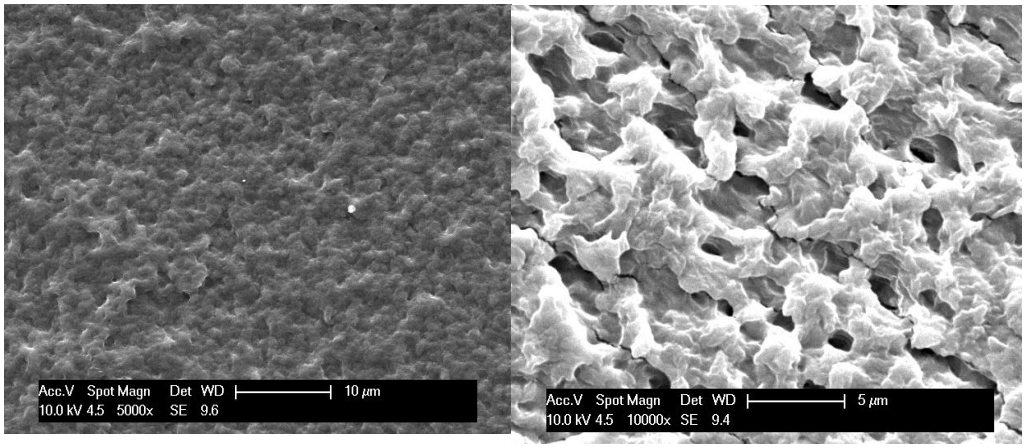


Figure 5.11: SEM image of untreated cellulose

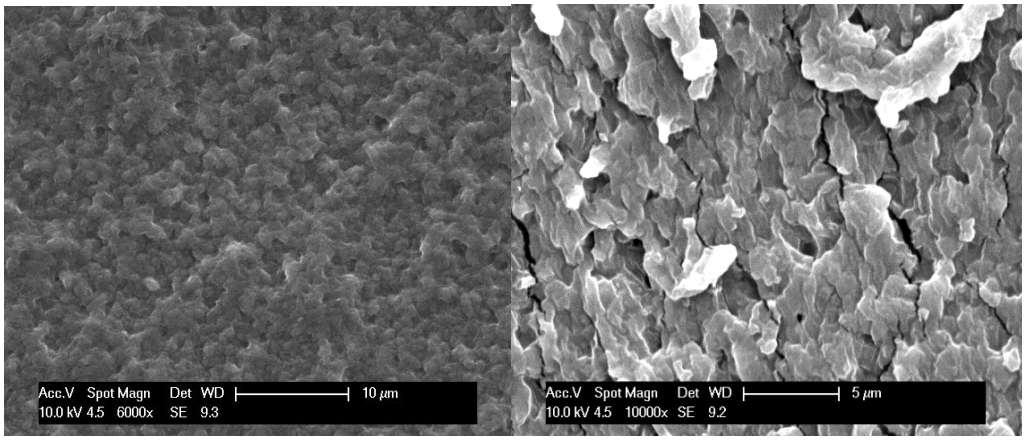
In contrast to earlier findings (Zhang H. *et al*., 2005; Xu A. *et al*., 2010; Pang J. *et al*., 2015; Reddy K. *et al*., 2017) a porous structure was observed for the films. Deng M. *et al*., (2009) discusses how different drying mechanism (oven drying and freeze drying) can be used to control the pore size of cellulose foams. Similarly, the films in this study were either left at room temperature or in a vacuum oven after removing from deionised water and this may have

contributed to the porous nature. From the SEM images (Figure 5.12A and B), pores were hardly visible on the top view for sample 11 and this may have contributed to the easily foldable nature of these films. The cracked behaviour for the films obtained from sample 12 may possibly be due to the highly porous network present both in top and cross-sectional view. This porous structure may allow water entrapment. Therefore, further characterisations must be conducted to verify the bound water concentration in the films.

Top Surface View **Cross Sectional View**

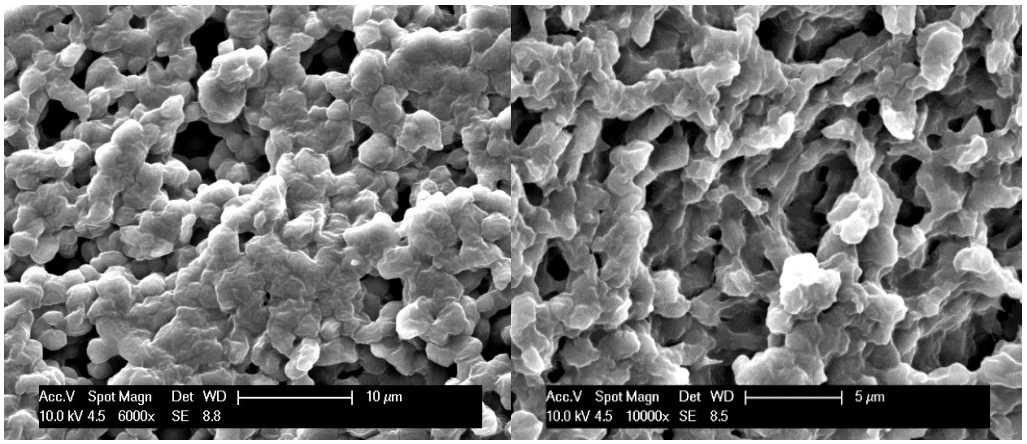


A Sample 11 ([C_2C_1Im][OAc] and cellulose) O.D, regen and rtm

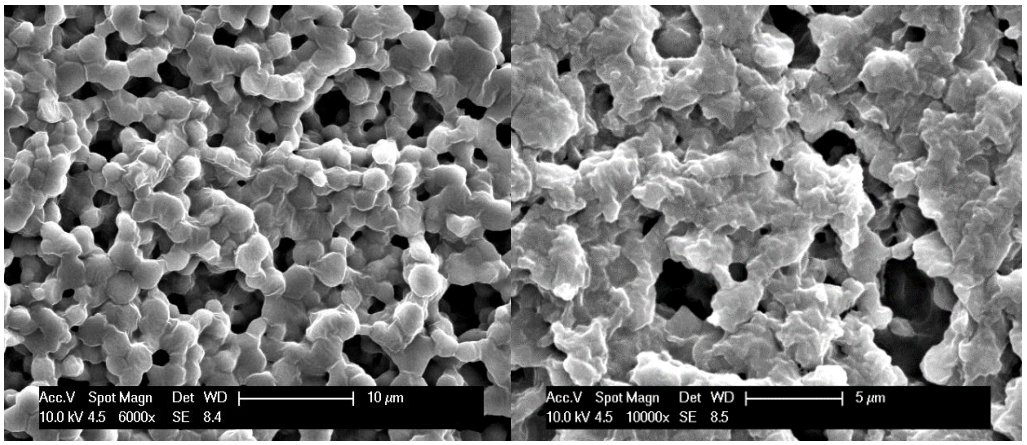


B Sample 11 ([C_2C_1Im][OAc] and cellulose) O.D, regen and vac. oven

Top Surface View **Cross Sectional View**



C Sample 12 ([C_4C_1Im][OAc] and cellulose) O.D, regen and rtm



D Sample 12 ([C_4C_1Im][OAc] and cellulose) O.D, regen and vac. oven

Figure 5.12: SEM images obtained after the cellulose recovery process

5.2.6 Characterisation of Regenerated Cellulose

Elemental Analysis

Comparing the chemical structures of the raw materials, nitrogen was present only in the ionic liquids. Therefore, the effectiveness of the cellulose recovery procedure can be measured based on the nitrogen content in the films. Table 5.8 reports the elemental analysis results for the pure chemicals, inks (sample 11 and sample 12) and the films obtained after the cellulose recovery process.

The carbon and hydrogen content in cellulose was in good agreement with previous studies conducted by Chen H., (2014) (C = 44.44 % and H = 6.17 %) and Kammiovira K. *et al*., (2016) (C = 44.14 % and H = 6.28 %).

Table 5.8: Summary of elemental analysis results

Material	Carbon	Hydrogen	Nitrogen
Cellulose	42.73 ± 0.21	6.31 ± 0.01	
$[C_2C_1Im][OAc]$	42.58 ± 1.80	8.77 ± 0.21	12.10 ± 0.94
$[C_4C_1Im][OAc]$	47.18 ± 0.71	9.66 ± 0.10	10.80 ± 0.25
$[C_2C_1Im][OAc]$ and cellulose (ink)	48.82 ± 0.36	8.37 ± 0.00	12.54 ± 0.17
Sample 11 (O.D, regen and rtm)	39.80 ± 0.08	7.30 ± 0.30	5.90 ± 0.05
Sample 11 (O.D, regen, and vac. oven)	38.84 ± 0.07	7.47 ± 0.30	6.60 ± 0.05
$[C_4C_1Im][OAc]$ and cellulose (ink)	52.16 ± 0.00	9.09 ± 0.16	11.33 ± 0.01
Sample 12 (O.D, regen and rtm)	44.82 ± 0.21	8.54 ± 0.04	6.50 ± 0.06
Sample 12 (O.D, regen, and vac. oven)	42.27 ± 0.06	8.42 ± 0.01	7.16 ± 0.04

Compared with the inks, nearly 50 % of nitrogen was lost in all the films. Also, both carbon and hydrogen percentages were reduced in all the films. Since carbon and hydrogen are present in all the raw materials used, this implies an increase in oxygen content, which could partially be accounted for by an increase in water content. Overall, it can be concluded that ionic liquid was not fully removed when the films were added to deionised water.

Fourier Transform Infrared Spectroscopy (FTIR) Analysis

The functional groups present in the pure chemicals and films obtained from samples 11 and 12 were identified using FTIR spectra (Figure 5.13 and Appendix Figure 9.21). All spectra looked identical with no new peaks, implying no chemical reaction took place during dissolution and when the printed films

were immersed in deionised water within the limits of detection for the FTIR (Zhang *et al*., H. 2005; Xu A. *et al*., 2010). This verifies that both the ionic liquids used were direct solvents for cellulose dissolution (Zhang H. *et al*., 2005), and not acting as reagents.

In the cellulose spectra, the broad absorption between 3339 and 3273 cm^{-1} was due to stretching vibrations of the cellulose hydroxyl group (O-H) (Zhang H. *et al*., 2005; Lateef H. *et al*., 2009; Jia N. *et al*., 2011; Yeng L. *et al*., 2015). The absorption was broad due to the presence of hydrogen bonds in cellulose (Zhang H. *et al*., 2005). The FTIR results on the cellulose films obtained in this study differ slightly from those of Zhang *et al*., (2005) and Xu A. *et al*., (2010) as they observed a shifting of the O-H vibrations in the regenerated cellulose films to a higher wavenumber, due to the destruction of the hydrogen bonding network (Zhang H. *et al*., 2005). However, in Figure 5.14C to F, a broader absorption was observed. The bound water was also responsible for the peak at 1654 cm^{-1} (Yeng L. *et al*., 2015), which became broader in the films (Figure 5.14C to F) and can be associated with large quantities of water introduced during the cellulose recovery process and further verify the WLI and elemental analysis results.

The peak at 1654 cm^{-1} due to bound water (Yeng L. *et al*., 2015) was negligible for both cellulose (Figure 5.14A) and ionic liquid (Figure 5.14B). This is in good agreement with the TGA and Karl Fischer Titration results (Chapter 4 Section

4.3.2) where the absorbed/bound water content for cellulose and the ionic liquids was minimum.

The absorption due to CH_2 scissoring vibrations in cellulose at 1426 cm^{-1} shifted to a lower wavenumber for the films obtained from the cellulose recovery process confirming previous findings in literature (Zhang H. *et al*., 2005; Xu A. *et al*., 2010). This is consistent with the destruction of intramolecular hydrogen bonds at C6 position (Nelson M. and O'Connor R., 1964).

The new shoulder present in the films (Figure 5.13C to F) close to 1000 cm^{-1} was due to the C-O stretching vibrations in the amorphous locations (Zhang H. *et al*., 2005). This implies that after the dissolution and cellulose recovery process cellulose rearranged to an amorphous state (Mikkola J. *et al*., 2007).

In the ionic liquid spectra (Figure 5.13B), C-H stretching and bending vibrations in the imidazole ring was responsible for the absorbance at 2962 and 1175 cm^{-1} (Jia N. *et al*., 2011). Even though the band at 1175 cm^{-1} was present for both $[C_2C_1Im]$ and $[C_4C_1Im]$ based films, the absorbance at 2962 cm^{-1} is of significantly lower intensity for $[C_2C_1Im]$ based films. This implies more ionic liquid was present in the films containing $[C_4C_1Im]$. In order to quantify the amount of ionic liquid left after the cellulose recovery process, further FTIR experiments must be conducted on the inks and the ionic liquid-water solution.

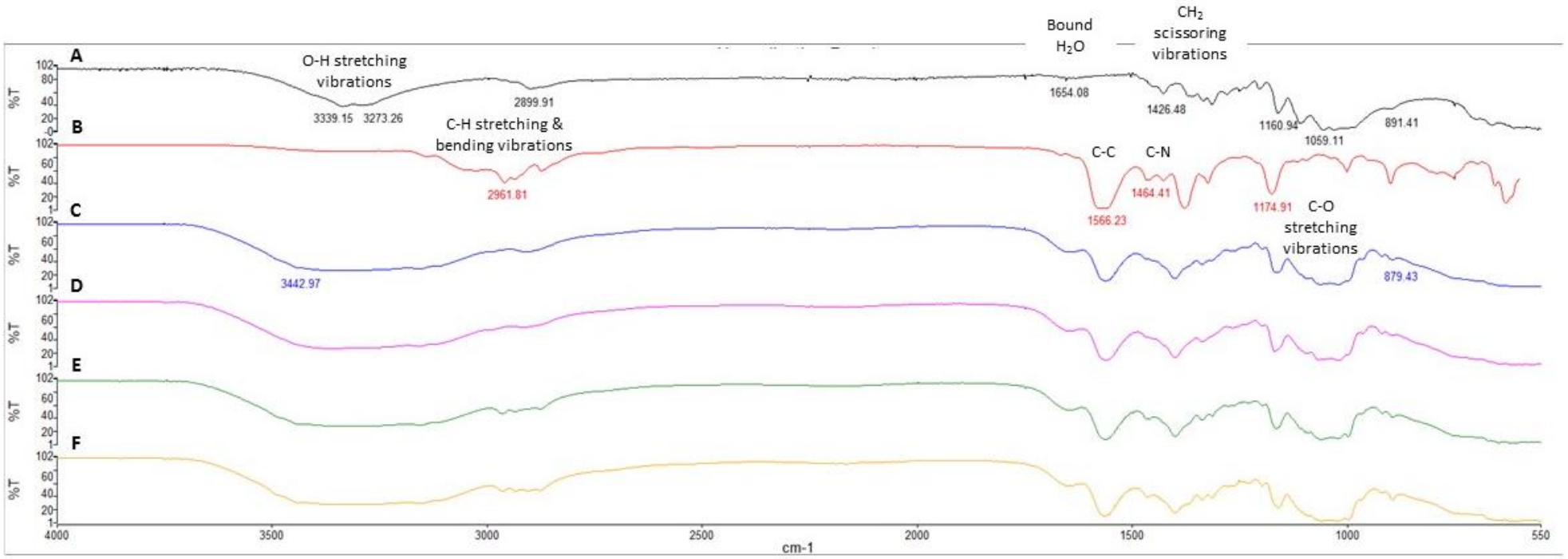


Figure 5.13: FTIR spectra obtained after the cellulose recovery process

(A)Cellulose (B) $[C_4C_1Im][OAc]$ (C) O.D, regen and rtm for sample 11 ($[C_2C_1Im][OAc]$ and cellulose) (D) O.D. regen and vac. oven for sample 11 ($[C_2C_1Im][OAc]$ and cellulose) (E) O.D, regen and rtm for sample 12 ($[C_4C_1Im][OAc]$ and cellulose) (F) O.D, regen and vac. dry for sample 12 ($[C_4C_1Im][OAc]$ and cellulose)

The major peaks present in ionic liquid due to stretching vibrations of C-C (1566 cm^{-1}) and C-N (1464 cm^{-1}) and C-H stretching and bending vibrations (1175 cm^{-1}) in the imidazolium ring (Jia N. *et al*., 2011) did not shift in the films obtained from the cellulose recovery process. The films obtained showed properties of both cellulose and ionic liquid confirming the formation of a polymer ionogel similar to that reported by Le Bideau J. *et al*., (2011) and P. C. Maar and A. C. Maar, (2016). In summary, these results are in accordance with the elemental analysis results that imply the presence of ionic liquid in the films.

Thermogravimetric Analysis (TGA)

Thermal stabilities of the multi-layered cellulose films were studied using a TGA and the results obtained are presented in Figures 5.14 and 5.15 along with the DTG curves. For comparison TGA and DTG curves for pure cellulose were also included. The initial weight loss between 50 to 150 °C was much higher for all the films (approximately 20 %) when compared to the loss from the cellulose-only sample (approximately 3 %). The removal of water during this stage was due to the hydrophilic nature of the cellulose polymer (Pang J. *et al*., 2015; Yeng L. *et al*., 2015). The TGA curves for the films obtained after cellulose recovery also differ significantly from some studies (Table 5.9) as they did not overlap at lower temperatures. The continuous weight loss that occurred in this region may also be due to the decrease in intermolecular forces and hydrogen bonds (Yeng L. *et al*., 2015) in the films caused by the disruption of the cellulose macromolecular structure.

A TGA study conducted by Kadokawa J. *et al*., (2008), showed an increase in the water content for a cellulose ionic liquid-based gel that was left between two glass plates at room temperature for a week compared to a cellulose and ionic liquid solution. Therefore, it can be concluded that another possible reason for the increase in water content observed from WLI, elemental analysis, FTIR and TGA occurred during overnight drying.

Similar to pure cellulose a two-step degradation was observed between 150 to 290 °C and 290 to 580 °C where the weight loss was approximately 60 % and 19 % for [C_2C_1Im] and 66 % and 12 % for [C_4C_1Im] containing films. During this weight loss stage, the films were completely burnt as a result of oxidative thermal degradation and loss of its crystallite structure (Yeng L. *et al*., 2015). Overall, the weight loss over this region for the films was lower compared to cellulose (77 % and 18 %) which could possibly be due to the higher amount of water present.

From the DTG curves, it is evident that all the films had a lower degradation temperature than that of cellulose (Table 5.10). This is consistent with previous findings in the literature (Table 5.9), where regenerated cellulose had a lower thermal stability than pure cellulose. The low thermal stability has been attributed to low crystallinity (Liu Z. *et al*., 2011; Reddy K. *et al*., 2014) and molecular weight (Yeng L. *et al*., 2015), that occurred due to the rupture of hydrogen bonds in cellulose during dissolution (Reddy K. *et al*., 2017). Table 5.10 also compares the degradation temperature for the pure chemicals and

the films. The degradation temperature of the films was close to that of the ionic liquids indicating the presence of ionic liquid in these films. Films obtained from [C_4C_1Im] (sample 12) had a degradation temperature similar to the corresponding ionic liquid indicating that more ionic liquid was present in sample 12 compared to sample 11.

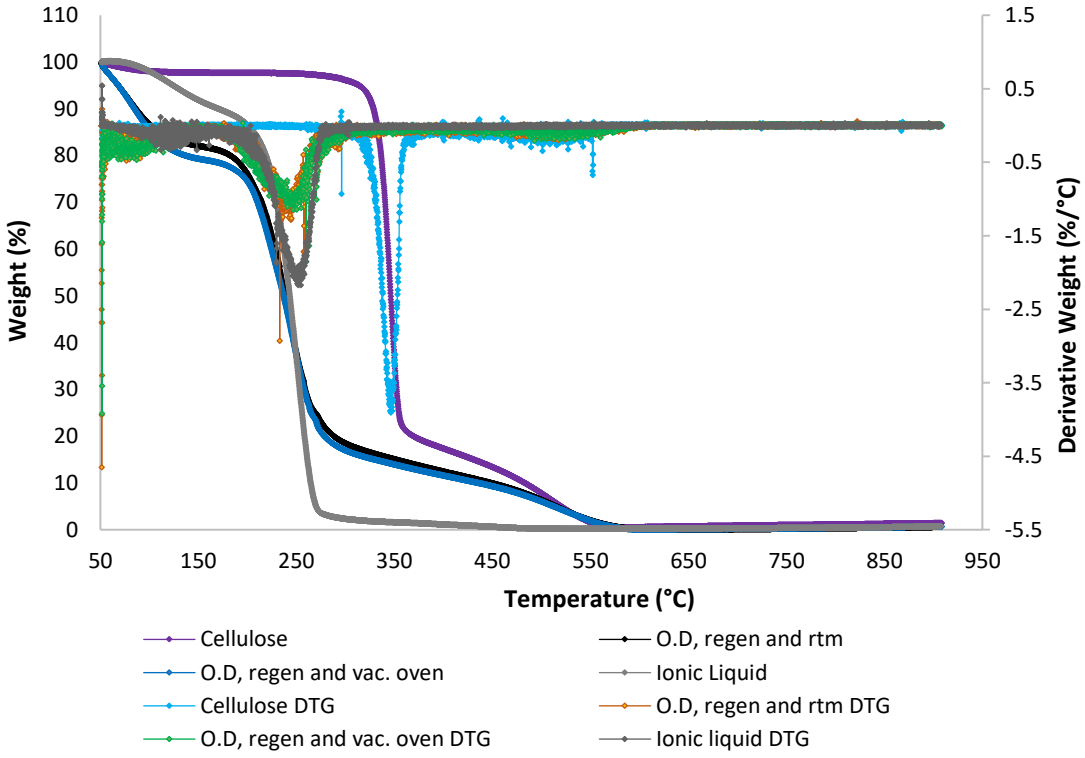


Figure 5.14: TGA and DTG curves for pure chemicals and films obtained from sample 11

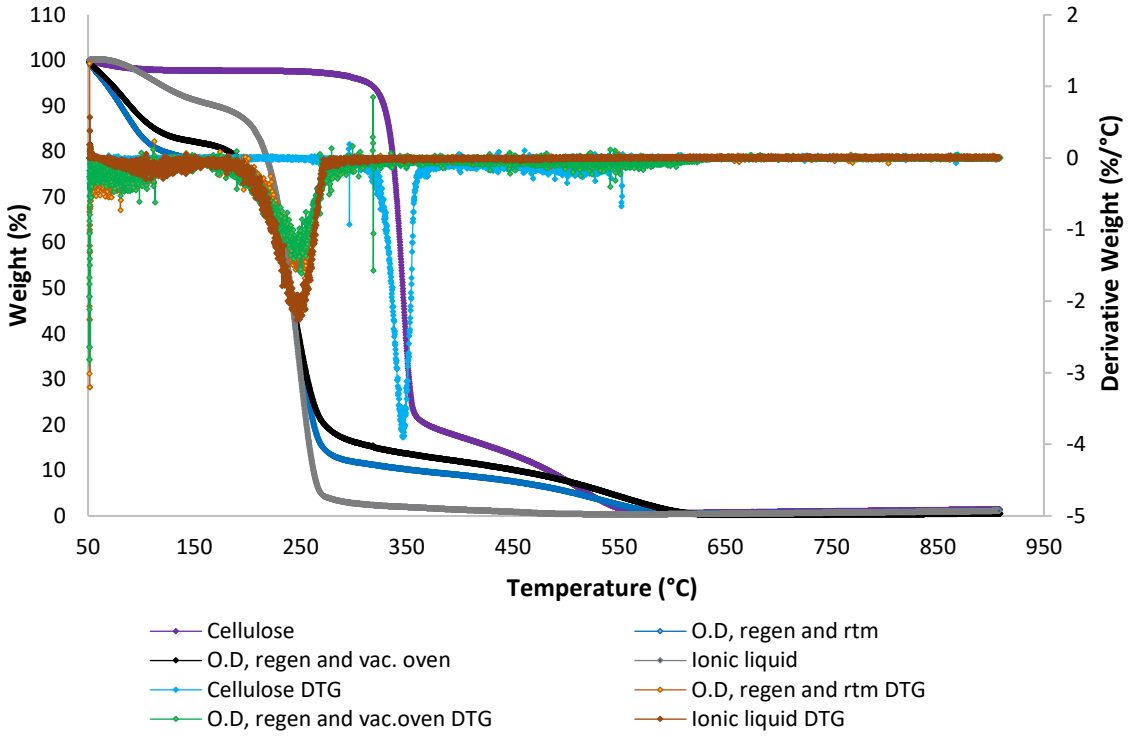


Figure 5.15: TGA and DTG curves for pure chemicals and films obtained from sample 12

Table 5.9: Summary of cellulose regeneration TGA results reported in literature

Ionic Liquid	Cellulose Type	Absorbed or Bound Water	Thermal Stability of Regenerated Cellulose	Char Yield in Regenerated Cellulose	Reference
$[C_4C_1Im][Cl]$	Cellulose pulp	More than raw cellulose	Lower than raw cellulose	Higher than raw cellulose	Swatloski R. *et al*., 2002
AMIM][Cl]/ $[C_4C_1Im][Cl]$	Cotton linter	Similar to raw cellulose	Lower than raw cellulose	Higher than raw cellulose	Mikkola J. *et al*., 2007
$[C_4C_1Im][Cl]$	Cellulose	More than raw cellulose	Lower than raw cellulose	Higher than raw cellulose	Kadokawa J. *et al*., 2008
$[C_4C_1Im][Cl]$	Cellulose	Similar to raw cellulose	Lower than raw cellulose	Higher than raw cellulose	Quan S. *et al*., 2010
$[C_4C_1Im][OAc]$	MCC	Similar to raw cellulose	Lower than raw cellulose	Higher than raw cellulose	Xu A. *et al*., 2010
$[C_4C_1Im][Cl]$	Cotton pulp	Similar to raw cellulose	Lower than raw cellulose	Higher than raw cellulose	Liu Z. *et al*., 2011
$[C_4C_1Im][Cl]$	Cellulose	Similar to raw cellulose	Lower than raw cellulose	Higher than raw cellulose	Lan W. *et al*., 2013

Ionic Liquid	Cellulose Type	Absorbed or Bound Water	Thermal Stability of Regenerated Cellulose	Char Yield in Regenerated Cellulose	Reference
[AMIM][Cl]	Cellulose microfibrils extracted from Agave raw fibres	Similar to raw cellulose	Lower than raw cellulose	Higher than raw cellulose	Reddy K. *et al*., 2014
[AMIM][Cl]	Cellulose extracted from borassus fruit raw fibres	Similar to raw cellulose	Lower than raw cellulose	Higher than raw cellulose	Reddy K. *et al*., 2017

Table 5.10: Degradation temperatures for pure chemicals and films obtained from the cellulose recovery process

Pure Chemical/Film Type	Degradation Temperature (°C)
Cellulose	345
$[C_2C_1Im][OAc]$	250
$[C_4C_1Im][OAc]$	245
Sample 11 – O.D, regen and rtm	240
Sample 11 – O.D, regen and vac. oven	245
Sample 12 – O.D, regen and rtm	245
Sample 12 – O.D, regen and vac. oven	245

The higher char yield present in regenerated cellulose compared with pure cellulose was due to the presence of impurities (Swatloski R. *et al*., 2002; Xu A. *et al*., 2010; Lan W. *et al*., 2013; Yeng L. *et al*., 2015). However, the cellulose films obtained in this study did not indicate the presence of impurities.

The thermal stability results were not affected by the type of ionic liquid used ($[C_2C_1Im]$/$[C_4C_1Im]$) and the manner in which the films were treated after they were removed from deionised water (leaving at room temperature/vacuum oven).

5.3 Chapter Summary

- The TGA study conducted for cellulose at isothermal conditions revealed that majority of the weight loss occurred within the first 5 minutes. However, this weight (0.12 %) was much lower than the previous TGA (3 %) results, indicating that water may be tightly bound as part of the hydrogen bonds.

- A maximum cellulose loading of 13 wt% and 10 wt% was achieved in the presence of the ionic liquids $[C_2C_1Im][OAc]$ and $[C_4C_1Im][OAc]$, respectively. Higher cellulose loading in $[C_2C_1Im][OAc]$ can be attributed to the short cation chain length and low pure ionic liquid viscosity (85.47 mPa s at 25 °C) compared to $[C_4C_1Im][OAc]$.
- Both the cellulose ionic liquid-based inks showed Newtonian behaviour between 50 to 90 °C, where the shear stress was proportional to the deformation of the liquid.
- The droplet formation study revealed that no printing was achieved at 40 °C and 90 °C. However, stable drops were printed at 65 °C. The droplet diameter was mainly dependent on the pressure and the ability to eject the ink from the nozzle was dependent on the ink temperature.
- The line formation study revealed that the lowest line width was observed at highest droplet spacing and highest line width was observed at the lowest droplet spacing. Lines printed at 60 % overlap showed lines with uniform edges and were used for the film formation study.
- Individual drops didn't merge to form a uniform film at 40 % overlap (for sample 11). However, at 60 % overlap uniform films were produced. Even though, uniform lines were printed at 60 % overlap when printing a film at a higher pulse time (0.7 ms) the inks started to bulge in the nozzle (for sample 12). Therefore, the selection of the printing condition for multi-layer printing was based on low pulse time and pressure, where smaller drops will be produced.

- When printing multiple layers, the printed films showed a sagging behaviour where majority of the ink was concentrated in the centre. This behaviour can be reduced by either using a support material, modifying the substrate surface or by spraying the anti-solvent over the printed layer.
- When the printed films (single and multi-layered) were soaked in deionised water immediately after printing they did not maintain their shape. However, films left to dry overnight didn't lose their shape. This was because, overnight drying allowed the rearrangement of hydrogen bonds into a more stable organised manner by forming a film with gel nature. But immersing the films straight in deionised water meant that the ions in the cellulose-ionic liquid mixture was drawn out too quickly resulting in loss of shape.
- Morphological data obtained from the SEM images showed that the, pores were hardly visible on the top surface for films obtained from $[C_2C_1Im][OAc]$. For $[C_4C_1Im][OAc]$ large number of pores were present both on the top and cross sectional view. Hence, the reason for the cracked nature of these films due to water entrapment.
- The colour changes that occurred during the cellulose recovery process may be due to the manner in which ionic liquid and cellulose ordered on the microscale and removal of ionic liquid from the printed films.
- A short cation like $[C_2C_1Im]$ can be removed easily compared to $[C_4C_1Im]$ from the cellulose ionic liquid mixture during the biopolymer recovery process. This is likely due to steric hindrance resulting from the higher molecular weight cation. This was validated by the FTIR results where more

ionic liquid was present in [C_4C_1Im]-based film after the biopolymer recovery process. This may have affected the difference in observations made during the cellulose recovery process with [C_2C_1Im][OAc] and [C_4C_1Im][OAc] ionic liquids where a easily foldable films was formed for [C_2C_1Im][OAc]-based films.

- In the FTIR spectrum, the peak due to bound water at 1654 cm^{-1} was not significant for both cellulose and ionic liquid indicating the absorbed/bound water was negligible. This further confirms the low water content observed for cellulose and the ionic liquids using TGA and Karl Fischer Titration.
- When multiple layers were printed, the average layer thickness increased, indicating the presence of water even after leaving at room temperature/vacuum oven. This was further verified by elemental analysis, FTIR and TGA results on the films obtained after the cellulose recovery process. From the elemental analysis both carbon and hydrogen content reduced implying an increase in oxygen content. In the FTIR spectra the absorptions due to the hydroxyl group (O-H) between 3339 and 3273 cm^{-1} and at 1654 cm^{-1} became broader for the films. From the TGA curve the initial water content of the films was nearly 20%. In summary, the introduction of water into the films occurred during overnight drying and when the films were immersed in deionised water.
- The TGA curve for the films followed a similar pattern like pure cellulose where the rapid weight loss occurred via a two-step process. However, weight loss during this stage was lower compared to cellulose further proving the presence of water.

- From the FTIR spectra the presence of a shoulder around 1000 cm^{-1}, indicated that after dissolution in ionic liquid and coagulation in deionised water, cellulose rearranged into an amorphous state.
- The presence of the absorbance in the FTIR spectra at 2962 cm^{-1} due to C-H stretching and bending vibration in the imidazolium ring showed that more ionic liquid was present in the [C_4C_1Im] containing films obtained after the cellulose recovery process. This was further supported by the TGA results where the degradation temperature for [C_4C_1Im][OAc] was similar to that of the films (245 °C).
- Even though, the elemental analysis results showed approximately a 50 % decrease in nitrogen content in the films recovered from cellulose and ionic liquid inks. The FTIR spectra for the films had characteristic absorbance for imidazole ring stretching and bending vibrations. Also, the degradation temperatures of the films were very close the ionic liquids. All these observations verify the formation of an ionogel type film.
- The lower thermal stability of the films obtained from the cellulose recovery process was due to the destruction of the cellulose macromolecular structure during dissolution, reducing the hydrogen bonds, crystallinity and molecular weight forming an amorphous film.

Chapter 6 : Three-Dimensional Printing of Wool and Blends using a PICO Pulse Printer

6.1 Background

In Chapter 5, cellulose and ionic liquid-based high viscosity inks were successfully printed and immersed in deionised water to obtain an ionogel type film. Building on this work, the ability to 3DP another biopolymer (wool) and blends (inks containing cellulose and wool) would provide a broader range of inks and properties.

Chapter 6, focused on preparing high viscosity inks with the ionic liquids; $[C_2C_1Im][OAc]$ and $[C_4C_1Im][OAc]$. Next, droplets, lines and films were printed at different printing parameters (pressure, temperature, pulse time and droplet spacing) to optimise the printing conditions. The optimum printing parameters were used to print single and multi-layered films which were immersed in deionised water to remove the ionic liquid. Finally, these films were characterised to evaluate the morphology and thermal stability.

6.2 Justification

Compared to cellulose dissolution in ionic liquid, research conducted on wool solubility is still at an early stage. The selection of the ionic liquids ($[C_2C_1Im][OAc]$ and $[C_4C_1Im][OAc]$) for wool dissolution was based on the justification provided in Chapter 4 Section 4.2.2. Wang L. *et al*., (2016b) and Li

R. and Wang D. (2013), studied the thermal stabilities of regenerated keratin obtained from different anti-solvents. They concluded that the thermal stabilities vary with the type of ionic liquid and anti-solvent used. However, keratin regenerated from water has shown good thermal stability. Therefore, deionised water was used as the anti-solvent in this study.

6.3 Result and Discussion

6.3.1 Preparation of High Viscosity Inks: Wool and Ionic Liquid

In order to identify a suitable temperature for wool dissolution in ionic liquids, a TGA analysis was performed for wool. The conditions used were similar to that reported before (Chapter 4 Section 4.3.2). However, a nitrogen flow rate of 20 mL/minute was used. From Figure 6.1, it can be seen that the initial weight loss was due to the evaporation of absorbed or bound water (Idris A. *et al*., 2013; Li R. and Wang D., 2013; Idris A. *et al*., 2014; Wang L. *et al*., 2016b; Liu X. *et al*., 2017). For wool, this was between 50 to 150 °C where the weight loss was approximately 7 %. Then there was a rapid weight loss during the second weight loss stage, indicating keratin decomposition (Wang L. *et al*., 2016b) and destruction of bonds (Li R. and Wang D., 2013). This occurred between 210 to 480 °C where the weight loss was approximately 57 %. This is in good agreement with Li R. and Wang D. (2013), as they observed a 60 % weight loss in wool keratin between 150 and 500 °C. Compared to cellulose (Figure 4.1), wool had a higher quantity of absorbed or bound water (3 % for cellulose) and a small char yield indicating the presence of impurities. The

degradation temperature ranges for keratin obtained from literature are summarised in Table 6.1.

Table 6.1: Degradation temperatures for keratin

Keratin Type	Degradation Temperature (°C)	Reference
Wool	325	In this work
Turkey feathers	Between 250 and 400	Idris A. *et al.*, 2013
Wool keratin	320	Li R. and Wang D., 2013
Goat wool	Between 240 and 450	Liu X. *et al.*, 2017

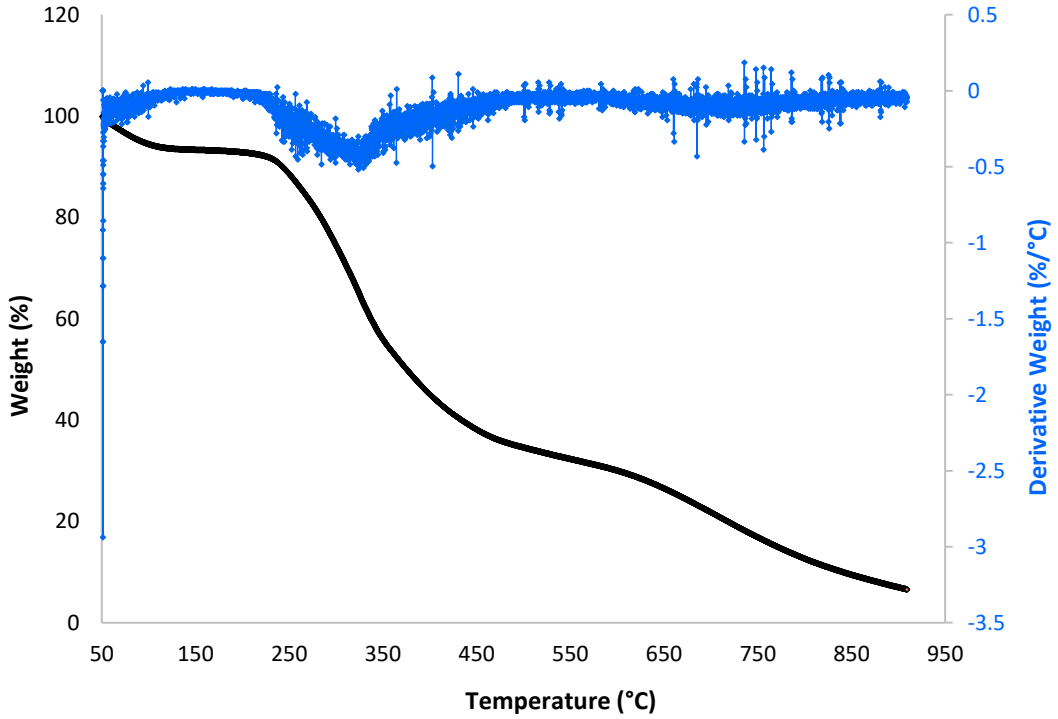


Figure 6.1: TGA and DTG curves for wool

A common dissolution temperature range used in the literature has between 120 to 130 °C (Table 2.4). However, it is not advisable to use higher temperatures for dissolution due to keratin degradation (Wang L. *et al.*, 2016b) and protein modification (Ghosh A. *et al.*, 2014). Therefore, after considering the wool (Table 6.1) and ionic liquid (Table 4.3) degradation temperatures, 100 °C was used as a suitable dissolution temperature for the inks containing wool.

The dissolution conditions used to prepare the high viscosity inks (stirring speed 800 rpm and oil bath) were similar to those used before (Chapter 4 Section 4.3.2). The samples were occasionally stirred manually using a spatula to enhance the dissolution process. Wool loading in the samples were gradually increased in increments of 5 wt%. Initially the dissolution was fast; further increasing the wool loading resulted in a viscous solution and slower dissolution rate. These observations are similar to those reported by Idris A. *et al*., (2013) for turkey feather dissolution in an ionic liquid. The maximum solubility for $[C_2C_1Im][OAc]$ and $[C_4C_1Im][OAc]$ was 20 wt% (sample 13) and 25 wt% (sample 14). Stepwise addition of keratin to ionic liquid has been reported by Idris A. *et al*., (2013) and Idris A. *et al*., (2014). The limiting solubility was recorded when the solution became too viscose to dissolve or when poor solubility was seen. However, this may represent a solubility lower than the actual solubility that can be achieved.

The dissolution results obtained in this study do not support previous dissolution trends (Idris A. *et al*., 2013; Li R. and Wang D., 2013), because the wool loading in the short cation chain length-based ionic liquid ($[C_2C_1Im][OAc]$) was lower than that of the long cation chain length-based ionic liquid ($[C_4C_1Im][OAc]$). A likely reason may be the validity of the method used to determine the wool solubility in the ionic liquids, as it may not represent the maximum solubility. Compared to cellulose ionic liquid-based inks prepared before (Chapter 5 Section 5.2.1), the amount of wool dissolved in the same ionic liquid was much higher. This could possibly because of the strong intra-

and intermolecular hydrogen bonds present in cellulose which was not broken as quickly as the intra- and inter chain bonds present in keratin.

The final solutions were viscous with no precipitates, in line with previous findings in the literature (Xie H. *et al*., 2005; Hameed N. and Guo Q., 2009; Hameed N. and Guo Q., 2010; Sun P. *et al*., 2009; Wang M. *et al*., 2014; Idris A. *et al*., 2013). Initially the solutions had an amber colour that became darker. This colour change has previously been attributed to protein modification (Ghosh A. *et al*., 2014), and is consistent with degradation of mixture components at higher temperatures used for dissolution.

Human hair fibre dissolution in the ionic liquid $[C_4C_1Im][Cl]$ was observed under the microscope by Wang M. *et al*., (2014). Initially the ionic liquid diffused into human hair and the fibres swelled, changing from an amorphous to a crystalline state. During this time, the ionic liquid was suggested to react with different functional groups present in hair fibre (*e.g.* –OH, $-NH_2$, -COOH etc.). With time, the fibres broke and were dispersed, after which they were not visible under the microscope, possibly due to the destruction of covalent and non-covalent interactions, leading to dissolution. These observations are consistent with those reported by Li R. and Wang D., (2013), Li R. *et al*., (2014), Zheng S. *et al*., (2015) and Liu X. *et al*., (2017), for keratin dissolution in the presence of an ionic liquid.

The inks containing wool and either $[C_2C_1Im][OAc]$ or $[C_4C_1Im][OAc]$, when left at room temperature (assumed to be 25 °C), showed an increase in viscosity. Similar observations were made by Idris A. *et al*., (2013), where the viscosity increased for a [AMIM][Cl] and turkey feather mixture when cooled down to room temperature. Hence, for handling, these inks were heated for 5 minutes at 100 °C before filling into the syringe barrel.

6.3.2 Rheological Properties of High Viscosity Inks: Wool and Ionic Liquid

Rheological properties of the high viscosity inks containing wool and ionic liquid (samples 13 and 14) were investigated similar to the procedure outlined in Chapter 5 Section 5.2.2. The logarithmic curve of viscosity Vs shear rate is presented in Figures 6.2 and 6.3. The non-Newtonian index (*n*) and the ink viscosities at the highest shear rate (100 s^{-1}) at different temperatures are shown in Table 6.2. Similar to the high viscosity samples prepared using cellulose (Table 5.1), the viscosity decreased with increasing temperature.

Table 6.2: Rheological properties of the high viscosity inks containing wool and ionic liquid

Temperature (°C)	Sample 13		Sample 14	
	Viscosity (mPa s)	Non-Newtonian Index (*n*)	Viscosity (mPa s)	Non-Newtonian Index (*n*)
40	1921 ± 75	0.82	11260 ± 746	0.87
50	1075 ± 41	0.81	5189 ± 189	0.86
60	662 ± 26	0.77	2712 ± 38	0.84
70	447 ± 19	0.74	1604 ± 52	0.79
80	328 ± 16	0.69	1067 ± 59	0.73
90	258 ± 11	0.62	781 ± 57	0.69

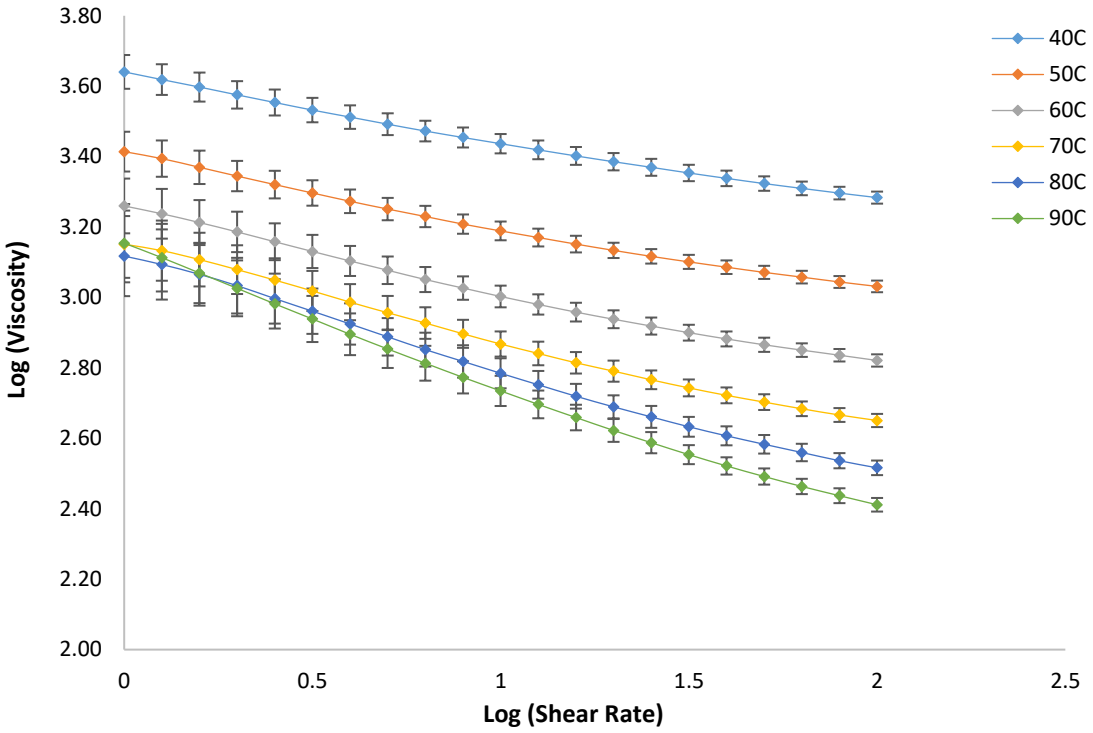


Figure 6.2: Rheological properties of sample 13 ([C_2C_1Im][OAc] and wool)

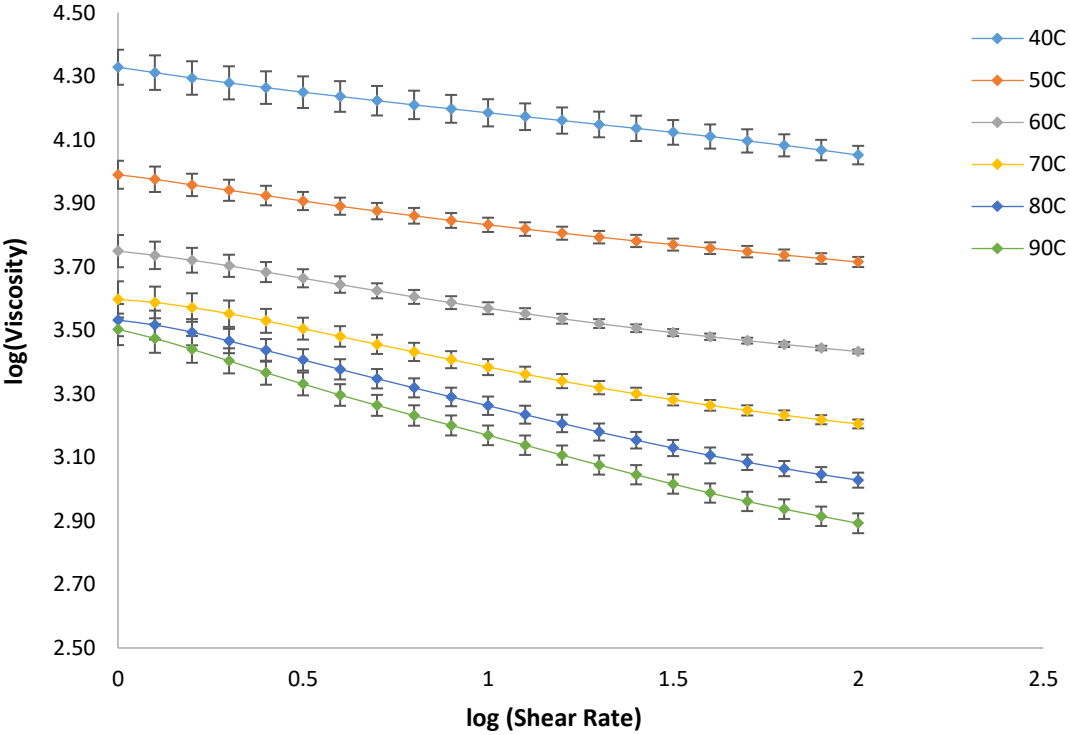


Figure 6.3: Rheological properties of sample 14 ([C_4C_1Im][OAc] and wool)

Shear thinning behaviour was exhibited for both sample 13 ([C_2C_1Im][OAc] and wool) and 14 ([C_4C_1Im][OAc] wool), as shown by a decrease in the non-Newtonian index (*n*) with increasing temperature. Similar studies have been conducted by Liu X. *et al*., (2017) and Zheng S. *et al*., (2015) where the non-Newtonian index, initially increased and then decreased (with increasing temperature) but remained between 0.8 and 0.9 for keratin-ionic liquid solutions. Even though the loading in the wool-based samples (20 to 25 wt%) were much higher than the cellulose-based samples (10 to 13 wt%), viscosity of the wool-based samples were low. Also, the cellulose-based samples showed Newtonian behaviour. The type of biopolymer and the loading may have contributed to these differences in the rheological properties.

Shear thinning behaviour allows to eject an ink at a lower viscosity and to maintain the shape of the printed pattern once the shear is removed (Detsch R. *et al*., 2008; Faddoul R. *et al*., 2012). Since the non-Newtonian index varied with increasing temperature for the wool-based inks, careful selection of printing temperature is crucial to achieve successful printing.

6.3.3 Printing Parameters Optimisation: Wool and Ionic Liquid

Optimisation of the printing parameters was achieved by selecting three variables (temperature, pressure and pulse time) and printing droplets (droplet formation study), lines (line formation study) and films (film formation study) at different droplet spacings, and observing their shapes and repeatability, mirroring the study carried out for cellulose inks (Chapter 5 Section 5.2.3).

Droplet Formation Study

For the droplet formation study, individual drops were printed on a glass substrate at a droplet spacing of 1300 µm for $[C_2C_1Im][OAc]$ containing ink (sample 13) and 1700 µm for $[C_4C_1Im][OAc]$ containing ink (sample 14). A higher droplet spacing was used for sample 14, to prevent the droplets from merging. These droplets were printed under different printing conditions (Table 6.3). A summary of the results and the microscopic images obtained from the droplet formation study are presented in Table 6.3 and Figures 9.22 and 9.23.

Table 6.3: Droplet formation study results

Printing Condition	Temperature (°C)	Pressure (bar)	Pulse Time (ms)	Sample 13	Sample 14
A	40	3	0.3	Missing drops and splashing	No ink ejected from the nozzle
B	40	5	0.3		
C	40	3	0.7	Small ligaments	
D	40	5	0.7	Droplets started to merge	
E	65	3	0.3	Lot of splashing	
F	65	5	0.3		
G	65	3	0.7	Small ligaments and some droplets started to merge	
H	65	5	0.7		
I	90	3	0.3	No printing, bulging in the nozzle observed	Printing
J	90	5	0.3		
K	90	3	0.7		
L	90	5	0.7		

The droplet formation study revealed that sample 13 was printable at 40 °C, but sample 14 was printable only at 90 °C. This was due to the lower viscosity of sample 13 relative to sample 14 at 40 °C (Table 6.2), making it easier to eject droplets at lower temperatures. The bulging behaviour of sample 13 (at 90 °C)

may be due to the low ink viscosity, where the ink did not have enough energy to break from the nozzle. Stable droplets were printed for sample 14 at 90 °C. For sample 13 both satellite drops that did not merge and splashing were observed at some printing conditions. A possible reason may be the distance between the substrate and the nozzle been too high (Wang L. *et al*., 2013). Some of the printed droplets also had air bubbles trapped, which disappeared within a few minutes. Cellulose ionic liquids-based inks (sample 11 and 12) were only printable at 65 °C (Table 5.3). Variations in rheological properties between cellulose and wool-based inks may have contributed to this difference.

The average droplet diameter measured from the microscope and the ImageJ software were similar (Table 6.4). Since the sample size used in ImageJ was higher, the average droplet diameter obtained from ImageJ was used in all the calculations.

Table 6.4: Average droplet diameter results

Sample	Printing Condition	ImageJ Analyzed Diameter (µm)	Microscope Measured Diameter (µm)
13	C	934 ± 27	923 ± 30
	D	1011 ± 38	978 ± 32
	G	990 ± 42	961 ± 39
	H	1100 ± 35	1057 ± 40
14	I	1142 ± 38	1102 ± 43
	J	1173 ± 38	1140 ± 31
	K	1283 ± 46	1221 ± 47
	L	1285 ± 46	1196 ± 48

Similar to cellulose ionic liquid-based inks, the average droplet diameter (Table 6.4) results revealed that, for the majority of the printing conditions used, there was an increase in droplet diameter as the pressure was increased from 3 to 5 bar. For $[C_4C_1Im][OAc]$ containing ink, when the valve was opened for a longer time (0.7 ms), more ink was deposited. Similar observations were made for the $[C_4C_1Im][OAc]$ and cellulose containing ink. For $[C_2C_1Im][OAc]$ containing ink, increasing temperature resulted in a higher droplet diameter, possibly due to the low ink viscosity ejecting higher ink volumes. Wang L. *et al*., (2013), also reported an increase in droplet diameter with increasing temperature and pressure. For the wool ionic liquid-based inks, it can be concluded that the droplet diameter was mainly dependent on the pressure and temperature and the ability to eject the ink from the nozzle was dependent on the ink temperature.

Line Formation Study

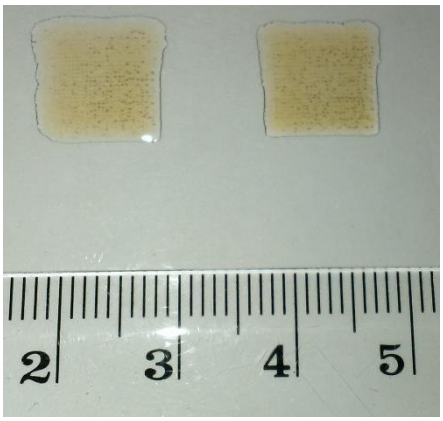
For the line formation study, printing conditions C, D and G were chosen sample 13 ($[C_2C_1Im][OAc]$ and wool), as they showed minimum splashing and droplet merging. For sample 14 ($[C_4C_1Im][OAc]$ and wool), printing conditions I, J and K were chosen. Printing conditions H (for sample 13) and L (for sample 14), were not selected due to the high pressure (5 bar) and pulse time (0.7 ms).

The observations made from the microscopic images obtained from the line formation study (Tables 9.1 and 9.2) were similar to those of cellulose ionic liquid-based inks where, the line width increased as the droplet spacing

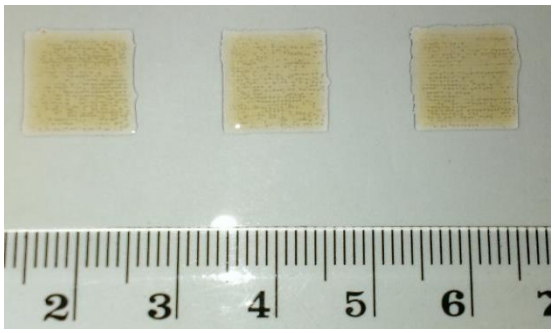
decreased. The lines showed a scalloped shape at an overlap of 20 % (highest droplet spacing) and become more uniform as the overlap was increased to 60 % (lower droplet spacing). As the lines printed at an overlap of 60 % showed a line with uniform edges compared to the others and therefore this condition was chosen to print films.

Film Formation Study

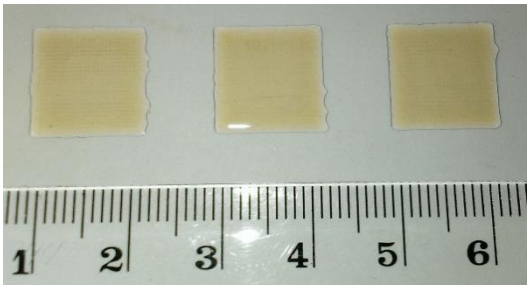
In the film formation study for both the samples, films were printed at an overlap of 60 %. The selection of the printing conditions C and D for sample 13 ($[C_2C_1Im][OAc]$ and wool) and I and K for sample 14 ($[C_4C_1Im][OAc]$ and wool) was based on the low temperature and pressure compared to the other printing conditions (G, H, J and L). Similar to the droplet and line formation study, the trapped air bubbles disappeared within a few minutes. For sample 13, printing condition D was selected to print multi-layer films, as the films were more uniform compared to printing condition C. For sample 14, printing condition I was selected to print multi-layer films, as it had the lowest pulse (0.3 ms) time therefore more likely to produce smaller drops (Figure 6.4). In summary, when the properties of the inks vary (*e.g.* type of biopolymer, loading and rheology) the optimum printing parameters also vary.



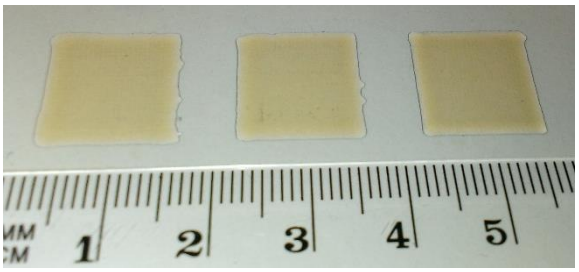
A Sample 13
Printing Condition C
Droplet Spacing: 375



B Sample 13
Printing Condition D
Droplet Spacing: 405



C Sample 14
Printing Condition I
Droplet Spacing: 460



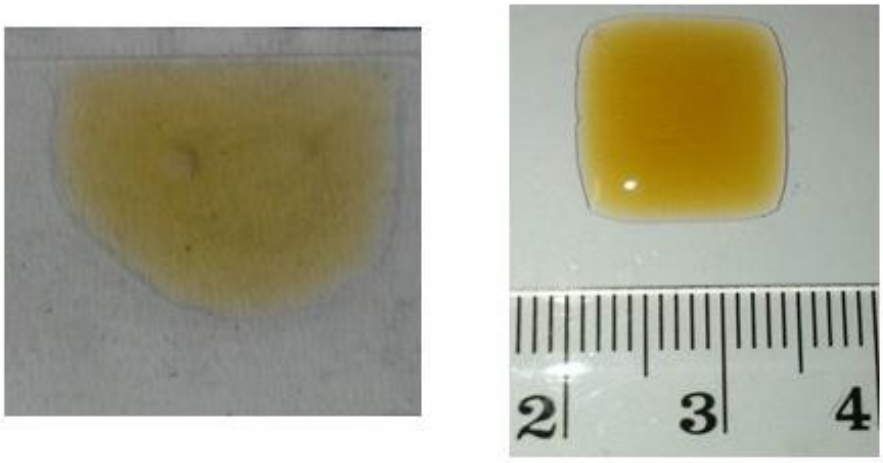
D Sample 14
Printing Condition K
Droplet Spacing: 515

Figure 6.4: Images obtained from the film formation study

6.3.4 Multi-Layer Printing and Regeneration: Wool and Ionic Liquid

The optimized printing parameters were used to print multi-layer (5 layers) films (Figure 6.5), demonstrating the possibility of forming 3D structures using wool and ionic liquid ($[C_4C_1Im][OAc]$). Compared to the single layer films (Figure 6.4), it can be seen that as the number of layers increased, sample 13 ($[C_2C_1Im][OAc]$ and wool) was not able to print 3D structures as it did not maintain the shape (Figure 6.5A). Even though this samples showed shear thinning behaviour the loss of shape is likely due to poor wettability of the ink

on the substrate. Dey T. and Naughton D. (2016), reported different methods that be used to modify substrate surfaces and thereby either increase/decrease the contact angle. Measuring the contact angle of the ink on the substrate will provide more information and to identify suitable methods that can be used in future to modify the substrate. For $[C_4C_1Im][OAc]$ wool containing ink (sample 14), as the number of layers increased the ink was not uniformly distributed across the printing area (Figure 6.5B). Instead majority of the ink was concentrated in the centre giving rise to a sagging behaviour similar to that observed for cellulose containing films.



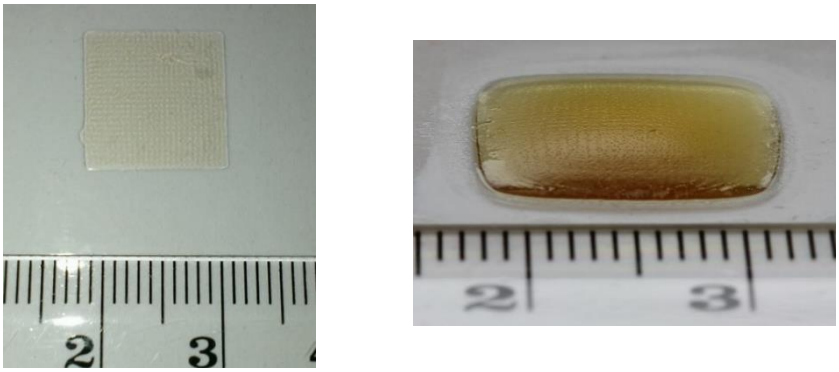
A – Sample 13 **B** – Sample 14

Figure 6.5: Multi-layered films printed using wool and ionic liquid

The wool recovery process used was similar to that reported in Chapter 5 Section 5.2.4. Rapid mixing and casting are some of the common methods reported in literature for keratin regeneration (Table 2.5). The printed films containing wool and ionic liquid, were treated using methods already established in the literature, namely either a vacuum oven (Hameed N. and Guo

Q., 2009; Idris A. *et al*., 2013; Idris A. *et al*., 2014; Zhang Z. *et al*., 2017a) or left at room temperature (Li R. and Wang D., 2013; Idris A. *et al*., 2014).

Single and multi-layered films printed using sample 14 ([C_4C_1Im][OAc] and wool) were able to maintain their shape when soaked in deionised water straight after printing (straight regen) (Figure 6.6). Single-layered films cracked and were very brittle, but the multi-layered films were very soft and sticky. A likely reason may be the entrapment of water in the multi-layered films after immersion in deionised water giving rise to a soft nature. However, cellulose films recovered from the same ionic liquid was not able to maintain the shape when subjected to the same conditions. This clearly shows that the biopolymers (cellulose and wool) behave differently when immersed in deionised water and this can even affect their final shape.



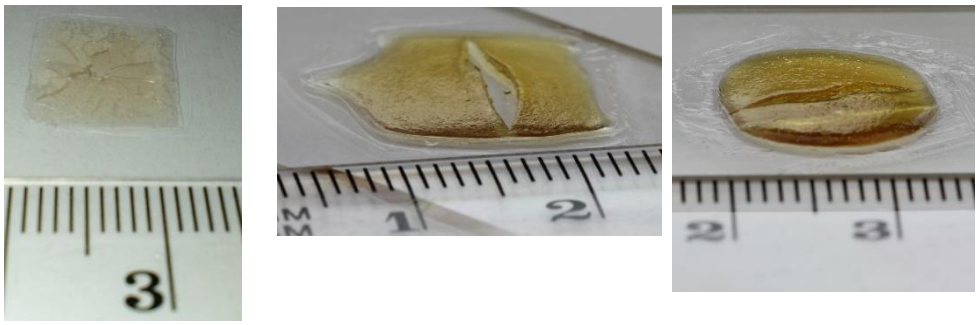
A 1 layer **B** 5 layers

Figure 6.6: Films obtained from sample 14 after the straight regeneration

When the printed films were left overnight at room temperature, single-layered films were able to maintain the shape, but the multi-layered films were not able to maintain their shape possibly due to the sagging behaviour. The

polymer gel formed was not rigid compared to cellulose. It is possible that the rearrangement of the bonds in wool during overnight drying was not very strong like in cellulose leading to the formation of a soft gel.

Both single and multi-layered, overnight dried films cracked when left at room temperature or in the vacuum oven (Figure 6.7). Similar to cellulose the colour change that occurred after the wool recovery process may be due to the manner in which ionic liquid and wool ordered on the microscale and removal of ionic liquid from the printed films. During wool dissolution, the solutions were very sticky and maybe the reason for the sticky nature of the films. In conclusion, the gel films formed with keratin were soft, formed cracks and sticky. Removal of the solvent (ionic liquid) from the printed structure may have resulted in these cracks.



A 1 layer – O.D, regen and rtm

B 5 layers – O.D, regen and rtm

C 5 layers – O.D, regen and vac. oven

Figure 6.7: Films obtained from sample 14 after wool recovery

A summary of the observations reported in the literature for recovered keratin is provided in Table 6.5 along with the observations made during this study.

Visually, both the films obtained by O.D, regen and rtm and O.D, regen and vac. oven were similar, and further characterisation experiments were conducted in order to understand the differences between them.

Table 6.5: Summary of keratin recovery observations

Ionic Liquid	Anti-Solvent	Observations	Reference
$[C_4C_1Im][OAc]$	Deionised water	Pale white/yellow film when immersed in water and turned pale yellow after left at room temperature. The final films cracked and were brittle.	Straight regen 1 layer In this work
		Yellow film when immersed in water and after left at room temperature. The final films were soft and sticky.	Straight regen 5 layers In this work
		Pale white/yellow film when immersed in water and turned pale yellow after left at room temperature. The final films cracked and were brittle.	O.D, regen and rtm 1 layer In this work
		Pale yellow film when immersed in water and turned yellow after left at room temperature/in the vacuum oven. The final films were soft, sticky, cracked and did not maintain its shape.	O.D, regen and rtm and O.D, regen and vac. oven In this work
$[C_4C_1Im][Cl]$	Methanol	Brittle keratin membrane	Xie H. *et al*., 2005
$[C_4C_1Im][Cl]$	Ethanol/ Water	Grayish-white particles	Sun P. *et al*., 2009
$[C_4C_1Im][Cl]$/ [AMIM][Cl]	Water	Fawn-coloured hard solid	Idris A. *et al*., 2013
[DMEA][Ofo]	Water	Transparent keratin films	Idris A. *et al*., 2014

6.3.5 Characterisation of Regenerated Wool: Wool and Ionic Liquid

Thermogravimetric Analysis (TGA)

Thermal stabilities of the multi-layered wool films were studied using a TGA and the results obtained are presented in Figure 6.8 along with the DTG curves. For comparison TGA and DTG curves for pure wool were also included. The initial weight loss between 50 to 150 °C was much higher for all films (approximately 13 %) when compared to the wool-only sample (approximately 7 %). This is consistent with the continued presence of water even after leaving the films in room temperature/vacuum oven, verifying the formation of gel-like films. Like cellulose films, overnight drying and immersion of films in deionised water may have contributed to this increase in water content. The rapid weight loss occurred between 150 to 450 °C where the weight loss was roughly between 65 to 70 %. Overall, the weight loss over this region for the films were much higher compared to pure wool (57 %). Similar to cellulose films the absence of char yield implies the amount of impurities left was insignificant.

From the DTG curves, it is evident that all the films had a lower degradation temperature than that of wool (Table 6.6). The low thermal stability of regenerated wool films strongly suggests that the hydrogen bonding network was broken to a certain extent (Idris A. *et al*., 2014). Table 6.6 also compares the degradation temperature for the pure chemicals and the films. The degradation temperature of the films was close to that of the ionic liquid indicating the presence of ionic liquid in the films and consistent with cellulose results. The variation in the degradation temperature based on the wool

recovery procedure used was minimal, but vacuum oven films showed a higher thermal stability even though the films cracked. This shows that the cracking phenomena observed has a negligible effect on the thermal stability of the recovered films and points to this being a more macroscopic than microscopic effect.

Comparing these TGA results to those reported in literature (Table 6.7), all the TGA curves were seen to vary based on the starting raw materials, keratin loading, recovery conditions and the type of anti-solvent used. A study conducted by Zhang Z. *et al*., (2017a) concluded that the presence of water in the ionic liquid had little effect on the thermal stability of the regenerated keratin. Therefore, it can be concluded that the thermal stabilities of recovered keratin can be optimised by varying any of the above-mentioned parameters.

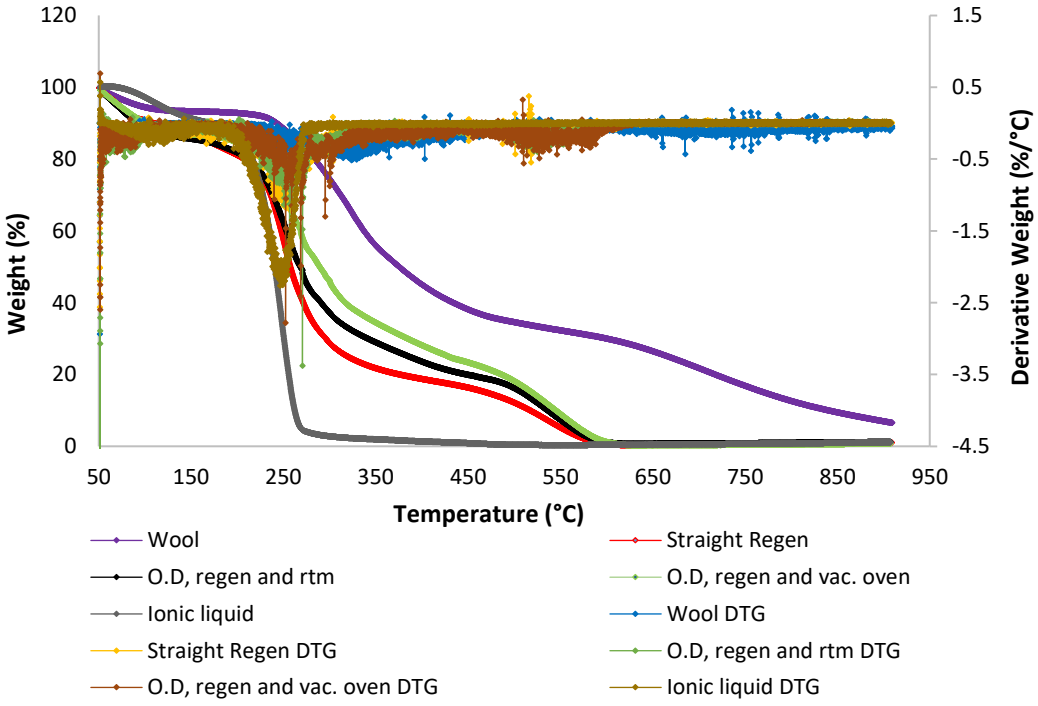


Figure 6.8: TGA and DTG curves for pure chemicals and films obtained from sample 14

Table 6.6: Degradation temperatures for pure chemicals and films obtained from the keratin recovery process

Pure Chemical/Film Type	Degradation Temperature (°C)
Wool	325
$[C_4C_1Im][OAc]$	245
Sample 14 – Straight regen	250
Sample 14 – O.D, regen and rtm	250
Sample 14 – O.D, regen and vac. oven	260

Another method adopted in the literature to improve stability was to formulate blends and was therefore trialled for this ionic liquid-based system.

Table 6.7: Summary of keratin regeneration TGA results reported in literature

Ionic Liquid	Keratin Type	Absorbed or Bound Water	Thermal Stability of Regenerated Keratin	Char Yield in Regenerated Keratin	Reference
$[C_4C_1Im][Cl]$	Wool	Less than raw wool	Higher than raw wool	Higher than raw wool	Xie H. *et al*., 2005
[AMIM][Cl]/ $[C_4C_1Im][Cl]$	Turkey feathers	Similar to raw feathers	Higher than raw feathers	Similar to raw feathers except for samples obtained from [AMIM][Cl]	Idris A. *et al*., 2013
[AMIM][Cl]/ $[C_4C_1Im][Cl]$	Wool		Lower than raw wool		Li R. and Wang D., 2013
[DMEA][Ofo]	Turkey feathers	Higher than raw feathers	Lower than raw feather	Higher than raw feathers	Idris A. *et al*., 2014
$[N_{2221}][DMP]$/ $[C_4C_1Im][OAc]$/ $[C_2C_1Im][DMP]$	Wool	Less than raw wool	Higher than raw wool for $[C_2C_1Im][DMP]$ and lower than raw wool for $[N_{2221}][DMP]$ and $[C_4C_1Im][OAc]$	Similar to raw wool	Zheng S. *et al*., 2015
[DBNE][DEP]/ $[C_2C_1Im][DEP]$/ [DBNH][OAc]	Goat wool	Less than raw wool	Higher than raw wool	Higher than raw wool	Liu X. *et al*., 2017

6.3.6 Preparation of High Viscosity Inks: Blend (cellulose and woo) and Ionic Liquid

An increasing number of studies have found that the regenerated blends containing both keratin and cellulose have improved mechanical strength and thermal stability as the cellulose loading increase (Hameed N. and Guo Q., 2009; Hameed N. and Guo Q., 2010; Rosewald M. *et al*., 2014; Wang M. *et al*., 2014; Tran C. and Mututuvari T., 2015; Kammiovirta K. *et al*., 2016; Tran C. and Mututuvari T., 2016, Tran C. *et al*., 2016b). Table 6.8 provides a literature summary of films and fibres that can be obtained from blends containing keratin and cellulose for a wide variety of applications.

Blend inks were prepared by first dissolving cellulose followed by wool at 100 °C. The dissolution conditions were similar to that reported in Chapter 4 Section 4.3.2. As a starting point, the blend ink consisted of 5 wt % cellulose and 5 wt% wool. The ink containing $[C_4C_1Im][OAc]$ (sample 16), when left at room temperature (assumed to be 25 °C), showed an increase in viscosity. Hence, for handling, it was heated for 5 minutes at 100 °C before filling into the syringe barrel.

Table 6.8: Summary of cellulose and keratin based blends reported in literature

Ionic Liquid	Blend Type	Regenerated Material Type	Applications	Reference
$[C_4C_1Im][Cl]$	Wool + cellulose	Fibers obtained by syringing and regenerated using methanol		Xie H. *et al*., 2005
$[C_4C_1Im][Cl]$	Wool + cellulose acetate	Membranes obtained by casting on to a glass slide and regenerated using water		Hameed N. and Guo Q., 2009
$[C_4C_1Im][Cl]$	Wool + cellulose	Films obtained by casting between two glass plates and regenerated using water		Hameed N. and Guo Q., 2010
$[C_4C_1Im][Cl]$	Cellulose + chitosan + sheep wool		Wound dressing	Rosewald M. *et al*., 2014
$[C_4C_1Im][Cl]$	Human hair + cellulose	Films obtained by casting on to a glass plate and regenerated using water		Wang M. *et al*., 2014
$[C_4C_1Im][Cl]$	Cellulose and/or chitosan + keratin	Films obtained by casting onto PTFE molds and regenerated using water	High performance bandage to treat chronic ulcerous wounds in diabetic patients	Tran C. and Mututuvari T., 2015

Ionic Liquid	Blend Type	Regenerated Material Type	Applications	Reference
$[C_2C_1Im][OAc]$	Cellulose + feathers	Filaments obtained by wet-jet spinning into an ethanol bath		Kammiovirta K. *et al*., 2016
$[C_4C_1Im][Cl]$	Cellulose and/or chitosan + keratin	Films obtained by casting onto PTFE molds and regenerated using water	Antibacterial activity and drug delivery	Tran C. and Mututuvari T., 2016
$[C_4C_1Im][Cl]$	Cellulose + keratin + silver nanoparticles	Films obtained by casting onto PTFE molds and regenerated using water	High performance dressing to treat chronic ulcerous infected wounds	Tran C. *et al*., 2016a
$[C_4C_1Im][Cl]$	Cellulose + keratin (wool, hair, chicken feather)	Films obtained by casting and regenerated using water	Water purification and wound healing	Tran C. *et al*., 2016b
$[C_4C_1Im][Cl]$	Cellulose + chitosan /keratin + copper oxide nano particles	Films obtained by casting onto a mould and regenerated using water	Dressing to treat chronic ulcerous infected wounds	Tran C. *et al*., 2017
$[C_4C_1Im][Cl]$	Cellulose + wool keratin + gold nanoparticles	Films obtained by casting onto PTFE molds and regenerated using water	Biosensors, therapeutic agents and other drug delivery systems	Tran C. *et al*., 2018

6.3.7 Rheological Properties of High Viscosity Inks: Blend (cellulose and wool) and Ionic Liquid

Rheological properties of the high viscosity blend inks containing cellulose, wool and ionic liquid (samples 15 and 16) were investigated similar to the procedure outlined in Chapter 5 Section 5.2.2. The logarithmic curve of viscosity Vs shear rate is presented in Figures 6.9 and 6.10. The non-Newtonian index (*n*) and the ink viscosities at the highest shear rate (100 s^{-1}) at different temperatures are shown in Table 6.9. Similar to the high viscosity samples prepared using cellulose (Table 5.1) and wool (Table 6.2), the viscosity of the blends also decreased with increasing temperature.

Table 6.9: Rheological properties of the high viscosity inks containing cellulose, wool and ionic liquid

Temperature (°C)	Sample 15		Sample 16	
	Viscosity (mPa s)	Non-Newtonian Index (*n*)	Viscosity (mPa s)	Non-Newtonian Index (*n*)
40	2648 ± 221	0.94	6988 ± 598	0.92
50	1492 ± 110	0.95	3507 ± 271	0.96
60	905 ± 62	0.94	1887 ± 150	0.96
70	591 ± 39	0.92	1102 ± 90	0.95
80	410 ± 25	0.90	694 ± 56	0.93
90	298 ± 17	0.88	465 ± 39	0.92

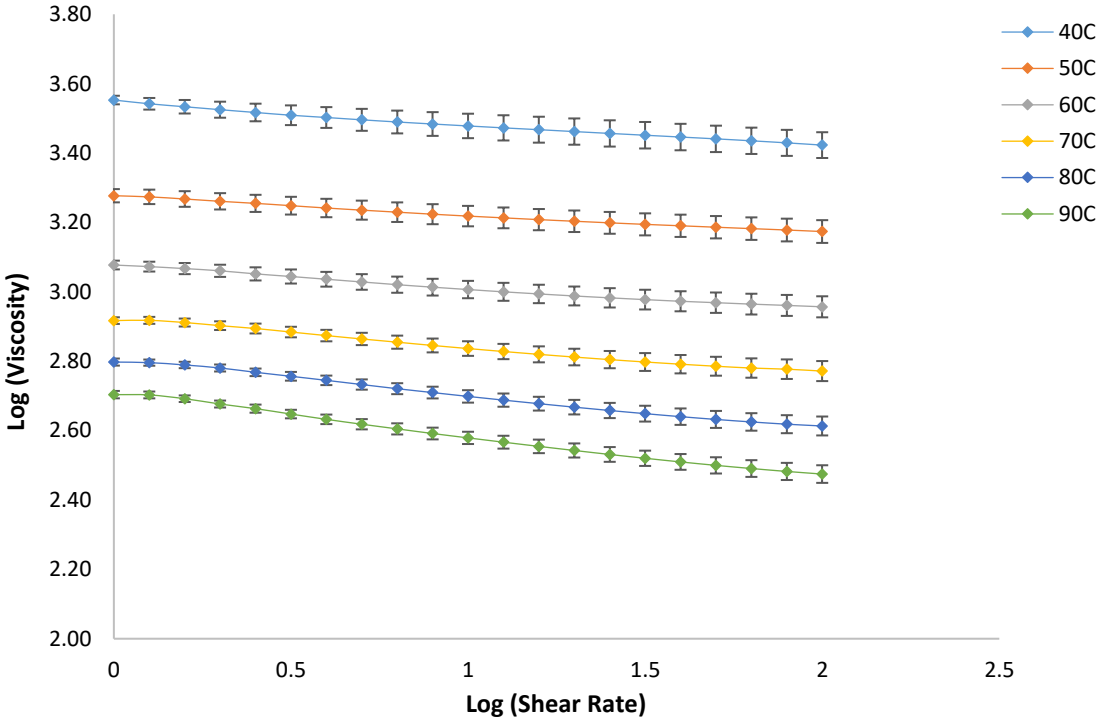


Figure 6.9: Rheological properties of sample 15 ([C_2C_1Im][OAc], cellulose and wool)

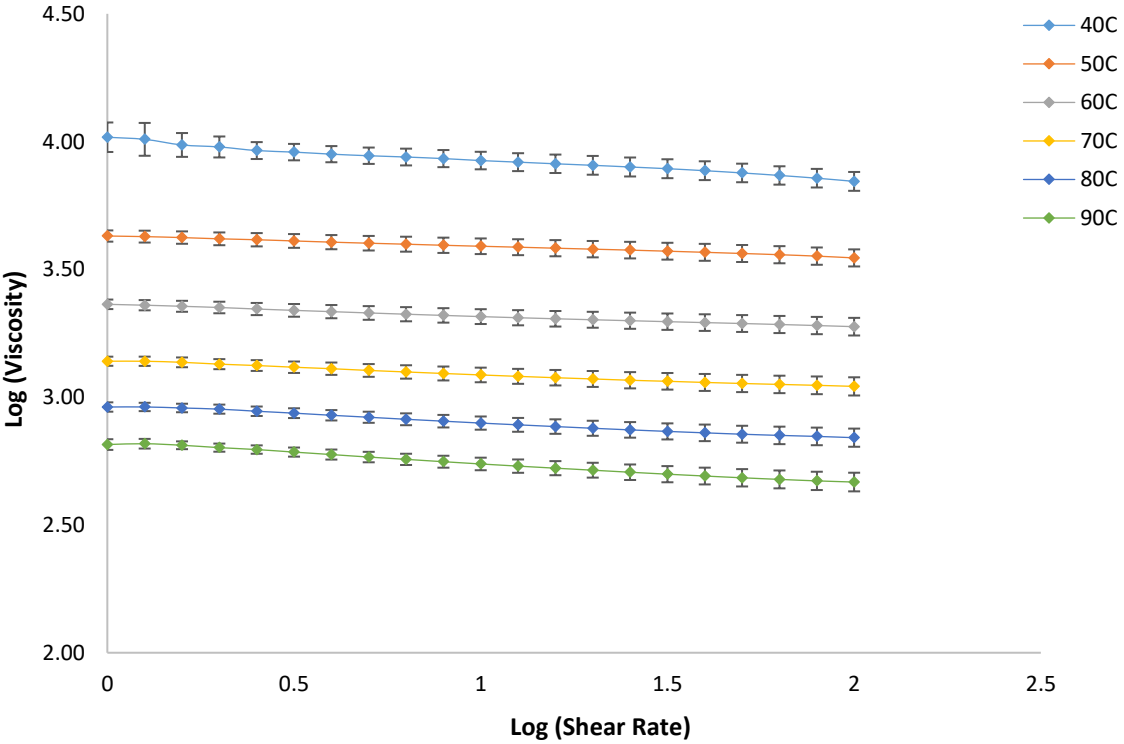


Figure 6.10: Rheological properties of sample 16 ([C_4C_1Im][OAc], cellulose and wool)

Shear thinning behaviour was exhibited for both sample 15 ([C_2C_1Im][OAc], cellulose and wool) and sample 16 ([C_4C_1Im], cellulose and wool), as shown by a decrease in the non-Newtonian index (*n*) from about 50 °C. Since both Newtonian (cellulose inks) and non-Newtonian (wool and blend inks) behaviour was observed for different inks, the rheological properties of the inks were governed by the type of biopolymer and the biopolymer loading.

Sample 16 ([C_4C_1Im][OAc] and blend) has a higher viscosity compared to sample 15 ([C_2C_1Im][OAc] and blend) (Table 6.9) consistent with the longer cation chain length. This further validates the increase in viscosity of sample 16 when left at room temperature. Since the non-Newtonian index varied with increasing temperature for the blend inks, careful selection of printing temperature is crucial to achieve successful printing.

6.3.8 Printing Parameters Optimisation: Blend (cellulose and wool) and Ionic Liquid

Optimisation of the printing parameters was achieved as per the previous work on cellulose and wool (Chapter 5 Sections 5.2.3 and Chapter 6 Section 6.3.3). For the droplet formation study, individual drops were printed on a glass substrate at a droplet spacing of 1300 µm for [C_2C_1Im][OAc] containing ink (sample 15) and 1500 µm for [C_4C_1Im][OAc] containing ink (sample 16). A higher droplet spacing was used for sample 16, to prevent the droplets from merging. A summary of the results and the microscopic images obtained from the droplet formation study are presented in Table 6.10 and Figures 9.24 and 9.25.

Table 6.10: Droplet formation study results

Printing Condition	Temperature (°C)	Pressure (bar)	Pulse Time (ms)	Sample 15	Sample 16
A	40	3	0.3	No ink ejected from the nozzle	No ink ejected from the nozzle
B	40	5	0.3		
C	40	3	0.7		
D	40	5	0.7		
E	65	3	0.3	Printing	Printing
F	65	5	0.3		
G	65	3	0.7		
H	65	5	0.7		
I	90	3	0.3		
J	90	5	0.3		
K	90	3	0.7		
L	90	5	0.7		

The droplet formation study revealed that both the samples were not printable at 40 °C, possibly due to the higher viscosity. Some of the printed droplets also had air bubbles trapped which disappeared with a few minutes. The average droplet diameter (Table 6.11) results revealed that, the droplet diameter was dependent on the pressure, pulse time and temperature, and the ability to eject the ink from the nozzle was dependent on the ink temperature.

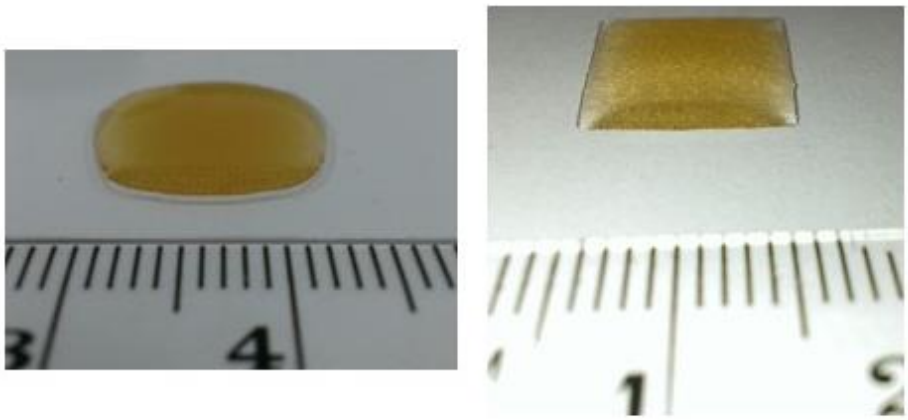
Observations made during the line formation study (Tables 9.3 and 9.4) were similar to cellulose/wool ionic liquid-based inks where, the line width increased as the droplet spacing decreased. Multi-layer printing was conducted at an overlap of 60 % using printing condition E, as it had the lowest temperature (65 °C), pressure (3 bar) and pulse time (0.3 ms) and therefore more likely to produce smaller drops.

Table 6.11: Average droplet diameter results

Sample	Printing Condition	ImageJ Analyzed Diameter (µm)	Microscope Measured Diameter (µm)
15	E	969 ± 24	929 ±36
	F	1000 ± 25	965 ± 24
	G	1041 ± 56	1022 ±37
	H	1099 ± 22	1052 ± 28
	I	1018 ± 32	968 ± 14
	J	951 ± 31	930 ± 25
	K	1086 ± 14	1050 ± 21
	L	1195 ± 11	1145 ± 40
16	E	1061 ± 29	1037 ± 27
	F	1078 ± 47	1040 ± 53
	G	1101 ± 31	1051 ± 31
	H	1068 ± 48	1018 ± 27
	I	1070 ± 43	1026 ± 25
	J	1043 ± 50	1024 ± 29
	K	1056 ± 65	1081 ± 65
	L	1143 ± 59	1097 ± 55

6.3.9 Multi-Layer Printing and Regeneration: Blend (cellulose and wool) and Ionic Liquid

The optimized printing parameters were used to print multi-layer (5 layers) films (Figure 6.11), demonstrating the possibility of forming 3D structures using cellulose, wool and ionic liquid-based ink. Some of the multi-layered films printed using $[C_2C_1Im][OAc]$ (sample 15), did not maintain the shape immediately after printing (Figure 6.11A) due to poor wettability of the ink on the substrate. The continuous presence of the sagging behaviour during multi-layer printing means that modifications must be made to the current printing procedure. These include; drying the films as it is printed so that the layers are solidified before another layer is printed, use a support material or by modifying the substrate surface to improve the wettability of the ink.

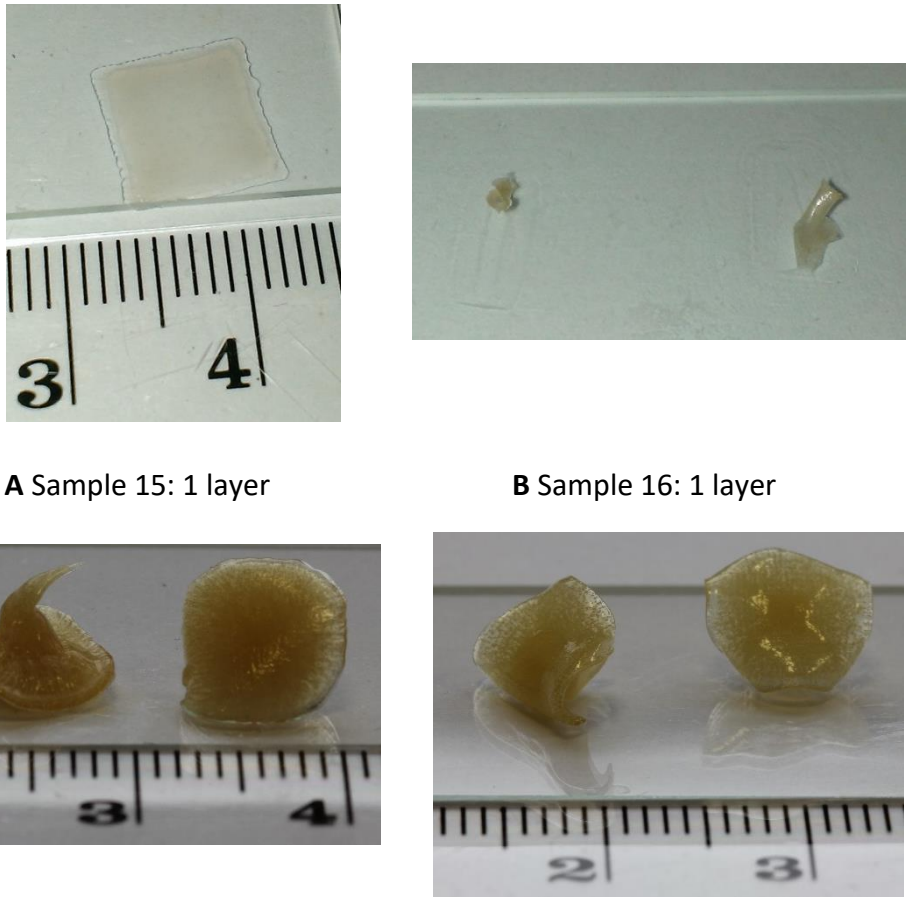


A – Sample 15 **B** – Sample 16

Figure 6.11:Multi-layered films printed using blends (cellulose and wool)

The biopolymer recovery process used was similar to that reported in Chapter 5 Section 5.2.4. Multi-layered films printed using sample 15 ($[C_2C_1Im][OAc]$, cellulose and wool) and 16 ($[C_4C_1Im][OAc]$, cellulose and wool) did not maintain the shape when soaked in deionised water straight after printing (straight regen) (Figure 6.12), indicating this method was not suitable for 3DP.

When the printed films were left overnight at room temperature, some ink spread out leaving a film with a gel nature, which could be lifted using tweezers. The formation of a gel film at room temperature for blend mixtures containing biopolymers and ionic liquid has been reported by Tran C. and Mututuvari T., (2015), Tran C. and Mututuvari T., (2016), Tran C. *et al*., (2016b) and Tran C. *et al*., (2017). The gel formed by blend inks were rigid compared to those formed by wool. Therefore, by adding cellulose the strength of the overnight dried gel film was improved.

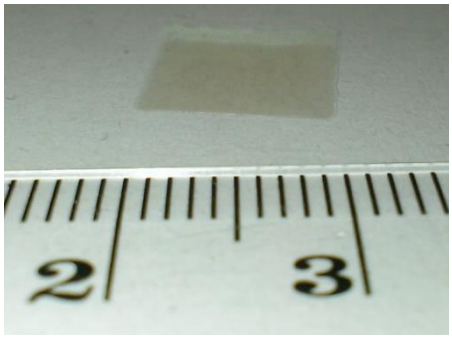


A Sample 15: 1 layer **B** Sample 16: 1 layer

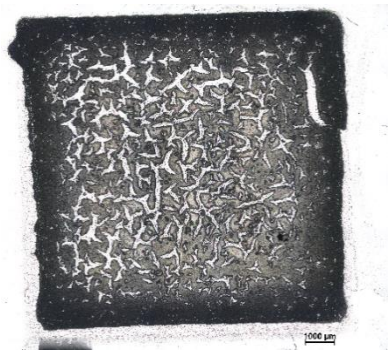
C Sample 15: 5 layers **D** Sample 16: 5 layers

Figure 6.12: Films obtained after straight regeneration

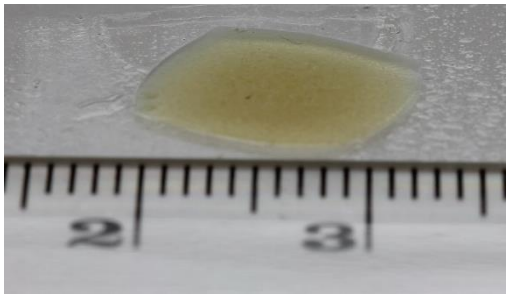
All the multi-layered films obtained after the biopolymer recovery process were soft and some formed multiple cracks ([C_4C_1Im][OAc]-based films) (Figure 6.13). These observations differ from previous studies where a dry film formed when left at room temperature in a humidity controlled environment (Tran C. and Mututuvari T., 2015; Tran C. and Mututuvari T., 2016) or when dried in an oven (Tran C. *et al.*, 2017). A number of factors like type and purity of the raw materials (biopolymer and ionic liquid), biopolymer loading and recovery procedure used could have affected this. A summary of the observations made during the blend recovery process is provided in Table 6.12.



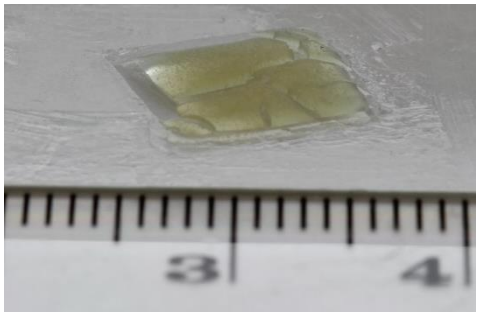
A Sample 15: 1 layer – O.D, regen and rtm



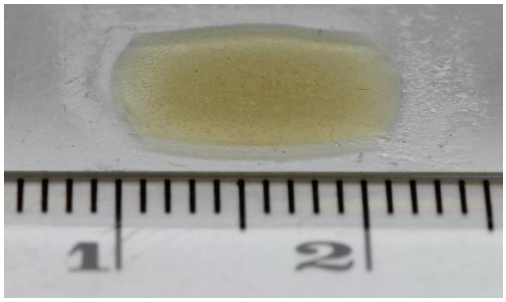
B Sample 16: 1 layer – O.D, regen and rtm



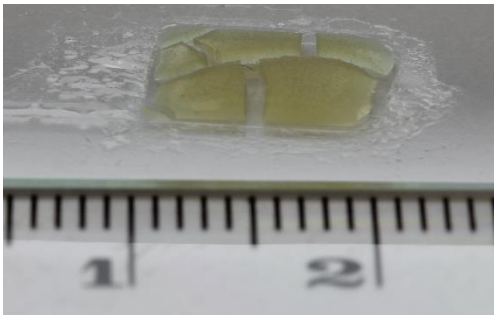
C Sample 15: 5 layers – O.D, regen and rtm



D Sample 16: 5 layers – O.D, regen and rtm



E Sample 15: 5 layers – O.D, regen and vac. oven



F Sample 16: 5 layers – O.D, regen and vac. oven

Figure 6.13: Films obtained after the blend (cellulose and wool) recovery

Table 6.12: Summary of blend (cellulose and wool) recovery observations

Ionic Liquid	Anti-Solvent	Observations	Reference
$[C_2C_1Im][OAc]$	Deionised water	Pale white film when immersed in water and after left at room temperature. The final films were brittle.	Straight regen 1 layer In this work
		Pale yellow film when immersed in water and turned yellow after left at room temperature. The final films did not maintain its shape and were soft.	Straight regen 5 layers In this work
		Pale white film when immersed in water and after left at room temperature. The final films were brittle.	O.D, regen and rtm 1 layer In this work
		Pale yellow/white film when immersed in water and turned pale yellow after left at room temperature/in the vacuum oven. The final films were soft.	O.D, regen and rtm and O.D, regen and vac. oven 5 layers In this work
$[C_4C_1Im][Cl]$	Deionised water	Pale white film when immersed in water and turned pale yellow after left at room temperature. The final films did not maintain its shape and were brittle.	Straight regen 1 layer In this work
		Yellow film when immersed in water and after left at room temperature. The final films did not maintain its shape and were soft.	Straight regen 5 layers In this work
		Pale white film when immersed in water and after left at room temperature. The final films formed cracks.	O.D, regen and rtm 1 layer In this work
		Pale yellow/white film when immersed in water and turned pale yellow after left at room temperature/in the vacuum oven. The final films formed cracks.	O.D, regen and rtm and O.D, regen and vac. oven 5 layers In this work

6.3.10 Characterisation of Regenerated Wool: Blend (cellulose and wool) and Ionic Liquid

Thermogravimetric Analysis (TGA)

Thermal stabilities of the multi-layered blend films were studied using a TGA and the degradation temperatures are presented in Table 6.13 (refer to Figures 9.26 and 9.27 for the TGA and DTG curves). The initial weight loss between 50 to 150 °C was much higher for all the films (between 20 to 25 %) compared to pure cellulose (approximately 3 %, Chapter 4 Section 4.3.2) and wool (approximately 7 %, Chapter 6 Section 6.3.1). This shows the presence of water even after leaving the films in room temperature/vacuum oven.

Table 6.13: Degradation temperatures for pure chemicals and films obtained from the blend recovery process

Pure chemical/Film type	Degradation Temperature (°C)
Cellulose	345
Wool	325
$[C_2C_1Im][OAc]$	250
$[C_4C_1Im][OAc]$	245
Sample 15 – O.D, regen and rtm	250
Sample 15 – O.D, regen and vac. oven	250
Sample 16 – O.D, regen and rtm	250
Sample 16 – O.D, regen and vac. oven	250

All the recovered films had a lower degradation temperature than wool and cellulose. However, compared to the films obtained from pure wool (Table 6.6), the thermal stability was not improved when cellulose was added. These findings contrast with literature where the thermal stability of the regenerated blends were higher than regenerated keratin and increased with the cellulose

loading (Hameed N. and Guo Q., 2009; Hameed N. and Guo Q., 2010; Wang M. *et al*., 2014; Tran C. and Mututuvari T., 2016). The maximum thermal stability was observed at about 60 wt% cellulose loading (Hameed N. and Guo Q., 2009; Hameed N. and Guo Q., 2010). This increase in thermal stability was due to the strong intermolecular hydrogen bonds between wool and cellulose (Hameed N. and Guo Q., 2009; Hameed N. and Guo Q., 2010). However, the results obtained in this study showed that the thermal stability of the recovered films were close to that of the ionic liquids indicating the presence of ionic liquid in the films and consistent with cellulose and wool results.

6.4 Chapter Summary

- The TGA study conducted on pure wool revealed that the absorbed or bound water was about 7 % which was much higher than that of cellulose (3 %). Unlike cellulose, a small char yield was present in wool indicting the presence of impurities.
- A maximum wool loading of 20 wt% and 25 wt% was achieved in the presence of the ionic liquids $[C_2C_1Im][OAc]$ and $[C_4C_1Im][OAc]$ respectively. A low viscosity ionic liquid with a short cation chain length generally has the ability to dissolve higher wool loadings as it is easy for the ionic liquid to penetrate into the wool structure. However, the method used to determine the solubility in this study does not accurately represent the highest wool loading that can be achieved and this may have contributed to the lower wool solubility observed in $[C_2C_1Im][OAc]$.

- The quantity of wool dissolved in the ionic liquids (20 and 25 wt%) was much higher than the cellulose-based inks (13 and 10 wt%). This is because, cellulose dissolution occurs due to the destruction of the hydrogen bonds which are much stronger than the intra- and inter chain bonds present in wool.
- Both wool and blend inks showed non-Newtonian shear thinning behaviour between 50 to 90 °C, where the viscosity decreased under shearing and increased when the shear was removed. However, the cellulose ionic liquid-based inks showed Newtonian behaviour within this temperature range. This suggests that the rheological properties of the biopolymer ionic liquid-based inks were governed by several factors like the type of biopolymer and the biopolymer loading.
- The droplet formation study for wool ionic liquid-based inks revealed that $[C_2C_1Im][OAc]$ containing ink was printable at 40 °C as it had a lower viscosity (≈ 2000 mPa s at 40 °C) compared to $[C_4C_1Im][OAc]$ (≈ 11,000 mPa s at 40 °C) containing ink. The blend inks were printable at temperatures ≥ 65 °C where the viscosity was ≈ 600 mPa s at 70 °C for $[C_2C_1Im][OAc]$ containing ink and ≈ 1100 mPa s at 70 °C for $[C_4C_1Im][OAc]$ containing ink.
- For biopolymer ionic liquid-based inks, the droplet diameter was dependent on a number of printing parameters like pressure, temperature and pulse time and the ability to eject an ink from the nozzle was dependant on the ink temperature. Therefore, careful optimisation of the printing parameters is crucial to obtain stable droplets.

- Similar to cellulose ionic liquid-based inks, the lines printed from wool ionic liquid-based inks and blend ionic liquid-based inks revealed that the lowest line width was observed at highest droplet spacing and highest line width was observed at the lowest droplet spacing. Lines printed at 60 % overlap showed lines with uniform edges and were used to print films.
- The selection of printing conditions to print films was based on the lowest temperature, pressure and pulse time as it is more likely to obtain smaller drops.
- Similar to cellulose ionic liquid-based inks multi-layer films printed using wool and blends also showed a sagging behaviour. Simple techniques like, substrate surface modification, using a support material or spraying the anti-solvent on the printed film can be incorporated in the future to overcome these problems.
- When multi-layered films were soaked in deionised water immediately after printing wool ionic liquid-based films were able to maintain their shape, but those obtained from blend inks did not maintain their shape.
- After overnight drying both wool and blend films formed a gel film. In terms of the strength of the overnight dried gels; cellulose > blend > wool. Therefore, the strength of the dried gel can be modified by changing the biopolymer composition.
- Similar to cellulose, a colour change was observed during wool and blend recovery process. This may be due to the manner in which ionic liquid and the biopolymer ordered on the microscale and removal of ionic liquid from the printed films.

- All multi-layered films obtained from wool were soft and sticky and those obtained from blend inks were soft and some formed cracks. Since the conditions used were similar to cellulose it can be assumed that the sticky nature was due to the presence of wool. Addition of cellulose to wool did not improve the mechanical strength of the blend films likely due to presence of large quantities of water. This was further verified by TGA results where the absorbed/bound water content of the blend-based films were between 20 to 25 %.
- In summary the thermal stability was also not improved when cellulose was added to wool. However, the thermal stability was much closer to the pure ionic liquid and it can be assumed that the films still contained large quantities of ionic liquid and the formation of an ionogel.

Chapter 7 : General Discussion

The aim of this work was to identify routes by which 3D printing of biopolymers will become possible, and this was achieved using ink-jet printing. However, this does not limit 3D printing of biopolymers to material jetting.

The ionic liquids selected for biopolymer dissolution ($[C_2C_1Im][OAc]$ and $[C_4C_1Im][OAc]$) have been commonly used in literature for cellulose and wool dissolution. They are also safe and environmentally friendly (Hermanutz F. *et al*., 2008; Zavrel M. *et al*., 2009; Liebert T., 2010). A maximum cellulose loading of 13 wt% and wool loading of 25 wt% was achieved in this study. This implies that the intra- and intermolecular bonds present in cellulose was much stronger compared to wool and may have reduced its solubility in ionic liquid compared to wool. The biopolymer loading in the final cellulose formulated ink was highest for the short cation chain length ionic liquid ($[C_2C_1Im][OAc]$). Similar results were reported by Kosan B. *et al*., (2008), Zavrel M. *et al*., (2009) and Liu Z. *et al*., (2011), where cellulose solubility decreased with increasing cation size. This is because, when the cation chain length in the ionic liquid is short, it has a lower viscosity and hence, can easily penetrate the biopolymer structure.

Cellulose and wool dissolved in ionic liquid, resulted in high viscosity solutions and it was observed that the viscosity increased as the cation chain length increased. For instance, 2 wt% cellulose dissolved in $[C_2C_1Im][OAc]$ had a

viscosity of 87.30 ± 2.56 mPa s, but for the same cellulose loading the viscosity was 163.90 ± 7.58 mPa s with a longer cation-based ionic liquid [C_4C_1Im][OAc]. Generally, inks prepared using cellulose had a much higher viscosity than wool even though the loading of cellulose was low. For instance, 10 wt% of cellulose dissolved in [C_4C_1Im][OAc] had a viscosity of 14,810 ± 340 mPa s at 50 °C. The viscosity was 5,189 ± 189 mPa s when 25 wt% wool was dissolved in the same ionic liquid. This is because, the foldable nature of wool allows it to be packed closely and in a compact manner with a low density whereas sheets of cellulose of a much a higher density cannot be treated in the same manner.

Addition of a co-solvent DMSO resulted in a viscosity less than 30 mPa s (viscosity was > 85 mPa s without DMSO) making these inks more suitable for DIMATIX ink-jet printing. However, when a rheological modifier like DMSO is added, majority of the final ink formulation consist of the co-solvent and the ionic liquid rather than the biopolymer.

In terms of rheological properties, cellulose-based inks showed Newtonian behaviour, wool and blend-based inks showed non-Newtonian shear thinning behaviour. This suggest that the rheological properties of different biopolymer ionic liquid-based inks are hard to predict and dependent on several variables likes type of biopolymer and loading.

During printing with DIMATIX ink-jet and PICO Pulse, the presence of ligaments and missing drops were common observations. This implies occasional nozzle

blockage and the presence of ligaments that did not have enough energy to merge with the leading drop. Optimising the printing parameters and regular cleaning/purging of the nozzle will help to resolve this problem in future.

For all the high viscosity inks printed using PICO Pulse printer, different inks were printable at different temperatures. For example, cellulose inks were printable at 65 °C, wool inks at 40, 65 and 90 °C and blend inks at 65 and 90 °C. The major factor contributing to this difference is the rheological properties. In terms of the droplet diameter, this was also dependant on printing parameters like pressure, temperature and pulse time. Therefore, careful optimisation of the printing parameters is crucial to obtain stable droplets. For all the lines printed, the lowest line width was observed at the highest droplet spacing and the highest line width at the lowest droplet spacing. Uniform lines were printed at an overlap of 60 % and therefore selected as a suitable overlap to print films. When printing multiple layers sagging behaviour was present in all the inks and this meant that further studies should focus on modifying the substrate, using a support material or spraying the anti-solvent on the printed film.

From the TGA results, the absorbed or bound water in pure cellulose and wool were 3 % and 7 %, respectively. However, the absorbed or bound water of the films obtained after immersing in deionised water was 20 % for cellulose films, 13 % for wool films and between 20 to 25 % for blend films. Also, the degradation temperature of all these films were closer to that of the pure ionic liquids and the thermal stability was lower than that of pure cellulose and/or

wool. This means that the films contained large quantities of water and the ionic liquid and resulted in the formation of an ionogel.

In term of mechanical strength and thermal stability, they were not improved when wool and cellulose were mixed to form a blend. A likely reason may be the presence of large quantities of water which was verified by TGA results to be between 20 to 25% for blend films.

Overall, overnight drying of multi-layered films was able to produce a polymer gel film. The strength of these films was highest for cellulose and lowest for wool. The strength of the films can be attributed to the rearrangement and the strength of the intra- and intermolecular bonds in cellulose and wool. Multi-layered films obtained from cellulose and ionic liquid $[C_2C_1Im][OAc]$ after immersing in water were easily foldable. However, wool films were soft and sticky and blend films were soft and formed cracks. Therefore, the overall strength of the film can be modified by changing the biopolymer composition.

Based on the observations made, Figures 7.1 and 7.2 represents schematic diagrams for the proposed interaction mechanism for cellulose and wool in the presence of acetate-based ionic liquids. Cellulose has strong intra- and intermolecular hydrogen bonds (represented in red dotted lines) both within the chain and between chains. When an ionic liquid is added, the ions in the ionic liquid (represented in green) interact with cellulose hydrogen bonds destroying the cellulose crystalline structure (Lan W. *et al*., 2013). When the

resultant solution is added to water some of the ions are removed/pushed away allowing the cellulose chains to come together reforming the intra- and intermolecular bonds resulting in a dense structure (Figure 7.1).

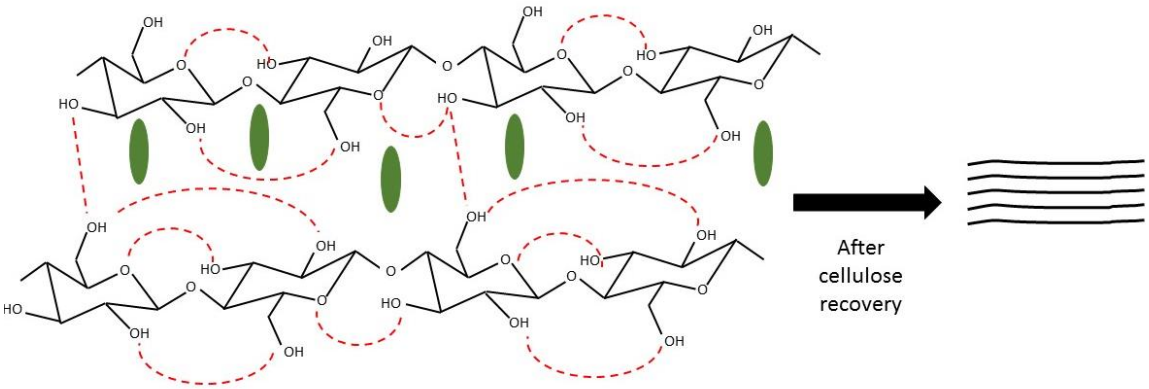


Figure 7.1: Schematic diagram for cellulose and ionic liquid interaction mechanism

Ionic liquid interacts with wool in a similar manner to cellulose during dissolution. However, wool has strong disulphide intramolecular bonds within the chains. When deionised water is added, the ions are removed/pushed away allowing the intramolecular bonds to form. The intermolecular bonds are not very strong in wool. Therefore, the resulting films soft compared to cellulose (Figures 7.2).

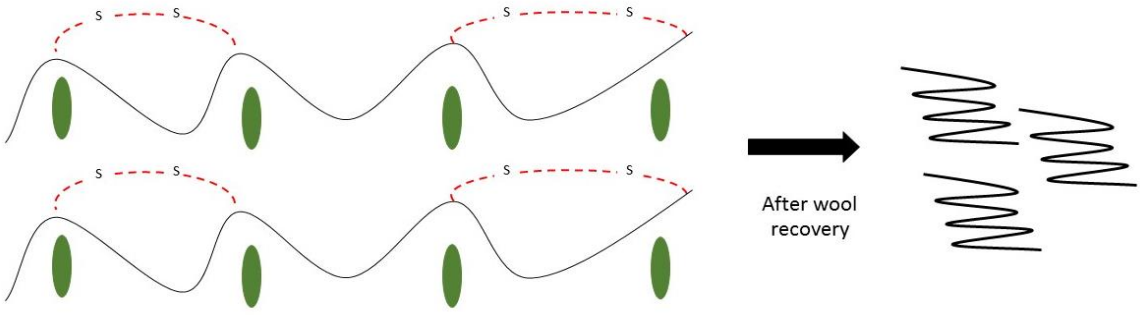


Figure 7.2: Schematic diagram for wool and ionic liquid interaction mechanism

To conclude, in terms of the efficiency of dissolution wool-based inks were able to achieve higher loadings. However, the quality of the films obtained after the recovery process did not have a self-supporting structure. Cellulose films produced from $[C_2C_1Im][OAc]$ ionic liquid had the best self-supporting structure with a maximum loading of 13 wt%. The biopolymer loading in the blend inks can be varied to enhance the final properties of the films. Although, the 50:50 proportion of cellulose and wool in the blend also did not produce a self-supporting structure.

Chapter 8 : Conclusions and Future Work

8.1 General Discussion

The work conducted in this study has demonstrated printability of different biopolymer inks; namely cellulose and/or keratin using ionic liquid as the solvent.

DIMATIX Ink-jet Printing

The major limitation in using the DIMATIX ink-jet printer was its requirement for low viscosity and low surface tension inks. Although a low viscosity ionic liquid was selected, the addition of the biopolymer increased the viscosity drastically, requiring the addition of a co-solvent and an increase in temperature to bring the ink formulation within the DIMATIX printing range. This resulted in formulating inks containing a cellulose loading less than the maximum loading. Low viscosity inks containing DMSO as the co-solvent resulted in complete dissolution, compared to those with 1-butanol. When printing the low viscosity inks, occasional nozzle blocks and ligaments were seen in the final printed pattern. In terms of a suitable substrate; the ionic liquids resulted in PET degradation, which was not observed when glass was used as the substrate. It was challenging to characterise the ink-jet printed samples using SEM, as deionised water dried leaving debris on the printed droplets.

PICO Pulse Printing

PICO Pulse printing overcame several the issues presented by the DIMATIX ink-jet printer. All the high viscosity inks showed a decrease in viscosity with increasing temperature, showing both non-Newtonian and Newtonian behaviour at different temperatures. The droplet diameter during printing was mainly dependent on the printing parameters (pressure, temperature and pulse time) and the ability to eject the ink from the nozzle was dependent on the ink temperature. Increasing the droplet spacing resulted in a decrease in line width. The droplet spacing was optimised to obtain stable lines with uniform edges.

Films printed using cellulose inks formed a film with gel-like nature, when dried overnight. However, the films obtained from wool were much softer compared to cellulose. The gel nature was visible for blend inks, indicating that the presence of cellulose had a stronger tendency to form a gel-type film during overnight drying. Overall, the type of ionic liquid, biopolymer, and the recovery conditions all impacted on the final structure of the films. Films obtained from cellulose and $[C_2C_1Im][OAc]$-based inks after the biopolymer recovery process were easily foldable. Other films obtained from keratin and blend-based inks resulted in cracks. This shows that the ionic liquid $[C_2C_1Im][OAc]$ and cellulose-based inks were able to rearrange the hydrogen bonds into a more organised manner. All the TGA results indicated presence of large quantities of water in the recovered films, even after leaving at room temperature and vacuum oven. The thermal stabilities of all the films were close to the respective ionic liquids

used, indicating that even after the recovery process, the films still contained large quantities of ionic liquid after the polymer recovery process.

Since the polymer gels formed exhibited properties of both cellulose (continuous phase) and ionic liquid (dispersed phase), it can be concluded that they corelates well with the polymer ionogels reported by Le Bideau J. *et al*., (2011) and P. C. Maar and A. C. Maar, (2016). A summary of the PICO Pulse printing results is shown in Table 8.1.

Table 8.1: Summary of PICO Pulse printing results

Parameter	$[C_2C_1Im][OAc]$ and Cellulose	$[C_4C_1Im][OAc]$ and Cellulose	$[C_2C_1Im][OAc]$ and Wool	$[C_4C_1Im][OAc]$ and Wool	$[C_2C_1Im][OAc]$, Cellulose and Wool	$[C_4C_1Im][OAc]$, Cellulose and Wool
Solubility	13 wt%	10 wt%	20 wt%	25 wt%	5 wt%	5 wt%
Ink Rheology	Newtonian	Newtonian	Non-Newtonian (shear thinning)	Non-Newtonian (shear thinning)	Non-Newtonian (shear thinning)	Non-Newtonian (shear thinning)
Printing Temperature/s	65 °C	65 °C	40 and 65 °C	90 °C	65 and 90 °C	65 and 90 °C
Droplet Diameter	Increased with pressure	Increased with pressure and pulse time	Increased with pressure and temperature	Increased with pressure and pulse time	Increased with temperature, pressure and pulse time	Increased with temperature, pressure and pulse time
Straight regen	Did not maintain shape	Did not maintain shape	Did not print films	Very soft and sticky	Did not maintain shape	Did not maintain shape
O.D, regen and rtm	Easily foldable	Soft and cracked	Did not print films	Very soft, sticky, cracked and did not maintain shape	Soft	Soft and cracked

Parameter	$[C_2C_1Im][OAc]$ and Cellulose	$[C_4C_1Im][OAc]$ and Cellulose	$[C_2C_1Im][OAc]$ and Wool	$[C_4C_1Im][OAc]$ and Wool	$[C_2C_1Im][OAc]$, Cellulose and Wool	$[C_4C_1Im][OAc]$, Cellulose and Wool
O.D, regen and vac. oven	Easily foldable	Soft	Did not print films	Very soft, sticky, cracked and did not maintain shape	Soft	Soft and cracked

Key
Straight regen – Straight regeneration
O.D, regen and rtm – Overnight drying, regeneration and leave at room temperature
O.D, regen and vac. oven - Overnight drying, regeneration and leave in the vacuum oven

8.2 Recommendations for Future Work

The aim of this research was to 3D print two different biopolymers (cellulose and wool) which can be easily sourced from waste. In order to use these 3D printed parts for end-user applications, it is essential that the 3D structure is not distorted during/after printing and the chemicals used are treated in an environmentally friendly and cost-effective manner. The following recommendations are ways that could be explored in future to improve on this current research.

Substrate Surface Modifications

Wool and blend inks printed using [C_2C_1Im] cation-based ionic liquid did not maintain their shape when printing multiple layers. Even though the other inks prepared using cellulose, wool and blends were able to retain their shape, further optimisation will ensure smoothening of their edges. This can be achieved by incorporating a substrate surface modification technique, which will engineer the surface to increase the hydrophobicity. When the substrate surface is hydrophobic (higher contact angle) it will reduce the spreading nature of the droplets. Coating or etching (Yu E. *et al*., 2015; Dey T. and Naughton D., 2016) can be used to modify the hydrophobicity. The most feasible way to achieve this is to deposit an ink drop on different treated substrates and measure the contact angle using a drop shape analyser. This will provide a good starting point to identify substrates suitable for different inks.

Printing Modifications

All the inks showed a sagging behaviour when printing multiple layers and this can be reduced by either directly printing the biopolymer and ionic liquid-based ink into an anti-solvent or by using a support material. Previous studies have shown successful extrusion printing of cellulose and ionic liquid-based ink onto an agar support (Markstedt K. *et al*., 2014). Building on this principle, if the biopolymer and ionic liquid-based ink is directly printed onto deionised water, the surface will be dried before another layer is deposited. However, to achieve this, modifications must be made to the current printing set-up, where the substrate will move down into a deionised water bath after printing each layer. A similar set-up was used by Boland T. *et al*., (2006), where the Z stage moved down as a new layer was deposited. A low-cost approach is to spray the anti-solvent onto the printed pattern during or directly after printing a layer. However, the spraying force must be optimised. This is because a higher force has the tendency distort the surface and at a lower force the amount of anti-solvent sprayed may not be enough.

Support materials are commonly used in AM, where it is printed using a material that will not react with the ink. If this method is utilised it can help solve the sagging behaviour observed when printing multi-layer films. The major disadvantages of this approach are removal of the support material after printing, material wastage and cost due to this additional step.

Ionic liquid is inherently hygroscopic. Therefore, the current printing studies must be conducted in a low moisture environment (in a glove box) to minimize or study the effect of ionic liquid hygroscopicity on the results obtained in this study.

Binder Jetting

This research was focused on ink-jet printing and the results can be used as a guide to identify other AM methods that can be used to print biopolymer and ionic liquid-based inks. A recommendation is to use binder jetting technology. This will involve printing a liquid-based ink directly onto a powder bed. Xanthan gum was successfully printed onto cellulose powder using a DIMATIX ink-jet printer (Holland S. *et al*., 2018). Building on this work and using the knowledge of selective laser sintering, the PICO pulse printing set-up can be modified to include a powder feed system that will deposit biopolymer powder layer by layer. Polymeric ionic liquids have been used as a binder for different applications (Pal A. *et al*., 2017) and can provide a starting point for ionic liquid binder jetting.

Efficient Experimental Planning

Printing and regeneration experiments in this study were conducted based on a few parameters. However, both these approaches involved a variety of different parameters and further optimisation is necessary with a statistical system to obtain the best possible outcomes. Therefore, further work should

concentrate on using a Design of Experiments (DoE) method that will allow a statistical means of selecting crucial parameters to be tested.

Ionic Liquid Recycling

The current regeneration technique used did not study the recycling of the ionic liquids, which is a major consideration given the expense and the environmental implications using these types of solvents. Ionic liquid recycling from the anti-solvent, in the first instance, will allow quantification of the amount of ionic liquid used, as well as that still left in the printed films after regeneration.

Ionic Liquid Quantification

The current experimental method focused only on the FTIR spectrum of the raw materials and the films obtained from the cellulose recovery process. In order to quantify the amount of ionic liquid remaining in the films, further experiments must focus on capturing the FTIR spectrum of the inks and the ionic liquid-water solution (obtained during the regeneration step).

Mixing Method

To enhance the dissolution, high viscosity inks were occasionally stirred using a spatula. This was not an efficient method since, there will be some level of biopolymer/ionic liquid loss during this step. Ultrasonication or overhead stirrers can be used in future studies to improve biopolymer dissolution.

Mikkola J. *et al*., (2007) used ultrasonication to significantly reduce the dissolution time and increase the cellulose loading.

Molecular Weight Determination

Molecular weights of the biopolymers used were unknown. Therefore, composition was calculated only on wt%. Gel permeation chromatography (GPC) or Nuclear magnetic resonance (NMR) spectroscopy, can be adopted in future studies to experimentally determine the molecular weight. This can be used to calculate the composition in mol%. Izunobi J. and Higginbotham C., (2011) conducted a study on experimentally determining the molecular weight of polymers. This can be used as a guideline for future work.

Further Characterisation of Cracked Films

Some of the cracked films obtained from the PICO pulse printed samples were not analysed using the SEM (those obtained from wool and blend films). SEM images would have provided further understanding on the surface topology of these cracked systems.

Chapter 9 : Appendix

Sample Calculation for Printability Parameter

$$\text{Printability Parameter (Z) of } [C_2C_1Im][OAc] = \frac{\sqrt{\sigma\rho d}}{\eta}$$

$$= \frac{\sqrt{39.94 \times 1.0 \times 21}}{85.47}$$



Figure 9.1: Drop watcher screen (Adapted from Fujifilm Dimatix Manual, 2010)

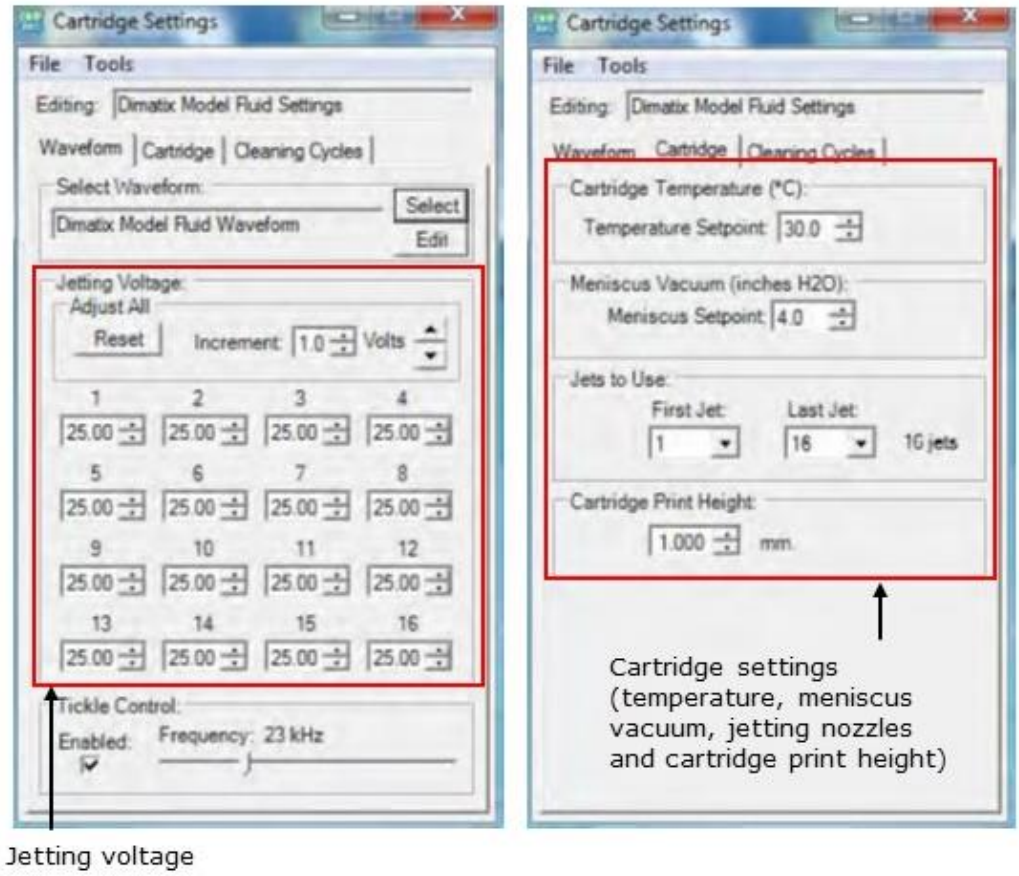


Figure 9.2: Cartridge settings window (Adapted from Fujifilm Dimatix Manual, 2010)

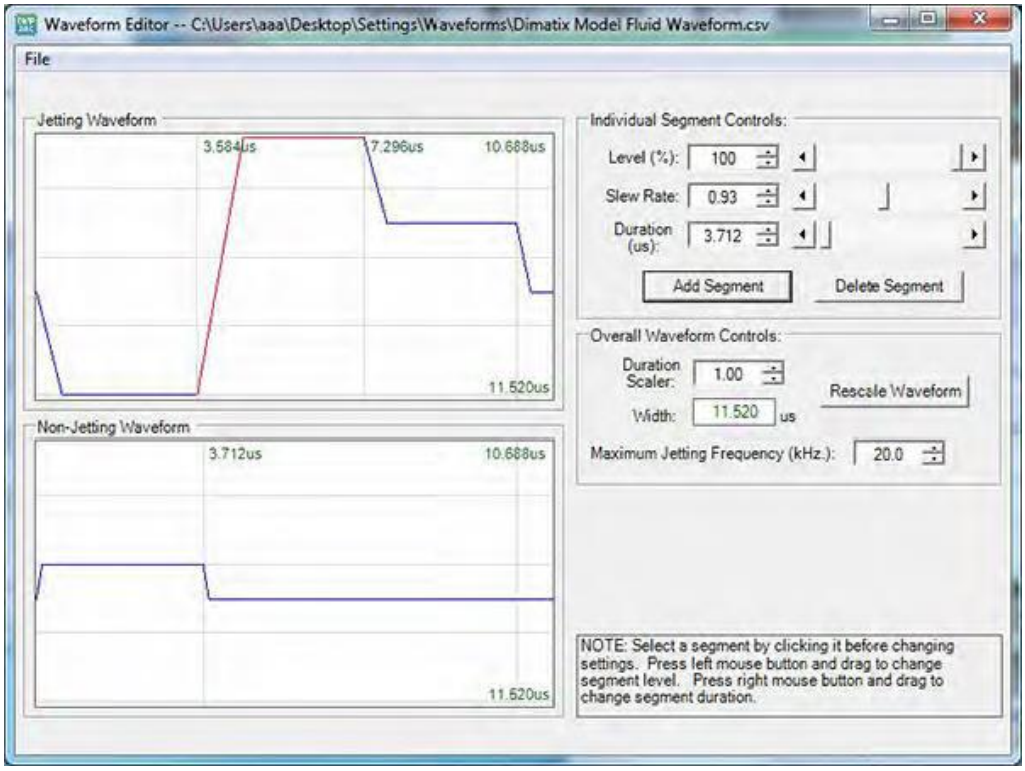


Figure 9.3:Waveform editor window (Adapted from Fujifilm Dimatix Manual, 2010)

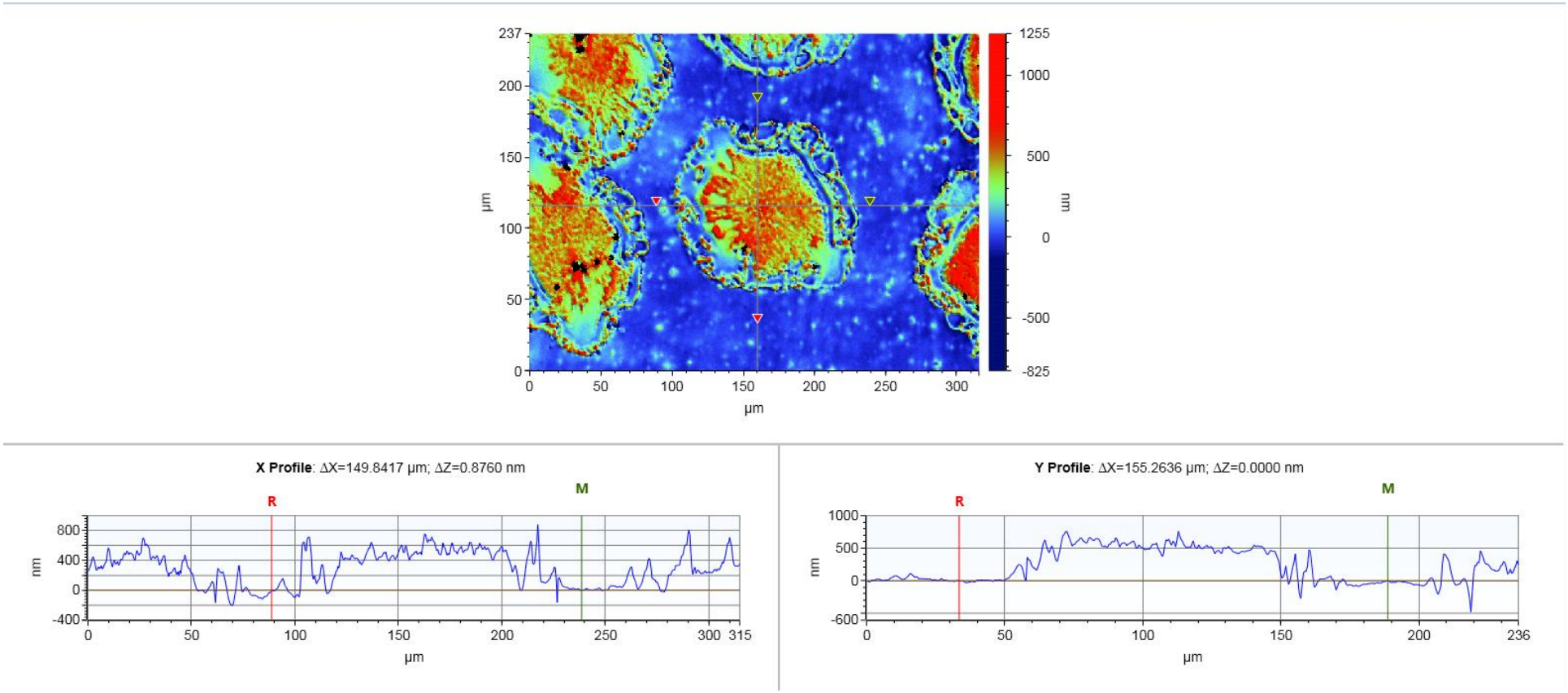


Figure 9.4: WLI results for sample 6 ink-jet printed on PET and dried for approximately 18 hours at room temperature

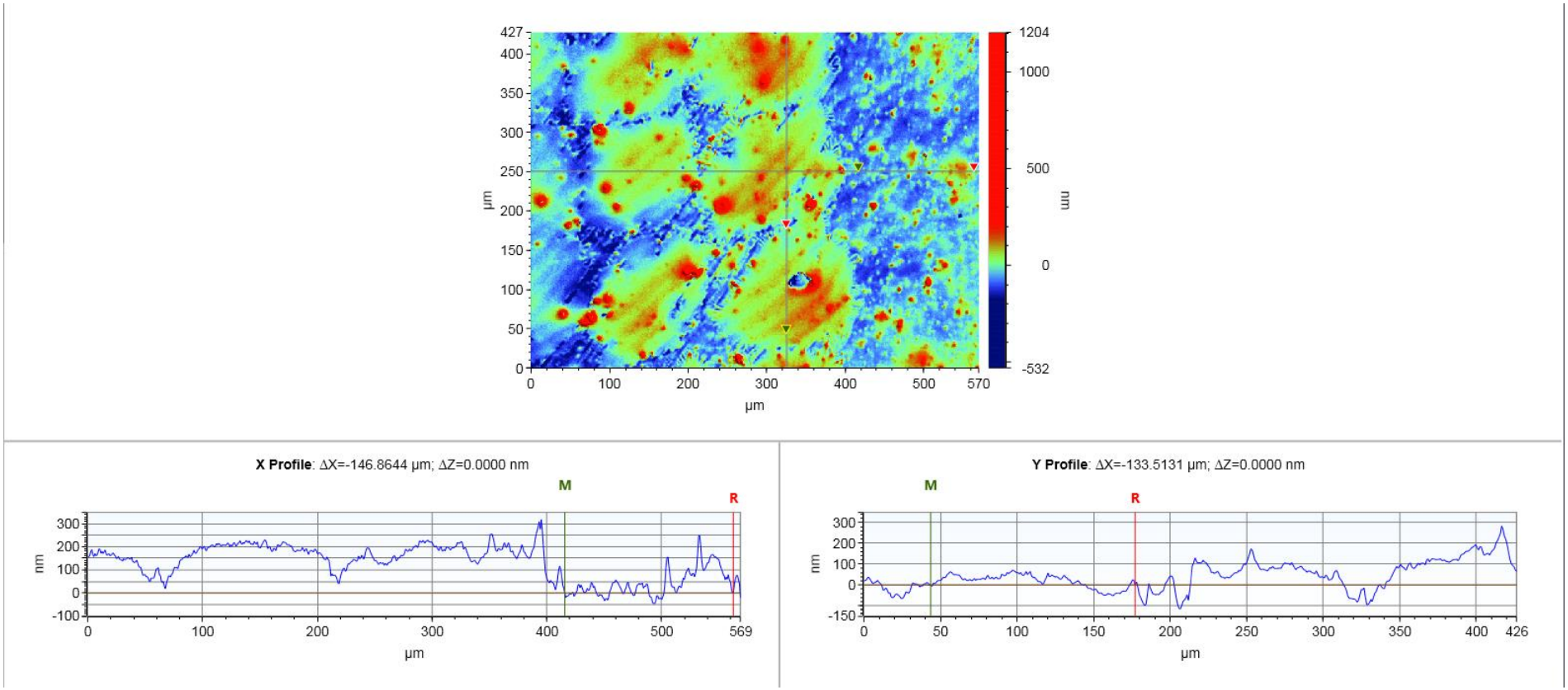


Figure 9.5: WLI results for sample 7 ink-jet printed on PET and dried for approximately 18 hours at room temperature

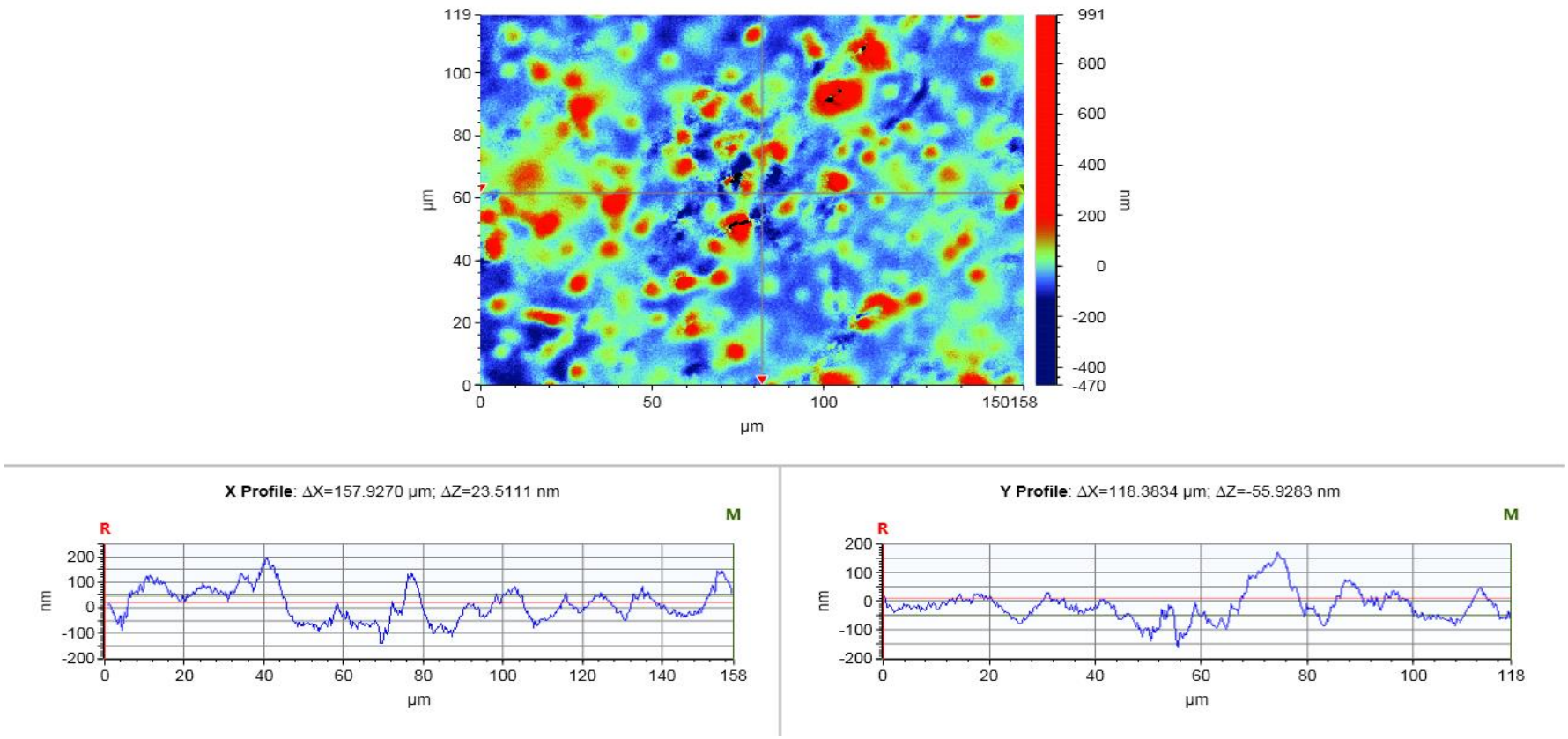


Figure 9.6: WLI results for sample 6 ink-jet printed on PET and regenerated by leaving deionised water for 30 minutes before heating for approximately 18 hours at 50 °C

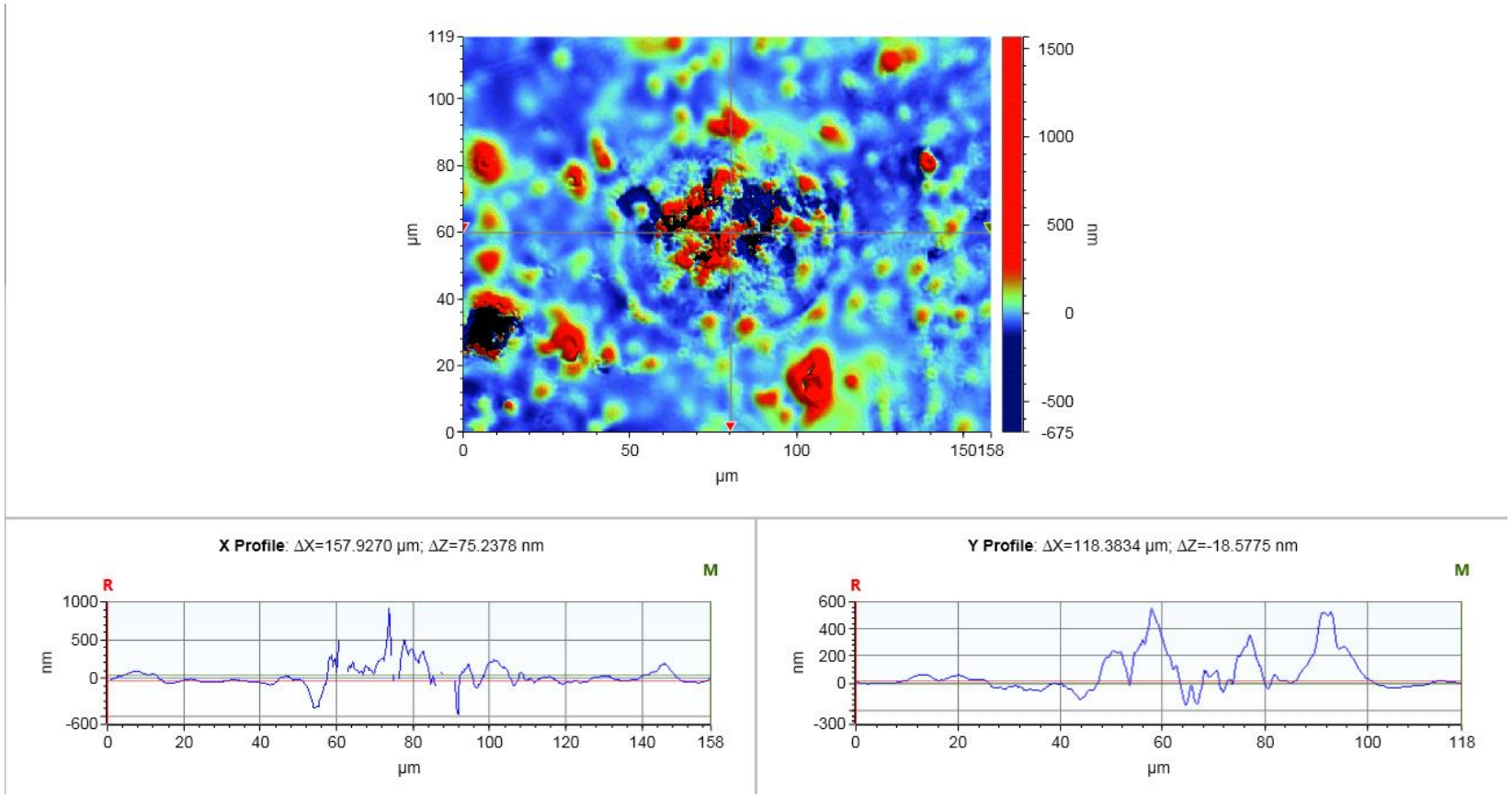


Figure 9.7: WLI results obtained for sample 6 ink-jet printed on PET and regenerated by leaving deionised water for 1 hour 30 minutes before heating for approximately 18 hours at 50 °C

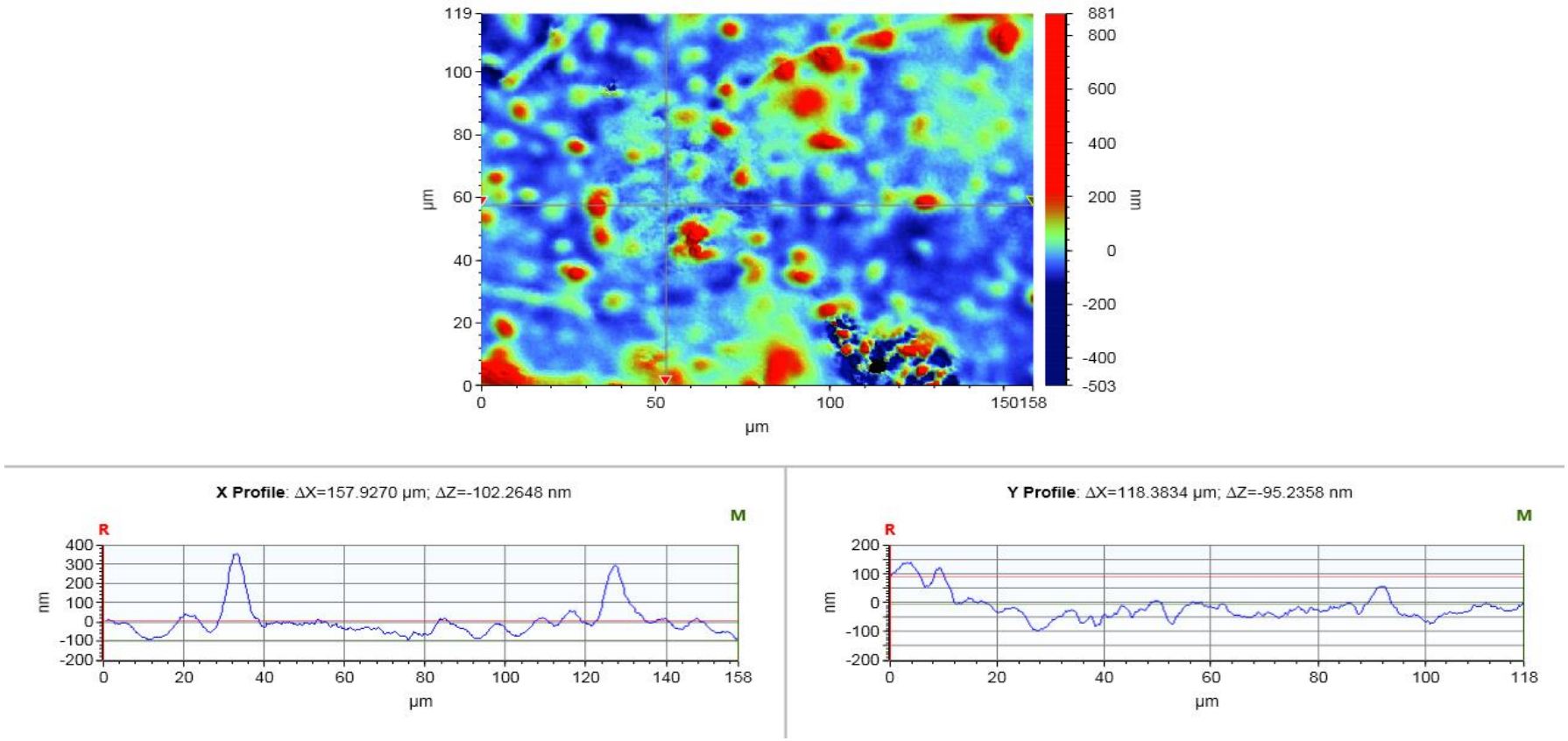


Figure 9.8: WLI results for sample 6 ink-jet printed on PET and regenerated by leaving deionised water for 2 hours before heating for approximately 18 hours at 50 °C

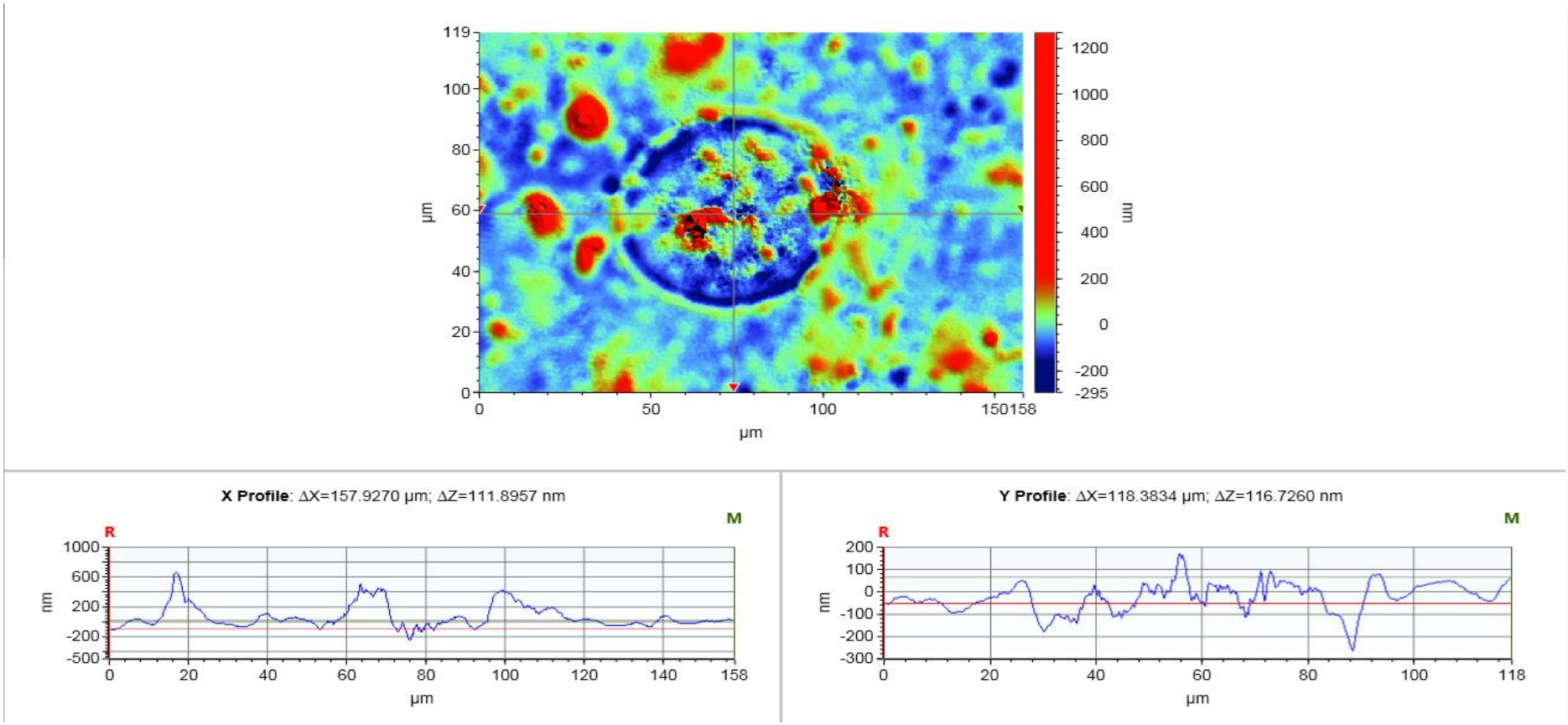


Figure 9.9: WLI results for sample 7 ink-jet printed on PET and regenerated by leaving deionised water for 30 minutes before heating for approximately 18 hours at 50 °C

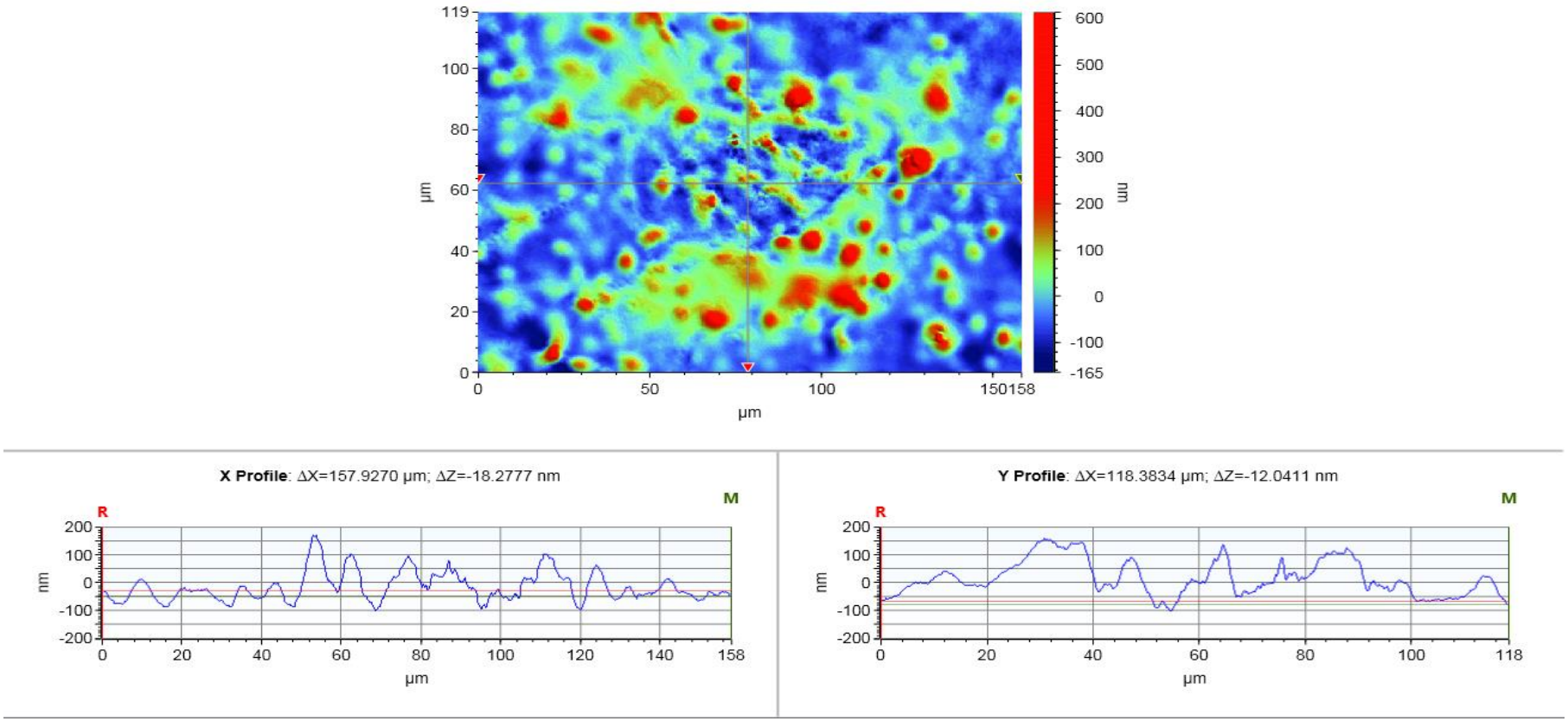


Figure 9.10: WLI results for sample 7 ink-jet printed on PET and regenerated by leaving deionised water for 1 hour before heating for approximately 18 hours at 50 °C

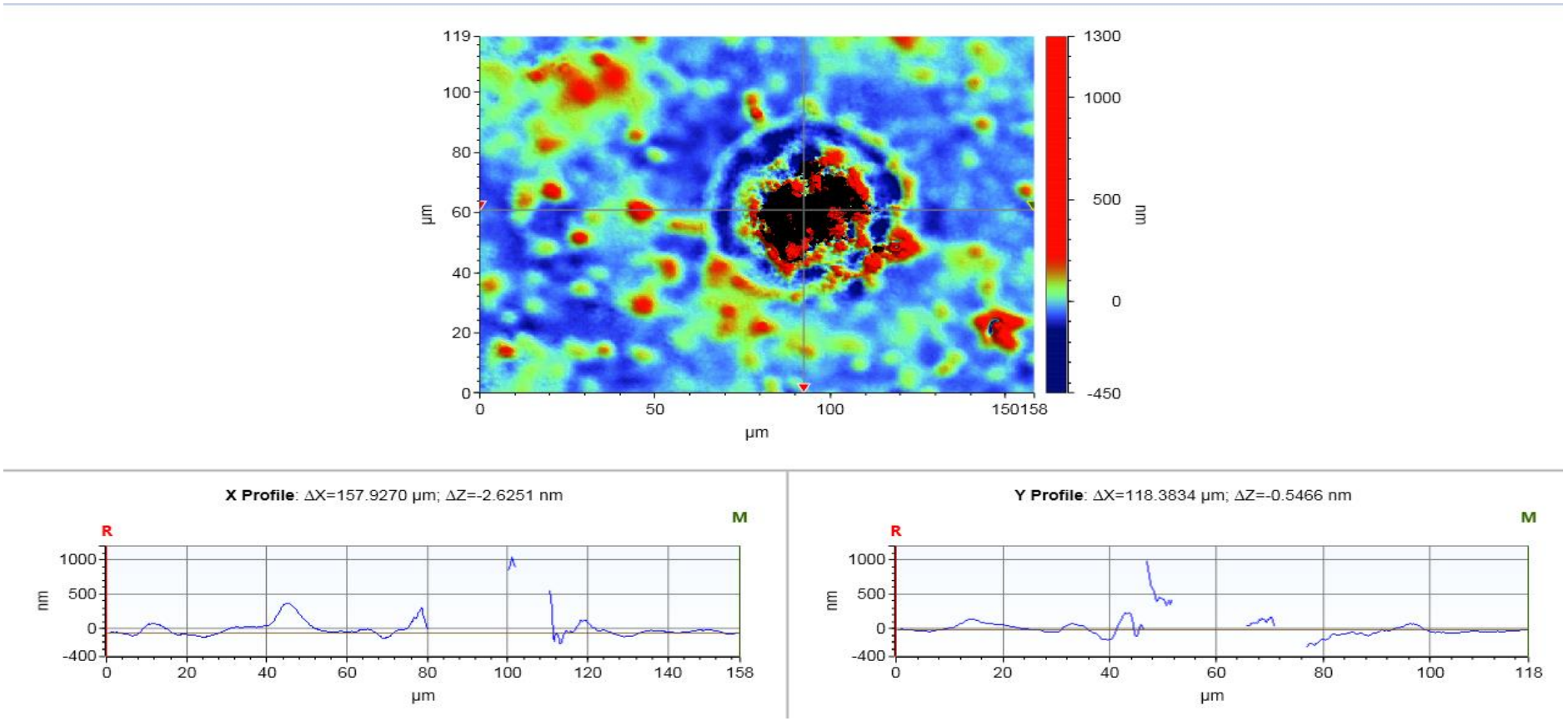


Figure 9.11: WLI results for sample 7 ink-jet printed on PET and regenerated by leaving deionised water for 1 hour 30 minutes before heating for approximately 18 hours at 50 °C

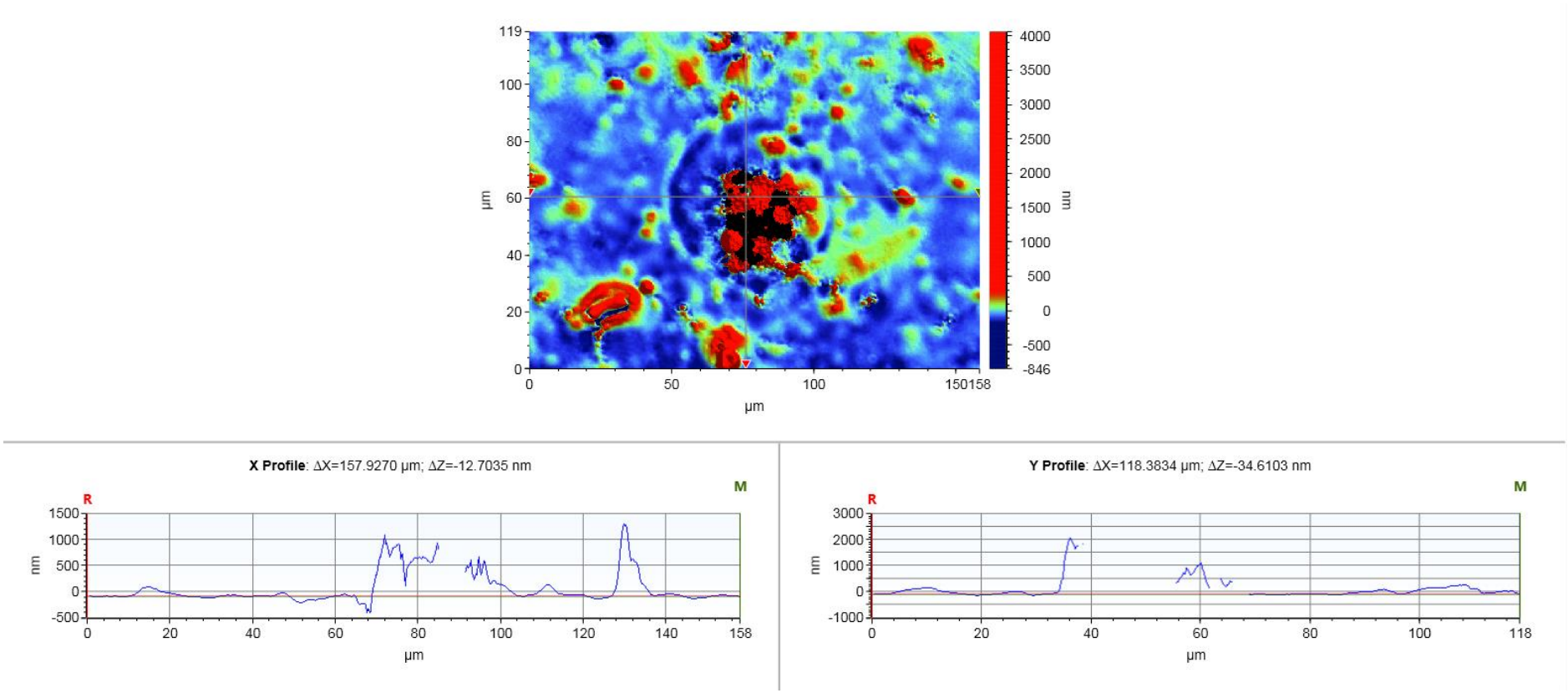


Figure 9.12: WLI results for sample 7 ink-jet printed on PET and regenerated by leaving deionised water for 2 hours before heating for approximately 18 hours at 50 °C

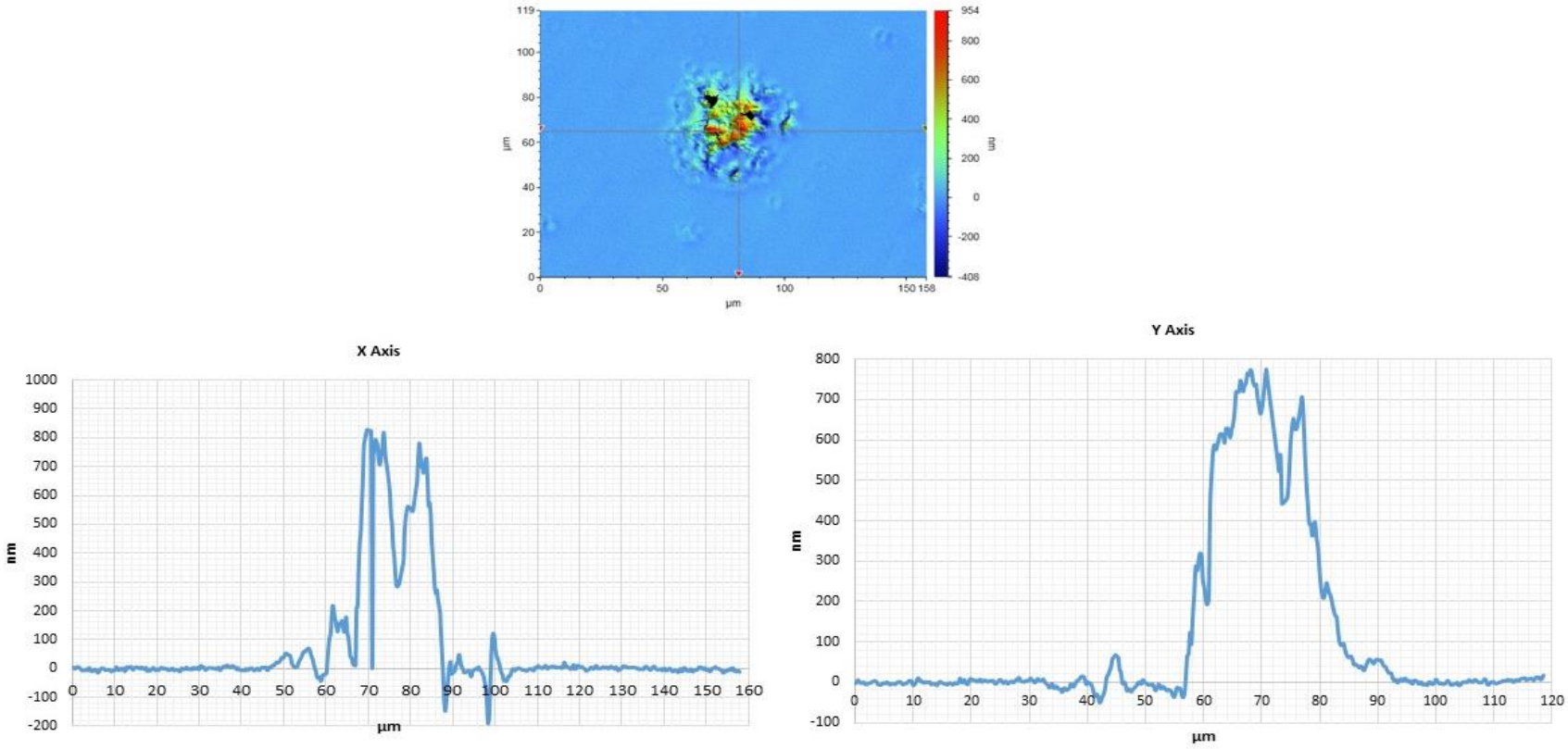


Figure 9.13: WLI results obtained for sample 6 ink-jet printed on glass and regenerated by leaving deionised water for 30 minutes before heating for approximately 18 hours at 50 °C

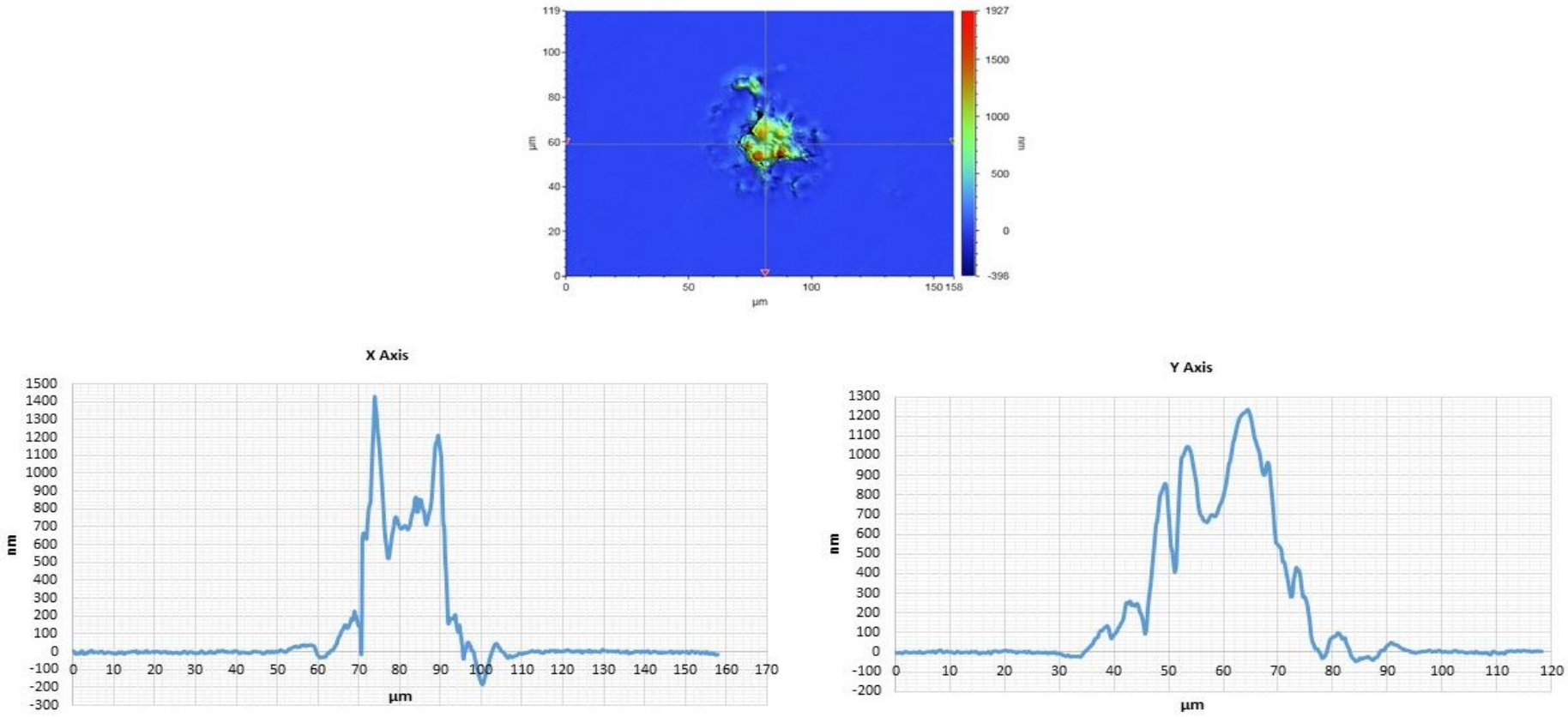


Figure 9.14: WLI results obtained for sample 6 ink-jet printed on glass and regenerated by leaving deionised water for 1 hour before heating for approximately 18 hours at 50 °C

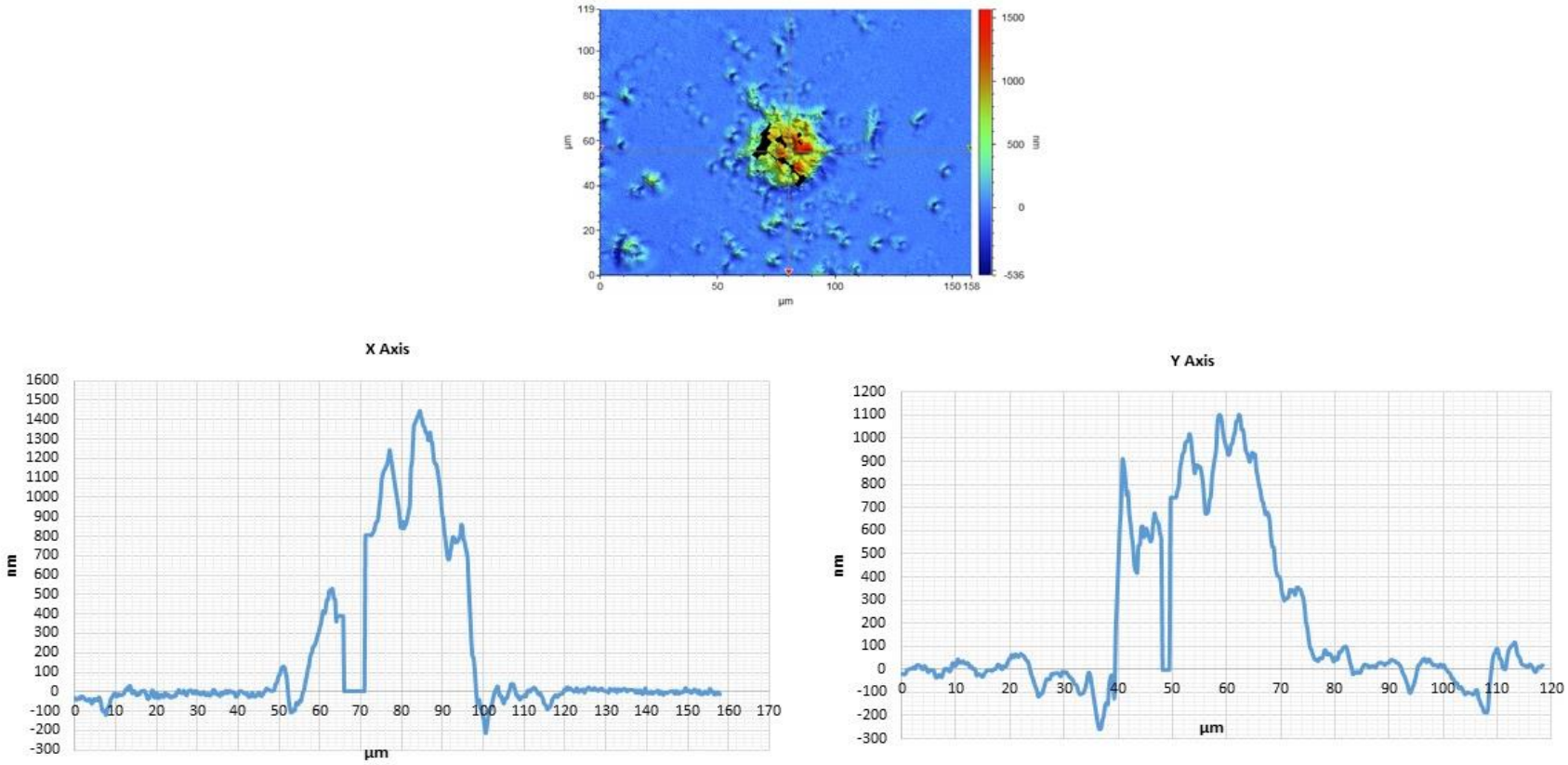


Figure 9.15: WLI results obtained for sample 6 ink-jet printed on glass and regenerated by leaving deionised water for 1 hour 30 minutes before heating for approximately 18 hours at 50 °C

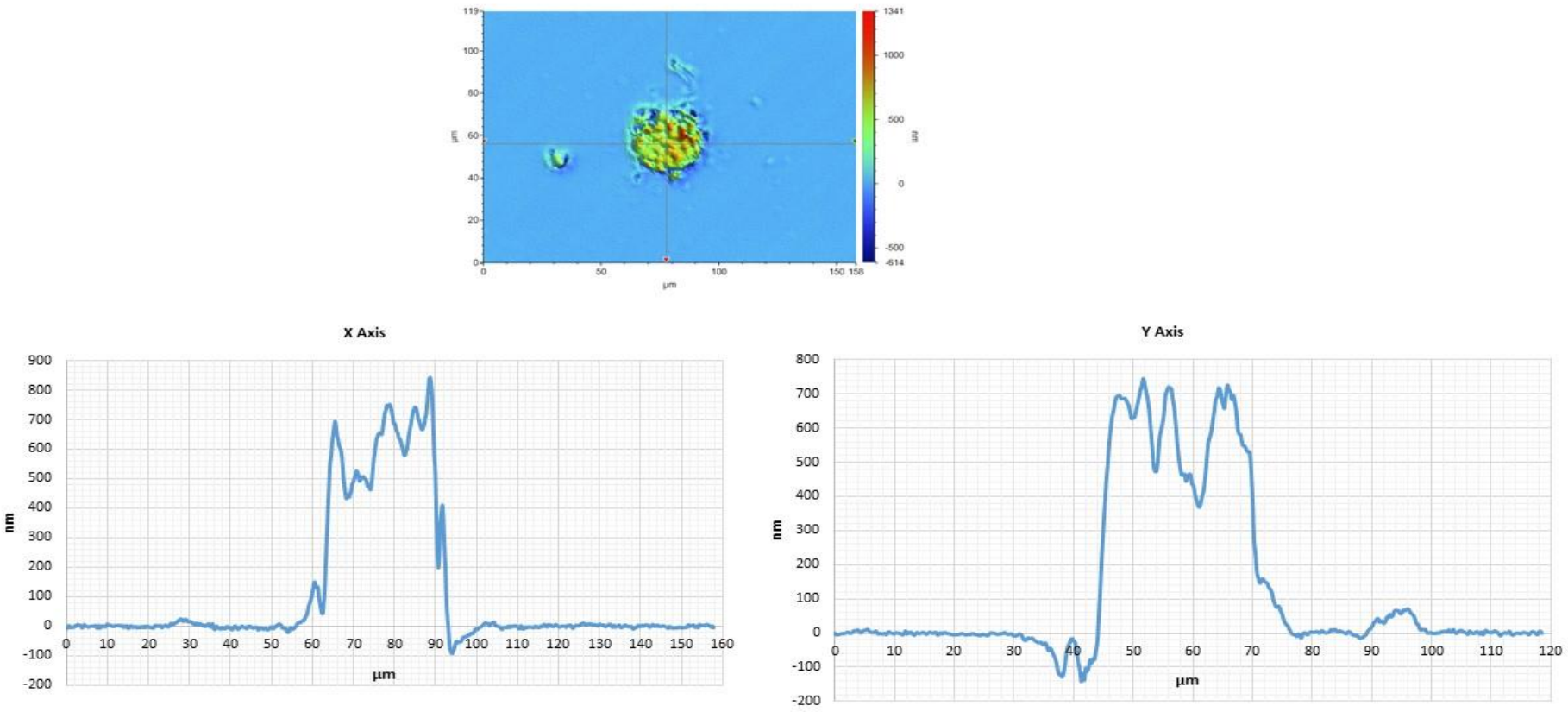


Figure 9.16: WLI results for sample 6 ink-jet printed on glass and regenerated by leaving deionised water for 2 hours before heating for approximately 18 hours at 50 °C

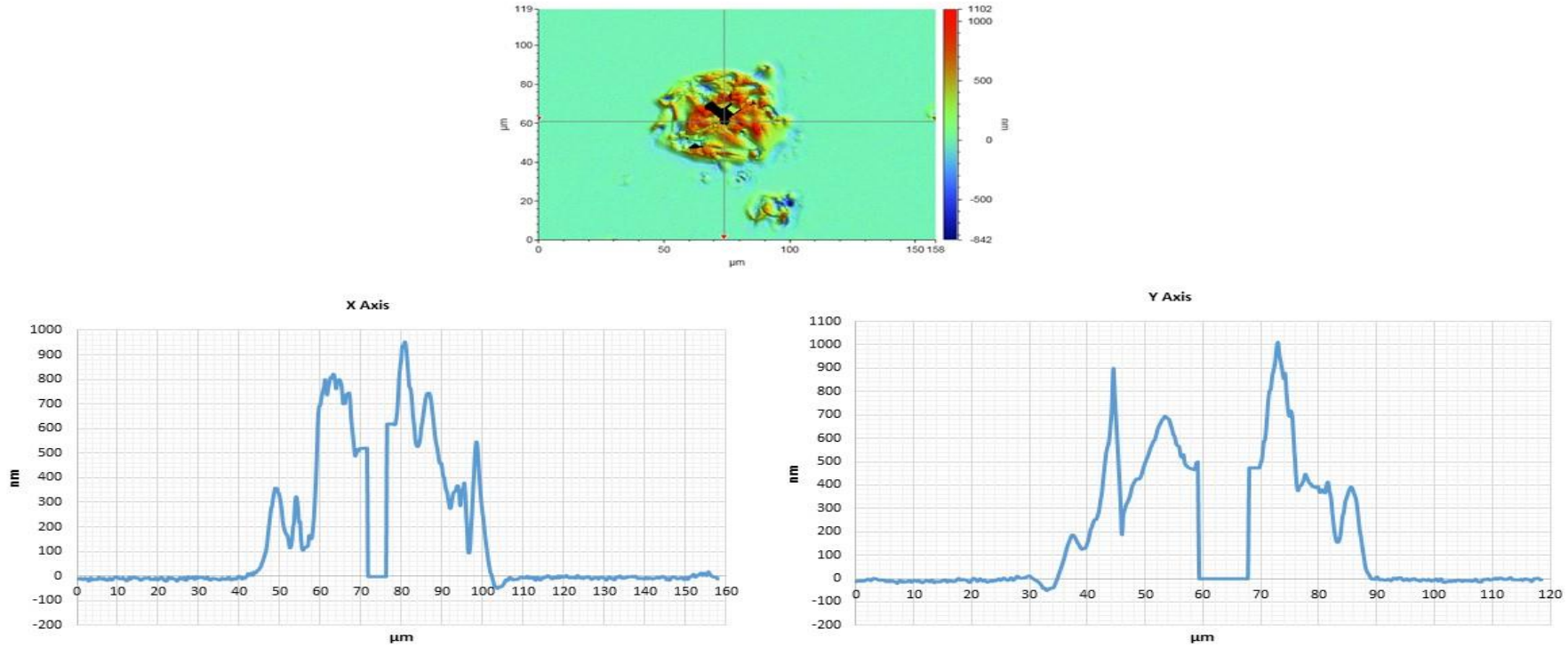


Figure 9.17: WLI results for sample 7 ink-jet printed on glass and regenerated by leaving deionised water for 30 minutes before heating for approximately 18 hours at 50 °C

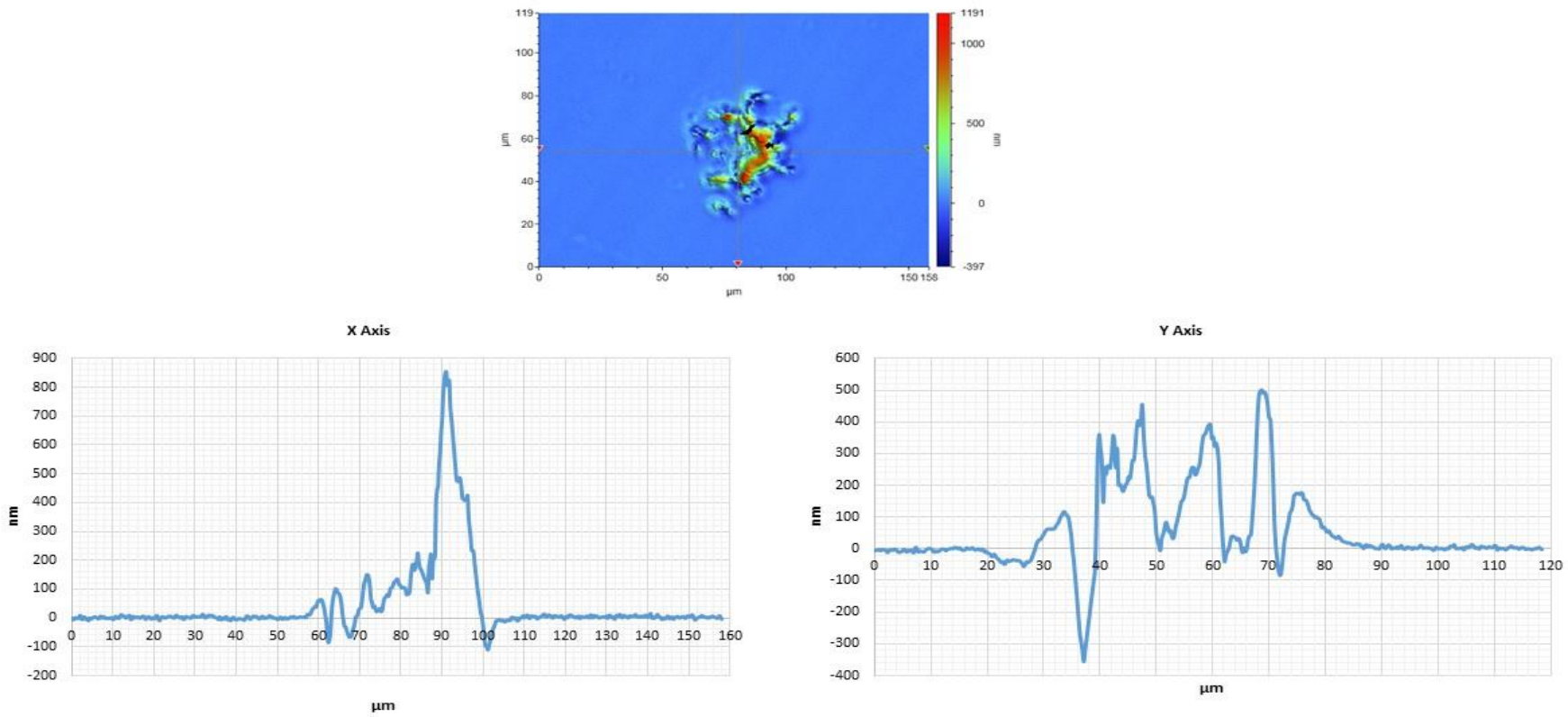


Figure 9.18: WLI results for sample 7 ink-jet printed on glass and regenerated by leaving deionised water for 1 hour before heating for approximately 18 hours at 50 °C

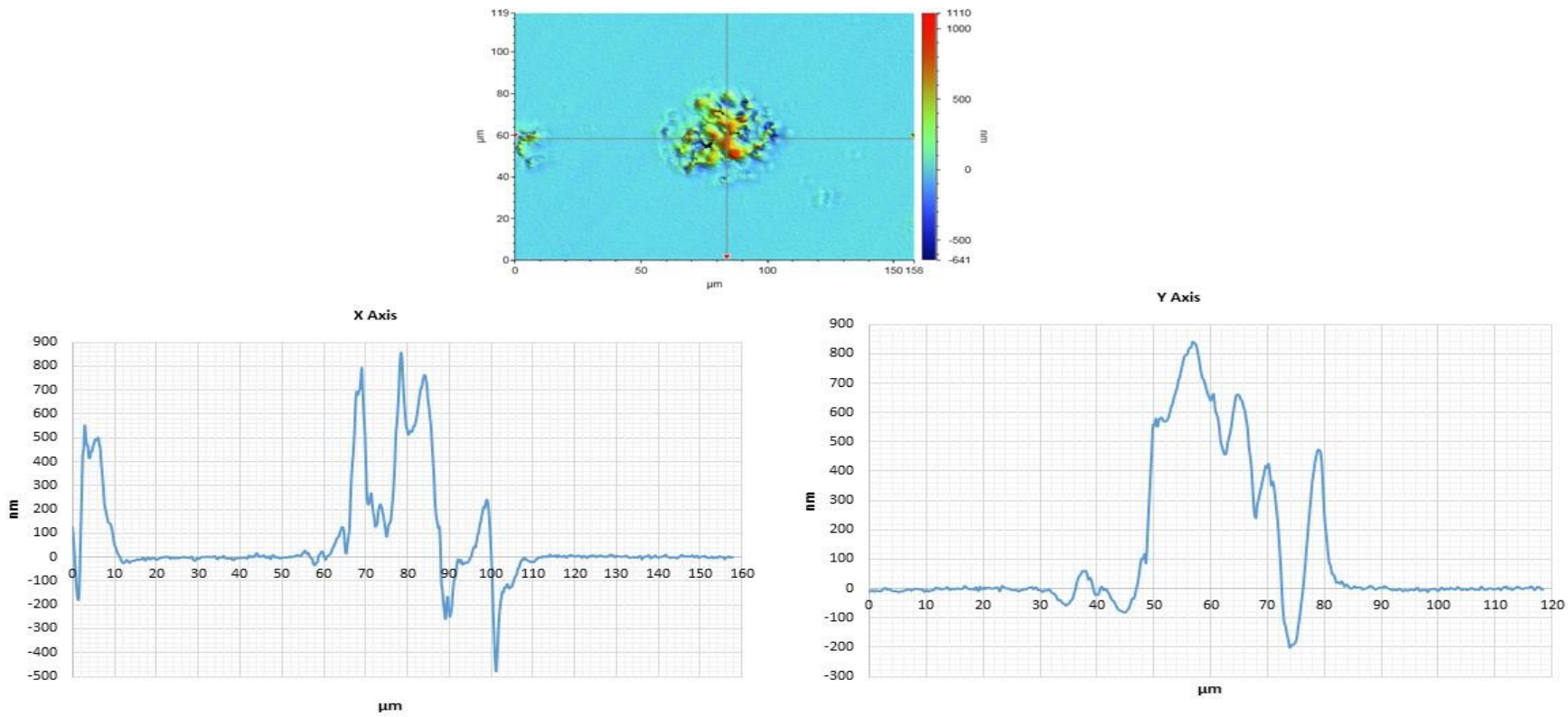


Figure 9.19: WLI results for sample 7 ink-jet printed on glass and regenerated by leaving deionised water for 1 hour 30 minutes before heating for approximately 18 hours at 50 °C

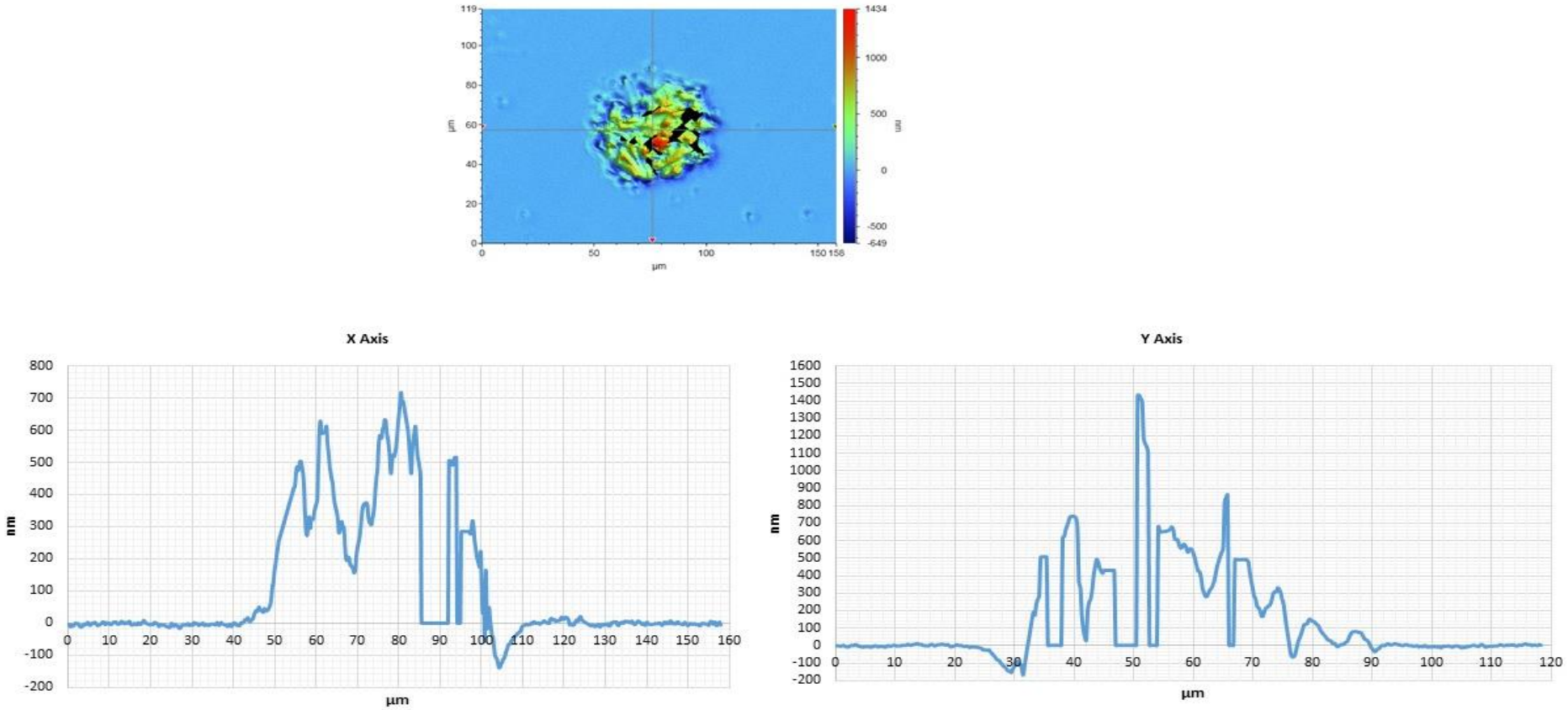


Figure 9.20: WLI results for sample 7 ink-jet printed on glass and regenerated by leaving deionised water for 2 hours before heating for approximately 18 hours at 50 °C

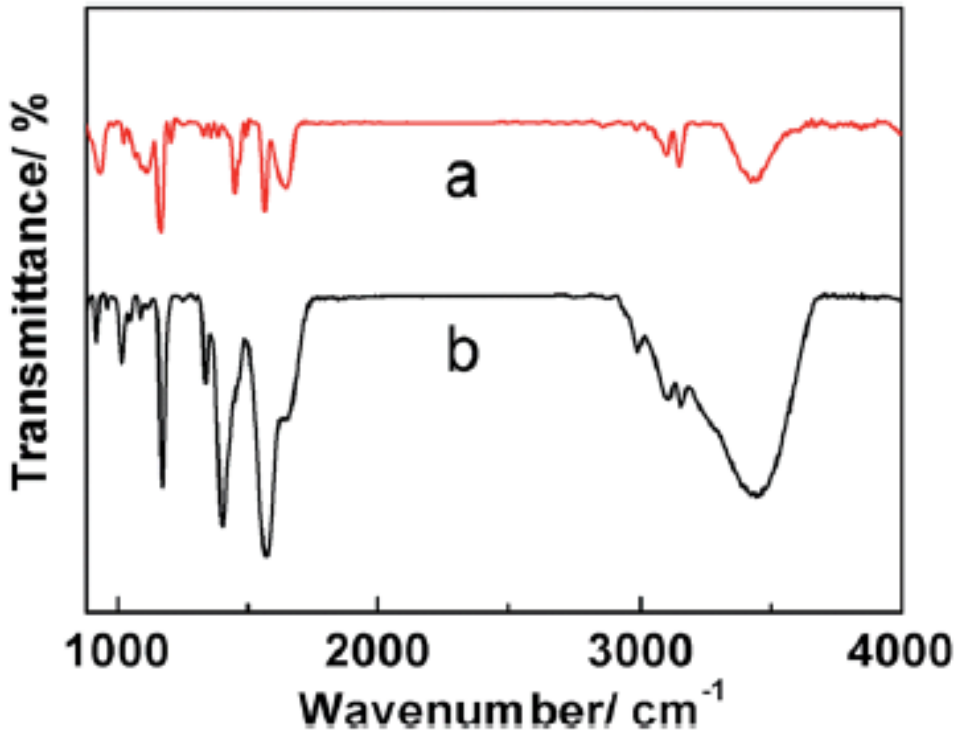
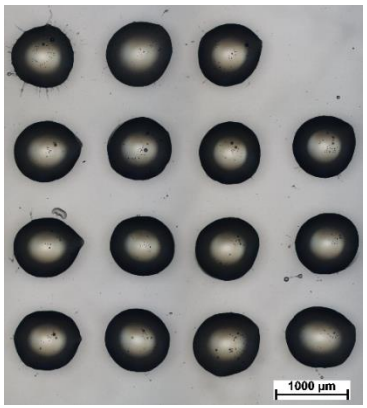
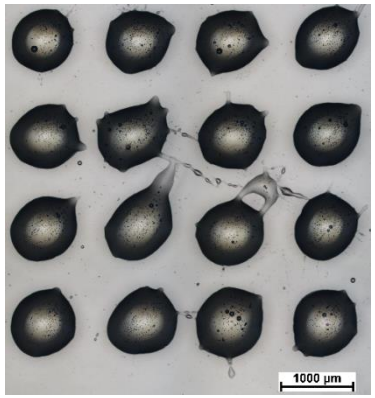


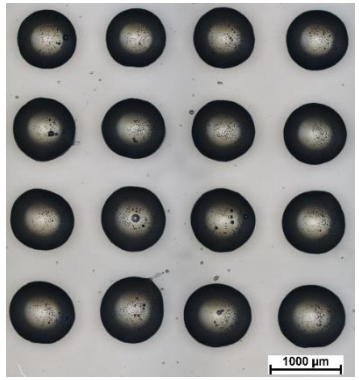
Figure 9.21: Graph b shows the FTIR spectra for $[C_2C_1Im][OAc]$ (Adapted from Zhang B. *et al*., 2015)



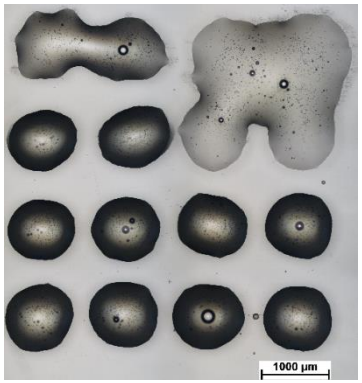
Printing Condition A



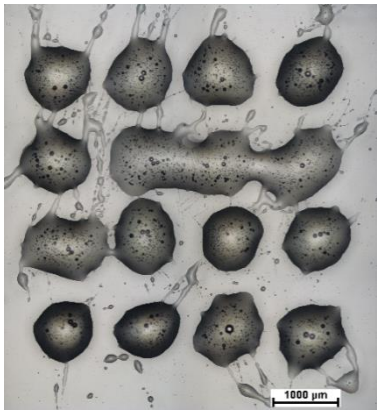
Printing Condition B



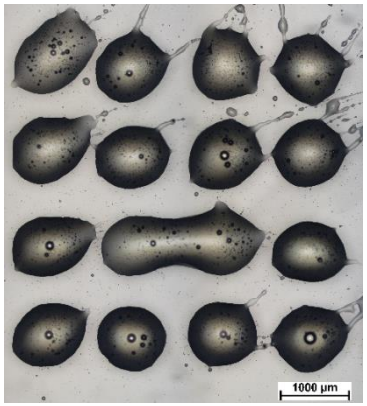
Printing Condition C



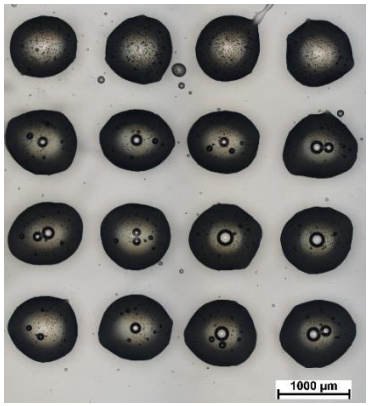
Printing Condition D



Printing Condition E



Printing Condition F

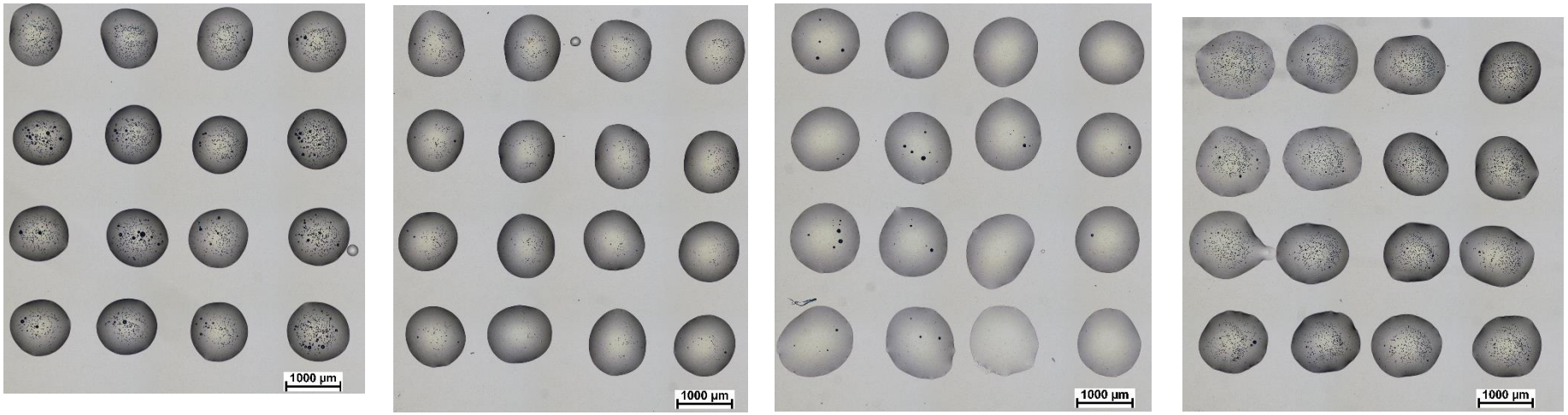


Printing Condition G



Printing Condition H

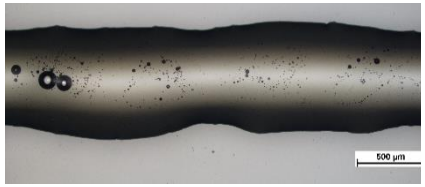
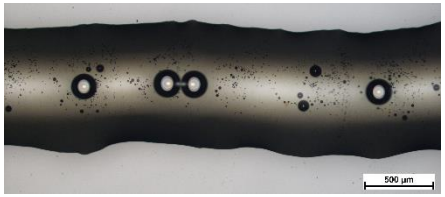
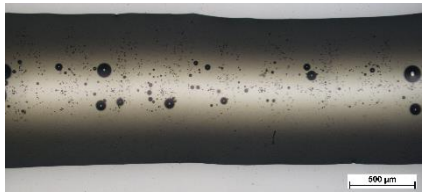
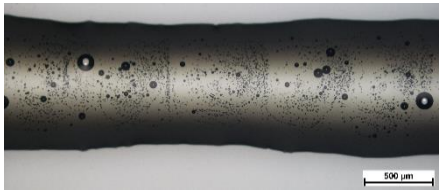
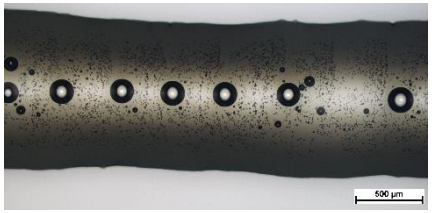
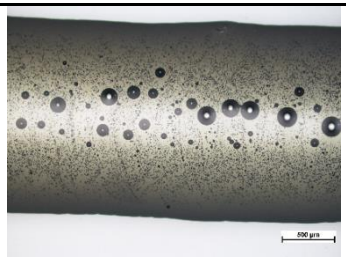
Figure 9.22: Microscopic images obtained from the droplet formation study for sample 13



Printing Condition I **Printing Condition J** **Printing Condition K** **Printing Condition L**

Figure 9.23: Microscopic images obtained from the droplet formation study for sample 14

Table 9.1: Microscopic images obtained from the line formation study for sample 13 ([C_2C_1Im][OAc]) and wool

	20 % Overlap	**40 % Overlap**	**60 % Overlap**	**80 % Overlap**
Printing Condition C				
Droplet Spacing (µm)	750	560	375	190
Average Line Width (µm)	N/A	N/A	1189 ± 112	1595 ± 131
Printing Condition D				
Droplet Spacing (µm)	810	605	405	200
Average Line Width (µm)	N/A	N/A	1175 ± 87	1703 ± 144

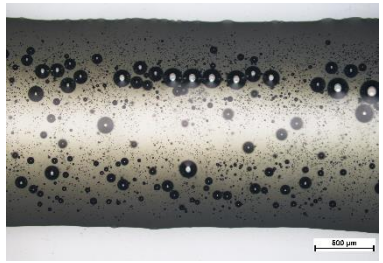
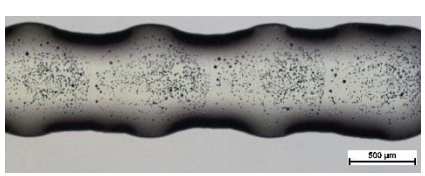
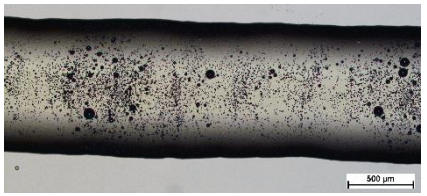
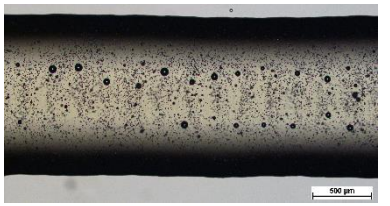
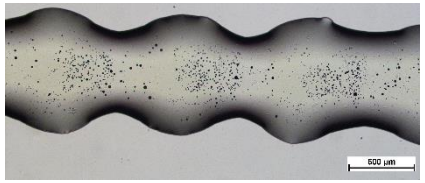
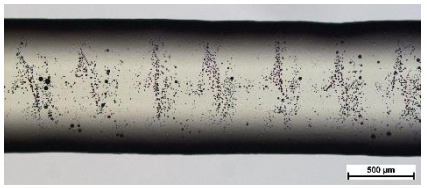
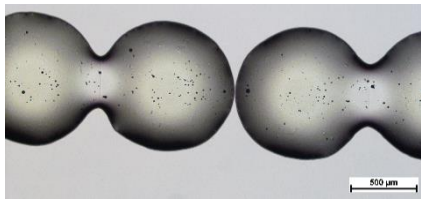
Printing Condition G				
Droplet Spacing (µm)	790	595	395	200
Average Line Width (µm)	N/A	N/A	1167 ± 25	1638 ± 111

Table 9.2: Microscopic images obtained from the line formation study for sample 14 ([C_4C_1Im][OAc] and wool)

	20 % Overlap	**40 % Overlap**	**60 % Overlap**	**80 % Overlap**
Printing Condition I				
Droplet Spacing (µm)	915	685	460	230
Average Line Width (µm)	N/A	N/A	1061 ± 13	1397 ± 37
Printing Condition J				
Droplet Spacing (µm)	940	705	470	235
Average Line Width (µm)	N/A	N/A	1029 ± 11	1217 ± 145

Printing Condition K				
Droplet Spacing (µm)	1025	770	515	260
Average Line Width (µm)	N/A	N/A	1022 ± 40	1316 ± 44

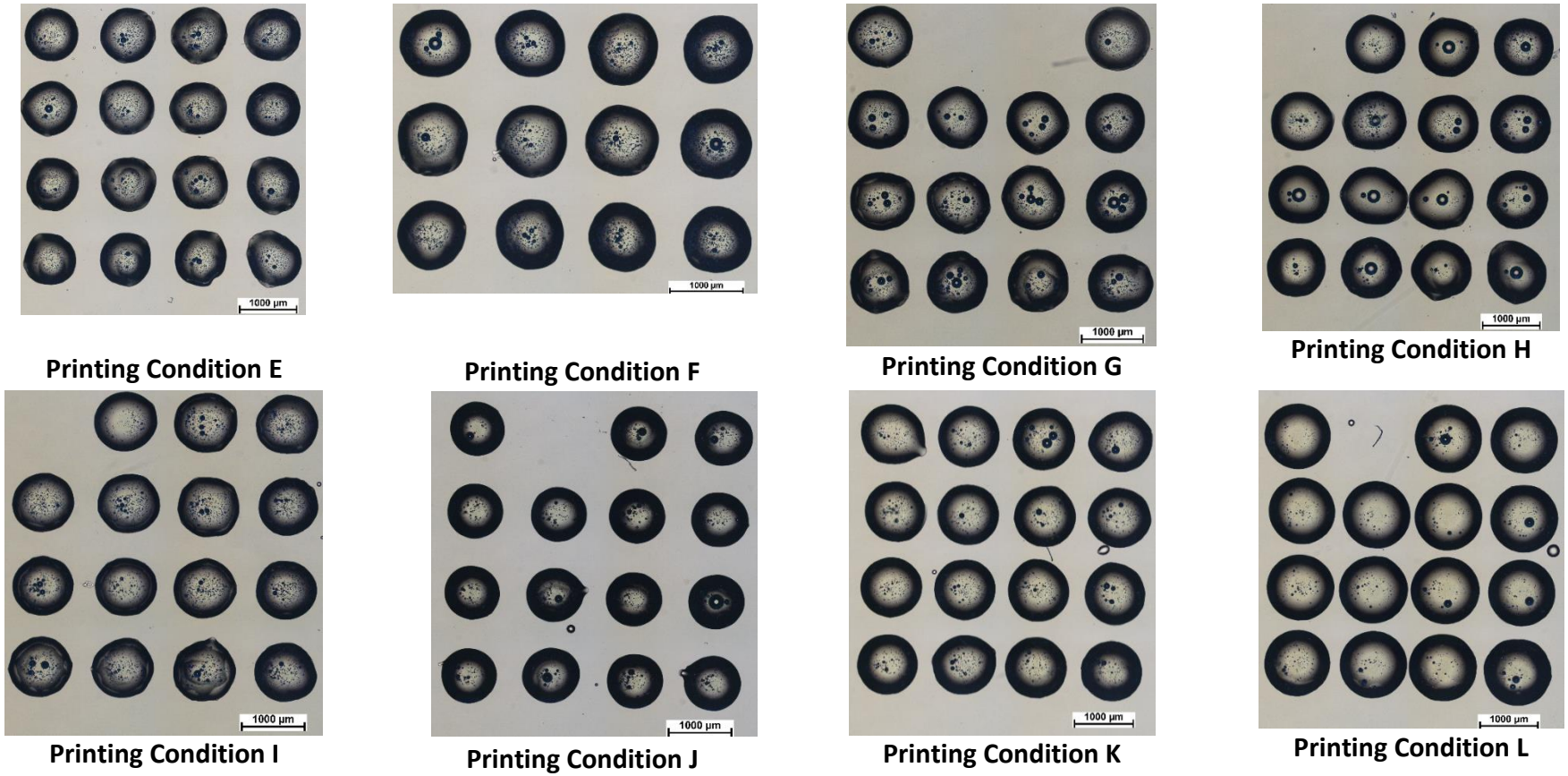
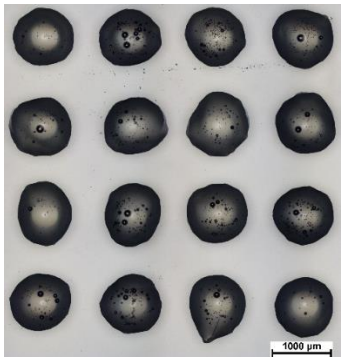
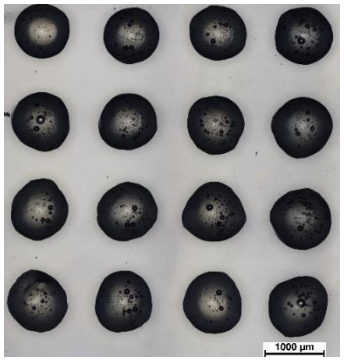


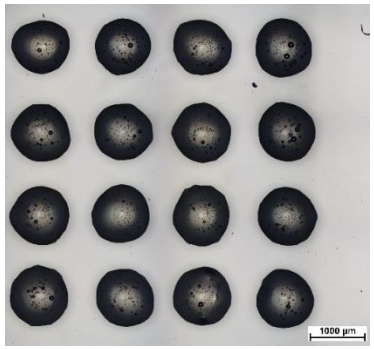
Figure 9.24: Microscopic images obtained from the droplet formation study for sample 15



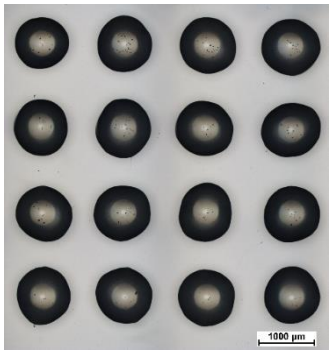
Printing Condition E



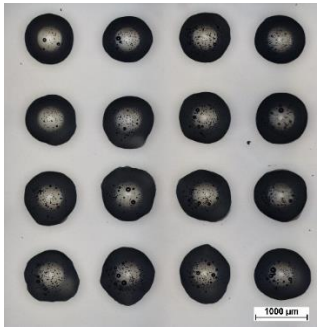
Printing Condition F



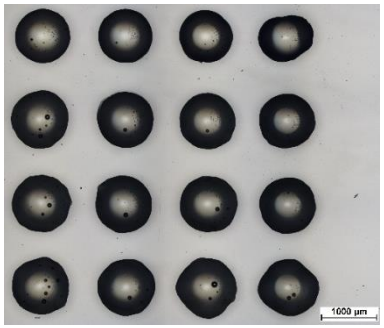
Printing Condition G



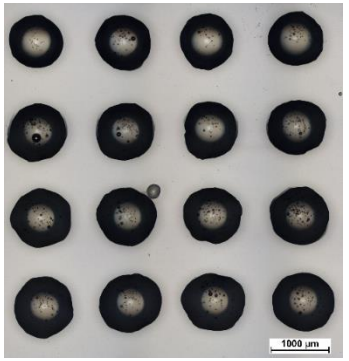
Printing Condition H



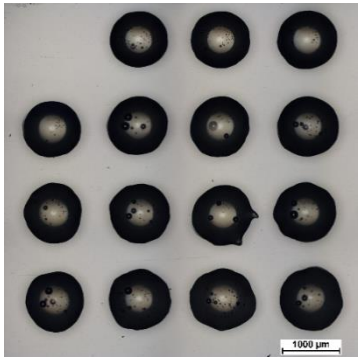
Printing Condition I



Printing Condition J



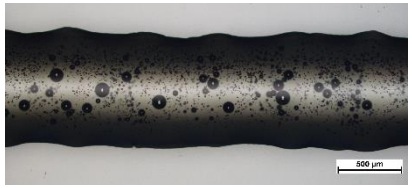
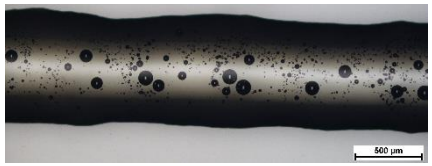
Printing Condition K



Printing Condition L

Figure 9.25: Microscopic images obtained from the droplet formation study for sample 16

Table 9.3: Microscopic images obtained from the line formation study for sample 15 ([C_2C_1Im][OAc], cellulose and wool)

	20 % Overlap	**40 % Overlap**	**60 % Overlap**	**80 % Overlap**
Printing Condition E				
Droplet Spacing (µm)	775	580	390	195
Average Line Width (µm)	N/A	N/A	1010 ± 35	1489 ± 44
Printing Condition F				
Droplet Spacing (µm)	800	600	400	200
Average Line Width (µm)	N/A	N/A	1086 ± 46	1615 ± 31

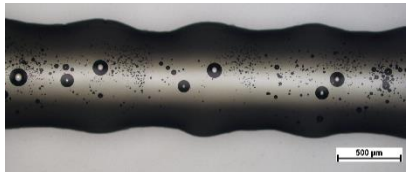
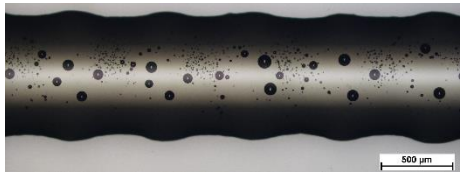
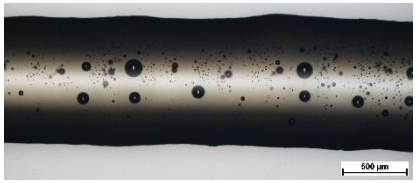
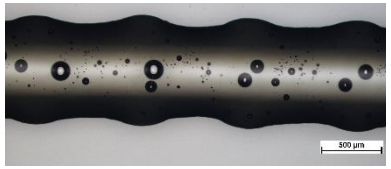
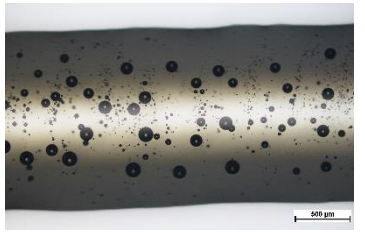
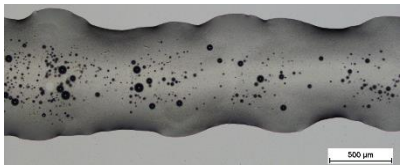
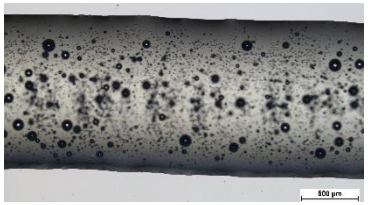
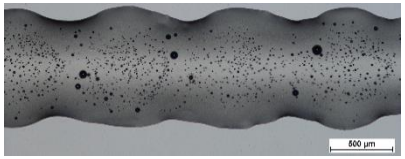
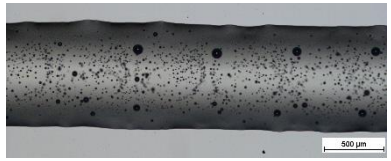
Printing Condition G				
Droplet Spacing (µm)	835	425	415	210
Average Line Width (µm)	N/A	N/A	1017 ± 24	1428 ± 71
Printing Condition H				
Droplet Spacing (µm)	880	660	440	220
Average Line Width (µm)	N/A	952 ± 23	1158 ± 20	1574 ± 44

Table 9.4: Microscopic images obtained from the line formation study for sample 16 ([C_4C_1Im][OAc], cellulose and wool)

	20 % Overlap	**40 % Overlap**	**60 % Overlap**	**80 % Overlap**
Printing Condition E				
Droplet Spacing (µm)	850	640	425	210
Average Line Width (µm)	N/A	875 ± 17	1039 ± 17	1395 ± 16
Printing Condition G				
Droplet Spacing (µm)	880	660	440	220
Average Line Width (µm)	N/A	876 ± 15	1098 ± 25	1538 ± 16

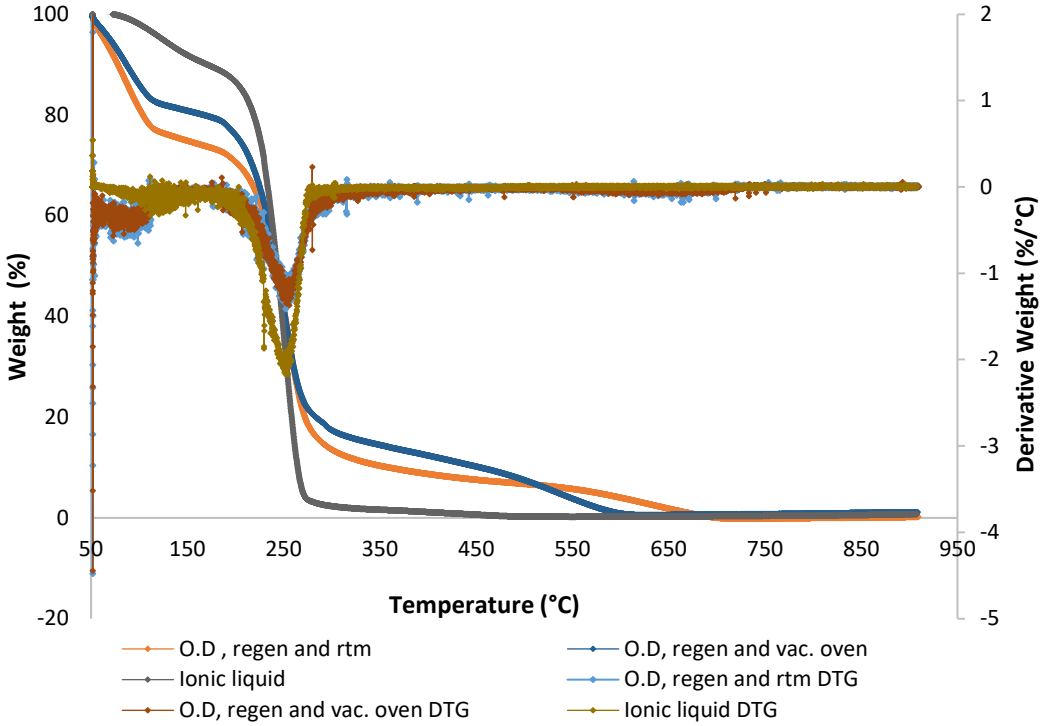


Figure 9.26: TGA and DTG curves for ionic liquid and blend films obtained from sample 15

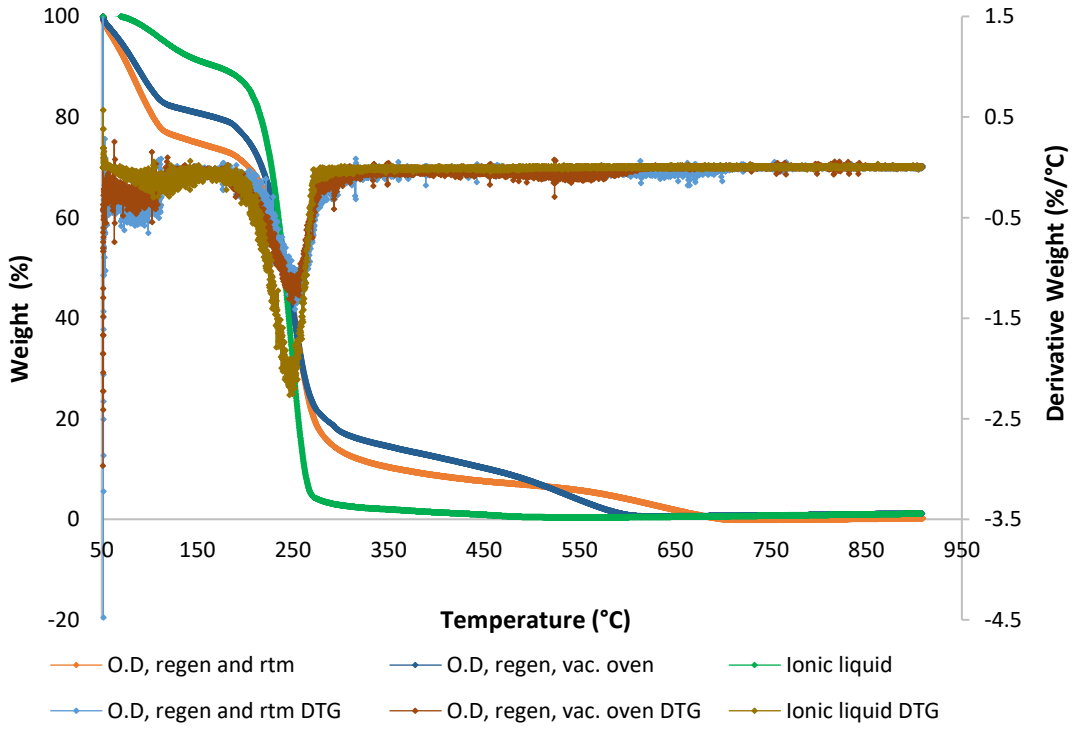


Figure 9.27: TGA and DTG curves for ionic liquid and blend films obtained from sample 16

Chapter 10 : References

AALTONEN, O. & JAUHIAINEN, O. 2009. The preparation of lignocellulosic aerogels from ionic liquid solutions. *Carbohydrate Polymers,* 75**,** 125-129.

ALMEIDA, H. F. D., TELES, A. R. R., LOPES-DA-SILVA, J. A., FREIRE, M. G. & COUTINHO, J. A. P. 2012a. Influence of the anion on the surface tension of 1-ethyl-3-methylimidazolium-based ionic liquids. *The Journal of Chemical Thermodynamics,* 54**,** 49-54.

ALMEIDA, H. F. D., PASSOS, H., LOPES-DA-SILVA, J. A., FERNANDES, A. M., FREIRE, M. G. & COUTINHO, J. A. P. 2012b. Thermophysical properties of five acetate-based ionic liquids. *Journal of Chemical & Engineering Data,* 57**,** 3005-3013.

AMBROSI, A. & PUMERA, M. 2016. 3D-printing technologies for electrochemical applications. *Chemical Society Reviews,* 45**,** 2740-2755.

ANDANSON, J.-M., BORDES, E., DEVÉMY, J., LEROUX, F., PÁDUA, A. A. H. & GOMES, M. F. C. 2014. Understanding the role of co-solvents in the dissolution of cellulose in ionic liquids. *Green Chemistry,* 16**,** 2528-2538.

ARASHIRO, E. Y. & DEMARQUETTE, N. R. 1999. Use of the pendant drop method to measure interfacial tension between molten polymers. *Materials Research,* 2**,** 23-32.

ASHRAFMANSOURI, S.-S. & ESFAHANY, M. N. 2015. The influence of silica nanoparticles on hydrodynamics and mass transfer in spray liquid–liquid extraction column. *Separation and Purification Technology,* 151**,** 74-81.

ASTM 2013. ASTM F2792-12a Standard terminology for additive manufacturing technologies.

BADGUJAR, K. C. & BHANAGE, B. M. 2015. Factors governing dissolution process of lignocellulosic biomass in ionic liquid: Current status, overview and challenges. *Bioresource Technology,* 178**,** 2-18.

BAJPAI, P. 2016. *Structure of lignocellulosic biomass. In: Pretreatment of Lignocellulosic Biomass for Biofuel Production*, Springer.

BANG, Y. H., LEE, S., PARK, J. B. & CHO, H. H. 1999. Effect of coagulation conditions on fine structure of regenerated cellulosic films made from cellulose/N-methylmorpholine-N-oxide/H2O systems. *Journal of Applied Polymer Science,* 73**,** 2681-2690.

BAPTISTA, A., FERREIRA, I. & BORGES, J. 2013. *Cellulose-based bioelectronic devices. In : Cellulose - Medical, Pharmaceutical and Electronic Applications*.

BARANYAI, K. J., DEACON, G. B., MACFARLANE, D. R., PRINGLE, J. M. & SCOTT, J. L. 2004. Thermal degradation of ionic liquids at elevated temperatures. *Australian Journal of Chemistry,* 57**,** 145-147.

BARBES, L., RADULESCU, C. & STIHI, C. 2014. ATR - FTIR spectrometry characterisation of polymeric materials. *Romanian Reports in Physics,* 66**,** 765-777.

BARNES, H. A. 2000. *A handbook of elementary rheology*, The University of Wales Institution of Non-Newtonaina Fluid.

BARTHEL, S. & HEINZE, T. 2006. Acylation and carbanilation of cellulose in ionic liquids. *Green Chemistry,* 8**,** 301-306.

BERMAN, B. 2012. 3-D printing: The new industrial revolution. *Business Horizons,* 55**,** 155-162.

BERROCAL, A., BAEZA, J., RODRÍGUEZ, J., ESPINOSA, M. & FREER, J. 2004. Effect of tree age on variation of pinus radiata d. don

chemical composition. *Journal of the Chilean Chemical Society,* 49**,** 251-256.
BERRY, J. D., NEESON, M. J., DAGASTINE, R. R., CHAN, D. Y. C. & TABOR, R. F. 2015. Measurement of surface and interfacial tension using pendant drop tensiometry. *Journal of Colloid and Interface Science,* 454**,** 226-237.
BOHLIN INSTRUMENTS LIMITED 1994. A basic introduction to rheology.
BOLAND, T., XU, T., DAMON, B. & CUI, X. 2006. Application of inkjet printing to tissue engineering. *Biotechnology Journal,* 1**,** 910-917.
BONHÔTE, P., DIAS, A.-P., PAPAGEORGIOU, N., KALYANASUNDARAM, K. & GRÄTZEL, M. 1996. Hydrophobic, highly conductive ambient-temperature molten salts. *Inorganic Chemistry,* 35**,** 1168-1178.
BRANDT, A., GRASVIK, J., HALLETT, J. P. & WELTON, T. 2013. Deconstruction of lignocellulosic biomass with ionic liquids. *Green Chemistry,* 15**,** 550-583.
BROWN, E. K., HAVERHALS, L. M., FOLEY, M. P., DE LONG, H. & TRULOVE, P. C. 2012. Electrospinning of biopolymers from ionic liquid - Co-solvent systems. *ECS Transactions,* 50**,** 595-602.
CAO, J. 2000. Is the α-β transition of keratin a transition of α-helices to β-pleated sheets? Part I. In situ XRD studies. *Journal of Molecular Structure,* 553**,** 101-107.
CAO, J. 2002. Is the alpha beta transition of keratin a transition of alpha-helices to beta-pleated sheets. II. Synchrotron investigation for stretched single specimens. *Journal of Molecular Structure,* 607**,** 69-75.
CAO, Y. & MU, T. 2014. Comprehensive investigation on the thermal stability of 66 ionic liquids by thermogravimetric analysis. *Industrial & Engineering Chemistry Research,* 53**,** 8651-8664.
CASTRO, M. C., RODRÍGUEZ, H., ARCE, A. & SOTO, A. 2014. Mixtures of ethanol and the ionic liquid 1-ethyl-3-methylimidazolium acetate for the fractionated solubility of biopolymers of lignocellulosic biomass. *Industrial & Engineering Chemistry Research,* 53**,** 11850-11861.
CHEN, H. 2014. *Chemical composition and structure of natural lignocellulose. In: Biotechnology of Lignocellulose.* , Springer.
CHEN, J., VONGSANGA, K., WANG, X. & BYRNE, N. 2014. What happens during natural protein fibre dissolution in ionic liquids. *Materials (Basel),* 7**,** 6158-6168.
CHEN, T., CHIDAMBARAM, M., LIU, Z., SMIT, B. & BELL, A. T. 2010. Viscosities of the mixtures of 1-ethyl-3-methylimidazolium chloride with water, acetonitrile and glucose: A molecular dynamics simulation and experimental study. *The Journal of Physical Chemistry B,* 114**,** 5790-5794.
CHEN, X., ZHANG, Y., CHENG, L. & WANG, H. 2009. Rheology of concentrated cellulose solutions in 1-butyl-3-methylimidazolium chloride. *Journal of Polymers and the Environment,* 17**,** 273-279.
CROSTHWAITE, J. M., MULDOON, M. J., DIXON, J. K., ANDERSON, J. L. & BRENNECKE, J. F. 2005. Phase transition and decomposition temperatures, heat capacities and viscosities of pyridinium ionic liquids. *The Journal of Chemical Thermodynamics,* 37**,** 559-568.
CROWHURST, L., MAWDSLEY, P. R., PEREZ-ARLANDIS, J. M., SALTER, P. A. & WELTON, T. 2003. Solvent–solute interactions in ionic liquids. *Physical Chemistry Chemical Physics,* 5**,** 2790-2794.
COULING, D. J., BERNOT, R. J., DOCHERTY, K. M., DIXON, J. K. & MAGINN, E. J. 2006. Assessing the factors responsible for ionic liquid toxicity to aquatic organisms via quantitative structure–property relationship modeling. *Green Chemistry,* 8**,** 82-90.

DALEV, P. G. 1994. Utilisation of waste feathers from poultry slaughter for production of a protein concentrate. *Bioresource Technology,* 48**,** 265-267.

DARBY, N. & CREIGHTON, T. E. 1993. *Protein structure* Oxford : IRL Press.

DE GANS, B. J., DUINEVELD, P. C. & SCHUBERT, U. S. 2004. Inkjet printing of polymers: State of the art and future developments. *Advanced Materials,* 16**,** 203-213.

DENG, M., ZHOU, Q., DU, A., VAN KASTEREN, J. & WANG, Y. 2009. Preparation of nanoporous cellulose foams from cellulose-ionic liquid solutions. *Materials Letters,* 63**,** 1851-1854.

DEPARTMENT OF ENVIRONMENT FOOD AND RURAL AFFAIRS 2016. UK Statistics on waste.

DERBY, B. 2010. Inkjet Printing of functional and structural materials: Fluid property requirements, feature stability, and resolution. *Annual Reviews of Materials Research,* 40**,** 395-414.

DETSCH, R., UHL, F., DEISINGER, U. & ZIEGLER, G. 2008. 3D-Cultivation of bone marrow stromal cells on hydroxyapatite scaffolds fabricated by dispense-plotting and negative mould technique. *Journal of Materials Science: Materials in Medicine,* 19**,** 1491-1496.

DEVILLEZ, A., LESKO, S. & MOZER, W. 2004. Cutting tool crater wear measurement with white light interferometry. *Wear,* 256**,** 56-65.

DEY, T. & NAUGHTON, D. 2016. Cleaning and anti-reflective (AR) hydrophobic coating of glass surface: a review from materials science perspective. *Journal of Sol-Gel Science and Technology,* 77**,** 1-27.

DOCHERTY, K. M. & KULPA, J. C. F. 2005. Toxicity and antimicrobial activity of imidazolium and pyridinium ionic liquids. *Green Chemistry,* 7**,** 185-189.

DOMINGUEZ, V. C., MCDONALD, C. R., JOHNSON, M., SCHUNK, D., KREUTER, R., SYKES, D., WIGTON, B. T. & CHOHAN, B. S. 2010. The characterization of a custom-built Coulometric Karl Fischer titration apparatus. *Journal of Chemical Education,* 87**,** 987-991.

EARLE, M., J. & SEDDON, K., R. 2000. Ionic liquids. Green solvents for the future. *Pure and Applied Chemistry,* 72**,** 1391-1398.

EGGENHUISEN, T. M., GALAGAN, Y., BIEZEMANS, A. F. K. V., SLAATS, T. M. W. L., VOORTHUIJZEN, W. P., KOMMEREN, S., SHANMUGAM, S., TEUNISSEN, J. P., HADIPOUR, A., VERHEES, W. J. H., VEENSTRA, S. C., COENEN, M. J. J., GILOT, J., ANDRIESSEN, R. & GROEN, W. A. 2015. High efficiency, fully inkjet printed organic solar cells with freedom of design. *Journal of Materials Chemistry A,* 3**,** 7255-7262.

EL SEOUD, O. A., DA SILVA, V. C., POSSIDONIO, S., CASARANO, R., ARÊAS, E. P. G. & GIMENES, P. 2011. Microwave-assisted derivatization of cellulose, 2 – The surprising effect of the structure of ionic liquids on the dissolution and acylation of the biopolymer. *Macromolecular Chemistry and Physics,* 212**,** 2541-2550.

EMORI, K., MIURA, T., KISHIDA, H. & YONEZU, A. 2019. Creep deformation behavior of polymer materials with a 3D random pore structure: Experimental investigation and FEM modeling. *Polymer Testing,* 80**,** 106097.

ERDMENGER, T., HAENSCH, C., HOOGENBOOM, R. & SCHUBERT, U. S. 2007. Homogeneous tritylation of cellulose in 1-butyl-3-methylimidazolium chloride. *Macromolecular Bioscience,* 7**,** 440-445.

FADDOUL, R., REVERDY-BRUAS, N. & BOUREL, J. 2012. Silver content effect on rheological and electrical properties of silver pastes. *Journal of Materials Science: Materials in Electronics,* 23**,** 1415-1426.

FAHAD, M., DICKENS, P. & GILBERT, M. 2011. Novel support materials for jetting based additive manufacturing processes. *Rapid Prototyping Journal,* 19**,** 230-239.

FANG, K., HAO, L., HU, X. & SHAO, H. 2003. Ester crosslinking treatmen for reducing the fibrillation tendency of lyocell fibers. *Textile Research Journal,* 73**,** 1013-1016.

FENDT, S., PADMANABHAN, S., BLANCH, H. W. & PRAUSNITZ, J. M. 2011. Viscosities of acetate or chloride-based ionic liquids and some of their mixtures with water or other common solvents. *Journal of Chemical & Engineering Data,* 56**,** 31-34.

FERNANDES, A. M., ROCHA, M. A. A., FREIRE, M. G., MARRUCHO, I. M., COUTINHO, J. A. P. & SANTOS, L. M. N. B. F. 2011. Evaluation of cation−anion interaction strength in ionic liquids. *The Journal of Physical Chemistry B,* 115**,** 4033-4041.

FORT, D. A., REMSING, R. C., SWATLOSKI, R. P., MOYNA, P., MOYNA, G. & ROGERS, R. D. 2007. Can ionic liquids dissolve wood? Processing and analysis of lignocellulosic materials with 1-n-butyl-3-methylimidazolium chloride. *Green Chemistry,* 9**,** 63-69.

FREEMANTLE, M. 2010. *An introduction to ionic liquids*, Royal Society of Chemistry.

FREIRE, M. G., TELES, A. R. R., ROCHA, M. A. A., SCHRÖDER, B., NEVES, C. M. S. S., CARVALHO, P. J., EVTUGUIN, D. V., SANTOS, L. M. N. B. F. & COUTINHO, J. A. P. 2011. Thermophysical characterization of ionic liquids able to dissolve biomass. *Journal of Chemical & Engineering Data,* 56**,** 4813-4822.

FUJIFILM DIMATIX 2006. Drop formation tunning and fluid characteristics.

FUJIFILM DIMATIX 2008. Materials printer & cartridges DMP-2831 & DMC-11601/11610.

FUJIFILM DIMATIX 2010. FUJIFILM Dimatix materials printer.

FUJII, T. & LI, D. 2008. Preparation and properties of protein films and particles from chicken feather *Journal of Biological Macromolecules,* 8**,** 48-55.

FUKAYA, Y., HAYASHI, K., WADA, M. & OHNO, H. 2008. Cellulose dissolution with polar ionic liquids under mild conditions: required factors for anions. *Green Chemistry,* 10**,** 44-46.

FUKAYA, Y., SUGIMOTO, A. & OHNO, H. 2006. Superior Solubility of Polysaccharides in Low Viscosity, Polar, and Halogen-Free 1,3-Dialkylimidazolium Formates. *Biomacromolecules,* 7**,** 3295-3297.

GERICKE, M., SCHLUFTER, K., LIEBERT, T., HEINZE, T. & BUDTOVA, T. 2009a. Rheological properties of cellulose/ionic liquid solutions: from dilute to concentrated states. *Biomacromolecules,* 10**,** 1188-1194.

GERICKE, M., LIEBERT, T. & HEINZE, T. 2009b. Interaction of ionic liquids with polysaccharides, 8 – Synthesis of cellulose sulfates suitable for polyelectrolyte complex formation. *Macromolecular Bioscience,* 9**,** 343-353.

GHATEE, M. H. & ZOLGHADR, A. R. 2008. Surface tension measurements of imidazolium-based ionic liquids at liquid–vapor equilibrium. *Fluid Phase Equilibria,* 263**,** 168-175.

GHOSH, A., CLERENS, S., DEB-CHOUDHURY, S. & DYER, J. M. 2014. Thermal effects of ionic liquid dissolution on the structures and properties of regenerated wool keratin. *Polymer Degradation and Stability,* 108**,** 108-115.

GIBSON, I., ROSEN, D. & STUCKER, B. 2014. *Additive manufacturing technologies: 3D Printing, Rapid Prototyping, and Direct Digital Manufacturing*, Springer New York.

GRAENACHER, C. 1934. *Cellulose Solution*. US PATENT 1943176

GUAN, W., MA, X.-X., LI, L., TONG, J., FANG, D.-W. & YANG, J.-Z. 2011. Ionic parachor and its application in acetic acid ionic liquid homologue 1-alkyl-3-methylimidazolium acetate {[Cnmim][OAc](n = 2,3,4,5,6)}. *The Journal of Physical Chemistry B,* 115**,** 12915-12920.

GUNTON, J. D., SHIRYAYEV, A. & PAGAN, D. L. 2007. *Protein condensation: kinetic pathways to crystallization and disease*, Cambridge University Press.

GUO, N. & LEU, M. 2013. Additive manufacturing: technology, applications and research needs. *Frontiers of Mechanical Engineering,* 8**,** 215-243.

GUPTA, K. M., HU, Z. & JIANG, J. 2013a. Cellulose regeneration from a cellulose/ionic liquid mixture: the role of anti-solvents. *RSC Advances,* 3**,** 12794-12801.

GUPTA, K. M., HU, Z. & JIANG, J. 2013b. Molecular insight into cellulose regeneration from a cellulose/ionic liquid mixture: effects of water concentration and temperature. *RSC Advances,* 3**,** 4425-4433.

HAGHTALAB, A. & SHOJAEIAN, A. 2014. Volumetric and viscometric behaviour of the binary systems of N-methyldiethanolamine and diethanolamine with 1-butyl-3-methylimidazolium acetate at various temperatures. *The Journal of Chemical Thermodynamics,* 68**,** 128-137.

HALLETT, J. P. & WELTON, T. 2011. Room-Temperature Ionic Liquids: Solvents for Synthesis and Catalysis. 2. *Chemical Reviews,* 111**,** 3508-3576.

HAMEED, N. & GUO, Q. 2009. Natural wool/cellulose acetate blends regenerated from the ionic liquid 1-butyl-3-methylimidazolium chloride. *Carbohydrate Polymers,* 78**,** 999-1004.

HAMEED, N. & GUO, Q. 2010. Blend films of natural wool and cellulose prepared from an ionic liquid. *Cellulose,* 17**,** 803-813.

HAVERHALS, L. M., BROWN, E. K., FOLEY, M. P., DE LONG, H. C. & TRULOVE, P. C. 2012. Formation of surface structures on biopolymers through the inkjet printing of ionic liquids. *ECS Transactions,* 50**,** 615-621.

HE, C. & WANG, Q. 1999. Rheological properties of cellulose solution in paraformaldehyde/dimethyl sulfoxide system (1). *Polymers for Advanced Technologies,* 10**,** 487-492.

HE, Y., TUCK, C. J., PRINA, E., KILSBY, S., CHRISTIE, S. D. R., EDMONDSON, S., HAGUE, R. J. M., ROSE, F. R. A. J. & WILDMAN, R. D. 2017a. A new photocrosslinkable polycaprolactone-based ink for three-dimensional inkjet printing. *Journal of Biomedical Materials Research Part B: Applied Biomaterials,* 105**,** 1645-1657.

HE, Y., WILDMAN, R. D., TUCK, C. J., CHRISTIE, S. D. R. & EDMONDSON, S. 2016. An investigation of the behavior of solvent based polycaprolactone ink for material jetting. *Scientific Reports,* 6**,** 20852.

HE, Y., ZHANG, F., SALEH, E., VAITHILINGAM, J., ABOULKHAIR, N., BEGINES, B., TUCK, C. J., HAGUE, R. J. M., ASHCROFT, I. A. & WILDMAN, R. D. 2017b. A tripropylene glycol diacrylate-based polymeric support ink for material jetting. *Additive Manufacturing,* 16**,** 153-161.

HEARLE, J. W. S. 1958. A fringed fibril theory of structure in crystalline polymers. *Journal of Polymer Science,* 28**,** 432-435.

HEINZE, T., DORN, S., SCHÖBITZ, M., LIEBERT, T., KÖHLER, S. & MEISTER, F. 2008. Interactions of ionic liquids with polysaccharides – 2: Cellulose. *Macromolecular Symposia,* 262**,** 8-22.

HEINZE, T. & KOSCHELLA, A. 2005. Solvents applied in the field of cellulose chemistry: A mini review. *Polímeros,* 15**,** 84-90.

HEINZE, T., SCHWIKAL, K. & BARTHEL, S. 2005. Ionic liquids as reaction medium in cellulose functionalization. *Macromolecular Bioscience,* 5**,** 520-525.

HERMANUTZ, F., GÄHR, F., UERDINGEN, E., MEISTER, F. & KOSAN, B. 2008. New developments in dissolving and processing of cellulose in ionic liquids. *Macromolecular Symposia,* 262**,** 23-27.

HIRAGA, Y., KATO, A., SATO, Y. & SMITH, R. L. 2015. Densities at pressures up to 200 mpa and atmospheric pressure viscosities of ionic liquids 1-ethyl-3-methylimidazolium methylphosphate, 1-ethyl-3-methylimidazolium diethylphosphate, 1-butyl-3-methylimidazolium acetate, and 1-butyl-3-methylimidazolium bis(trifluoromethylsulfonyl)imide. *Journal of Chemical & Engineering Data,* 60**,** 876-885.

HIRAGA, Y., KOYAMA, K., SATO, Y. & SMITH, R. L. 2017. High pressure densities for mixed ionic liquids having different functionalities: 1-butyl-3-methylimidazolium chloride and 1-butyl-3-methylimidazolium bis(trifluoromethylsulfonyl)imide. *The Journal of Chemical Thermodynamics,* 108**,** 7-17.

HOLLAND, S., FOSTER, T., MACNAUGHTAN, W. & TUCK, C. 2018. Design and characterisation of food grade powders and inks for microstructure control using 3D printing. *Journal of Food Engineering,* 220**,** 12-19.

HU, G., ALBROW-OWEN, T., JIN, X., ALI, A., HU, Y., HOWE, R. C. T., SHEHZAD, K., YANG, Z., ZHU, X., WOODWARD, R. I., WU, T.-C., JUSSILA, H., WU, J.-B., PENG, P., TAN, P.-H., SUN, Z., KELLEHER, E. J. R., ZHANG, M., XU, Y. & HASAN, T. 2017. Black phosphorus ink formulation for inkjet printing of optoelectronics and photonics. *Nature Communications,* 8**,** 278.

IDRIS, A., VIJAYARAGHAVAN, R., PATTI, A. F. & MACFARLANE, D. R. 2014. Distillable protic ionic liquids for keratin dissolution and recovery. *ACS Sustainable Chemistry & Engineering,* 2**,** 1888-1894.

IDRIS, A., VIJAYARAGHAVAN, R., RANA, U. A., FREDERICKS, D., PATTI, A. F. & MACFARLANE, D. R. 2013. Dissolution of feather keratin in ionic liquids. *Green Chemistry,* 15**,** 525-534.

IZUNOBI, J. U. & HIGGINBOTHAM, C. L. 2011. Polymer Molecular Weight Analysis by 1H NMR Spectroscopy. *Journal of Chemical Education,* 88**,** 1098-1104.

JI, Y., CHEN, J., LV, J., LI, Z., XING, L. & DING, S. 2014. Extraction of keratin with ionic liquids from poultry feather. *Seperation and Purification Technology,* 132**,** 577-583.

JIA, N., LI, S.-M., MA, M.-G., SUN, R.-C. & ZHU, L. 2011. Green microwave-assisted synthesis of cellulose/calcium silicate nanocomposites in ionic liquids and recycled ionic liquids. *Carbohydrate Research,* 346**,** 2970-2974.

JOHNSON, D. L. 1970. *Method of preparing polymers from a mixture of cyclic amine oxides and polymers*.US Patent US3508941A

JØRGENSEN, H., KRISTENSEN, J. B. & FELBY, C. 2007. Enzymatic conversion of lignocellulose into fermentable sugars: challenges and opportunities. *Biofuels, Bioproducts and Biorefining,* 1**,** 119-134.

KADOKAWA, J.-I., MURAKAMI, M.-A. & KANEKO, Y. 2008. A facile preparation of gel materials from a solution of cellulose in ionic liquid. *Carbohydrate Research,* 343**,** 769-772.

KAMLET, M. J. & TAFT, R. W. 1976. The solvatochromic comparison method. I. The .beta.-scale of solvent hydrogen-bond acceptor

(HBA) basicities. *Journal of the American Chemical Society,* 98**,** 377-383.
KAMMIOVIRTA, K., JAASKELAINEN, A.-S., KUUTTI, L., HOLOPAINEN-MANTILA, U., PAANANEN, A., SUURNAKKI, A. & ORELMA, H. 2016. Keratin-reinforced cellulose filaments from ionic liquid solutions. *RSC Advances,* 6**,** 88797-88806.
KIM, U.-J., EOM, S. H. & WADA, M. 2010. Thermal decomposition of native cellulose: Influence on crystallite size. *Polymer Degradation and Stability,* 95**,** 778-781.
KLEMM, D., HEUBLEIN, B., FINK, H. P. & BOHN, A. 2005. Cellulose: fascinating biopolymer and sustainable raw material. *Angewandte Chemie International Edition,* 44**,** 3358-3393.
KLEMM, D., PHILIPP, B., HEINZE, T., HEINZE, U. & WAGENKNECHT, W. 1998. *Comprehensive cellulose chemistry, comprehensive cellulose chemistry: Fundamentals and Analytical Methods*, Wiley.
KOSAN, B., MICHELS, C. & MEISTER, F. 2008. Dissolution and forming of cellulose with ionic liquids. *Cellulose,* 15**,** 59-66.
KRUTH, J. P., LEU, M. C. & NAKAGAWA, T. 1998. Progress in additive manufacturing and rapid prototyping. *CIRP Annals,* 47**,** 525-540.
LAMOOLPHAK, W., DE-EKNAMKUL, W. & SHOTIPRUK, A. 2008. Hydrothermal production and characterization of protein and amino acids from silk waste. *Bioresource Technology,* 99**,** 7678-7685.
LAN, W., LIU, C.-F., YUE, F.-X. & SUN, R.-C. 2013. Rapid dissolution of cellulose in ionic liquid with different methods. In: Cellulose Fundamental Aspects. InTech.
LATEEF, H., GRIMES, S., KEWCHAROENWONG, P. & FEINBERG, B. 2009. Separation and recovery of cellulose and lignin using ionic liquids: a process for recovery from paper-based waste. *Journal of Chemical Technology & Biotechnology,* 84**,** 1818-1827.
LE BIDEAU, J., VIAU, L. & VIOUX, A. 2011. Ionogels, ionic liquid based hybrid materials. *Chemical Society Reviews,* 40**,** 907-925.
LE, H. P. 1998. Progress and trends in ink-jet printing technologies. *Journal of Imaging Science and Technology,* 42**,** 49-62.
LEAL, G. F., RAMOS, L. A., BARRETT, D. H., CURVELO, A. A. S. & RODELLA, C. B. 2015. A thermogravimetric analysis (TGA) method to determine the catalytic conversion of cellulose from carbon-supported hydrogenolysis process. *Thermochimica Acta,* 616**,** 9-13.
LEE, H. V., HAMID, S. B. A. & ZAIN, S. K. 2014. Conversion of lignocellulosic biomass to nanocellulose: Structure and chemical process. *The Scientific World Journal,* 2014**,** 20.
LEVIS, S. R. & DEASY, P. B. 2001. Production and evaluation of size reduced grades of microcrystalline cellulose. *International Journal of Pharmaceutics,* 213**,** 13-24.
LEVY, G. N., SCHINDEL, R. & KRUTH, J. P. 2003. Rapid Manufacturing and rapid tooling with layer manufacturing (LM) technologies, state of the art and future perspectives. *CIRP Annals,* 52**,** 589-609.
LEWIS, D. M. & RIPPON, J. A. 2013. *The coloration of wool and other keratin fibres* John Wiley & Sons, Inc.
LI, L., ZHU, Y. & YANG, J. 2018. 3D bioprinting of cellulose with controlled porous structures from NMMO. *Materials Letters,* 210**,** 136-138.
LI, R., HE, J., WEN, F. & WANG, D. 2014. Fabrication and properties of nano indium tin oxide/wool keratin composites. *Journal of Applied Polymer Science,* 131**,** 39641/1-39641/6.
LI, R. & WANG, D. 2013. Preparation of regenerated wool keratin films from wool keratin-ionic liquid solutions. *Journal of Applied Polymer Science,* 127**,** 2648-2653.

LIAW, C.-Y. & GUVENDIREN, M. 2017. Current and emerging application of 3D printing in medicine. *Biofabrication,* 9.

LIEBERT, T. 2010. Cellulose Solvents – Remarkable history, bright future. *cellulose solvents: For Analysis, Shaping and Chemical Modification.* American Chemical Society.

LIU, H., SALE, K. L., HOLMES, B. M., SIMMONS, B. A. & SINGH, S. 2010. Understanding the interactions of cellulose with ionic liquids: a molecular dynamics study. *The Journal of Physical Chemistry B,* 114**,** 4293-4301.

LIU, X., NIE, Y., MENG, X., ZHANG, Z., ZHANG, X. & ZHANG, S. 2017. DBN-based ionic liquids with high capability for the dissolution of wool keratin. *RSC Advances,* 7**,** 1981-1988.

LIU, Z., WANG, H., LI, Z., LU, X., ZHANG, X., ZHANG, S. & ZHOU, K. 2011. Characterization of the regenerated cellulose films in ionic liquids and rheological properties of the solutions. *Materials Chemistry and Physics,* 128**,** 220-227.

LOPES, J. M., KARETH, S., BERMEJO, M. D., MARTÍN, Á., WEIDNER, E. & COCERO, M. J. 2016. Experimental determination of viscosities and densities of mixtures carbon dioxide+1-allyl-3-methylimidazolium chloride. Viscosity correlation. *The Journal of Supercritical Fluids,* 111**,** 91-96.

LU, B., XU, A. & WANG, J. 2014a. Cation does matter: how cationic structure affects the dissolution of cellulose in ionic liquids. *Green Chemistry,* 16**,** 1326-1335.

LU, F., WANG, L., JI, X., CHENG, B., SONG, J. & GOU, X. 2014b. Flow behavior and linear viscoelasticity of cellulose 1-allyl-3-methylimidazolium formate solutions. *Carbohydrate Polymers,* 99**,** 132-139.

MA, X.-X., WEI, J., ZHANG, Q.-B., TIAN, F., FENG, Y.-Y. & GUAN, W. 2013. Prediction of thermophysical properties of acetate-based ionic liquids using semiempirical methods. *Industrial & Engineering Chemistry Research,* 52**,** 9490-9496.

MACLAREN, J. 1962. The extent of reduction of wool proteins by thiols. *Australian Journal of Chemistry,* 15**,** 824-831.

MAHADEVA, S. K., WALUS, K. & STOEBER, B. 2015. Paper as a platform for sensing applications and other devices: A Review. *ACS Applied Materials & Interfaces,* 7**,** 8345-8362.

MÄKI-ARVELA, P., ANUGWOM, I., VIRTANEN, P., SJÖHOLM, R. & MIKKOLA, J. P. 2010. Dissolution of lignocellulosic materials and its constituents using ionic liquids—A review. *Industrial Crops and Products,* 32**,** 175-201.

MARKSTEDT, K., SUNDBERG, J. & GATENHOLM, P. 2014. 3D Bioprinting of cellulose structures from an ionic liquid. *3D Printing Additive Manufacturing,* 1**,** 115-121.

MARR, P. C. & MARR, A. C. 2016. Ionic liquid gel materials: applications in green and sustainable chemistry. *Green Chemistry,* 18**,** 105-128.

MARSH, K. N., BOXALL, J. A. & LICHTENTHALER, R. 2004. Room temperature ionic liquids and their mixtures—a review. *Fluid Phase Equilibria,* 219**,** 93-98.

MARTIN, G. D., HOATH, S. D. & HUTCHINGS, I. M. 2008. Inkjet printing - the physics of manipulating liquid jets and drops. *Journal of Physics: Conference Series,* 105.

MCKITTRICK, J., CHEN, P.-Y., BODDE, S. G., YANG, W., NOVITSKAYA, E. E. & MEYERS, M. A. 2012. The structure, functions, and mechanical properties of keratin. *The Journal of the Minerals, Metals and Materials Society,* 64**,** 449-468.

MEDRONHO, B. & LINDMAN, B. 2014. Competing forces during cellulose dissolution: From solvents to mechanisms. *Current Opinion in Colloid & Interface Science,* 19**,** 32-40.
MENG, Z., ZHENG, X., TANG, K., LIU, J. & QIN, S. 2012. Dissolution of natural polymers in ionic liquids: A review. *e-Polymers,* 12**,** 317.
METTLER TOLEDO 2011. Good titration practice in Karl Fischer titration.
MIKKOLA, J.-P., KIRILIN, A., TUUF, J.-C., PRANOVICH, A., HOLMBOM, B., KUSTOV, L. M., MURZIN, D. Y. & SALMI, T. 2007. Ultrasound enhancement of cellulose processing in ionic liquids: from dissolution towards functionalization. *Green Chemistry,* 9**,** 1229-1237.
MOON, R. J., MARTINI, A., NAIRN, J., SIMONSEN, J. & YOUNGBLOOD, J. 2011. Cellulose nanomaterials review: structure, properties and nanocomposites. *Chemical Society Reviews,* 40**,** 3941-3994.
NAGAI, Y. & NISHIKAWA, T. 1970. Alkali solubilization of chichken feather keratin. *Agricultural and Biological Chemistry,* 34**,** 16-22.
NAZET, A., SOKOLOV, S., SONNLEITNER, T., MAKINO, T., KANAKUBO, M. & BUCHNER, R. 2015. Densities, viscosities, and conductivities of the imidazolium ionic liquids [Emim][Ac], [Emim][FAP], [Bmim][BETI], [Bmim][FSI], [Hmim][TFSI], and [Omim][TFSI]. *Journal of Chemical & Engineering Data,* 60**,** 2400-2411.
NELSON, M. L. & O'CONNOR, R. T. 1964. Relation of certain infrared bands to cellulose crystallinity and crystal latticed type. Part I. Spectra of lattice types I, II, III and of amorphous cellulose. *Journal of Applied Polymer Science,* 8**,** 1311-1324.
NGO, T. D., KASHANI, A., IMBALZANO, G., NGUYEN, K. T. Q. & HUI, D. 2018. Additive manufacturing (3D printing): A review of materials, methods, applications and challenges. *Composites Part B: Engineering,* 143**,** 172-196.
NOGUEIRA, R., QUEIROZ, S. M., SILVA, G. E. B., ROCHA, W. F. C., SARMANHO, G. F., ALMEIDA, R. R. R. & MOREIRA, G. F. 2012. Determination of volatiles in pharmaceutical certified reference materials. *Journal of the Brazilian Chemical Society,* 23**,** 1636-1646.
NORDSON 2015a. PICO Pulse jetting valve operating manual.
NORDSON 2015b. PICO Touch controller operating manual.
NOVOSELOV, N. P., SASHINA, E. S., PETRENKO, V. E. & ZABORSKY, M. 2007. Study of dissolution of cellulose in ionic liquids by computer modeling. *Fibre Chemistry,* 39**,** 153-158.
NULWALA, H., MIRJAFARI, A. & ZHOU, X. 2018. Ionic liquids and poly(ionic liquid)s for 3D printing – A focused mini-review. *European Polymer Journal,* 108**,** 390-398.
O'MAHONY, A. M., SILVESTER, D. S., ALDOUS, L., HARDACRE, C. & COMPTON, R. G. 2008. Effect of water on the electrochemical window and potential limits of room-temperature ionic liquids. *Journal of Chemical & Engineering Data,* 53**,** 2884-2891.
OLIVIER-BOURBIGOU, H., MAGNA, L. & MORVAN, D. 2010. Ionic liquids and catalysis: Recent progress from knowledge to applications. *Applied Catalysis A: General,* 373**,** 1-56.
OLSSON, C. & WESTMAN, G. 2013. Direct dissolution of cellulose: background, means and applications. *Cellulose - Fundamental Aspects.* InTech.
OSHIMA, T., SAKAMOTO, T., OHE, K. & BABA, Y. 2014. Cellulose aerogel regenerated from ionic liquid solution for immobilized metal affinity adsorption. *Carbohydrate polymers,* 103**,** 62-69.
PAL, A., SHAHROM RAJA SHAHROM, M., MONIRUZZAMAN, M., DEVI WILFRED, C., MITRA, S., THU, K. & SAHA, B. 2017. Ionic liquid as a

new binder for activated carbon based consolidated composite adsorbents. 326.
PANG, J., WU, M., ZHANG, Q., TAN, X., XU, F., ZHANG, X. & SUN, R. 2015. Comparison of physical properties of regenerated cellulose films fabricated with different cellulose feedstocks in ionic liquid. *Carbohydrate Polymers,* 121**,** 71-78.
PATEL, D. D. & LEE, J.-M. 2012. Applications of ionic liquids. *The Chemical Record,* 12**,** 329-355.
PERIYASAMY, A. & KHANUM, R. 2012. Effect of fibrillation on pilling tendency of lyocell fiber. *Textile Today*.
PETROVIC, V., VICENTE HARO GONZALEZ, J., JORDÁ FERRANDO, O., DELGADO GORDILLO, J., RAMÓN BLASCO PUCHADES, J. & PORTOLÉS GRIÑAN, L. 2011. Additive layered manufacturing: sectors of industrial application shown through case studies. *International Journal of Production Research,* 49**,** 1061-1079.
PHAM, D. T. & GAULT, R. S. 1998. A comparison of rapid prototyping technologies. *International Journal of Machine Tools and Manufacture,* 38**,** 1257-1287.
PINKERT, A., MARSH, K. N., PANG, S. & STAIGER, M. P. 2009. Ionic liquids and their interaction with cellulose. *Chemical Reviews,* 109**,** 6712-6728.
PINTO, A. M., RODRÍGUEZ, H., ARCE, A. & SOTO, A. 2014. Combined physical and chemical absorption of carbon dioxide in a mixture of ionic liquids. *The Journal of Chemical Thermodynamics,* 77**,** 197-205.
POLETTO, M., PISTOR, V. & ZATTERA, A. J. 2013. Structural characteristics and thermal properties of native cellulose. In : Cellulose Fundamental Aspects. InTech.
POOLE, A. J., CHURCH, J. S. & HUSON, M. G. 2009. Environmentally sustainable fibers from regenerated protein. *Biomacromolecules,* 10**,** 1-8.
POOLE, A. J., LYONS, R. E. & CHURCH, J. S. 2011. Dissolving feather keratin using sodium sulfide for bio-polymer applications. *Journal of Polymers and the Environment,* 19**,** 995-1004.
QI, H., CHANG, C. & ZHANG, L. 2008a. Effects of temperature and molecular weight on dissolution of cellulose in NaOH/urea aqueous solution. *Cellulose,* 15**,** 779-787.
QI, W., DING, D. & SALVI, R. J. 2008b. Cytotoxic effects of dimethyl sulphoxide (DMSO) on cochlear organotypic cultures. *Hearing Research,* 236**,** 52-60.
QUAN, S.-L., KANG, S.-G. & CHIN, I.-J. 2010. Characterization of cellulose fibers electrospun using ionic liquid. *Cellulose,* 17**,** 223-230.
QUIJADA-MALDONADO, E., VAN DER BOOGAART, S., LIJBERS, J. H., MEINDERSMA, G. W. & DE HAAN, A. B. 2012. Experimental densities, dynamic viscosities and surface tensions of the ionic liquids series 1-ethyl-3-methylimidazolium acetate and dicyanamide and their binary and ternary mixtures with water and ethanol at T = (298.15 to 343.15 K). *Journal of Chemical Thermodynamics,* 51**,** 51-58.
RABIDEAU, B. D., AGARWAL, A. & ISMAIL, A. E. 2013. Observed mechanism for the breakup of small bundles of cellulose iα and iβ in ionic liquids from molecular dynamics simulations. *The Journal of Physical Chemistry B,* 117**,** 3469-3479.
RANKE, J., STOLTE, S., STÖRMANN, R., ARNING, J. & JASTORFF, B. 2007. Design of sustainable chemical productsthe example of ionic liquids. *Chemical Reviews,* 107**,** 2183-2206.

REDDY, K. O., MAHESWARI, C. U., DHLAMINI, M. S., MOTHUDI, B. M., ZHANG, J., ZHANG, J., NAGARAJAN, R. & RAJULU, A. V. 2017. Preparation and characterization of regenerated cellulose films using borassus fruit fibers and an ionic liquid. *Carbohydrate polymers,* 160**,** 203-211.

REDDY, K. O., ZHANG, J., ZHANG, J. & RAJULU, A. V. 2014. Preparation and properties of self-reinforced cellulose composite films from Agave microfibrils using an ionic liquid. *Carbohydrate Polymers,* 114**,** 537-545.

REIN, M. 1993. Phenomena of liquid drop impact on solid and liquid surfaces. *Fluid Dynamics Research,* 12**,** 61-93.

REMSING, R. C., HERNANDEZ, G., SWATLOSKI, R. P., MASSEFSKI, W. W., ROGERS, R. D. & MOYNA, G. 2008. Solvation of carbohydrates in n,n'-dialkylimidazolium ionic liquids: A multinuclear NMR spectroscopy study. *The Journal of Physical Chemistry B,* 112**,** 11071-11078.

REMSING, R. C., SWATLOSKI, R. P., ROGERS, R. D. & MOYNA, G. 2006. Mechanism of cellulose dissolution in the ionic liquid 1-n-butyl-3-methylimidazolium chloride: a 13C and 35/37Cl NMR relaxation study on model systems. *Chemical Communications***,** 1271-1273.

RIOBOO, R., MARENGO, M. & TROPEA, C. 2002. Time evolution of liquid drop impact onto solid, dry surfaces. *Experiments in Fluids,* 33**,** 112-124.

RIOBOO, R., TROPEA, C. & MARENGO, M. 2001. Outcomes from a drop impact on solid surfacses. 11**,** 12.

ROSENAU, T., POTTHAST, A., SIXTA, H. & KOSMA, P. 2001. The chemistry of side reactions and byproduct formation in the system NMMO/cellulose (Lyocell process). *Progress in Polymer Science,* 26**,** 1763-1837.

ROSEWALD, M., HOU, F. Y. S., HARKINS, A. L., MUTUTUVARI, T. & TRAN, C. D. 2014. Cellulose-chitosan-keratin composite materials: Synthesis, immunological and antibacterial properties. *ECS Transactions,* 64**,** 499-505.

ROUSE, J. G. & VAN DYKE, M. E. 2010. A review of keratin-based biomaterials for biomedical applications. *Materials,* 3**,** 999-1014.

SAALWÄCHTER, K., BURCHARD, W., KLÜFERS, P., KETTENBACH, G., MAYER, P., KLEMM, D. & DUGARMAA, S. 2000. Cellulose solutions in water containing metal complexes. *Macromolecules,* 33**,** 4094-4107.

SAFAROV, J., GEPPERT-RYBCZYŃSKA, M., KUL, I. & HASSEL, E. 2014. Thermophysical properties of 1-butyl-3-methylimidazolium acetate over a wide range of temperatures and pressures. *Fluid Phase Equilibria,* 383**,** 144-155.

SASHINA, E. S. & NOVOSELOV, N. P. 2009. Effect of structure of ionic liquids on their dissolving power toward natural polymers. *Russian Journal of General Chemistry,* 79**,** 1057-1062.

SCHROOYEN, P. M. M., DIJKSTRA, P. J., OBERTHÜR, R. C., BANTJES, A. & FEIJEN, J. 2000. Partially carboxymethylated feather keratins. 1. properties in aqueous systems. *Journal of Agricultural and Food Chemistry,* 48**,** 4326-4334.

SCHROOYEN, P. M. M., DIJKSTRA, P. J., OBERTHÜR, R. C., BANTJES, A. & FEIJEN, J. 2001. Stabilization of solutions of feather keratins by sodium dodecyl sulfate. *Journal of Colloid and Interface Science,* 240**,** 30-39.

SESCOUSSE, R., LE, K. A., RIES, M. E. & BUDTOVA, T. 2010. Viscosity of cellulose−imidazolium-based ionic liquid solutions. *The Journal of Physical Chemistry B,* 114**,** 7222-7228.

SHARMA, R. K. & FRY, J. L. 1983. Instability of anhydrous tetra-n-alkylammonium fluorides. *The Journal of Organic Chemistry,* 48**,** 2112-2114.
SHARMA, S. & GUPTA, A. 2016. Sustainable management of keratin waste biomass: applications and future perspectives. *Brazilian Archives of Biology and Technology,* 59.
SHEN, W., HU, T. & FAN, W. 2014. Cellulose generated-microporous carbon nanosheets with nitrogen doping. *RSC Advances,* 4**,** 9126-9132.
SHOKRI, J. & ADIBKI, K. 2013. *Application of cellulose and cellulose derivatives in pharmaceutical Industries. In: Cellulose Medical, Pharmaceutical and Electronic Applications*
SILVA, N. H. C. S., VILELA, C., MARRUCHO, I. M., FREIRE, C. S. R., PASCOAL NETO, C. & SILVESTRE, A. J. D. 2014. Protein-based materials: from sources to innovative sustainable materials for biomedical applications. *Journal of Materials Chemistry B,* 2**,** 3715-3740.
SIMPSON, W. S. & CRAWSHAW, G. 2002. *Wool: science and technology*, Elsevier Science.
SOLTMAN, D. & SUBRAMANIAN, V. 2008. Inkjet-printed line morphologies and temperature control of the coffee ring effect. *Langmuir,* 24**,** 2224-2231.
SONG, B. & SPRINGER, J. 1996. Determination of interfacial tension from the profile of a pendant drop using computer-aided image processing: 1. theoretical. *Journal of Colloid and Interface Science,* 184**,** 64-76.
SONG, H., LUO, Z., ZHAO, H., LUO, S., WU, X., GAO, J. & WANG, Z. 2013. High tensile strength and high ionic conductivity bionanocomposite ionogels prepared by gelation of cellulose/ionic liquid solutions with nano-silica. *RSC Advances,* 3**,** 11665-11675.
SOUČKOVÁ, M., KLOMFAR, J. & PÁTEK, J. 2017. Group contribution and parachor analysis of experimental data on density and surface tension for members of the homologous series of 1-Cn-3-methylimidazolium chlorides. *Fluid Phase Equilibria,* 454**,** 43-56.
SPANGE, S., REUTER, A., VILSMEIER, E., HEINZE, T., KEUTEL, D. & LINERT, W. 1998. Determination of empirical polarity parameters of the cellulose solvent N,N-dimethylacetamide/LiCl by means of the solvatochromic technique. *Journal of Polymer Science Part A: Polymer Chemistry,* 36**,** 1945-1955.
STRINGER, J. & DERBY, B. 2010. Formation and stability of lines produced by inkjet printing. *Langmuir,* 26**,** 10365-10372.
SUN, N., RODRIGUEZ, H., RAHMAN, M. & ROGERS, R. D. 2011. Where are ionic liquid strategies most suited in the pursuit of chemicals and energy from lignocellulosic biomass? *Chemical Communications,* 47**,** 1405-1421.
SUN, P., LIU, Z.-T. & LIU, Z.-W. 2009. Particles from bird feather: A novel application of an ionic liquid and waste resource. *Journal of Hazardous Materials,* 170**,** 786-790.
SWATLOSKI, R. P., SPEAR, S. K., HOLBREY, J. D. & ROGERS, R. D. 2002. Dissolution of cellose with ionic liquids. *Journal of the American Chemical Society,* 124**,** 4974-4975.
SWEELY, K. D., FOX, E. T., BROWN, E. K., HAVERHALS, L. M., DE LONG, H. C. & TRULOVE, P. C. 2014. Inkjet printing ionic liquids for the formation of surface structures on biopolymer substrates. *ECS Transactions,* 64**,** 575-582.

TAFT, R. W. & KAMLET, M. J. 1976. The solvatochromic comparison method. 2. The .alpha.-scale of solvent hydrogen-bond donor (HBD) acidities. *Journal of the American Chemical Society,* 98**,** 2886-2894.

TENGBORG, C., STENBERG, K., GALBE, M., ZACCHI, G., LARSSON, S., PALMQVIST, E. & HAHN-HÄGERDAL, B. 1998. Comparison of SO2 and H2SO4 impregnation of softwood prior to steam pretreatment on ethanol production. *Applied Biochemistry and Biotechnology,* 70**,** 3-15.

THERMOFISCHER SCIENTIFIC. 2013. *Introduction to Fourier transform infrared spectroscopy* [Online].

THOORENS, G., KRIER, F., LECLERCQ, B., CARLIN, B. & EVRARD, B. 2014. Microcrystalline cellulose, a direct compression binder in a quality by design environment—A review. *International Journal of Pharmaceutics,* 473**,** 64-72.

TOLVIK CONSULTING LTD 2011. The UK waste wood market.

TRAN, C. D., BENZI, G., PROSENC, F. & FRANKO, M. 2016a. One-pot synthesis of biocompatible silver nanoparticle composites from cellulose and keratin: Characterization and antimicrobial activity. *ACS Appl Materials and Interfaces,* 8**,** 34791-34801.

TRAN, C. D., MAKUVAZA, J., MUNSON, E. & BENNETT, B. 2017. Biocompatible copper oxide nanoparticle composites from cellulose and chitosan: Facile synthesis, unique structure, and antimicrobial activity. *ACS Applied Materials and Interfaces,* 9**,** 42503-42515.

TRAN, C. D. & MUTUTUVARI, T. M. 2015. Cellulose, chitosan, and keratin composite materials. Controlled drug release. *Langmuir,* 31**,** 1516-26.

TRAN, C. D. & MUTUTUVARI, T. M. 2016. Cellulose, chitosan and keratin composite materials: Facile and recyclable synthesis, conformation and properties. *ACS Sustain Chemistry and Engineering,* 4**,** 1850-1861.

TRAN, C. D., PROSENC, F. & FRANKO, M. 2018. Facile synthesis, structure, biocompatibility and antimicrobial property of gold nanoparticle composites from cellulose and keratin. *Journal of Colloid and Interface Science,* 510**,** 237-245.

TRAN, C. D., PROSENC, F., FRANKO, M. & BENZI, G. 2016b. Synthesis, structure and antimicrobial property of green composites from cellulose, wool, hair and chicken feather. *Carbohydrate Polymers,* 151**,** 1269-1276.

TSUDA, Y. & NOMURA, Y. 2014. Properties of alkaline-hydrolyzed waterfowl feather keratin. *Animal Science Journal,* 85**,** 180-185.

VALOT, L., MARTINEZ, J., MEHDI, A. & SUBRA, G. 2019. Chemical insights into bioinks for 3D printing. *Chemical Society Reviews,* 48**,** 4049-4086.

VEHOVEC, T., GARTNER, A., PLANINŠEK, O. & OBREZA, A. 2012. Influence of different types of commercially available microcrystalline cellulose on degradation of perindopril erbumine and enalapril maleate in binary mixtures *Acta Pharm,* 62**,** 515.

VITZ, J., ERDMENGER, T., HAENSCH, C. & SCHUBERT, U. S. 2009. Extended dissolution studies of cellulose in imidazolium based ionic liquids. *Green Chemistry,* 11**,** 417-424.

VOET, D., VOET, J. G. & PRATT, C. W. 2016. *Fundamentals of biochemistry: Life at the molecular level, 5th Edition*, Wiley.

VYAZOVKIN, S. 2012. Thermogravimetric analysis. *Characterization of Materials.* John Wiley & Sons, Inc.

WANG, H., GURAU, G. & ROGERS, R. D. 2012. Ionic liquid processing of cellulose. *Chemical Society Reviews,* 41**,** 1519-1537.

WANG, H., LI, Z., LIU, Y., ZHANG, X. & ZHANG, S. 2009. Degradation of poly(ethylene terephthalate) using ionic liquids. *Green Chemistry,* 11**,** 1568-1575.
WANG, L., DU, J., LUO, Z., DU, X., LI, Y., LIU, J. & SUN, D. 2013. Design and experiment of a jetting dispenser driven by piezostack actuator. *IEEE Transactions on Components, Packaging and Manufacturing Technology,* 3**,** 147-156.
WANG, S., LU, A. & ZHANG, L. 2016a. Recent advances in regenerated cellulose materials. *Progress in Polymer Science,* 53**,** 169-206.
WANG, L., NIE, Y., ZHANG, X., ZENG, S., ZHANG, S. & ZHENG, S. 2016b. Synergistic effects of cosolvents on the dissolution of wool keratin using ionic liquids. *Chemical Engineering & Technology,* 39**,** 979-986.
WANG, M., ZHAO, T., WANG, G. & ZHOU, J. 2014. Blend films of human hair and cellulose prepared from an ionic liquid. *Textile Research Journal,* 84**,** 1315-1324, 10 pp.
WATANABE, M., THOMAS, M. L., ZHANG, S., UENO, K., YASUDA, T. & DOKKO, K. 2017. Application of ionic liquids to energy storage and conversion materials and devices. *Chemical Reviews,* 117**,** 7190-7239.
WELTON, T. 2018. Ionic liquids: a brief history. *Biophysical reviews,* 10**,** 691-706.
WERTZ, J.-L., MERCIER, J. P. & BÉDUÉ, O. 2010. *Cellulose science and technology*, EPFL Press.
WIECHERS, S., UNGER, F. & MEYER, J. 2015. *Use of powdered cellulose in cosmetic applications*. US Patent US2015/0110841 A1.
WILKES, J. S. 2002. A short history of ionic liquids—from molten salts to neoteric solvents. *Green Chemistry,* 4**,** 73-80.
WONG, K. V. & HERNANDEZ, A. 2012. A review of additive manufacturing. *ISRN Mechanical Engineering,* 2012**,** 10.
WONG, S. Y., LEE, C. C., ASHRAFZADEH, A., JUNIT, S. M., ABRAHIM, N. & HASHIM, O. H. 2016. A high-yield two-hour protocol for extraction of human hair shaft proteins. *PLOS ONE,* 11**,** e0164993.
XIE, H., LI, S. & ZHANG, S. 2005. Ionic liquids as novel solvents for the dissolution and blending of wool keratin fibers. *Green Chemistry,* 7**,** 606-608.
XU, A., WANG, J. & WANG, H. 2010. Effects of anionic structure and lithium salts addition on the dissolution of cellulose in 1-butyl-3-methylimidazolium-based ionic liquid solvent systems. *Green Chemistry,* 12**,** 268-275.
XU, A., WANG, J., ZHANG, Y. & CHEN, Q. 2012a. Effect of alkyl chain length in anions on thermodynamic and surface properties of 1-butyl-3-methylimidazolium carboxylate ionic liquids. *Industrial & Engineering Chemistry Research,* 51**,** 3458-3465.
XU, A., ZHANG, Y., LI, Z. & WANG, J. 2012b. Viscosities and conductivities of 1-butyl-3-methylimidazolium carboxylates ionic liquids at different temperatures. *Journal of Chemical & Engineering Data,* 57**,** 3102-3108.
YAMAUCHI, K., YAMAUCHI, A., KUSUNOKI, T., KOHDA, A. & KONISHI, Y. 1996. Preparation of stable aqueous solution of keratins, and physiochemical and biodegradational properties of films. *Journal of Biomedical Materials Research,* 31**,** 439-444.
YANG, H., HE, Y., TUCK, C., WILDMAN, R., ASHCROFT, I., DICKENS, P. & HAGUE, R. High viscosity jetting system for 3D reactive inkjet printing. Solid Freeform Fabrication Proceedings, 2013. 505-513.
YARIN, A. L. 2006. Drop impact dynamics : splashing, spreading, receding, bouncing…. *Annual Review of Fluid Mechanics,* 38**,** 159-192.

YENG, L. C., WAHIT, M. U. & OTHMAN, N. 2015. Thermal and flexural properties of regenerated cellulose (RC)/poly(3-hydroxybutyrate) (PHB) bicomposited. *Jurnal Teknologi,* 75**,** 107-112.

YIN, J., RASTOGI, S., TERRY, A. E. & POPESCU, C. 2007. Self-organization of oligopeptides obtained on dissolution of feather keratins in superheated water. *Biomacromolecules,* 8**,** 800-806.

YOUNGS, T. G. A., HARDACRE, C. & HOLBREY, J. D. 2007. Glucose solvation by the ionic liquid 1,3-dimethylimidazolium chloride: A simulation study. *The Journal of Physical Chemistry B,* 111**,** 13765-13774.

YOUNGS, T. G. A., HOLBREY, J. D., MULLAN, C. L., NORMAN, S. E., LAGUNAS, M. C., D'AGOSTINO, C., MANTLE, M. D., GLADDEN, L. F., BOWRON, D. T. & HARDACRE, C. 2011. Neutron diffraction, NMR and molecular dynamics study of glucose dissolved in the ionic liquid 1-ethyl-3-methylimidazolium acetate. *Chemical Science,* 2**,** 1594-1605.

YU, E., KIM, S.-C., LEE, H. J., OH, K. H. & MOON, M.-W. 2015. Extreme wettability of nanostructured glass fabricated by non-lithographic, anisotropic etching. *Scientific Reports,* 5**,** 9362.

YUAN, Y. & LEE, T. R. 2013. Contact angle and wetting properties. In: Surface Science Techniques. Springer Berlin Heidelberg.

ZAVREL, M., BROSS, D., FUNKE, M., BÜCHS, J. & SPIESS, A. C. 2009. High-throughput screening for ionic liquids dissolving (ligno-)cellulose. *Bioresource Technology,* 100**,** 2580-2587.

ZHANG, B., XUE, Z., XUE, Y., HUANG, Z., LI, Z. & HAO, J. 2015. Ionic liquid-assisted synthesis of morphology-controlled TiO2 particles with efficient photocatalytic activity. *RSC Advances,* 5**,** 81108-81114.

ZHANG, F., TUCK, C., HAGUE, R., HE, Y., SALEH, E., LI, Y., STURGESS, C. & WILDMAN, R. 2016. Inkjet printing of polyimide insulators for the 3D printing of dielectric materials for microelectronic applications. *Journal of Applied Polymer Science,* 133.

ZHANG, H., WANG, Z. G., ZHANG, Z. N., WU, J., ZHANG, J. & HE, J. S. 2007. Regenerated-cellulose/multiwalled- carbon-nanotube composite fibers with enhanced mechanical properties prepared with the ionic liquid 1-allyl-3-methylimidazolium chloride. *Advanced Materials,* 19**,** 698-704.

ZHANG, H., WU, J., ZHANG, J. & HE, J. 2005. 1-Allyl-3-methylimidazolium chloride room temperature ionic liquid: A new and powerful nonderivatizing solvent for cellulose. *Macromolecules,* 38**,** 8272-8277.

ZHANG, J., ZHANG, H., WU, J., ZHANG, J., HE, J. & XIANG, J. 2010. NMR spectroscopic studies of cellobiose solvation in EmimAc aimed to understand the dissolution mechanism of cellulose in ionic liquids. *Physical Chemistry Chemical Physics,* 12**,** 1941-1947.

ZHANG, Z., ZHANG, X., NIE, Y., WANG, H., ZHENG, S. & ZHANG, S. 2017a. Effects of water content on the dissolution behavior of wool keratin using 1-ethyl-3-methylimidazolium dimethylphosphate. *Science China Chemistry,* 60**,** 934-941.

ZHANG, J., WU, J., YU, J., ZHANG, X., HE, J. & ZHANG, J. 2017b. Application of ionic liquids for dissolving cellulose and fabricating cellulose-based materials: state of the art and future trends. *Materials Chemistry Frontiers,* 1**,** 1273-1290.

ZHAO, H., BAKER, G. A., SONG, Z., OLUBAJO, O., CRITTLE, T. & PETERS, D. 2008. Designing enzyme-compatible ionic liquids that can dissolve carbohydrates. *Green Chemistry,* 10**,** 696-705.

ZHAO, H., JONES, C. L. & COWINS, J. V. 2009. Lipase dissolution and stabilization in ether-functionalized ionic liquids. *Green Chemistry,* 11**,** 1128-1138.
ZHAO, S., WANG, X. & ZHANG, L. 2013. Rapid and efficient Knoevenagel condensation catalyzed by a novel protic ionic liquid under ultrasonic irradiation. *Royal Society of Chemistry Advances,* 3**,** 11691-11696.
ZHAO, W., YANG, R., ZHANG, Y. & WU, L. 2012. Sustainable and practical utilization of feather keratin by an innovative physicochemical pretreatment: high density steam flash-explosion. *Green Chemistry,* 14**,** 3352-3360.
ZHENG, S., NIE, Y., ZHANG, S., ZHANG, X. & WANG, L. 2015. Highly efficient dissolution of wool keratin by dimethylphosphate ionic liquids. *ACS Sustainable Chemistry & Engineering,* 3**,** 2925-2932.
ZOCCOLA, M., ALUIGI, A. & TONIN, C. 2009. Characterisation of keratin biomass from butchery and wool industry wastes. *Journal of Molecular Structure,* 938**,** 35-40.